Functional Colloidal Systems Containing Probiotic Bacteria

Natalia Burlaga, MSc Eng.

Doctor of Philosophy Dissertation

Supervised by Professor Ewa Kaczorek

Institute of Chemical Technology and Engineering

Poznan University of Technology

Poland, 2026

Research conducted within this dissertation was supported by the National Science Centre in Poland, PRELUDIUM 22 project entitled *MiCo: new microbe-colloids for oral delivery of probiotics*.

Grant number: 2023/49/N/NZ9/02128

Grant Recipient: Natalia Burlaga

ACKNOWLEDGMENTS

I would like to express my sincere gratitude to all those who contributed to the completion of this doctoral dissertation.

In particular, I would like to thank my supervisor, Professor Ewa Kaczorek, for her valuable scientific guidance, kindness, time, and support at every stage of the preparation of this work.

I would also like to thank all my colleagues, co-workers and members of the research team for inspiring discussions, substantive assistance, and a friendly working atmosphere.

My sincere thanks go to Katarzyna Adamska, Aleksandra Rybak, Oliwia Degórska, Aleksandra Banasiak, and Witold Stachowiak for their motivation, kindness, and companionship throughout the entire period of my doctoral studies.

I am especially grateful to Zofia Rybacka and Marta Wojcieszak-Michalak for their invaluable support, kindness, and belief in me.

I would also like to express my special thanks to Adam Grzywaczyk and Wojciech Smułek for our shared scientific and professional journey, mutual support, and for always being someone I could rely on, especially in the moments when I needed it the most, as well as for all the challenges we continue to undertake together. Our collaboration, both during the doctoral studies and in the creation of our joint venture, has been and continues to be extremely important to me.

Finally, I would like to thank my family for their patience, understanding, and constant presence.

PODZIĘKOWANIA

Pragnę złożyć serdeczne podziękowania wszystkim osobom, które przyczyniły się do powstania niniejszej rozprawy doktorskiej.

W szczególności chciałabym wyrazić wdzięczność mojej Promotorce, Pani Profesor Ewie Kaczorek, za cenne wskazówki naukowe, życzliwość, poświęcony czas oraz pomoc na każdym etapie przygotowywania tej pracy.

Dziękuję również wszystkim współpracownikom i członkom zespołu badawczego za inspirujące dyskusje, pomoc merytoryczną oraz przyjazną atmosferę pracy.

Serdeczne podziękowania kieruję do Katarzyny Adamskiej, Aleksandry Rybak, Oliwii Degórskiej, Aleksandry Banasiak oraz Witolda Stachowiaka za motywację, życzliwość oraz towarzyszenie mi w trakcie całego okresu realizacji doktoratu.

Szczególnie wdzięczna jestem Zofii Rybackiej oraz Marcie Wojcieszak-Michalak za nieocenione wsparcie, życzliwość oraz wiarę we mnie.

Osobne podziękowania chciałabym złożyć Adamowi Grzywaczykowi i Wojciechowi Smułkowi – za wspólną drogę naukową i zawodową, wzajemne wsparcie oraz za to, że zawsze mogłam na Was liczyć, szczególnie w momentach, w których najbardziej tego potrzebowałam, a także za wszystkie wyzwania, które podejmujemy razem. Nasza współpraca, zarówno w trakcie doktoratu, jak i przy tworzeniu wspólnego przedsięwzięcia, była i jest dla mnie niezwykle ważna.

Na końcu chciałabym podziękować mojej rodzinie za cierpliwość, zrozumienie oraz stałą obecność.

TABLE OF CONTENT

ABSTRACT

The limited viability and stability of probiotic bacteria during processing and storage remain a key challenge in the development of effective food and nutraceutical formulations. Although numerous encapsulation strategies have been proposed, integrated evaluations linking carrier architecture with probiotic physiology, storage stability, and functional performance remain limited. This dissertation investigates colloidal carrier systems designed to enhance probiotic functional potential.

The study was based on the hypothesis that encapsulation in hydrogel-based matrices and association with liposome-based carriers improves storage stability compared with free cells, and that the incorporation of supportive or bioactive components further enhances probiotic viability. The objective was to design and comprehensively evaluate such colloidal systems through formulation development, structural and physicochemical characterization, and biological assessment using multiple parameters.

The results indicate that probiotic stabilization is influenced by the composition and structural organization of the colloidal matrix. Preformulation screening revealed strain-dependent additive effects and identified trehalose, inulin, and gum arabic as the most favorable components for further development, with *Lactiplantibacillus plantarum* selected as the model strain. Hydrogel systems were associated with improved probiotic performance compared with free cells, with protective effects governed by matrix composition and microenvironmental factors rather than by physical entrapment alone. Liposomal formulations introduced an additional stabilization mechanism through formation of an external pericellular lipid corona. Two studied lipid-based systems maintained organized colloidal structures and supported physiologically relevant bacterial subpopulations. The fluvastatin-loaded lipid formulation represented a dual-function system integrating probiotic stabilization with a bioactive liposomal phase. Overall, the developed systems preserved functional activity, maintained controlled oxidative responses, and exhibited stable electrokinetic behavior at both room and physiological temperatures.

The findings are consistent with the proposed hypothesis and indicate that the defined research objectives were addressed within the scope of the work.

STRESZCZENIE

Ograniczona żywotność i stabilność bakterii probiotycznych w trakcie procesów technologicznych oraz przechowywania stanowią istotne wyzwanie w opracowywaniu skutecznych produktów spożywczych i nutraceutycznych. Pomimo licznych proponowanych strategii enkapsulacji, nadal brakuje zintegrowanych analiz łączących architekturę nośnika z fizjologią probiotyków, ich stabilnością w trakcie przechowywania oraz funkcjonalną aktywnością. Niniejsza rozprawa doktorska dotyczy badania koloidalnych układów nośnikowych zaprojektowanych w celu zwiększenia potencjału funkcjonalnego probiotyków.

Badanie oparto na hipotezie, że enkapsulacja w hydrożelowych matrycach oraz oddziaływanie z liposomowymi nośnikami poprawiają stabilność podczas przechowywania w porównaniu z wolnymi komórkami, a włączenie składników wspierających lub bioaktywnych dodatkowo zwiększa przeżywalność probiotyków. Celem pracy było zaprojektowanie oraz kompleksowa ocena takich układów koloidalnych poprzez opracowanie formulacji, ich charakterystykę strukturalną i fizykochemiczną oraz wieloparametrową ocenę biologiczną.

Uzyskane wyniki wskazują, że stabilizacja probiotyków zależy od składu oraz organizacji strukturalnej matrycy koloidalnej. Badania wstępne wykazały zależne od szczepu działanie dodatków oraz pozwoliły wytypować trehalozę, inulinę i gumę arabską jako najbardziej korzystne składniki do dalszego opracowania formulacji, przy czym jako szczep modelowy wybrano *Lactiplantibacillus plantarum*. Zastosowanie systemów hydrożelowych prowadziło do poprawy funkcjonowania probiotyków w porównaniu z wolnymi komórkami, a obserwowany efekt ochronny był determinowany przez skład matrycy i czynniki mikrośrodowiskowe, a nie wyłącznie przez fizyczne uwięzienie komórek. Formulacje liposomalne zapewniały dodatkowy mechanizm stabilizacji poprzez tworzenie zewnętrznej, okołokomórkowej lipidowej otoczki. Oba badane układy lipidowe utrzymywały uporządkowaną strukturę koloidalną oraz umożliwiały utrzymanie fizjologicznie istotnych subpopulacji bakterii. Z kolei formulacja lipidowa zawierająca fluwastatynę stanowiła układ o podwójnej funkcji, łączący stabilizację probiotyku z obecnością bioaktywnej fazy liposomalnej. Opracowane systemy pozwoliły na zachowanie aktywności funkcjonalnej komórek, utrzymanie kontrolowanej odpowiedzi oksydacyjnej oraz stabilnych właściwości elektrokinetycznych zarówno w temperaturze pokojowej, jak i w temperaturze fizjologicznej.

Uzyskane wyniki są zgodne z postawioną hipotezą badawczą oraz wskazują, że założone cele badawcze zostały zrealizowane w zakresie określonym w pracy.

LIST OF ABBREVIATIONS

AB – AlamarBlue

AFM – atomic force microscopy

ALG – sodium alginate

B/L – lipid-coated probiotic cells

B/L/F – probiotic cells with a surrounding layer of liposomes loaded with fluvastatin

CDNB – 1-chloro-2,4-dinitrobenzene

CFU – colony forming units

CR – Congo red

CRB – Congo red binding

CRP – cellular redox potential

cryoSEM – cryogenic scanning electron microscopy

CS – corn starch

CTRL – control sample

CV – crystal violet

DBS – diluted bacterial suspensions

DMPC – 1,2-dimyristoyl-sn-glycero-3-phosphocholine

DMSO – dimethyl sulfoxide

DNPH – 2,4-dinitrophenylhydrazine

DOPG – dioleoylphosphatidylglycerol

DPBS – Dulbecco's phosphate-buffered saline

GA – gum arabic

GA-IN – alginate probiotic beads with the addition of gum arabic and with the incorporation of inulin

GA-IN/TRE – alginate probiotic beads with the addition of gum arabic and with the incorporation of the mixture of inulin and trehalose

GA-TRE – alginate probiotic beads with the addition of gum arabic and with the incorporation of trehalose

GI – gastrointestinal

GRAS – Generally Recognized as Safe

GSH – reduced glutathione

GSTs – glutathione S-transferases

GUVs – giant unilamellar vesicles

ICP-MS – inductively coupled plasma mass spectrometry

IN – inulin

L – formulation with liposomes alone

LAB – lactic acid bacteria

L/P – lipid-coated probiotic cells

LUVs – large unilamellar vesicles

MD – maltodextrin

MLVs – multilamellar vesicles

MMS – minimal medium solution

MRU – MTT reducing units

MRS – de Man, Rogosa, and Sharpe (medium)

MSG – monosodium glutamate

MTT – 3-(4,5-dimethylthiazol-2-yl)-2,5-diphenyltetrazolium bromide

MVLs – multivesicular liposomes

OD – optical density

PCM – Polish Collection of Microorganisms

PCC – protein carbonyl content

PDI – polydispersity index

PH – psyllium husk

PH-IN – alginate probiotic beads with the addition of psyllium husk and with the incorporation of inulin

PH-IN/TRE – alginate probiotic beads with the addition of psyllium husk and with the incorporation of the mixture of inulin and trehalose

PH-TRE – alginate probiotic beads with the addition of psyllium husk and with the incorporation of trehalose

PI – propidium iodide

PPA – potentially protective agent

PSD – particle size distribution

Ra – surface roughness

ROS – reactive oxygen species

RSG – RedoxSensor Green

SCFAs – short-chain fatty acids

SI – standardized inocula

SUVs – small unilamellar vesicles

TEM – transmission electron microscopy

TMP – total membrane permeability

TRE – trehalose

VBNC – viable but non-culturable

VC – vitamin C

WFCC – World Federation for Culture Collections

I. LITERATURE REVIEW

1. PROBIOTICS AND THEIR IMPORTANCE IN FOOD AND HEALTH SCIENCES

1.1. Classification and characteristics of the main groups of probiotic bacteria

Probiotics are defined as "live microorganisms that, when administered in adequate amounts, confer a health benefit on the host" [1]. According to this definition, a demonstrable health effect is required for microorganisms to be classified as probiotics. From a taxonomic perspective, most probiotic bacteria are Gram-positive and are mainly associated with lactic acid bacteria (LAB) belonging to the order *Lactobacillales*, as well as with the genus *Bifidobacterium*. The key probiotic genera within *Lactobacillales* include members of the former genus *Lactobacillus* (recently reclassified into several genera), as well as *Lactococcus*, *Streptococcus*, and *Enterococcus*. Although species of the genus *Bifidobacterium* are not considered LAB, they represent one of the most important groups of probiotic bacteria [2]. Together, these genera include the majority of microorganisms currently used in probiotic foods and dietary supplements. Despite differences in taxonomy and physiology, probiotic bacteria share several common features. They are non-pathogenic and able to survive food or pharmaceutical matrices, as well as to persist, at least temporarily, in the gastrointestinal (GI) tract. The main characteristics of the principal probiotic genera are summarized in Figure 1.

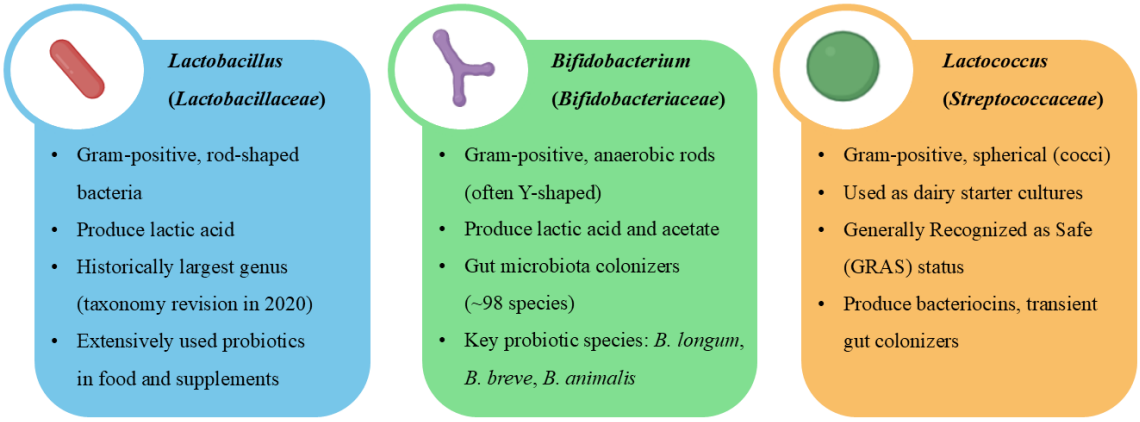

Figure 1. Main characteristics of major probiotic genera, including members of the former genus *Lactobacillus*, as well as *Bifidobacterium* and *Lactococcus* [3–5].

Not all strains within a given species are suitable for use as probiotics. For this reason, the selection and characterization of probiotic strains are based on clearly defined criteria. In general, a candidate strain must be identified at the genus, species, and strain level and must be safe for use (i.e. with no virulence factors or transferable antibiotic resistances) [2].

In addition, a probiotic strain should demonstrate a measurable health benefit in the target host. For strains used in foods or dietary supplements, such effects are typically supported by at least one well-designed human clinical trial. The strain must also remain viable at an effective dose in the final product throughout its shelf life [6]. Beyond safety and documented health effects, probiotic strains are evaluated for a range of functional and technological properties. These properties determine their suitability for incorporation into food or pharmaceutical products and their performance under practical conditions. The key functional and technological characteristics considered during strain selection are summarized in Figure 2. Only strains that meet these requirements are likely to provide the expected benefits to consumers.

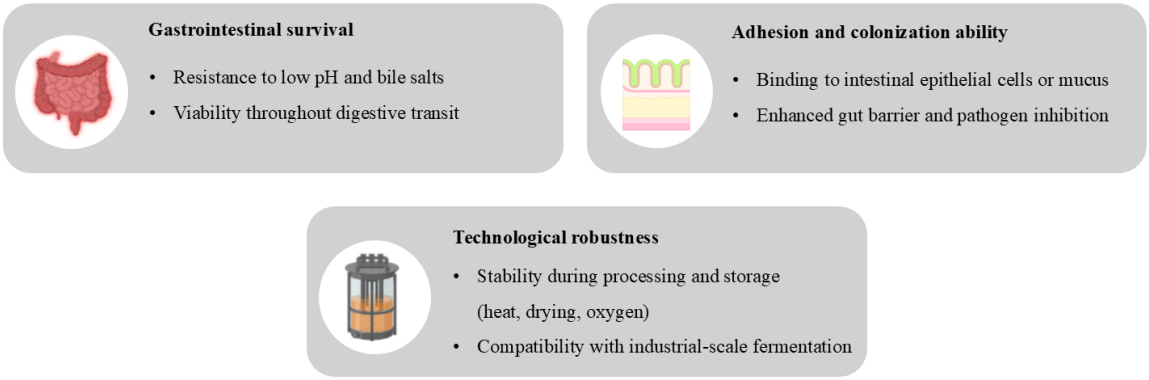

Figure 2. Key functional and technological characteristics considered during probiotic strain selection [2,7,8].

1.2. Mechanisms of health-promoting effects of probiotic bacteria

Probiotic bacteria modulate the gut microbiota mainly through competition with pathogenic microorganisms for nutrients and adhesion sites. In addition, many probiotic strains produce antimicrobial metabolites, including organic acids and bacteriocins. The formation of lactic acid and short-chain fatty acids (SCFAs) lowers intestinal pH, which limits the growth of pathogenic bacteria and supports balanced microbial community. Through these mechanisms, probiotics contribute to the preservation of mucosal integrity, support microbial diversity, and strengthen gut barrier function, thereby reducing the risk of GI disturbances [9].

Moreover, probiotic bacteria interact with the host immune system. Selected strains have been shown to promote regulatory immune responses and enhance epithelial barrier function. Metabolites produced by probiotics also contribute to immune regulation by supporting anti-inflammatory pathways and maintaining immune responsiveness [9,10].

Probiotics may also influence host metabolism, particularly lipid metabolism and micronutrient availability. Certain LAB have been shown to reduce serum cholesterol levels through mechanisms such as bile salt deconjugation and direct assimilation of cholesterol, which can decrease its intestinal absorption. Clinical studies report small but consistent reductions in total cholesterol and low-density lipoprotein (LDL) cholesterol after probiotic consumption [11]. In addition, some probiotic bacteria are able to synthesize vitamins (i.e. folate, riboflavin, vitamin B_{12}, and vitamin K), which may improve their availability and absorption in the host [12].

1.3. Impact of technological and environmental conditions on probiotic cell viability

Probiotic cell viability is influenced by processing methods and environmental conditions during production and storage. In particular, dehydration-based preservation techniques, such as freeze-drying and spray-drying, expose cells to physicochemical stresses, and probiotic strains differ in their tolerance to these conditions.

Freeze-drying stabilizes probiotic cultures by removing water through freezing followed by sublimation under reduced pressure, resulting in dry powdered products. However, during the freezing stage, extracellular ice formation can cause osmotic imbalance and mechanical damage to cell envelopes. In addition, changes in solute concentration during drying, together with intracellular ice formation, may lead to membrane deformation and loss of structural integrity. These effects can be further intensified by oxidative stress associated with the formation of reactive oxygen species (ROS). As a result, freeze-drying may lead to reductions in cell viability if process parameters are not properly controlled, with reported survival rates sometimes falling below 5% [13]. Although freeze-drying remains a widely used preservation method, it is associated with several limitations, including high operational costs, long processing times, and limited protection of probiotic cells under non-optimized conditions [14].

Spray-drying involves the atomization of probiotic suspensions into a stream of hot air to remove moisture. This method is economically attractive and suitable for large-scale production, but it exposes probiotic cells to thermal and dehydration-related stress. Exposure to high temperatures during drying can lead to protein denaturation, enzyme inactivation, and damage to cellular membranes. In addition, water removal during the drying process creates osmotic and oxidative stress, which may further affect membrane integrity and nucleic acids, resulting in reduced cell viability [13,15]. As a consequence, spray-drying often leads to low

immediate survival rates, particularly in strains with limited heat tolerance. For example, species sensitive to heat, such as *Bifidobacterium pseudocatenulatum* may show viability losses above 99% at drying temperatures of 75-85 °C [16].

Freeze-drying and spray-drying often require the use of protective additives, such as cryoprotective agents, to reduce damage to probiotic cells. These compounds can form protective matrices around cells during drying. However, achieving consistent and satisfactory survival rates remains difficult. In addition, dried probiotic powders require controlled storage conditions, including low humidity, temperature control, and limited oxygen exposure, to minimize further viability loss and oxidative degradation. Maintaining such conditions during storage and distribution increases technological complexity and costs [17,18].

The response of probiotic bacteria to stress associated with drying is strongly strain-dependent and reflects differences in cell structure, antioxidant capacity, and stress response mechanisms. As a result, drying tolerance varies widely among probiotic strains. To address these challenges, approaches such as encapsulation, stress adaptation before drying, and the selection of more robust strains are used to improve the stability of probiotics in final products. Table 1 presents selected examples of strains with lower and higher tolerance to drying, together with physiological features that influence their survival.

Table 1. Comparison of drying tolerance among selected probiotic strains.

Probiotic strain/species	Tolerance to drying	Key physiological factors	Example drying performance	Ref.
Low tolerance strains				
Bifidobacterium longum	Low	Strict anaerobe, highly sensitive to oxygen, poor antioxidative defense	High viability loss during spray-drying (>99%), severe oxidative damage	[19,20]
Lactobacillus delbrueckii subsp. *bulgaricus*	Low	Sensitive cell membranes, low thermotolerance	>60% cell death during spray-drying, poor survival without protectants	[19,21]
Akkermansia muciniphila	Very low	Strict anaerobe, extreme oxygen sensitivity, poor thermal tolerance	Unable to survive standard drying without special encapsulation and anaerobic conditions	[22]
High tolerance strains				
Lactiplantibacillus plantarum	Moderate-high	Robust antioxidative and osmotic stress responses, flexible metabolism	Low mortality (~19%) during spray-drying, good freeze-drying survival (>90%) with protectants	[21,23,24]
Bacillus coagulans (spore-forming)	High	Forms endospores, high thermal and oxidative resistance	Minimal viability loss during spray-drying, survives baking and long-term storage	[25,26]

1.4. Directions in probiotic development

Recent research on probiotics has increasingly focused on the development of new delivery formats and systems composed of multiple components designed to improve stability, safety, and functional performance. Among these approaches, prebiotics, synbiotics, and postbiotics are commonly discussed in the context of contemporary probiotic formulations (Figure 3).

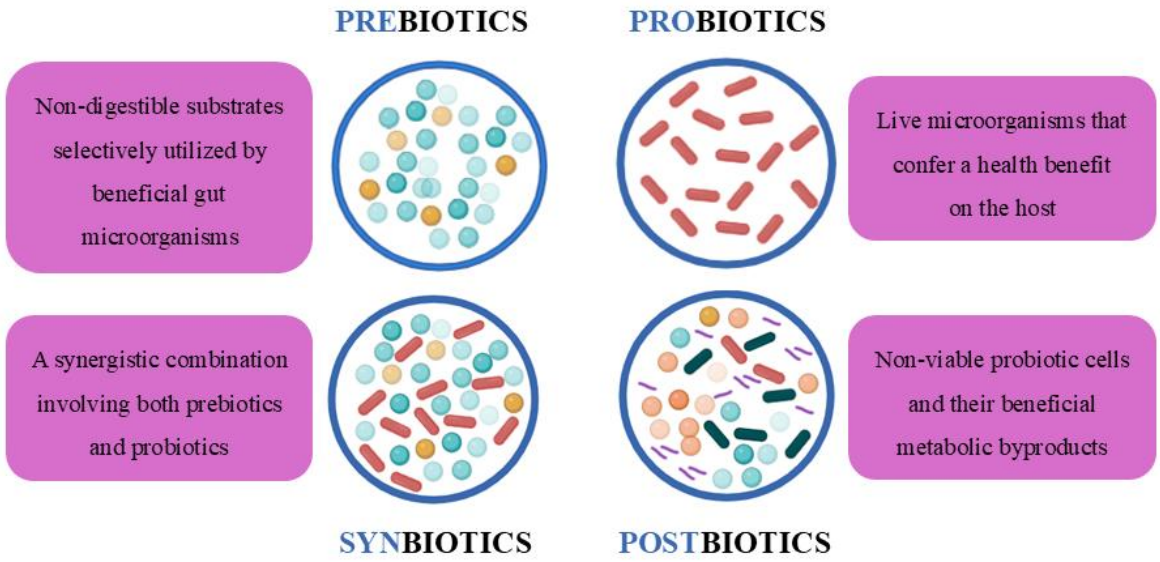

Figure 3. Conceptual illustration of probiotic-related terms highlighting their definitions [27–29].

Prebiotics are substrates that cannot be digested and are selectively utilized by beneficial gut microorganisms, supporting their growth and metabolic activity. Fermentation of prebiotics by probiotic bacteria leads to the production of SCFAs, which contribute to gut barrier function and immune regulation [27].

Synbiotics combine probiotic microorganisms with selected prebiotics to support their survival and activity in the GI tract. In such formulations, the prebiotic component serves as a substrate for the probiotic strain, which may improve persistence and metabolic activity compared with probiotics used alone. Several studies have reported improved probiotic performance in synbiotic products, particularly with respect to survival effect on the gut microbiota [28,29].

Postbiotics consist of non-viable microbial cells and their metabolic products, including cell components, enzymes, vitamins, and bioactive compounds. The absence of live microorganisms provides advantages in terms of stability, dosing consistency, and safety. As a result, postbiotics are being explored for use in functional foods, nutraceuticals, and dietary supplements [30].

Taken together, prebiotics, synbiotics, and postbiotics represent structured approaches to probiotic formulation that address limitations associated with the use of live microorganisms. Their development reflects a broader trend toward multi-component products designed to improve product stability and functionality.

2. INTRODUCTION TO COLLOIDAL SYSTEMS

2.1. Characteristics and classification of colloids

Colloids are heterogeneous mixtures in which one substance is dispersed as small particles, typically ranging from 1 to 1000 nm in size, within a continuous medium. Due to their size and relatively large surface area, colloidal particles show physicochemical properties that differ from those of true solutions. One characteristic feature of colloidal particles is Brownian motion, which refers to their random thermal movement and helps prevent sedimentation under the influence of gravity [31].

Colloidal systems are also characterized by a large interfacial area between the dispersed and continuous phases. This results in increased surface energy and a natural tendency of particles to aggregate. To maintain stability, colloids rely on stabilizing mechanisms that limit interactions between particles. These include electrostatic stabilization, in which particles acquire surface charge through ion adsorption, as well as steric stabilization provided by polymers or surfactants adsorbed at the particle surface. As a result, the stability of colloidal systems is determined by the balance between attractive and repulsive forces acting between particles. Depending on this balance, colloids may remain dispersed or undergo aggregation. In this sense, colloids combine interactions occurring at a small scale with a distinct dispersed structure, which underlies their use in many scientific and technological fields (i.e. chemistry, biology, and materials science) [32].

Colloidal systems can be classified according to their structural organization, formation mechanisms, and composition. An overview of these classifications, together with selected examples related to food and probiotic applications, is presented in Table 2. Such systems are widely used in food and biotechnological applications, where they support the delivery, stability, and functionality of bioactive compounds and microorganisms. Representative examples of these applications are summarized in Table 3.

Table 2. Classification and examples of colloidal systems used in food and probiotic applications.

Classification approach	Colloid type	Description	Food examples or applications	Ref.
By phases of dispersed and continuous components	Sol	Solid particles dispersed in liquid	Beverage stabilizers, starch suspensions	[33]
	Emulsion	Liquid droplets dispersed in another immiscible liquid	Milk, mayonnaise, salad dressings	
	Foam	Gas bubbles dispersed in liquid or solid matrix	Whipped cream, meringue	
	Gel	Semi-solid network immobilizing liquid within its structure	Yogurt, jam, tofu	[33–35]
By structural assembly	Association colloids (self-assembled)	Structures spontaneously formed (micelles, vesicles, microemulsions)	Casein micelles (milk), engineered liposomes for encapsulation	[33,35]
	Dispersive colloids	Mechanically or physically dispersed particles or droplets	Oil droplets dispersed mechanically (homogenized emulsions)	[33]
By composition	Biopolymer-based colloids	Natural edible biopolymers (proteins, polysaccharides, lipids)	Alginate, pectin, gelatin, chitosan hydrogels for probiotics encapsulation	[34,35]
	Inorganic or synthetic colloids	Industrial formulations (not food-grade)	Silica, synthetic polymer colloids	[36]

Table 3. Key roles and applications of colloidal systems in food and biotechnological applications.

Application domain	Role of colloidal systems	Examples and benefits	Ref.
Functional food formulations	Encapsulation and controlled release of bioactive compounds	• Nanoemulsions/liposomes for vitamins, omega-3, carotenoids (improved solubility and bioavailability) • Protein or polysaccharide nanoparticles for antioxidants, minerals (enhanced stability and controlled release)	[33]
	Protection and stabilization of probiotics	• Alginate or gelatin microcapsules to maintain probiotic viability in yogurts, cheeses, beverages (protection during storage and digestion)	[34,35]
Industrial biotechnology	Control of product quality	• Managing colloidal stability in brewing (preventing haze formation caused by interactions between proteins and polyphenols in beer and wine via fining agents)	[37]
	Immobilization of enzymes	• Silica, polymer or magnetic nanoparticles for enzyme immobilization (enhanced stability, activity, and reusability in biocatalysis) • Lipase immobilization for food processing (fat modification and flavor synthesis) • Nanobiocatalysts in environmental biotechnology (wastewater treatment, pollutant degradation)	[36]

In the context of probiotic delivery, the choice of an appropriate colloidal system is particularly important. Systems such as biopolymer-based hydrogels and emulsions are commonly investigated for probiotic encapsulation, as they can improve bacterial survival during processing, storage, and passage through the gastrointestinal tract. The use of colloidal carriers therefore provides practical solutions for maintaining probiotic viability in food products. Recent studies also describe the application of more advanced colloidal structures, including food-grade nanocarriers and responsive hydrogel systems, in functional food design [33,36]. These examples illustrate that colloid classification is not limited to theoretical considerations but has direct relevance for the development and optimization of complex food and biotechnological formulations.

2.1.1. Hydrogels

Hydrogels are hydrophilic polymer networks that are cross-linked and able to absorb and retain large amounts of water while preserving their 3D structure. Due to their high water content and soft mechanical properties, hydrogels show similarities to biological tissues and are generally considered biocompatible, biodegradable, and non-toxic [38]. The properties of hydrogels, including swelling behavior, pore size, mechanical strength, and degradation rate, depend on polymer composition and the degree of cross-linking. Hydrogels can be formed through physical cross-linking, such as ionic interactions or hydrogen bonding, or through chemical cross-linking involving covalent bonds. The type of cross-linking affects their stability and response to environmental conditions such as pH or temperature [39]. Because of these characteristics, hydrogels are widely studied as carrier systems in food and pharmaceutical applications. Their structure can be adjusted to protect sensitive components and to allow controlled release under defined conditions.

Natural biopolymers are used to form hydrogels for probiotic encapsulation because of their safety and ability to form stable gel structures. Typical examples include polysaccharides such as alginate, pectin, and gums derived from plants (i.e. guar gum, xanthan gum, and gum arabic) [40]. Alginate is a linear polyuronic acid obtained from seaweed that forms cross-linked hydrogels in the presence of divalent cations, most often calcium ions. These gels are stable under acidic gastric conditions and tend to swell or partially dissolve at the neutral pH of the intestine. However, hydrogels formed from calcium alginate may exhibit relatively high porosity, which can result in early release of encapsulated probiotic cells. For this reason, alginate is frequently combined with other polymers to reinforce the gel structure and reduce permeability [41].

Hydrogels may also be designed as synbiotic systems by incorporating prebiotic compounds together with probiotic microorganisms. In such systems, prebiotics are included within the hydrogel matrix [42]. Several studies have shown that the inclusion of prebiotics in hydrogel formulations improves probiotic survival under simulated gastric conditions. In synbiotic hydrogel systems, probiotic bacteria are therefore protected during transit through the upper GI tract and released together with a local nutrient source, which supports their persistence and activity in the host [40,41,43].

2.1.2. Colloidal carriers based on lipids

Liposomes are spherical lipid vesicles composed of one or more phospholipid bilayers that surround an internal aqueous compartment. Because of this structure, liposomes can encapsulate hydrophilic compounds within the aqueous core, while lipophilic substances can be incorporated into the lipid bilayer [44].

Liposomes are classified according to their size and lamellarity (Figure 4). Unilamellar liposomes consist of a single bilayer and include small unilamellar vesicles (SUVs), typically with diameters of about 30-100 nm, as well as large unilamellar vesicles (LUVs), which are larger than 100 nm. Giant unilamellar vesicles (GUVs) exceed 1000 nm in diameter. Multilamellar vesicles (MLVs) contain several concentric bilayers, whereas multivesicular liposomes (MVLs) consist of multiple aqueous compartments enclosed within a single lipid structure [45].

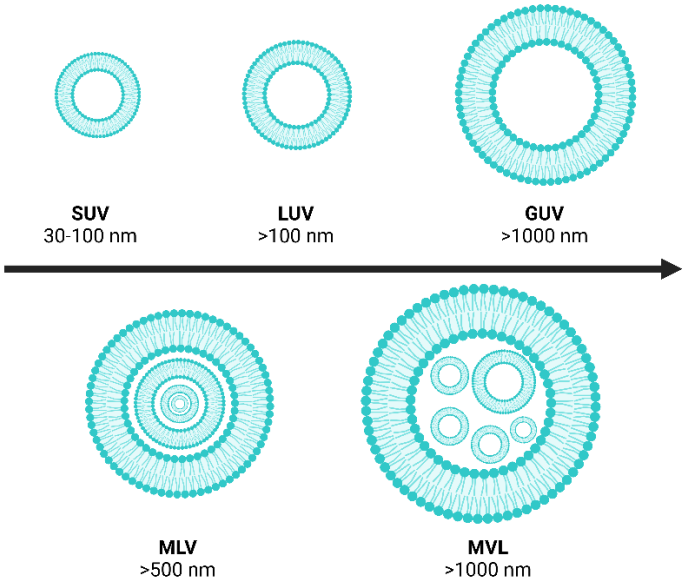

Figure 4. Representation of the different classes of liposomes based on size and lamellarity (SUV – small unilamellar vesicles; LUV – large unilamellar vesicles; GUV – giant unilamellar vesicles; MLV – multilamellar vesicles; MVL – multivesicular liposomes) [44,45].

The properties of liposomes, including size, number of bilayers, and lipid composition, influence encapsulation efficiency and behavior in biological systems. For this reason, liposomes are commonly characterized by parameters such as particle size distribution, zeta potential, lamellarity, and stability, which are directly related to their performance as delivery systems [46].

Liposomes are used as carriers in both applications related to food and in pharmaceutical or biomedical fields. Examples of liposomal systems applied in these areas are summarized in Table 4, including the types of encapsulated compounds, key functional aspects, and practical limitations. Ongoing work in this area focuses on adapting liposome-based technologies to different application requirements, including food-grade formulations. Despite current limitations, the transfer of liposome technologies from pharmaceutical research to food applications underscores future potential. Advances in liposome engineering are expected to drive broader adoption, improving efficacy, stability, and functionality across both therapeutic and nutraceutical domains.

Table 4. Comparative applications and characteristics of liposomal systems in functional foods, pharmaceuticals and biomedicine.

	Functional food sector	Pharmaceutical and biomedical sector	Ref.
Typical encapsulated agents	Vitamins, antioxidants, polyphenols, natural colorants, probiotics	Drugs, nucleic acids, diagnostic imaging agents	[45–49]
Main benefits	• Enhanced bioavailability and stability of bioactive ingredients • Improved probiotic survival and controlled gut release	• Targeted drug delivery • Controlled release • Biocompatibility • Protection of sensitive payloads	[45–49]
Commercial maturity	Emerging, mostly experimental and limited commercial use	Well-established, clinically approved products widely used in oncology, infectious diseases, vaccines	[45–47,49]
Typical compositions and requirements	• Food-grade ingredients • Stability during processing • Cost-effective production	• Highly purified lipids • Strict manufacturing conditions (sterility, defined particle size, stringent quality control)	[44–49]
Challenges and limitations	• Stability in complex food matrices • Cost and regulatory barriers • Limited industrial scalability	• High manufacturing costs • Complex regulatory approval for pharmaceuticals	[45–49]
Future perspectives	• Developments inspired by pharmaceutical advances • Broader use in probiotic and nutraceutical delivery	• Ongoing innovation (advanced targeting, enhanced stability) • Expanding therapeutic application (personalized medicine)	[44–49]

2.2. Importance of colloidal systems in food, pharmaceutical, and cosmetic industries

Colloidal systems can remain uniformly dispersed and are able to encapsulate active substances, which helps protect them from degradation and allows controlled release. Because of these properties, systems based on colloids are widely used in food, pharmaceutical, and cosmetic products, where they support product stability, functionality, and effectiveness [50,51]. An overview of selected applications of colloidal systems in these fields is presented in Figure 5. These examples illustrate the critical importance and broad utility of colloidal systems as advanced formulation tools across multiple sectors.

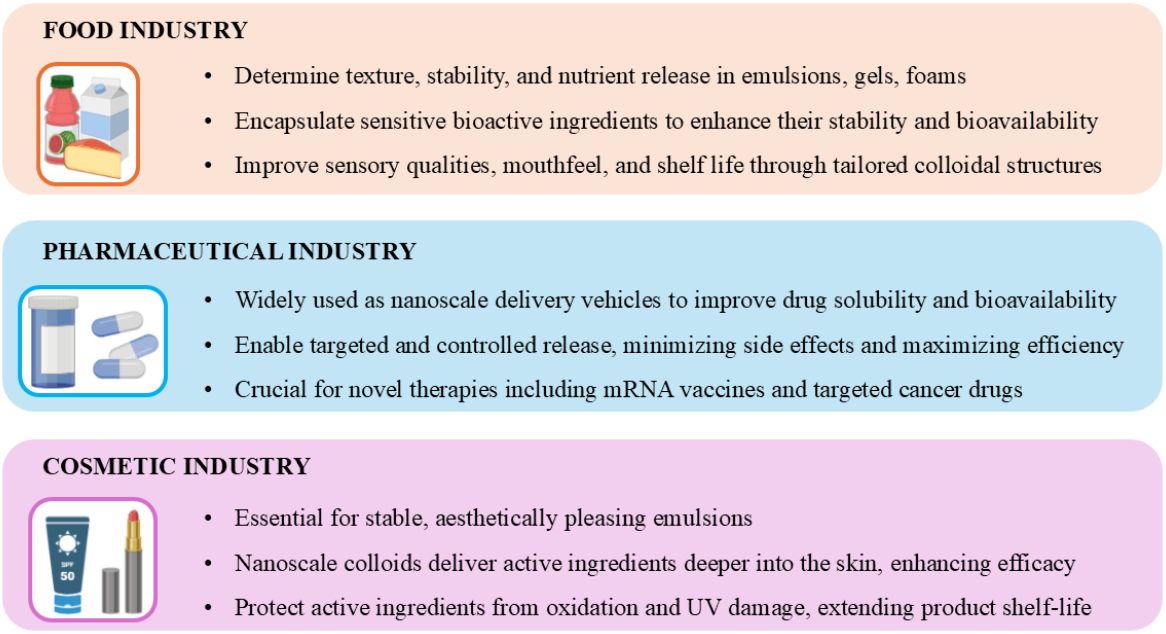

Figure 5. Overview of colloidal system applications, highlighting their roles in product performance [33,51–53].

3. APPLICATION OF COLLOIDS IN ENCAPSULATION OF ACTIVE SUBSTANCES

3.1. Polymeric hydrogel beads and liposomes as bioactive compound delivery systems

Polymeric hydrogel beads and liposomes are used as encapsulation systems for the delivery and protection of bioactive compounds. Each system is characterized by different structural features that influence its performance in different applications.

Hydrogel beads are typically prepared from polymers of natural origin, which are GRAS and suitable for use in food and dietary supplements. The composition of the polymer matrix and the degree of cross-linking can be adjusted to control properties such as swelling behavior, resistance to enzymatic degradation, and responsiveness to changes in pH. These features allow the release of encapsulated compounds to be tailored to specific conditions within the GI tract. In food and nutraceutical applications, hydrogel beads are used to incorporate ingredients related to health benefits. They have been applied for the encapsulation of vitamins, antioxidants, and flavor compounds, helping to limit degradation during processing and storage, and enabling release after ingestion. The gel structure of hydrogel beads and their adjustable mechanical properties also make them suitable for incorporation into food matrices, where they can be dispersed as discrete particles without markedly affecting product texture [35,54].

Liposomes differ from hydrogel beads in both structure and mode of action, and are commonly used as carriers for bioactive compounds. Their amphiphilic bilayer structure allows the encapsulation of hydrophilic substances within the aqueous core and lipophilic compounds within the lipid membrane. Encapsulation within the lipid bilayer can improve the stability of sensitive compounds and support their absorption or uptake by cells [35,47]. Liposome-based delivery systems are well established in pharmaceutical applications, where several formulations have been approved for clinical use. These systems have been applied for the delivery of chemotherapeutic agents, antibiotics, and nucleic acids. In biological systems, liposomes may interact with cell membranes or be internalized by endocytosis, which allows the transport of encapsulated compounds across biological barriers. Liposomes have also been investigated for use in functional foods and dietary supplements. Encapsulation of nutraceuticals, including polyphenols, omega-3 fatty acids, and vitamins, may support their availability after consumption [55]. In addition, both liposomal systems and hydrogel beads are applied in cosmetic formulations, where they are used to stabilize and deliver active ingredients such as vitamins or extracts derived from plants in topical products [56].

Although hydrogel beads and liposomes provide effective encapsulation of bioactive substances, both systems present technical challenges that limit their application under certain conditions. These challenges, which include stability, scalability, and cost-related factors, are summarized in Table 5.

Table 5. Technical challenges associated with hydrogel beads and liposome delivery systems.

Technical challenge	Hydrogel beads	Liposomes	Ref.
Long-term stability	• Prone to dehydration, swelling, deformation or aggregation • Challenging structural integrity in food matrices or gastrointestinal conditions	• Instability of lipid bilayers • Leakage of encapsulated compounds • Limited storage stability without careful formulation	[47,54,57]
Encapsulation efficiency and payload capacity	• Hydrophilic compounds may diffuse out of hydrogel matrix • High loading while maintaining bead integrity requires careful optimization	• Low efficiency for encapsulating large polar molecules • High encapsulation of hydrophilic compounds is difficult, limiting commercial formulations	[47,54,55,57]
Controlled release kinetics	• Difficulties in precisely controlling release rate/location • Requires careful adjustment of cross-link density or polymer choice	• Release can be unpredictable (usually upon membrane disruption or fusion)	[47,54,55,57]
Scale-up and manufacturing costs	• Costly and technically complex processes to produce uniform beads at industrial scale	• Complex large-scale production • Challenging for low-margin products	[47,54,57]
Regulatory and formulation issues	• Reproducibility, quality control, and biocompatibility of polymers must be rigorously managed	• Strict regulatory control • Ensuring safety and reproducibility of lipid components • Particularly for pharmaceutical and nutraceutical uses	[55,57]

3.2. Colloidal systems containing probiotic bacteria

3.2.1. Functional advantages

Colloidal encapsulation of probiotic bacteria influences the stability and performance of probiotic formulations during storage and use. One of the main effects of encapsulation is improved cell survival during storage. The encapsulating matrix forms a physical barrier around probiotic cells, which limits their exposure to oxygen, moisture, and other environmental factors that may reduce viability [58]. As a result, encapsulated probiotics generally maintain higher survival rates over time than non-encapsulated cells [59].

Encapsulation also provides protection against stresses encountered during processing and passage through the GI tract. Many probiotic bacteria are sensitive to oxygen, which can cause oxidative damage to cellular components, such as membranes and DNA. Putting cells within matrices that limit oxygen diffusion or contain antioxidant components can reduce this type of stress. In addition, the physical structure of microcapsules can protect bacteria from mechanical forces generated during processing or digestion, lowering the risk of cell damage [60].

Another functional aspect of colloidal systems is the possibility of co-encapsulating probiotic bacteria together with other bioactive compounds. In these systems, probiotics and accompanying ingredients are incorporated within the same carrier matrix. This approach can simplify formulation and help preserve the stability of both components. After release, the accompanying compounds may support probiotic activity or contribute additional functional effects, depending on the composition of the formulation [60].

Another functional aspect of colloidal encapsulation is the possibility of controlling the release of probiotic bacteria along the GI tract. Protective coatings can be applied to colloidal carriers to limit probiotic exposure to acidic gastric conditions and allow release at the neutral pH of the intestine. In this way, more viable bacteria can reach the intestinal environment, where they are able to persist and interact with the host [59,61].

3.2.2. Major technological challenges

The development of stable colloidal systems containing probiotic bacteria is associated with several technological limitations. One of the main challenges is maintaining probiotic viability over extended storage periods, together with the physical stability of the colloidal dispersion. Even when encapsulated, probiotic cell numbers may gradually decrease during storage, particularly under unfavorable conditions.

Differences between probiotic strains further complicate this issue. For example, encapsulated *Lactobacillus fermentum* and *Lactobacillus johnsonii* have been reported to retain high viability for up to 12 months at 4 °C, whereas *Lactobacillus acidophilus* encapsulated in a comparable system maintained viable cell counts for only about 4 months [62]. Such observations indicate that encapsulation does not provide uniform protection across strains and that interactions between the bacterial cells and the encapsulating matrix play an important role in determining prolonged survival. In addition to biological factors, maintaining a uniform colloidal dispersion during storage presents practical difficulties. In liquid formulations, encapsulated particles may aggregate or settle over time, leading to sedimentation or phase separation and a non-uniform distribution of probiotic cells within the product [63].

Probiotic stability is also influenced by formulation composition and storage conditions. The choice of encapsulating materials, the presence of additives, moisture content, and product pH all affect cell survival. Storage temperature and humidity are particularly relevant, as higher temperatures and insufficient moisture control can accelerate viability loss, even in encapsulated systems. These effects have been linked to processes such as membrane lipid oxidation and protein denaturation. Exposure to light may further reduce stability by degrading encapsulating materials or promoting the formation of ROS. For these reasons, encapsulation strategies must be tailored to the specific probiotic strain and the intended storage conditions. Even with such optimization, reduced stability outside refrigerated conditions remains a limitation, as many encapsulated probiotics show higher survival at 4 °C than at room temperature [62].

Additional challenges are related to production costs and the scalability of colloidal systems containing probiotic bacteria. Many encapsulation approaches rely on specialized equipment and multiple processing steps, which can limit their feasibility for large-scale production. Drying methods also involve trade-offs between cost and probiotic viability. Techniques such as freeze-drying generally support higher cell survival but require high capital investment and operating costs. In contrast, more economical processes, including spray-drying, are easier to scale but may result in lower probiotic viability. Balancing these factors remains a practical challenge in the design of encapsulated probiotic products. Scaling up encapsulation processes also requires careful consideration of regulatory and quality control requirements. All materials and processing steps must be food-grade, safe, and reproducible at an industrial scale, which further constrains formulation choices and process design [64]. Taken together, limitations related to storage stability, formulation optimization, and production scalability continue

to restrict the broader application of colloidal encapsulation strategies for probiotics in commercial products.

4. SIGNIFICANCE AND FUTURE PERSPECTIVES OF RESEARCH ON COLLOIDAL PROBIOTIC SYSTEMS

4.1. Justification of originality and innovative character

The present research addresses key challenges related to the stability and functionality of probiotic bacteria in different applications. Unencapsulated probiotic cells are known for reduced viability during processing and storage [65]. It has led to growing interest in encapsulation approaches based on protective colloidal matrices [66].

In this context, this doctoral work is about development and systematic evaluation of colloidal probiotic systems based on polymeric hydrogel beads and liposomal carriers. These systems were designed to improve probiotic survival and performance under conditions relevant to food and nutraceutical applications, extending beyond commonly applied encapsulation approaches.

A distinctive element of this research is the incorporation of prebiotic compounds into hydrogel-based probiotic carriers, resulting in synbiotic capsules. In these systems, prebiotic substrates are embedded within the hydrogel matrix, where they can support probiotic cells by providing a local nutrient source and contributing to stress resistance. The use of hydrogel beads enriched with prebiotics therefore represents a novel synbiotic delivery approach that combines physical protection with nutritional support for encapsulated probiotics. The originality of this strategy lies in the integration of probiotics and prebiotics within a single colloidal carrier, allowing their combined effects to be assessed in a controlled manner. While synbiotic concepts have been described previously, their application within hydrogel-based colloidal systems for probiotic stabilization remains a relatively limited area of study [55,67].

Another innovative element of this work is the application of liposomal encapsulation for probiotic delivery, adapted from approaches commonly used in pharmaceutical carrier systems. In food applications, probiotic encapsulation has traditionally relied on techniques such as spray-drying or polymer microcapsules. In contrast, this study investigates lipid bilayer vesicles at the nanoscale as carriers for live probiotic cells. While liposomes are well established as delivery systems for drugs with low molecular weight, their application to whole probiotic bacteria remains comparatively limited. The use of liposomes offers several functional features relevant to probiotic formulations, including improved physical stability, control over particle

size, and the ability to incorporate both hydrophilic and lipophilic components [60]. The novelty of this work lies in adapting these characteristics to the delivery of probiotic microorganisms and evaluating their performance under conditions relevant to food and nutraceutical applications. In this way, the study links concepts from pharmaceutical carrier design with challenges specific to probiotic stabilization.

In addition, this research examines the co-encapsulation of probiotic bacteria together with other bioactive compounds within a single colloidal system. Such multi-component formulations have been discussed in the literature but remain less explored in practical probiotic delivery systems. The originality of this approach lies in the parallel development of hydrogel beads and liposomal carriers that simultaneously incorporate live probiotic cells and complementary bioactive substances. Co-encapsulation allows the interaction between probiotics and accompanying bioactives to be studied within the same delivery matrix. Depending on the formulation, the additional bioactive may contribute to probiotic protection or functionality, while the probiotic component may influence the stability or release behavior of the co-delivered compound [68]. In this work, co-encapsulation is therefore examined as an extension of conventional probiotic formulations containing a single component, providing a basis for the development of combined probiotic and bioactive systems.

4.2. Future directions and research outlook

The results obtained in this study indicate several directions that may be explored in future research on colloidal systems for probiotic encapsulation. One area of interest is the further optimization of encapsulation matrices, including their composition and internal structure. Although the hydrogel beads and liposomal systems investigated here improved probiotic stability under the tested conditions, additional adjustments to formulation parameters may allow further improvement of their performance. Future studies may examine alternative combinations of food-grade biopolymers, emulsifiers, and cross-linking agents to evaluate their influence on encapsulation efficiency and probiotic viability. The incorporation of additional co-encapsulated components, as well as the assessment of different processing routes, could also contribute to a better understanding of how formulation choices affect system behavior at both laboratory and pilot scales. Beyond formulation aspects, further work may focus on evaluating colloidal probiotic systems under conditions that more closely reflect practical use, including extended storage, processing variability, and GI models. In addition, controlled in vivo or clinical studies would be required to assess the functional relevance of encapsulation strategies observed in experimental settings.

Taken together, the colloidal systems developed in this work provide a structured basis for continued investigation of probiotic delivery approaches. Their further study may contribute to the development of more reliable and application-oriented probiotic formulations for food and nutraceutical products.

II. RESEARCH HYPOTHESIS AND OBJECTIVES

Based on literature review and preliminary studies, the following research hypothesis was formulated: ***It is hypothesized that hydrogel-based encapsulation matrices and liposome-based carriers improve probiotic viability during storage compared with non-encapsulated cells***. It was further assumed that the incorporation of prebiotic or other bioactive components into these encapsulation systems provides additional protection, contributing to higher viable cell counts and improved stability over the product shelf life.

To test this hypothesis, the main objective of this doctoral research was to **develop and evaluate colloidal systems containing probiotic bacteria, with a particular focus on hydrogel-based encapsulation matrices and liposome-based carriers**. The study aimed to assess the effect of these systems on probiotic viability and stability under conditions relevant to food and nutraceutical applications.

An additional objective was to **investigate the co-encapsulation of supportive agents**, such as prebiotic fibers or selected bioactive compounds, and to examine their influence on probiotic survival within the colloidal carriers. A schematic overview of the research concept applied in this doctoral study is presented in Figure 6.

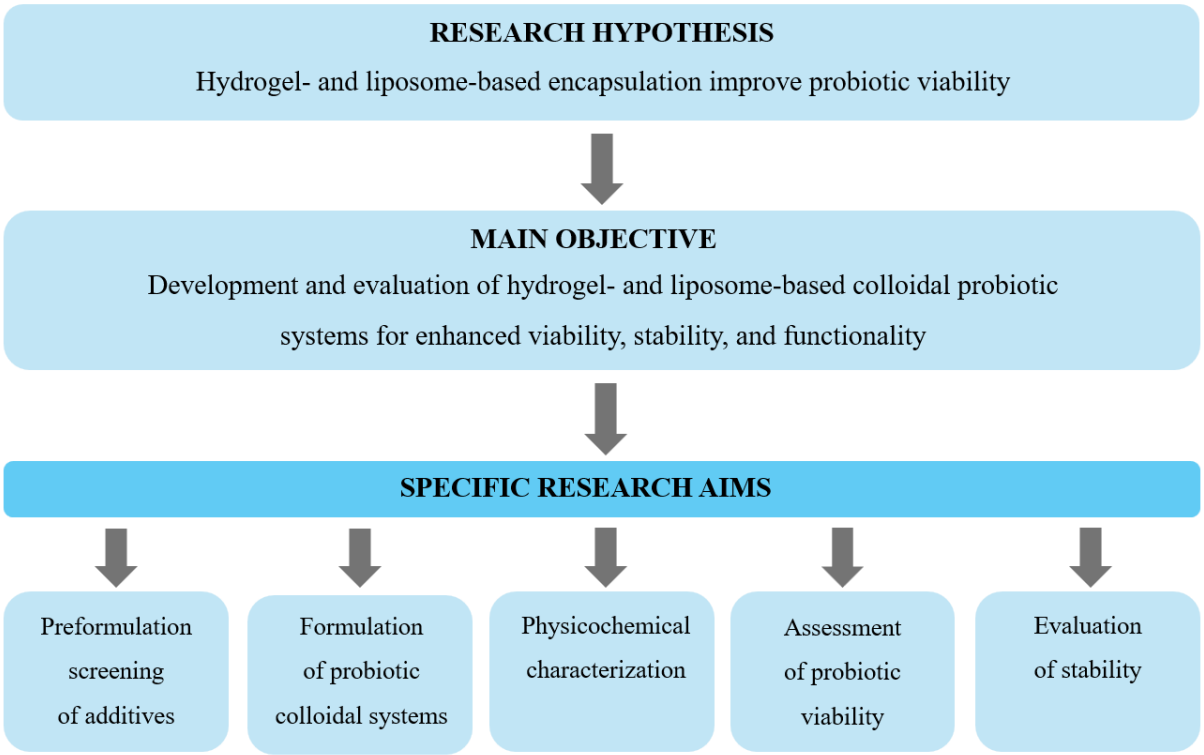

Figure 6. Overview of the research concept applied in this doctoral study.

The main objective of this doctoral research and the verification of the research hypothesis were addressed through the following specific aims:

- **A.** To perform preformulation screening of selected formulation additives in order to assess their compatibility with free probiotic cells and to evaluate their protective effects under controlled culture conditions.
- **B.** To formulate probiotic colloidal systems based on hydrogel and liposomal matrices, designed to incorporate selected probiotic strains, with or without the addition of prebiotic or other bioactive compounds.
- **C.** To characterize the developed colloidal probiotic systems with respect to their structural and physicochemical properties.
- **D.** To assess probiotic viability within the formulated colloidal systems in order to determine the protective effect of encapsulation on probiotic cell survival.
- **E.** To evaluate the stability of probiotic-loaded colloidal systems during storage by monitoring formulation integrity and probiotic viability under relevant storage conditions.

These specific objectives are directly related to the main research goal and collectively address the research hypothesis by examining whether hydrogel-based encapsulation matrices and liposome-based carriers, with or without co-encapsulated functional additives, improve probiotic viability and stability compared with non-encapsulated probiotic cells.

III. SCIENTIFIC RESEARCH

1. MATERIALS

1.1. Probiotic microorganisms

The probiotic bacterial strains used in this doctoral research were standard reference microorganisms obtained as pure cultures from the Polish Collection of Microorganisms (PCM; WFCC No. 106). The following strains were applied: *Lactiplantibacillus plantarum* subsp. *plantarum* (PCM 2675), *Lacticaseibacillus rhamnosus* (PCM 2677), *Lacticaseibacillus paracasei* subsp. *paracasei* (PCM 3039), and *Lactococcus lactis* subsp. *lactis* (PCM 2678).

All strains are Gram-positive, facultatively anaerobic LAB and are stored in the Department of Organic and Bioorganic Chemistry at the Institute of Chemical Technology and Engineering, Poznan University of Technology. The bacterial strains were routinely stored at -80 °C (CryoCube F101h, Eppendorf, Germany) to ensure long-term viability and genetic stability throughout the research period. The selected probiotic microorganisms represent probiotic species that are well characterized and commonly used in research and industrial applications, and are recognized for their documented health benefits and GRAS status [69–71].

1.2. Microbiological media, buffers, and other cultivation components

This subsection describes microbiological media, buffers, and other solutions used for the cultivation, processing, and analysis of probiotic bacteria and colloidal probiotic systems.

1.2.1. Cultivation and maintenance media

A. MRS agar

MRS (de Man, Rogosa, and Sharpe) agar is a selective microbiological medium commonly used for the cultivation, isolation, and enumeration of LAB. In this study, commercially available dehydrated MRS agar powder (Oxoid, USA) was used.

The medium was prepared according to the manufacturer's instructions using ultra-purified Milli-Q water (Arium Pro, Sartorius, Poland). After preparation, the medium was sterilized by steam sterilization (HMC-Europe, Germany) at 121 °C for 15 min. The sterilized medium was then poured into sterile Petri dishes and allowed to solidify at room temperature before use.

The composition of MRS agar medium was as follows ($g \cdot L^{-1}$):

agar	10.0
di-potassium phosphate (K_2HPO_4)	2.0
d-glucose	20.0

magnesium sulfate heptahydrate ($MgSO_4 \cdot 7H_2O$)	0.2
manganese(II) sulphate tetrahydrate ($MnSO_4 \cdot 4H_2O$)	0.05
meat extract	8.0
peptone	10.0
sodium acetate trihydrate	5.0
sorbitan monooleate	1.0 mL
tri-ammonium citrate	2.0
yeast extract	4.0

B. MRS broth

MRS broth is a microbiological medium commonly used for the cultivation and propagation of LAB. In this study, dehydrated MRS broth powder (Oxoid) was used primarily for the preparation of probiotic inocula.

The medium was prepared according to the manufacturer's instructions using ultra-purified Milli-Q water. After preparation, the broth was sterilized by steam sterilization at 121 °C for 15 min and allowed to cool to room temperature before use.

The composition of MRS broth medium was as follows ($g \cdot L^{-1}$):

di-potassium phosphate (K_2HPO_4)	2.0
d-glucose	20.0
magnesium sulfate heptahydrate ($MgSO_4 \cdot 7H_2O$)	0.2
manganese(II) sulphate tetrahydrate ($MnSO_4 \cdot 4H_2O$)	0.05
meat extract	8.0
peptone	10.0
sodium acetate trihydrate	5.0
tri-ammonium citrate	2.0
Tween 80 (polysorbate 80)	1.0 mL
yeast extract	4.0

C. Minimal medium solution

A minimal medium solution (MMS) with a defined composition was prepared and used as a simplified nutrient medium for the controlled cultivation of probiotic bacterial strains. All reagents were purchased from Merck (Germany).

The medium components were dissolved in ultra-purified Milli-Q water. The prepared medium was sterilized by steam sterilization at 121 °C for 15 min and allowed to cool before use.

The composition of the MMS was as follows ($g \cdot L^{-1}$):

casein peptone	0.2
di-potassium phosphate (K_2HPO_4)	2.0
d-glucose	0.5
magnesium sulfate heptahydrate ($MgSO_4 \cdot 7H_2O$)	0.2
manganese(II) sulphate tetrahydrate ($MnSO_4 \cdot 4H_2O$)	0.05
sodium acetate trihydrate	5.0
tri-ammonium citrate	2.0
Tween 80 (polysorbate 80)	0.2 mL
yeast extract	0.2

1.2.2. Buffers and solutions for sample processing and storage

A. Dulbecco's phosphate buffered saline

Dulbecco's phosphate buffered saline (DPBS) is a balanced salt buffer commonly used in microbiological and cell culture procedures. In this study, DPBS was used for rinsing cultured bacterial cells to remove residual metabolites and medium components, for the preparation of uniform bacterial cell suspensions, and as a component of selected microbiological assays.

The buffer was prepared according to the manufacturer's instructions by dissolving DPBS powder (Merck) in ultra-purified Milli-Q water. The solution was then sterilized by steam sterilization at 121 °C for 15 min and allowed to cool before experimental use.

The DPBS buffer maintains physiological pH in the range of 7.1-7.5 and had the following composition ($g \cdot L^{-1}$):

potassium chloride (KCl)	0.2
potassium phosphate monobasic (KH_2PO_4)	0.2
sodium chloride (NaCl)	8.0
sodium phosphate dibasic (Na_2HPO_4)	1.2

B. Peptone salt solution

Peptone salt solution is an isotonic diluent commonly used for the recovery, dilution, and temporary storage of microorganisms. In this study, it was used as an isotonic storage medium for probiotic-loaded colloidal systems, providing stable osmotic conditions without promoting bacterial growth.

The powdered peptone salt medium (Merck) was dissolved in ultra-purified Milli-Q water according to the manufacturer's instructions. The prepared solution was then sterilized by steam sterilization at 121 °C for 15 min and allowed to cool before use.

The peptone salt solution maintains a pH range of 6.8-7.2 and had the following composition ($g \cdot L^{-1}$):

casein peptone	1.0
sodium chloride (NaCl)	8.5

C. Peptone water

Peptone water is a non-selective enrichment medium commonly used as a diluent in microbiological analyses. In this study, it was used for the disintegration of probiotic-loaded colloidal systems in order to release encapsulated bacterial cells for subsequent analyses.

The powdered peptone water medium (Merck) was dissolved in ultra-purified Milli-Q water according to the manufacturer's instructions. The prepared solution was then sterilized by steam sterilization at 121 °C for 15 min and allowed to cool before use.

The peptone water solution maintains a pH range of 7.0-7.4 and had the following composition ($g \cdot L^{-1}$):

casein peptone	10.0
sodium chloride (NaCl)	5.0

1.3. Compounds used in probiotic formulations

This subsection describes the chemical compounds and functional ingredients used in the preparation of probiotic formulations. The listed compounds were selected based on their documented functional roles in probiotic encapsulation and their applicability in colloidal formulations.

General notes for Section 1.3.

All reagents listed in Sections 1.3.1-1.3.3 and 1.3.5 were purchased from Merck. Phospholipid reagents described in Section 1.3.4 were obtained from Avanti Polar Lipids (USA). All chemicals were of analytical grade and were used as received without further purification.

Ultra-purified Milli-Q water was used for the preparation of all aqueous solutions, except for those described in Sections 1.3.4 and 1.3.5, which were prepared according to dedicated procedures detailed in the *Research Methods* chapter.

For reagents described in Sections 1.3.1-1.3.3, solid compounds were dissolved in water, with the temperature adjusted according to the solubility of each substance, and mixed using a magnetic stirrer until complete dissolution was achieved. All prepared solutions were sterilized by steam sterilization at 121 °C for 15 min, with the exception of the ascorbic acid solution, which was sterilized by filtration through a 0.22 μm membrane filter (Labsolute, Germany). Additional details of solution handling are given where relevant in the *Research Methods* chapter.

1.3.1. Sugars and oligosaccharides

A. Trehalose

Trehalose is a disaccharide that does not have reducing properties and is characterized by high chemical stability and the ability to replace water. It is known to stabilize cellular structures by maintaining hydration and preserving protein conformation under stress conditions, as well as by supporting membrane integrity during environmental changes [72]. In probiotic formulations, trehalose was used as a functional additive in drying media. Its application is associated with improved protection of probiotic cells during freeze-drying and storage, primarily through replacement of water molecules surrounding phospholipid membranes and other cellular components [73,74].

B. Maltodextrin

Maltodextrin is a carbohydrate polymer obtained by partial hydrolysis of starch. It is supplied as a powder that is soluble in water and is commonly used as a food additive. Maltodextrin solutions exhibit moderate viscosity, depending on concentration and degree of polymerization [75–77]. In probiotic encapsulation systems, maltodextrin was applied as a protective carrier component. Its inclusion in microencapsulation formulations has been reported to support

probiotic survival by reducing osmotic stress and limiting mechanical damage during processing. Maltodextrin can function as a cryoprotective and lyoprotective agent by forming an amorphous glassy matrix that reduces cellular injury during drying and storage [78,79].

1.3.2. Organic acids and amino acid derivatives

A. Ascorbic acid

Ascorbic acid (vitamin C) is an organic acid soluble in water with antioxidant properties. It is sensitive to high temperatures and alkaline pH, but is commonly used in food systems as a preservative and vitamin supplement. From a biological perspective, ascorbic acid is involved in collagen synthesis and immune function [80]. In probiotic formulations, ascorbic acid was used as an antioxidant additive to support probiotic stability. By scavenging oxygen and ROS, it can limit oxidative stress during processing and storage. In addition, the presence of ascorbic acid may contribute to the formation of a more anaerobic microenvironment, which is beneficial for probiotic strains sensitive to oxygen. For these reasons, ascorbic acid was included in selected encapsulation matrices to support probiotic viability and functional integrity [40,81].

B. Monosodium glutamate

Monosodium glutamate is the sodium salt of the amino acid L-glutamic acid. It is supplied as a crystalline powder that is readily soluble in water and is widely used in food applications, primarily as a flavor enhancer. In addition, monosodium glutamate is applied in fermentation media as a nitrogen source for microbial growth [82,83]. In probiotic formulations, monosodium glutamate was used as a stabilizing excipient with cryoprotective properties. Its presence has been associated with improved preservation of cellular proteins and enzymes through electrostatic interactions between amino groups and acidic residues of protein molecules, which can limit denaturation during stress conditions. Monosodium glutamate may also retain residual moisture within the formulation, contributing to protection against damage caused by dehydration during processing and storage [84,85].

1.3.3. Polysaccharide fibers and gums

A. Inulin

Inulin is a plant-derived polysaccharide classified as a fructooligosaccharide. It is a soluble dietary fiber that is not digested by human enzymes but can be selectively fermented by beneficial gut microorganisms [86,87]. From a physicochemical perspective, inulin

dissolves in water to form a slightly viscous solution and is capable of gel formation at higher concentrations. Inulin is commonly applied in food systems as a dietary fiber supplement, a sugar-reducing agent, and a stabilizer, particularly in dairy products [88]. In probiotic formulations, inulin was used as a co-encapsulated component to form synbiotic systems. Its presence within the encapsulating matrix can provide a protective microenvironment during GI transit due to its capacity to retain water and its buffering properties. In addition, inulin serves as a fermentable substrate supporting probiotic growth in the intestinal environment [89].

B. Gum arabic

Gum arabic is a complex heteropolysaccharide containing a minor protein fraction and is obtained as a natural exudate from acacia tree bark. It is highly soluble in water and forms solutions with low viscosity, even at relatively high concentrations [90]. Gum arabic exhibits functional properties such as emulsification and film formation and is widely used in food applications, including soft drink syrups, confectionery products, and spray-dried flavor encapsulation [91]. In probiotic encapsulation systems, gum arabic was applied as a wall-forming material in microcapsules. Its film-forming ability enables the formation of a protective coating around probiotic cells, while its high solubility facilitates capsule rehydration [92].

C. Corn starch

Corn starch is a polysaccharide obtained from maize kernels and consists of two glucose polymers, amylose and amylopectin. Native corn starch is supplied as a fine powder and is insoluble in cold water but undergoes gelatinization upon heating in the presence of water [93,94]. Corn starch is widely used in food systems for its thickening and texturizing properties and in pharmaceutical applications as a filler or disintegrant [95]. In probiotic microencapsulation systems, corn starch was used as a supportive matrix component. Its inclusion has been reported to improve probiotic stability by absorbing water, moderating acidic conditions, and contributing to the formation of a solid protective matrix during drying, which can limit cellular damage [96].

D. Sodium alginate

Sodium alginate is the sodium salt of alginic acid, a naturally occurring polysaccharide extracted from brown seaweeds. Chemically, it is composed of β-D-mannuronic acid and α-L-guluronic acid residues arranged in varying sequences along the polymer chain. Sodium alginate is supplied as a granular powder that dissolves in water to form viscous solutions. In the presence of divalent cations, such as calcium ions, alginate undergoes ionic cross-linking,

resulting in the formation of a gel network. Alginate gels are heat stable, biocompatible, and non-toxic. Alginate is commonly used in food systems as a thickener and stabilizer, as well as in biomedical applications such as wound dressings and drug delivery systems [97,98]. In probiotic encapsulation, sodium alginate was used as a polymer that forms the hydrogel matrix. Alginate gels remain stable under acidic gastric conditions and undergo partial dissociation at higher pH values, which enables the release of encapsulated cells in the intestinal environment [99].

E. Psyllium husk

Psyllium husk is a dietary fiber obtained from the seed husks of *Plantago ovata*. It is primarily composed of hemicellulosic mucilage, which swells in the presence of water to form a gel-like structure. Psyllium is classified as a soluble fiber that is resistant to digestion in the small intestine but can be fermented by intestinal microbiota in the colon [100]. A key physicochemical characteristic of psyllium husk is its high water absorption capacity, which leads to the formation of viscous gels. This property has resulted in its use in food and pharmaceutical applications, including products intended to support digestive function, as a thickening agent, and as a structural component in gluten-free formulations [101,102]. In probiotic formulations, psyllium husk was used as a gel-forming prebiotic fiber. Matrices containing psyllium can provide protection under acidic gastric conditions and contribute to a more gradual release of probiotics upon transit to the colonic environment [103].

1.3.4. Phospholipids

A. DMPC

DMPC (1,2-dimyristoyl-sn-glycero-3-phosphocholine) is a glycerophospholipid composed of a phosphatidylcholine headgroup and two saturated myristic acid (C14:0) acyl chains. It is a zwitterionic phospholipid that is used in liposome formulations because of its biocompatibility and its ability to form stable bilayer membranes that resemble biological membranes. DMPC bilayers exhibit a relatively low gel-to-liquid crystalline phase transition temperature of approximately 23.6 °C, which results in membrane fluidity at physiological temperatures [104,105]. This physicochemical property facilitates the formation of flexible lipid bilayers under conditions relevant to biological and food-related applications. In addition, DMPC is characterized by chemical stability, which supports its use in lipid-based encapsulation systems. The formation of a lipid corona between bacterial cells provides a physical barrier that may protect them from the external aqueous environment. The fluid state

of DMPC-based membranes at physiological temperature was considered relevant for interactions with biological interfaces during GI transit [48,106].

B. DOPG

DOPG (dioleoylphosphatidylglycerol) is a glycerophospholipid with a phosphatidylglycerol headgroup and two unsaturated oleic acid (C18:1) acyl chains. It is an anionic phospholipid that occurs naturally in bacterial membranes, including those of many Gram-positive bacteria such as LAB. DOPG exhibits a low gel-to-liquid crystalline phase transition temperature, below 0 °C, and therefore remains in a fluid state at physiological temperatures [107,108]. This property supports the formation of flexible lipid bilayers under conditions relevant to biological systems. The anionic character of DOPG contributes to the overall surface charge of the liposomal membrane and influences bilayer organization. In addition, the fluid nature of DOPG-containing membranes affects membrane [109–111].

1.3.5. Pharmaceutical agent – fluvastatin

Fluvastatin is a pharmaceutical compound with low molecular weight belonging to the statin class. It is a synthetic inhibitor of 3-hydroxy-3-methylglutaryl coenzyme A reductase, the key enzyme involved in cholesterol biosynthesis in the liver. Fluvastatin is relatively hydrophobic and is commonly formulated as fluvastatin sodium for oral administration [112,113]. Clinically, it is used in the treatment of hypercholesterolemia and in the prevention of cardiovascular diseases [114]. In the present work, fluvastatin served as a representative pharmaceutical agent for studying co-encapsulation in probiotic colloidal systems. Its physicochemical properties and well characterized biological activity make it suitable for investigating co-encapsulation strategies. The selection of fluvastatin was further motivated by previous reports describing effects related to cholesterol metabolism associated with certain probiotic strains, including mechanisms such as bile salt deconjugation, alongside the established inhibitory action of statins on cholesterol synthesis [60,115].

2. RESEARCH METHODS

This chapter describes the experimental methods applied in this doctoral research. All procedures were selected to address the research hypothesis and to achieve the defined research objectives. The methodological workflow composed of bacterial strain preparation, preliminary evaluation of selected probiotic additives, formulation of colloidal probiotic systems, and characterization of the developed formulations. The applied research methods are presented below in accordance with the sequence of experimental stages.

2.1. General aseptic procedures

All glassware used in microbiological experiments was sterilized by steam sterilization at 121 °C for 15 min before use. Disposable plasticware was supplied sterile by the manufacturer. All procedures involving bacterial samples were conducted under aseptic conditions using a biological safety cabinet (Labculture Class II, Esco, Singapore) to minimize the risk of contamination.

2.2. Preparation of probiotic bacteria

A. Bacterial culture and inoculum preparation

For routine cultivation, frozen stocks of probiotic strains were thawed, streaked onto MRS agar plates, and incubated for 24 h at 35 °C under a 5% CO_2 atmosphere (Incubator S41i, Eppendorf). To obtain enrichment cultures, a loopful of cells from freshly grown MRS agar plates was collected.

Single colonies were then inoculated into MRS broth and cultivated to the defined physiological growth phase under strain-specific conditions. Cultivation was typically carried out overnight at 35 °C in a 5% CO_2 atmosphere with shaking at 100 rpm. These cultivation parameters were determined individually for each strain based on preliminary growth curve experiments conducted before the main studies.

B. Preparation of bacterial cell suspensions

After cultivation in MRS broth, bacterial cells were harvested by centrifugation at 4500 RCF for 20 min (Centrifuge 5910R, Eppendorf). The cell pellets were washed twice with sterile DPBS to remove residual medium components. After cultivation in MRS broth, bacterial cells were harvested by centrifugation at 4500 RCF for 20 min (Centrifuge 5910R, Eppendorf). The cell pellets were washed twice with sterile DPBS to remove residual medium components.

After washing, the pellets were resuspended in DPBS, and the optical density (OD) of the resulting suspensions was adjusted to an OD_{600} of 1.5 ± 0.1 using a spectrophotometer (Jasco V-650, JASCO Corporation, Japan). The standardized bacterial suspensions corresponded to a viable cell concentration of approximately 10^7 colony forming units $CFU \cdot mL^{-1}$. These standardized inocula (SI) were then used for the preparation of probiotic colloidal systems.

2.3. Preformulation screening – evaluation of the effect of selected probiotic additives directly on probiotic bacterial cells

A. Cultivation of probiotic bacteria

This experiment was performed using *Lactiplantibacillus plantarum* subsp. *plantarum* (PCM 2675), *Lacticaseibacillus rhamnosus* (PCM 2677), and *Lacticaseibacillus paracasei* subsp. *paracasei* (PCM 3039). Liquid cultures were prepared by combining MMS, a potentially protective agent (PPA) working solution, and SI at a volumetric ratio of 5:4:1 (MMS:PPA:SI).

The following PPAs were evaluated: trehalose (TRE), vitamin C (VC), maltodextrin (MD), monosodium glutamate (MSG), inulin (IN), gum arabic (GA), and corn starch (CS). The final concentrations of PPAs in the cultures were as follows: TRE 10% (v/v), VC 0.5% (v/v), MD 5% (v/v), MSG 0.5% (v/v), IN 3% (v/v), GA 3% (v/v), and CS 3% (v/v).

Control samples (CTRL) without the addition of PPA were prepared in parallel. In addition, sterile abiotic controls were included. Abiotic samples were obtained by autoclaving the bacterial biomass at 121 °C for 15 min and supplementing the samples with 2% (v/v) sodium azide (Merck) to inhibit potential bacterial proliferation. All cultures were incubated at 30 °C with shaking at 120 rpm for 48 h before further analyses.

B. Assessment of the effect of PPAs on probiotic cells

Within the preformulation screening, the direct effects of the evaluated PPAs on probiotic cells were assessed using methods described in Sections 2.5.1 (A, B, and D), 2.5.2 (A-D), 2.5.3 (A and B), and 2.5.5 (A and B).

2.4. Formulation of colloidal probiotic systems

2.4.1. Preparation of hydrogel-based probiotic formulations

A. Preparation of probiotic mixtures for encapsulation

Sterile working solutions of sodium alginate (ALG) were prepared in combination with a thickening agent, either gum arabic (GA) or psyllium husk (PH). In addition, selected PPAs, including IN, TRE, or a 1:1 (v/v) mixture of IN/TRE, were incorporated. The individual components were combined to obtain pre-encapsulation mixtures.

Then, SI of *L. plantarum* (PCM 2675) was added at a volumetric ratio of 2:1 (mixture:cells). Sterile MRS broth was then added to support short-term probiotic viability before encapsulation. The final concentrations of the components in the mixtures before encapsulation

were as follows: ALG 2% (v/v), GA or PH 0.5% (v/v), IN or TRE or IN/TRE 1% (v/v), and MRS broth 5% (v/v). The resulting fully prepared probiotic mixtures were used directly for the encapsulation procedure.

A CTRL was prepared by mixing the *L. plantarum* SI with 0.1% (v/v) peptone salt solution at a volumetric ratio of 1:2 (cells:diluent), followed by supplementation with sterile MRS broth to a final concentration of 5% (v/v). This CTRL was not subjected to the encapsulation process.

B. Preparation of alginate-based probiotic beads

Alginate-based probiotic beads were prepared by ionic cross-linking, as illustrated in Figure 7. Fully formulated probiotic mixtures were introduced dropwise into a 5% (w/v) calcium chloride ($CaCl_2$) solution using an 18G needle connected to a syringe pump (HK-400, Hawk Medical Instrument, China) operated at a flow rate of 25 mL · h^{-1}. The needle tip was positioned at a distance of 5 cm above the surface of the $CaCl_2$ solution to ensure consistent droplet formation.

The resulting beads were allowed to cross-link in the $CaCl_2$ bath for 30 min under constant stirring at 80 rpm using a magnetic stirrer. After cross-linking, the beads were separated from the $CaCl_2$ solution and washed with ultra-purified Milli-Q water to remove remined calcium ions. The washed beads were then resuspended in 0.1% (v/v) peptone salt solution. Encapsulated probiotic beads were stored at 4 °C for 7 days before further analyses.

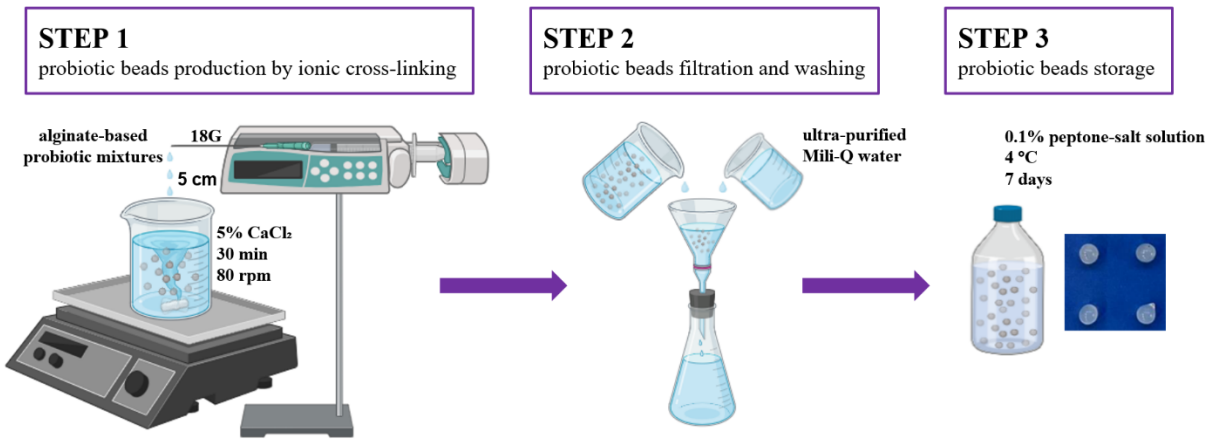

Figure 7. Schematic representation of alginate-based probiotic beads prepared by ionic cross-linking.

C. Disintegration of beads and recovery of encapsulated bacteria

For analyses requiring direct measurements on released bacterial cells, hydrogel beads were disintegrated using peptone water as a diluent to disrupt the colloidal structure. Briefly, 1 g of probiotic-loaded beads was transferred to a sterile container, and 200 mL of peptone water was

added, corresponding to a ratio of 1:200 (w/v). The suspension was agitated continuously at room temperature for 1 h using a laboratory shaker (Vortex TTS 2, IKA, Germany) until complete disintegration of the hydrogel matrix was observed.

The resulting suspension was passed through a sterile 40 µm filter (pluriSelect Life Science, Germany) to remove residual gel fragments. The filtrate was then centrifuged at 4500 RCF for 20 min, and the cell pellet was washed twice with sterile DPBS. After washing, the pellet was resuspended in DPBS, and the resulting bacterial suspension was used for further analyses.

2.4.2. Preparation of liposome-based probiotic formulations

A. Method I – preparation of lipid nanoparticle-stabilized probiotic formulations

This method corresponds to the patent application (P.446869; *Układ do dostarczania mikroorganizmów probiotycznych stabilizowany za pomocą nanocząstek lipidowych*; N. Burlaga, A. Grzywaczyk, A. Pacholak, E. Kaczorek). In view of ongoing IP protection, the procedure is described at a general level sufficient for academic reporting, without disclosing protected technical details.

Lipid nanoparticles were prepared using a thin-film hydration approach and then brought into contact with probiotic bacterial cells. Briefly, DMPC was dissolved in chloroform (Merck) at a concentration of 2% (w/v). The organic solvent was removed under reduced pressure using a rotary evaporator (Rotavapor R-210, Büchi, Switzerland) to obtain a uniform phospholipid film deposited on the walls of a sterile round-bottom flask.

All procedures involving organic solvents were carried out with complete solvent removal before contact with bacterial cells. After solvent evaporation, the SI of *L. lactis* (PCM 2678) was added directly onto the dried lipid film. The system was subjected to gentle agitation for 4 h to allow film hydration and the self-assembly of lipids in the presence of bacterial cells. Under these conditions, lipid nanoparticles were formed at the interface between the bacterial surface and the surrounding medium, resulting in the formation of an external lipid corona associated with the cell surface.

The obtained liposome-stabilized probiotic formulations were divided into two storage groups: (1) stored at room temperature and (2) stored at 4 °C. A CTRL consisting of the bacterial SI without lipid nanoparticles was stored under identical conditions. The produced systems were

analyzed at several time points over a period of 28 days (details are given where relevant in the *Results* chapter).

B. Method II – preparation of fluvastatin-loaded liposome-stabilized probiotic formulations

Fluvastatin-loaded liposomes were prepared using a combination of thin-film hydration, freeze-thaw cycling, membrane extrusion, and gel filtration. The resulting liposomal vesicles were then combined with probiotic bacteria to obtain colloidal probiotic systems (Figure 8).

A DOPG lipid film containing fluvastatin was prepared in round-bottom flasks. DOPG was dissolved in chloroform at a concentration of 2.5% (w/v) and mixed with a fluvastatin solution in dimethyl sulfoxide (DMSO) at a concentration of 20 $mg \cdot mL^{-1}$, using a volumetric ratio of 1:1 (v/v). Organic solvents were removed under reduced pressure using a rotary evaporator equipped with a water bath set to 60 °C and operated at 200 rpm. Solvent removal was performed using a stepwise vacuum program consisting of 150 mbar for 1 min, 100 mbar for 2 min, and 50 mbar for 5 min, resulting in the formation of a uniform lipid film containing fluvastatin on the flask walls. The lipid film was then placed in a sealed desiccator and subjected to high vacuum for 5 days to ensure complete removal of residual organic solvents.

The dried lipid film containing fluvastatin was hydrated with sterile DPBS using a volume equivalent to the initial solvent volume used for lipid dissolution. Hydration was carried out under gentle agitation until complete detachment of the film from the flask walls was achieved. The resulting liposomal dispersion was subjected to eight freeze-thaw cycles (-80 °C ↔ room temperature), with brief vortex mixing between each cycle. Liposome size homogenization was performed using an extruder (Avanti Polar Lipids) equipped with a 200 nm polycarbonate membrane. The suspension was passed through the membrane 25 times, changing the direction of extrusion with each pass.

The extruded liposome dispersion was purified by gel filtration using a Sephadex G-25 (Merck) column (size B19), with DPBS used as the eluent. Liposome fractions were collected, pooled, and diluted with DPBS to the desired final working volume. The purified liposome dispersion was mixed with the SI of *L. plantarum* (PCM 2675) to obtain final optical density of both the bacterial suspension and the liposome dispersion of $OD_{600} = 0.10 \pm 0.01$. Optical density measurements were performed in a 96-well plate using a working volume of 200 µL per well. Sodium succinate was added to the formulation at a final concentration of 2% (v/v) as a readily

utilizable energy source. The resulting fluvastatin-loaded probiotic liposome systems were stored at 4 °C.

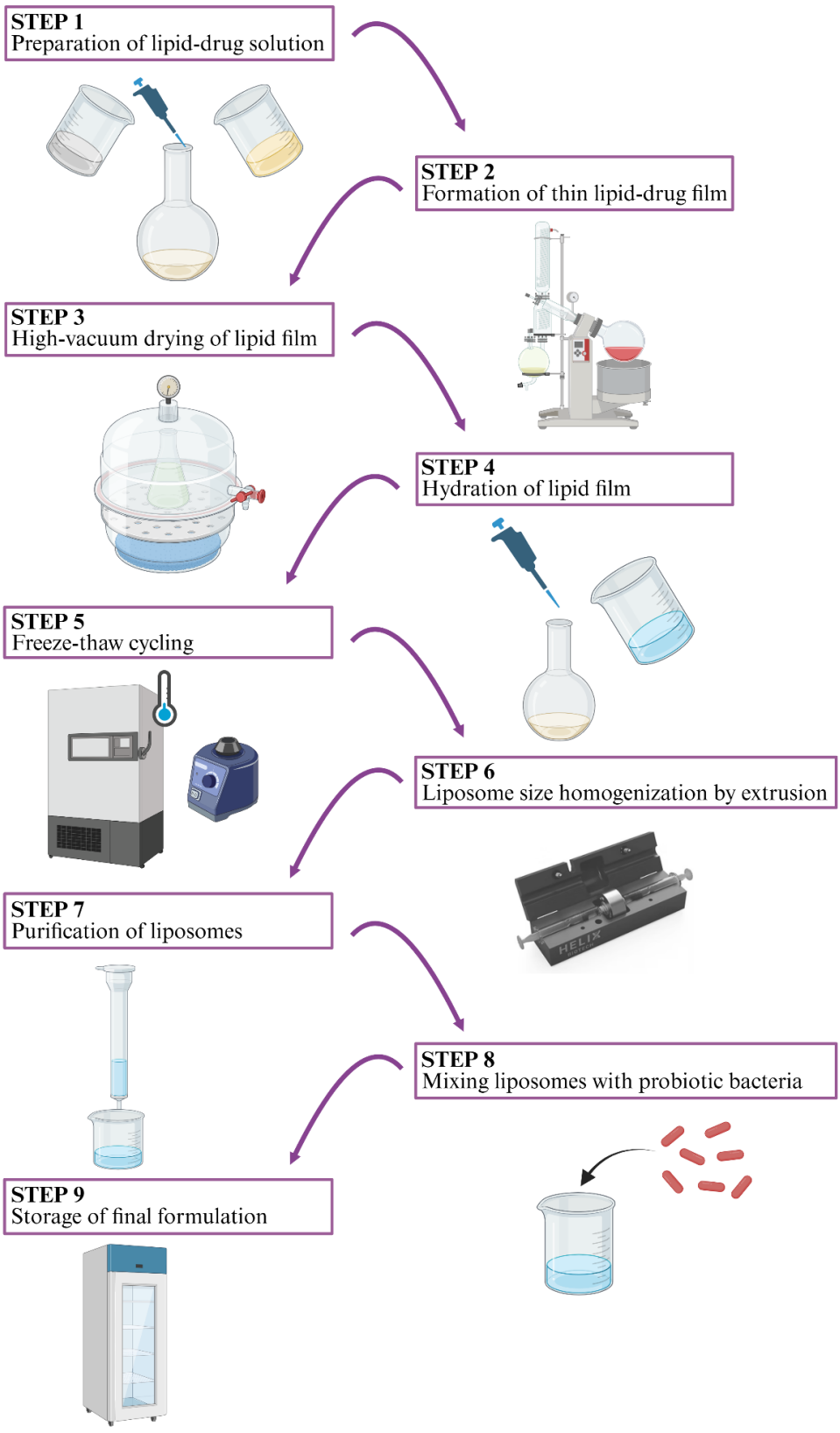

Figure 8. Schematic representation of the preparation of fluvastatin-loaded probiotic liposome systems.

A CTRL consisted of the bacterial SI without lipid nanoparticles, stored under identical conditions. An additional sample was prepared by combining bacterial cells with unloaded DOPG liposomes prepared using the same procedure but without fluvastatin. The produced systems were analyzed at several time points over a period of 28 days (details are given where relevant in the *Results* chapter).

2.5. Analysis and characterization of colloidal probiotic systems

2.5.1. Methods for evaluation of probiotic cell viability and metabolic activity

A. Metabolic activity assay

The metabolic activity of probiotic cells was determined using a colorimetric assay based on the enzymatic reduction of the yellow, water-soluble compound 3-(4,5-dimethylthiazol-2-yl)-2,5-diphenyltetrazolium bromide (MTT) to insoluble purple formazan crystals. Formazan was then dissolved and measured spectrophotometrically. The procedure was based on an improved formazan dissolution method described by Benov [116].

Before analysis, each bacterial suspension was normalized to OD_{600} = 0.10 ± 0.01, measured in a 96-well plate using a working volume of 200 µL per well, with sterile DPBS used as the diluent. From each normalized suspension, 200 µL was transferred into sterile, flat-bottom 96-well microplates. Then, 20 µL of freshly prepared MTT solution (5 mg·mL^{-1}) was added to each well. The contents of the wells were mixed thoroughly, and the plates were incubated for 2-4 h at 30 °C with shaking at 120 rpm to allow for formazan formation. After incubation, the plates were centrifuged at 4500 RCF for 20 min, and the supernatants were carefully removed.

The resulting pellets were resuspended in 200 µL of DMSO and incubated for 15 min at 30 °C to ensure complete dissolution of formazan. The plates were centrifuged again at 4500 RCF for 20 min, after which 120 µL of each DMSO extract was transferred to a new 96-well microplate for absorbance measurement. Absorbance was recorded at a wavelength of 560 nm using a microplate spectrophotometer (Multiskan Sky, Thermo Fisher Scientific, USA). Metabolic activity was expressed as MTT reducing units (MRU) according to:

$$MRU = \left(\frac{A_{560} \cdot SV}{TV}\right) \cdot \left(\frac{K}{OD_{600}}\right) \quad (-)$$

where:

A_{560} = absorbance of the DMSO extract at 560 nm,

SV = volume of the cell suspension used for reaction before adding MTT,

TV = total reaction volume in the well with MTT,

K = net dilution factor applied to the DMSO extract before reading,

OD_{600} = optical density of the bacterial suspension measured immediately before adding MTT.

B. AlamarBlue cytotoxicity assay

The cytotoxic effects of selected formulation components on probiotic cells were evaluated using the AlamarBlue (AB) assay. The AB reagent is an indicator based on resazurin that assesses cell viability based on the reducing capacity of metabolically active cells. In viable cells, resazurin is reduced to resorufin, a red and fluorescent compound. The assay protocol was based on an improved method described previously [117].

Before analysis, each bacterial suspension was normalized to OD_{600} = 0.60 ± 0.01, measured in a 96-well plate using a working volume of 200 µL per well, with sterile DPBS used as the diluent. From each normalized suspension, 200 µL was dispensed into sterile, flat-bottom 96-well microplates. Then, 20 µL of AB reagent was added to each well. The contents were mixed thoroughly, and the plates were incubated for 4 h at 30 °C with shaking at 120 rpm.

After incubation, the plates were centrifuged at 4500 RCF for 30 min. A volume of 120 µL of the supernatant from each well was transferred to a new microplate for absorbance measurements. Absorbance was measured at wavelengths of 570 nm and 600 nm using a microplate spectrophotometer. The AB reduction for each experimental condition was calculated relative to the untreated control, defined as 100% viability, using the dual-wavelength absorbance difference:

$$AB\ reduction = \frac{(O_2 \cdot A_1) - (O_1 \cdot A_2)}{(O_2 \cdot P_1) - (O_1 \cdot P_2)} \cdot 100 \quad (\%)$$

where:

O_1 = molar extinction coefficient of oxidized AB reagent at 570 nm (ε = 80,586 $M^{-1} \cdot cm^{-1}$),

O_2 = molar extinction coefficient of oxidized AB reagent at 600 nm (ε = 117,216 $M^{-1} \cdot cm^{-1}$),

A_1 = absorbance of test well at 570 nm,

A_2 = absorbance of test well at 600 nm,

P_1 = absorbance of growth control well (untreated control cells) at 570 nm,

P_2 = absorbance of growth control well (untreated control cells) at 600 nm.

C. Plate count method

Viable cell numbers were determined using the plate count method, which quantifies metabolically active cells. Colony counts within the ISO countable range were used for the calculation of CFU. Serial decimal dilutions were prepared at a ratio of 1:10 by mixing one part of the sample with nine parts of sterile 0.9% (w/v) sodium chloride (NaCl) solution (Merck). Each dilution step was followed by vortex mixing. The dilution range was selected in advance to obtain countable plates containing 15-300 colonies per plate after incubation, in accordance with the counting criteria specified in ISO 15214:1998 and ISO 7218:2007 [118,119].

From each selected dilution, 100 µL volume were spread onto MRS agar plates prepared in duplicate. The plates were incubated at 30 °C for 48 h under a 5% CO_2 atmosphere to support the growth of LAB. After incubation, two consecutive dilutions that met the acceptance criteria were selected for enumeration. Colonies were counted, and the colony counts from duplicate plates at each retained dilution were recorded and used for CFU calculations. Colony forming units were calculated using the ISO equation:

$$N = \frac{\sum C}{V(n_1 + 0.1n_2) \cdot d} \quad (CFU \cdot mL^{-1})$$

where:

$\sum C$ = sum of the colonies counted on all the dishes from two successive dilutions,

V = volume of inoculum applied to each dish (mL),

n_1 = number of plates at the first (lower) retained dilution,

n_1 = number of plates at the second retained dilution,

d = dilution factor of the first retained dilution.

D. Flow cytometry method

Flow cytometry was used to assess the viability of probiotic cells using an adapted protocol described by Sielatycka et al. [120]. Before analysis, each probiotic sample was diluted 500-fold in sterile DPBS to reduce event coincidence and to optimize acquisition rates. Metabolic activity and membrane integrity were evaluated using the BacLight Redox Sensor Green Vitality Kit (Thermo Fisher Scientific).

Diluted bacterial suspensions (DBS) were stained with RedoxSensor Green (RSG) and propidium iodide (PI) at final concentrations corresponding to a volumetric ratio of 250:3:0.8 (DBS:RSG:PI), with PI used at a final concentration of 20 mM. RedoxSensor Green is a fluorogenic redox indicator that is converted by intracellular reductases into a green

fluorescent product, with fluorescence intensity proportional to the cellular redox potential (CRP). PI was used as an indicator of membrane integrity. Staining was performed for 15 min at room temperature in the dark. Immediately after incubation, 100 µL of each stained sample was analyzed using a FlowSight imaging flow cytometer (Luminex Corporation, USA) equipped with 405, 488, and 642 nm lasers, five charge-coupled device (CCD) fluorescence detection channels, and a side-scatter (SSC) detector. The 488 nm laser was used for excitation of both RSG and PI. Data acquisition was performed using logarithmic signal amplification, and 5000 events were recorded per sample. Post-acquisition data analysis was carried out using IDEAS software (Luminex Corporation).

Morphological parameters and fluorescence intensity thresholds were applied to discriminate discrete subpopulations of bacterial cells. Based on differences in CRP and membrane integrity, cells were classified into the following physiological states: non-active (dead), intermediate (mid-active), or active. In selected experiments, two additional states were distinguished: dormant (undisturbed membrane with low metabolic activity) and injured (partially damaged membrane).

2.5.2. Methods for assessing bacterial cell surface properties and membrane integrity

A. Membrane permeability assay

Total membrane permeability was evaluated by measuring the uptake of crystal violet (CV) by bacterial cells using a protocol described by Halder et al., with minor modifications [121]. Before the assay, samples were centrifuged at 4500 RCF for 10 min and washed with sterile DPBS. Each bacterial suspension was normalized to OD_{600} = 0.30 ± 0.01, measured in a 96-well plate using a working volume of 200 µL per well, with DPBS used as the diluent. The assay was conducted in sterile, flat-bottom 96-well microplates with a final reaction volume of 0.22 mL per well.

For each reaction, 200 µL of the normalized bacterial suspension was mixed with 20 µL of CV solution (0.1 $mg \cdot mL^{-1}$). The mixtures were mixed thoroughly and incubated for 15 min at 30 °C. After incubation, the samples were centrifuged at 4500 RCF for 20 min. After centrifugation, 120 µL of the supernatant from each well was transferred to a new microplate for absorbance measurement.

Absorbance was recorded at 590 nm using a microplate reader to quantify the amount of CV remaining in the supernatant. Total membrane permeability (TMP) was expressed as the percentage of CV uptake relative to the reagent blank:

$$TMP = \frac{A_{CV\ blank} - A_{sample}}{A_{CV\ blank}} \cdot 100 \quad (\%)$$

where:

$A_{CV\ blank}$ = absorbance of CV in DPBS without cells at 590 nm,

A_{sample} = absorbance of the sample supernatant at 590 nm.

The membrane disruption index was calculated as the ratio of TMP in the tested sample to the TMP of the control sample, with the control value set to 1.

B. Cell surface hydrophobicity assay

Cell surface hydrophobicity was assessed using the Congo red (CR) adsorption assay, which is based on the binding of the dye to bacterial cell surfaces and provides an indirect measure of surface hydrophobicity. Congo red binding (CRB) was determined using a method described by Ambalam et al., with minor modifications [122].

Before analysis, samples were centrifuged at 4500 RCF for 10 min and washed with sterile DPBS. Each bacterial suspension was normalized to OD_{600} = 0.30 ± 0.01, measured in a 96-well plate using a working volume of 200 µL per well, with DPBS used as the diluent. The assay was conducted in sterile, flat-bottom 96-well microplates with a final reaction volume of 0.21 mL per well.

For each reaction, 200 µL of the normalized bacterial suspension was mixed with 10 µL of CR solution (2 $mg \cdot mL^{-1}$). The mixtures were mixed thoroughly and incubated for 15 min at 30 °C. After incubation, samples were centrifuged at 4500 RCF for 20 min. After centrifugation, 120 µL of the supernatant from each well was transferred to a new microplate for absorbance measurement. Absorbance was recorded at 480 nm using a microplate reader to quantify the amount of CR remaining in the supernatant.

CRB was expressed as the percentage of CR uptake relative to the reagent blank:

$$CRB = \frac{A_{CR\ blank} - A_{sample}}{A_{CR\ blank}} \cdot 100 \quad (\%)$$

where:

$A_{CR\ blank}$ = absorbance of CR in DPBS without cells at 480 nm,

A_{sample} = absorbance of the sample supernatant at 480 nm.

The relative hydrophobicity index was calculated as the ratio of CRB in the tested sample to the CRB of the control sample, with the control value set to 1.

C. Atomic force microscopy (AFM)

This method corresponds to the patent application (P.447941; *Sposób przygotowania próbki żywych komórek bakteryjnych do ich obrazowania za pomocą mikroskopii sił atomowych*; A. Pacholak, F. Jaworski, N. Burlaga, E. Kaczorek). In view of ongoing IP protection, the procedure is described at a general level sufficient for academic reporting, without disclosing protected technical details.

Before analysis, bacterial samples were centrifuged at 4500 RCF for 10 min and washed twice with sterile DPBS. Each cell suspension was normalized to OD_{600} = 0.10 ± 0.01, measured in a 96-well plate using a working volume of 200 µL per well, in order to obtain separated single cells within the microscope field of view. The normalized cell suspensions were deposited onto polycarbonate membrane filters (Merck) with a pore size of 0.2 µm and a diameter of 25 mm using a vacuum filtration setup. Filtration was continued until the liquid phase had completely passed through the membrane, leaving undisturbed bacterial cells retained on the filter surface.

The filter was then transferred to an atomic force microscope (Park NX10, Park Systems Corporation, Korea), and imaging was performed immediately to analyze bacterial cell surface topography. Measurements were conducted in non-contact mode using an All-in-One cantilever, type D (BudgetSensors, Bulgaria), with operational parameters set according to a previously described protocol [123].

The acquired AFM images were analyzed using Gwyddion open-source software (Czech Metrology Institute, Czech Republic). Surface roughness (Ra) and bacterial cell dimensions were calculated over a linear profile of the cells from images of 5 × 5 µm size. For each experimental condition, measurements were performed on at least 15 individual bacterial cells.

D. Transmission electron microscopy (TEM)

Transmission electron microscope (HT7700, Hitachi, Japan) was used to examine the morphology of the bacterial cells. Before analysis, bacterial samples were centrifuged at 4500 RCF for 10 min and washed twice with sterile DPBS. Each bacterial suspension was normalized to OD_{600} = 0.10 ± 0.01, measured in a 96-well plate using a working volume of 200 µL per well, to obtain separated single cells within the microscope field of view.

A volume of the normalized bacterial suspensions were deposited onto copper grids coated with a carbon support film and negatively stained with 2% (v/v) tungstic acid (Merck). The prepared grids were air-dried at room temperature for 2 h before imaging to ensure complete evaporation of the staining solution.

2.5.3. Methods for evaluation of oxidative and cellular stress

A. Glutathione S-transferases (GSTs) activity assay

GSTs activity was measured as an indicator of oxidative stress in probiotic cells. GSTs are detoxification enzymes that catalyze the conjugation of reduced glutathione (GSH) with electrophilic compounds, including products of oxidative stress and xenobiotics. Measurement of GSTs activity therefore provides an indirect assessment of the cellular antioxidant response. The assay is based on the conjugation of GSH with 1-chloro-2,4-dinitrobenzene (CDNB). Formation of the GSH-CDNB conjugate results in an increase in absorbance, and the rate of absorbance change is proportional to the total GSTs activity in the sample [124].

Before analysis, samples were centrifuged at 4500 RCF for 10 min and washed twice with sterile DPBS. Each bacterial suspension was adjusted to OD_{600} = 1.00 ± 0.10, measured in a 96-well plate using a working volume of 200 µL per well. Bacterial cells were lysed using the CelLytic B Plus Kit (Merck).

Total protein content in the lysates was determined using the Pierce BCA Protein Assay (Thermo Fisher Scientific). Total GSTs activity was measured using a Glutathione S-Transferase Assay Kit (Merck) in accordance with the manufacturer's protocol (#CS0410, Sigma-Aldrich, USA) [125].

Spectrophotometric measurements were performed using a microplate reader at a wavelength of 340 nm. The increase in absorbance was recorded kinetically over time.

GSTs activity was calculated according to the following equation:

$$GSTs\ activity = \frac{\Delta A_{340}\ /\ \Delta t \cdot V \cdot 1000}{\varepsilon \cdot C_{protein} \cdot V_{enz}} \quad (\mu mol \cdot min^{-1} \cdot mg^{-1}\ of\ protein)$$

where:

ΔA_{430} / Δt = slope of absorbance increase from the kinetic measurement (min^{-1}),

V = total reaction volume (mL),

ε = extinction coefficient for CDNB conjugate at 340 nm (ε = 5.3 $mM^{-1} \cdot cm^{-1}$),

$C_{protein}$ = protein concentration in the sample determined by the BCA method ($mg \cdot mL^{-1}$)

V_{enz} = volume of the enzyme sample tested [mL].

B. Protein carbonyl content (PCC) assay

PCC was measured as an indicator of oxidative protein damage in probiotic cells. Oxidative modification of proteins results in the formation of stable carbonyl groups, which can be quantified as markers of oxidative stress. The assay is based on the derivatization of protein carbonyl groups with 2,4-dinitrophenylhydrazine (DNPH), leading to the formation of dinitrophenyl (DNP) hydrazone derivatives that are detectable spectrophotometrically in proportion to the carbonyl content [126].

Before analysis, bacterial samples were centrifuged at 3000 RCF for 15 min at 4 °C and washed twice with sterile DPBS. The cell pellets were resuspended in cold sterile water and adjusted to OD_{600} = 1.00 ± 0.10, measured in a 96-well plate using a working volume of 200 µL per well. The prepared bacterial suspensions were subjected to cell disruption by sonication using an ultrasonic homogenizer (Sonoplus HD 3100, Bandelin, Germany). Sonication was performed using the following parameters: power output of 75 W, pulse mode of 5 s ON and 10 s OFF, with samples maintained in a 4 °C water bath, and a total sonication time of 8 min. After sonication, the lysates were centrifuged at 4500 RCF for 15 min, and the supernatants were transferred to new tubes.

Protein extracts were concentrated using a vacuum concentrator (Concentrator Plus, Eppendorf). Protein carbonyl content was determined using a Protein Carbonyl Assay Kit (Merck) according to the manufacturer's protocol (#MAK094, Sigma-Aldrich) [127].

Spectrophotometric measurements were performed in a microplate reader at a wavelength of 375 nm. Total protein concentration in the samples was determined using the Pierce BCA Protein Assay (Thermo Fisher Scientific).

PCC was calculated according to the following equation:

$$PCC = \frac{(A_{375} - A_{375\,blank}) \cdot V \cdot 1000 \cdot DF}{\varepsilon \cdot P} \quad (nmol \cdot mg^{-1})$$

where:

A_{375} = absorbance of the sample at 375 nm,

$A_{375\ blank}$ = absorbance of DNPH in water without cells at 375 nm,

V = total volume in well (µL),

DF = dilution factor for sample (DF = 1 for undiluted samples),

ε = extinction coefficient for the enclosed 96-well plate (ε = 6.364 $mM^{-1} \cdot cm^{-1}$),

P = amount of protein from well (µg).

2.5.4. Methods for structural and morphological characterization of colloidal systems

A. Keyence digital microscope analysis

To characterize the shape and surface characteristics of alginate-based beads, digital optical microscopy was performed using a VHX-7000 microscope (Keyence, Belgium). Before analysis, individual beads were gently rinsed with ultra-purified Milli-Q water to remove residual salts, placed on a clean surface, and allowed to air-dry at room temperature to obtain a stable shape suitable for imaging.

Dried beads were transferred onto the microscope stage immediately before imaging to minimize handling artifacts. Low magnification optics were used to capture overview images of entire beads to assess their overall geometry, while higher magnification objectives were used to evaluate surface texture and the presence of surface defects. Images were recorded using the instrument's default settings, ensuring appropriate contrast, focus, and scale calibration. Scale bars were generated automatically based on the instrument's internal calibration.

B. Ash Omni 3 inspection microscope analysis

The inspection microscopy analysis was conducted to complement digital optical microscopy and to provide high-resolution visualization of the morphology, diameter, and surface properties of alginate-based probiotic beads. Before analysis, individual beads were gently rinsed with ultra-purified Milli-Q water to remove residual salts, placed on a clean surface, and carefully dried using a lint-free cotton cloth to avoid surface damage.

Imaging was performed with an Ash Omni 3 inspection microscope with a Plan 1x objective (both from Ash Technologies, Ireland) fitted with a polarization filter. Samples were

illuminated using polarized ring light in combination with the microscope's integrated transmitted light stage. To improve depth of field, the Z-stacking module of the system was applied to reconstruct images from multiple focal planes. This approach allowed visualization of entire bead morphology at low magnification and surface features at higher magnification.

Scale bars were automatically generated based on the instrument's internal calibration. Bead diameter was determined using Digimizer software (MedCalc Software, Belgium), with at least 15 beads measured per sample.

C. Cryogenic scanning electron microscopy (cryoSEM)

The morphology of liposome-based systems was examined by cryoSEM using a JSM-7001F TTLS thermal field emission scanning electron microscope (JEOL, Japan) equipped with a cryo preparation system.

After brief sonication to disperse aggregates, the suspension was applied onto a cryo holder and rapidly vitrified in liquid nitrogen. The vitrified samples were transferred to the load-lock chamber while being maintained at cryogenic temperature. In the chamber, the surface was fractured with a cryo knife and then sputter-coated with argon plasma at 10 mA for 120 seconds. The specimens were then moved into the microscope chamber, maintained at a vacuum of $2 \cdot 10^{-4}$ mbar. Imaging was performed at an accelerating voltage of 5 kV, with a working distance of 10 mm, using secondary electron (SE) detection mode under field-emission conditions. Representative images were prepared at various magnifications to visualize both overall morphology and nanoscale features of the structures.

2.5.5. Methods for physicochemical characterization of colloidal systems

A. Zeta potential measurement

The stability of bacterial suspensions and probiotic colloidal systems was assessed by determining the zeta potential based on the Smoluchowski equation using electrophoretic light scattering (ELS). Before analysis, samples were diluted 100-fold with ultra-purified Milli-Q water to ensure appropriate conductivity for electrophoretic measurements. Zeta potential was calculated from the electrophoretic mobility of particles in an applied electric field and measured using disposable folded capillary cells (DTS1070, Malvern Panalytical, UK). Measurements were performed using a Litesizer 500 instrument (Anton Paar, Austria) and a Zetasizer Nano ZS (Malvern Panalytical).

B. Particle size distribution (PSD) analysis

PSD and polydispersity index (PDI) of the bacterial suspensions and probiotic systems were determined using dynamic light scattering (DLS). Before analysis, the samples were diluted 100-fold with ultra-purified Milli-Q water. Measurements were performed in disposable cuvettes at a scattering angle of 90°. Data were acquired and analyzed using a Litesizer 500 instrument (Anton Paar) and a Zetasizer Nano ZS (Malvern Panalytical).

C. Inductively coupled plasma mass spectrometry (ICP-MS)

To assess the effect of alginate encapsulation on intracellular trace metals, probiotic cells were first released from alginate beads and then quantified for manganese, iron, and zinc. Beads were transferred to a 50 mM sodium citrate solution and mixed gently at room temperature for 30 min until complete gel disintegration was observed. The suspension was then passed through a 40 µm sterile filter (pluriSelect Life Science) to remove gel fragments. Filtrates were centrifuged at 4500 RCF for 20 min and washed three times with ultra-purified Milli-Q water. The final cell pellet was retained for acid digestion in HNO_3, using a volume sufficient to cover the pellet and applying gentle heating at 60 °C until the solution became clear.

Each digest was diluted 50-fold with ultra-purified Milli-Q water before analysis. The concentrations of manganese (^{55}Mn), iron (^{56}Fe), and zinc (^{66}Zn) were determined by ICP-MS (Agilent Technologies, USA) operated in no-gas mode. Calibration was performed using certified standard solutions (Sigma-Aldrich) for Mn, Fe, and Zn at concentrations of 1.25, 2.5, 5, 10, and 20 $mg \cdot L^{-1}$. Both calibration standards and diluted samples were introduced into the autosampler, and the ICP-MS instrument was programmed to analyze the selected isotopes accordingly. Measured concentrations were reported as $mg \cdot L^{-1}$ of solution.

2.6. Statistical analysis

Results are presented as mean values calculated from at least three independent biological replicates. For each biological replicate, a minimum of two technical replicates were performed. Data are expressed as the mean ± standard deviation (SD). Statistical significance of differences between experimental groups was evaluated using one-way analysis of variance (ANOVA). When statistically significant effects were detected, pairwise comparisons were performed using the Sidak-Holm post hoc test. The level of statistical significance was set at $p < 0.05$. Data analysis and graphical presentation were performed using OriginPro (OriginLab Corporation, USA).

IV. RESULTS AND DISCUSSION

This chapter presents the experimental results together with their interpretation in relation to the research hypothesis and specific research objectives. The results are organized according to following experimental stages reflecting the chronology of the study.

1. PREFORMULATION SCREENING OF SELECTED ADDITIVES

This stage focused on evaluating the compatibility and direct effects of selected PPAs (trehalose – TRE, vitamin C – VC, maltodextrin – MD, monosodium glutamate – MSG, inulin – IN, gum arabic – GA, and corn starch – CS) when applied to free probiotic cells (*L. plantarum*, *L. rhamnosus*, and *L. paracasei*). The objective of this stage was to compare the effects of the tested additives on probiotic viability, membrane integrity, surface properties, and selected stress markers, thereby providing a basis for selecting suitable components for next encapsulation experiments.

1.1. Metabolic activity and cell viability

The effects of selected PPAs on the survival of probiotic cells were evaluated using complementary analytical approaches. Metabolic activity was assessed by the MTT assay, potential cytotoxicity by the AlamarBlue (AB) assay, and cell viability by flow cytometry.

Lactiplantibacillus plantarum

As shown in Figure 9, metabolic activity of *L. plantarum* varied depending on the applied PPA. Treatment with TRE and VC resulted in a significant increase in metabolic activity, with MRU values of 1.47 ± 0.05 and 1.38 ± 0.16, respectively ($p < 0.001$ for both). This increase suggests that TRE and VC supported metabolic activity of *L. plantarum* under the tested conditions. This observation is consistent with previous reports describing the osmoprotective role of TRE and the antioxidative properties of VC in bacterial systems [128,129]. MD was associated with a moderate but statistically significant increase in metabolic activity (0.95 ± 0.12, $p < 0.001$). This effect may be related to the availability of MD as an additional carbon source for bacterial metabolism [130]. In contrast, treatment with IN resulted in a significant decrease in metabolic activity, with MRU value of 0.52 ± 0.01 ($p < 0.001$). This result indicates an inhibitory effect on *L. plantarum* under the tested conditions. Although IN is commonly described as a prebiotic compound that supports probiotic growth, the observed effect suggests that its direct application to free cells may influence metabolism differently than its action within the GI environment. [87].

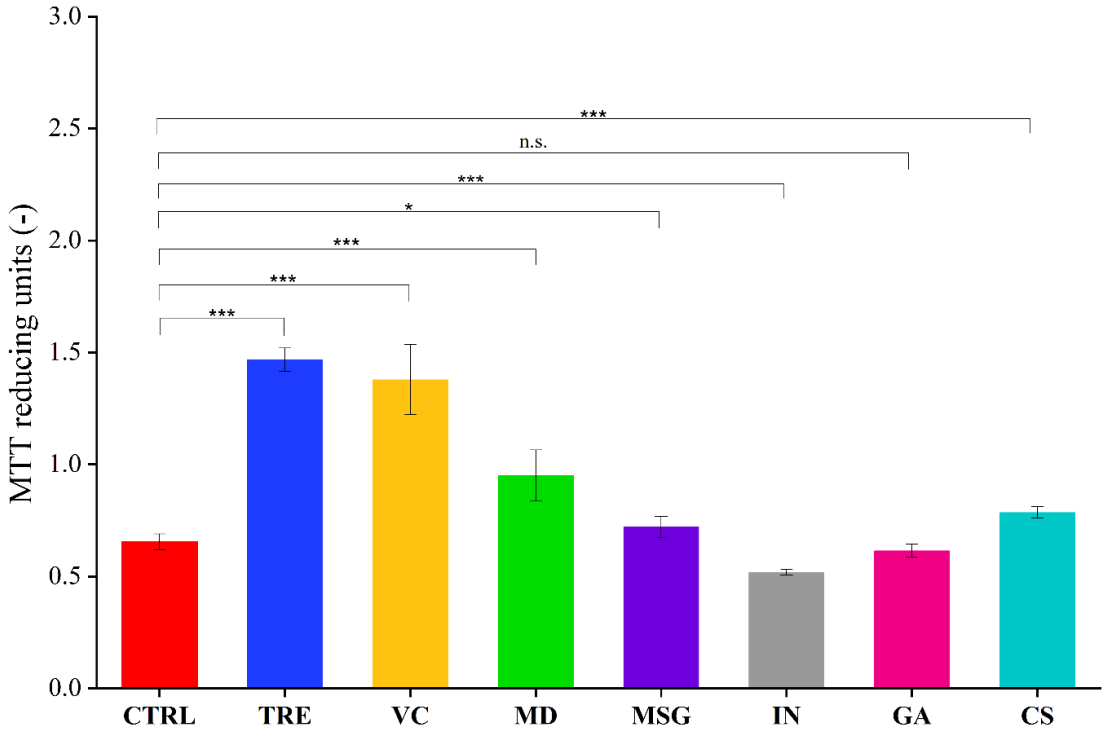

Figure 9. Results of metabolic activity (MTT reducing units – MRU) for *L. plantarum* exposed to trehalose (TRE), vitamin C (VC), maltodextrin (MD), monosodium glutamate (MSG), inulin (IN), gum arabic (GA), and corn starch (CS). The control sample (CTRL) represents free (untreated) cells. Comparisons without asterisks are not statistically significant (n.s.). Statistical significance: (*) $p < 0.05$; (***) $p < 0.001$.

The AlamarBlue assay revealed significant differences in the reduction of the AB reagent after exposure of *L. plantarum* to selected PPAs (Figure 10). Treatment with TRE and VC resulted in a statistically significant decrease in AB reduction, with values of 56.50 ± 1.55 and 50.20 ± 1.72%, respectively ($p < 0.001$ for both). A decrease in AB reduction reflects changed cellular redox activity and may indicate increased cellular stress under the tested conditions. In this context, the observed decrease suggests that exposure to TRE and VC affected metabolic processes associated with cellular redox balance in *L. plantarum*. Similar observations have been reported for conditions in which increased metabolic activity is accompanied by elevated intracellular stress levels [135]. In contrast, treatment with IN and CS resulted in statistically significant increases in AB reduction, reaching 135.10 ± 5.63 and 149.40 ± 4.86%, respectively ($p < 0.001$) for both). These values indicate higher redox activity relative to the CTRL, which is consistent with a lower level of cellular stress under the tested conditions.

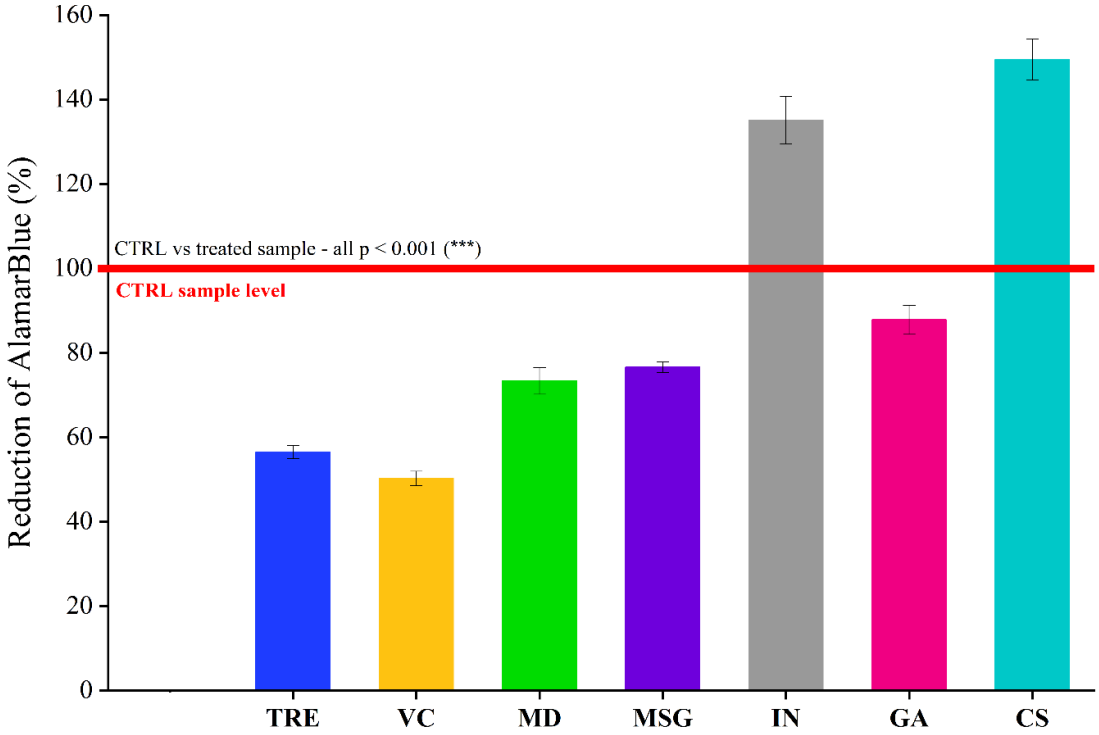

Figure 10. Results of cytotoxicity for *L. plantarum* exposed to trehalose (TRE), vitamin C (VC), maltodextrin (MD), monosodium glutamate (MSG), inulin (IN), gum arabic (GA), and corn starch (CS). The control sample (CTRL) represents free (untreated) cells.

As shown in Table 6, treatment with TRE and VC resulted in the maintenance of high levels of active cells of *L. plantarum* (89.88 ± 0.52 and 94.80 ± 0.06%, respectively, $p < 0.001$ for both). This pattern suggests a balance between increased metabolic activity and the induction of cellular stress, in which higher metabolic demand does not translate into a loss of overall viability. In contrast, exposure to IN resulted in a significant reduction in the proportion of active cells to 70.27 ± 1.39% ($p < 0.001$), accompanied by a corresponding increase in the fraction of mid-active cells. This shift indicates changed physiological status of the bacterial population, consistent with a stress or metabolism related response under the tested conditions.

Lacticaseibacillus rhamnosus

As shown in Figure 11, exposure of *L. rhamnosus* to TRE and VC resulted in a significant increase in metabolic activity, with MRU values of 4.57 ± 0.33 and 3.64 ± 0.61, respectively ($p < 0.001$ for both). MD MSG were also associated with a significant increase in metabolic activity compared with the CTRL, indicating a stimulatory effect on *L. rhamnosus* metabolism. This response may be related to the availability of MSG as a nitrogen source for bacterial metabolic processes [131,132]. In contrast, treatment with IN, GA, and CS did not result

in statistically significant changes in metabolic activity compared to the CTRL, indicating a neutral effect under the tested conditions.

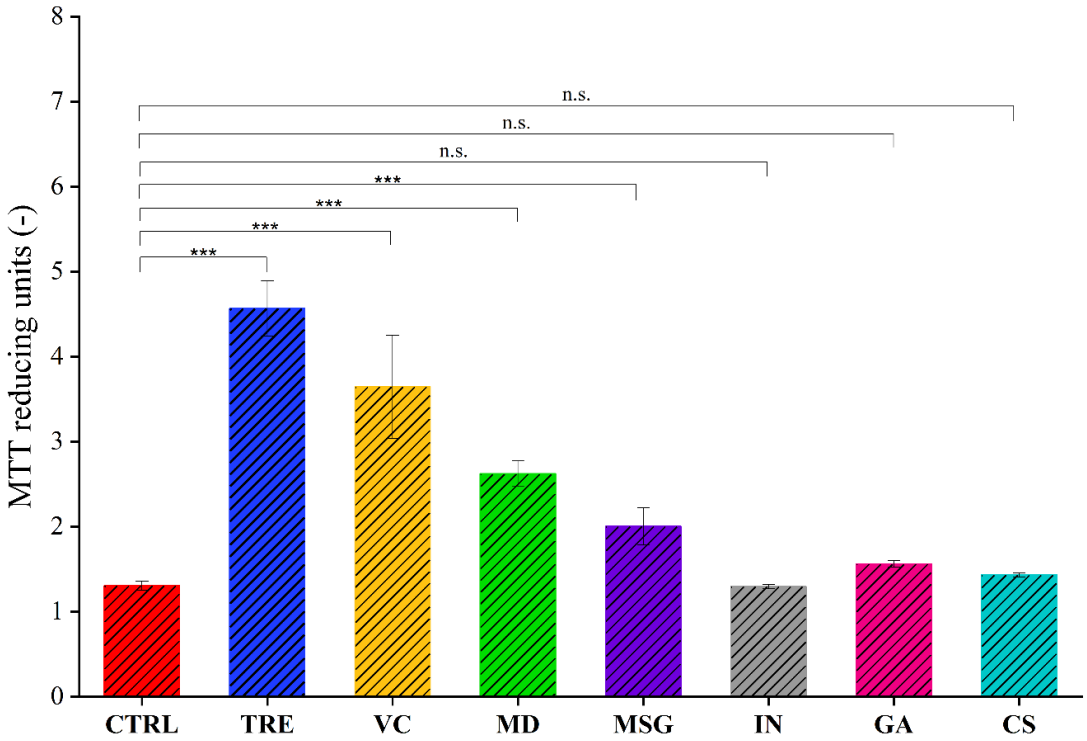

Figure 11. Results of metabolic activity (MTT reducing units – MRU) for *L. rhamnosus* exposed to trehalose (TRE), vitamin C (VC), maltodextrin (MD), monosodium glutamate (MSG), inulin (IN), gum arabic (GA), and corn starch (CS). The control sample (CTRL) represents free (untreated) cells. Comparisons without asterisks are not statistically significant (n.s.). Statistical significance: (***) $p < 0.001$.

As shown in Figure 12, results of the AB assay indicated a significant decrease in AB reduction after exposure of *L. rhamnosus* to TRE, reaching 22.50 ± 0.81% ($p < 0.001$). This finding contrasts with the increase in metabolic activity observed in the MTT assay for the same treatment. A decrease in AB reduction may indicate increased intracellular stress under the tested conditions. In this context, the observed discrepancy between MTT and AB results suggests that stimulation of metabolic activity by TRE may be accompanied by changes in redox balance rather than by improved overall cellular homeostasis. In contrast, CS resulted in higher AB reduction values relative to CTRL, indicating reduced redox stress. This observation is consistent with the neutral effect of CS on metabolic activity measured by the MTT assay, suggesting that CS does not impose additional metabolic or oxidative burden on *L. rhamnosus* cells under the applied conditions.

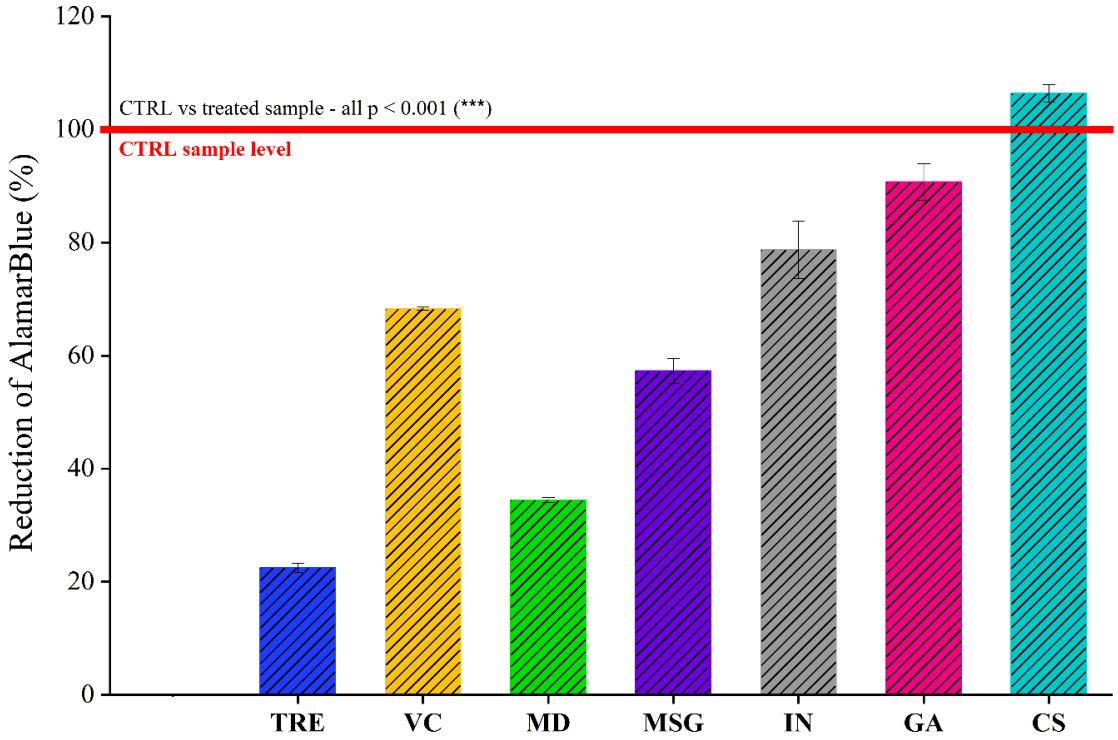

Figure 12. Results of cytotoxicity for *L. rhamnosus* exposed to trehalose (TRE), vitamin C (VC), maltodextrin (MD), monosodium glutamate (MSG), inulin (IN), gum arabic (GA), and corn starch (CS). The control sample (CTRL) represents free (untreated) cells.

As shown in Table 6, treatment with VC and GA resulted in a significant increase in the proportion of active *L. rhamnosus* cells, reaching 55.88 ± 1.86 and 60.50 ± 1.50%, respectively ($p < 0.001$ for both). The observed increase in active cells suggests improved maintenance of cellular integrity under these conditions. Similar effects have been reported for systems in which antioxidant compounds or polysaccharide-based matrices contribute to cellular stabilization [131]. In contrast, exposure to TRE and CS resulted in a decrease in the proportion of active cells relative to the CTRL. This observation indicates that enhanced metabolic activity does not necessarily correspond to higher levels of cellular vitality. Taken together, these results highlight the need to consider both metabolic responses and stress-related indicators when evaluating the performance of probiotic formulations.

Lacticaseibacillus paracasei

The response of *L. paracasei* to selected PPAs is shown in Figure 13. Exposure to TRE resulted in a significant increase in metabolic activity, with an MRU value of 4.31 ± 0.20 ($p < 0.001$). Similar increases in metabolic activity were observed in treatment with VC and IN. MD and CS were associated with smaller increases in metabolic activity compared with the

CTRL. The observed effects may be related to the availability of MD and CS as additional carbon sources for bacterial metabolism, providing a limited contribution to cellular energy supply under the tested conditions [132].

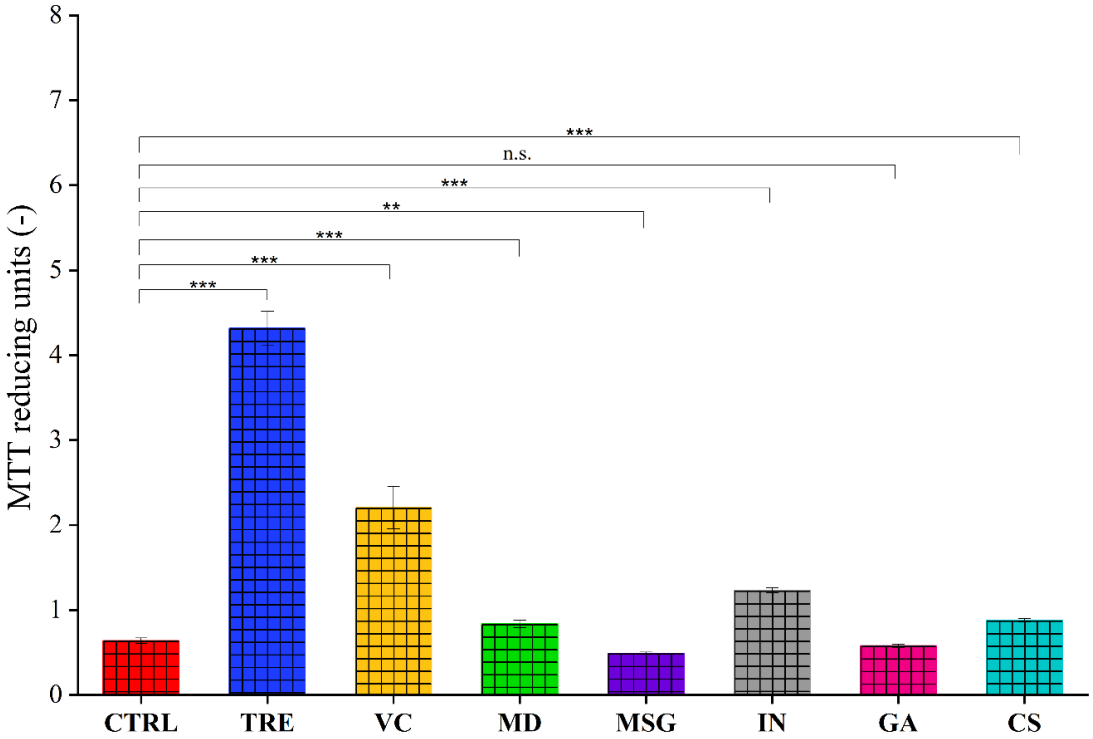

Figure 13. Results of metabolic activity (MTT reducing units – MRU) for *L. paracasei* exposed to trehalose (TRE), vitamin C (VC), maltodextrin (MD), monosodium glutamate (MSG), inulin (IN), gum arabic (GA), and corn starch (CS). The control sample (CTRL) represents free (untreated) cells. Comparisons without asterisks are not statistically significant (n.s.). Statistical significance: (**) $p < 0.01$; (***) $p < 0.001$.

As shown in Figure 14, results of the AB assay for *L. paracasei* showed a marked reduction in AB reagent after exposure to MD and MSG. In the case of MD, AB reduction decreased to 4.20 ± 0.10% ($p < 0.001$), indicating strongly changed redox-dependent cellular activity under the tested conditions. Decreased AB reduction reflects changes in intracellular redox balance and may be associated with elevated metabolic demand. In contrast, treatment with IN and GA resulted in higher AB reduction values relative to the CTRL, consistent with lower redox-associated stress levels. These observations align with the previously observed effects of IN and GA in other assays, supporting their role as stabilizing components under the applied conditions. Taken together, the AB assay results for *L. paracasei* highlight that stimulation of metabolic activity does not necessarily correspond to reduced cellular stress.

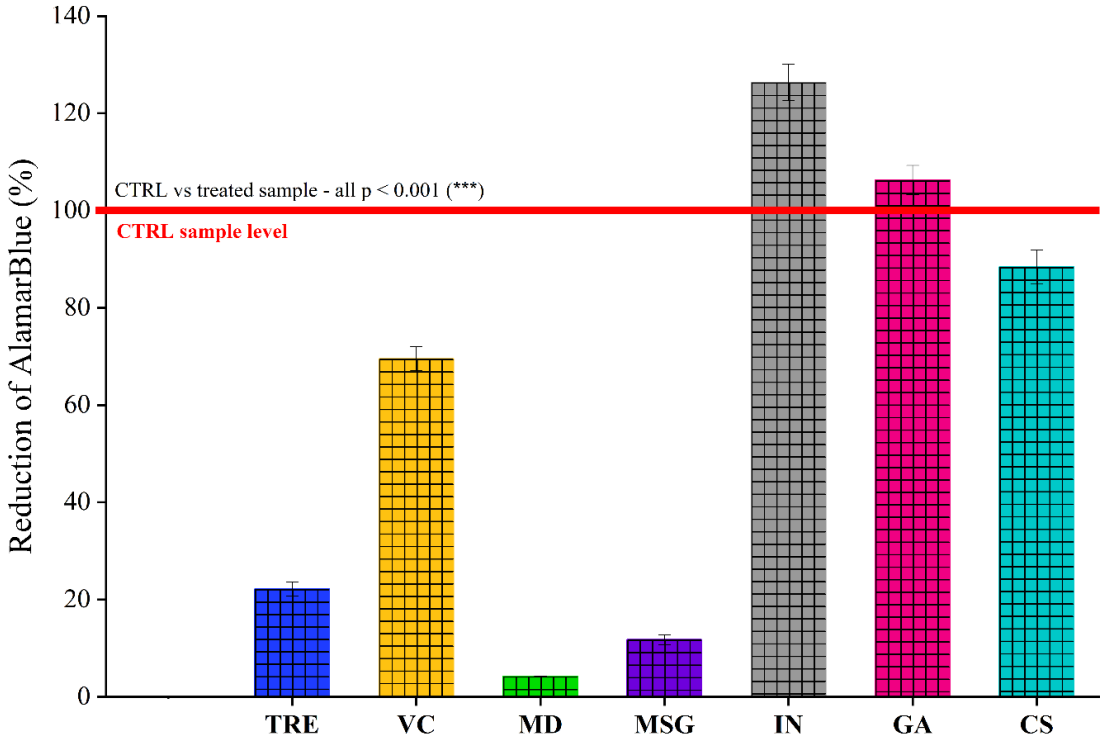

Figure 14. Results of cytotoxicity for *L. paracasei* exposed to trehalose (TRE), vitamin C (VC), maltodextrin (MD), monosodium glutamate (MSG), inulin (IN), gum arabic (GA), and corn starch (CS). The control sample (CTRL) represents free (untreated) cells.

As shown in Table 6, treatment with MD and GA resulted in a significant increase in the proportion of active *L. paracasei* cells, reaching 81.57 ± 1.23 and 83.22 ± 2.81%, respectively ($p < 0.001$ for both). These values indicate improved maintenance of cell vitality under the tested conditions. Exposure to TRE and CS was associated with a reduction in the proportion of dead cells, suggesting a favorable effect on overall cell viability. In contrast, treatment with MSG and IN did not result in statistically significant changes in the proportion of active cells relative to the CTRL, indicating a neutral response under the applied conditions.

Across all tested strains, TRE consistently increased metabolic activity. At the same time, several assays indicated changes in redox balance under TRE exposure, suggesting that enhanced metabolic activity does not necessarily correspond to improved cellular homeostasis. The effects VC on metabolic activity were strain-dependent, highlighting that its antioxidative properties may provide benefits under specific conditions but may also impose stress depending on concentration and bacterial physiology. MD and GA were associated with improved maintenance of probiotic viability, consistent with their role as matrix components or stabilizing agents.

Table 6. Results of cell viability assessed by flow cytometry for *L. plantarum*, *L. rhamnosus*, and *L. paracasei* exposed to trehalose (TRE), vitamin C (VC), maltodextrin (MD), monosodium glutamate (MSG), inulin (IN), gum arabic (GA), and corn starch (CS). The control sample (CTRL) represents free (untreated) cells. Data are expressed as mean ± standard deviation. Comparisons without asterisks are not statistically significant (n.s.). Statistical significance: (*) $p < 0.05$; (**) $p < 0.01$; (***) $p < 0.001$.

	Fractional composition of cell populations (%)								
	L. plantarum			***L. rhamnosus***			***L. paracasei***		
	active	**mid-active**	**dead**	**active**	**mid-active**	**dead**	**active**	**mid-active**	**dead**
CTRL	92.98 ± 0.60	3.30 ± 0.49	0.67 ± 0.05	23.78 ± 0.77	53.82 ± 0.70	8.97 ± 0.51	40.78 ± 1.07	23.87 ± 1.28	32.07 ± 0.83
TRE	89.88 ± 0.52 (***)	4.13 ± 0.48 (**)	0.28 ± 0.08 (***)	18.07 ± 3.26 (***)	51.55 ± 1.89 (n.s.)	7.08 ± 0.42 (n.s.)	67.65 ± 1.92 (***)	14.32 ± 1.58 (***)	13.32 ± 0.71 (***)
VC	94.80 ± 0.06 (***)	3.05 ± 0.12 (n.s.)	0.60 ± 0.09 (n.s.)	55.88 ± 1.86 (***)	28.80 ± 1.36 (***)	4.83 ± 0.42 (*)	24.00 ± 0.73 (***)	36.17 ± 2.03 (***)	37.52 ± 1.88 (*)
MD	92.70 ± 0.65 (n.s.)	4.50 ± 0.42 (***)	0.42 ± 0.08 (**)	49.57 ± 2.34 (***)	26.80 ± 0.63 (***)	3.50 ± 0.19 (**)	81.57 ± 1.23 (***)	10.37 ± 0.83 (***)	4.95 ± 0.43 (***)
MSG	92.52 ± 0.44 (n.s.)	4.05 ± 0.23 (**)	0.55 ± 0.05 (n.s.)	28.38 ± 7.16 (*)	48.80 ± 6.61 (**)	6.13 ± 1.47 (n.s.)	37.08 ± 1.28 (n.s.)	29.37 ± 3.69 (*)	29.00 ± 6.84 (n.s.)
IN	70.27 ± 1.39 (***)	5.35 ± 0.61 (***)	0.58 ± 0.18 (n.s.)	24.07 ± 3.13 (n.s.)	47.97 ± 2.44 (***)	8.35 ± 1.30 (n.s.)	40.98 ± 3.13 (n.s.)	26.43 ± 1.29 (n.s.)	28.15 ± 1.34 (n.s.)
GA	88.48 ± 1.31 (***)	5.13 ± 0.62 (***)	1.15 ± 0.23 (***)	60.50 ± 1.50 (***)	24.30 ± 1.04 (***)	3.12 ± 0.23 (***)	83.22 ± 2.81 (***)	9.22 ± 1.70 (***)	4.92 ± 0.71 (***)
CS	92.33 ± 0.36 (n.s.)	4.18 ± 0.42 (**)	0.58 ± 0.12 (n.s.)	17.93 ± 1.08 (***)	57.73 ± 1.22 (*)	9.58 ± 0.69 (n.s.)	67.07 ± 1.76 (***)	15.07 ± 1.39 (***)	13.12 ± 0.25 (***)

Differences observed between metabolic activity, cytotoxicity, and viability across different PPAs emphasize that probiotic performance is influenced by multiple interacting factors, including the physicochemical properties of the additives, their concentration, and the metabolic and stress response characteristics of individual strains. In this context, increased metabolism may be accompanied by increased cellular stress if metabolic stimulation disrupts osmotic balance or promotes generation of ROS [133].

1.2. Modifications of cell envelope

Crystal violet (CV) and Congo red (CR) assays were used to evaluate the effects of PPAs on bacterial membrane permeability and cell surface hydrophobicity, respectively.

Lactiplantibacillus plantarum

As shown in Figure 15, treatment with TRE, VC, MD, MSG, and CS was associated with reduced membrane permeability in *L. plantarum*, indicating enhanced barrier properties relative to the CTRL. This reduction suggests improved membrane integrity under the tested conditions. In contrast, exposure to IN and GA did not result in statistically significant changes in membrane permeability.

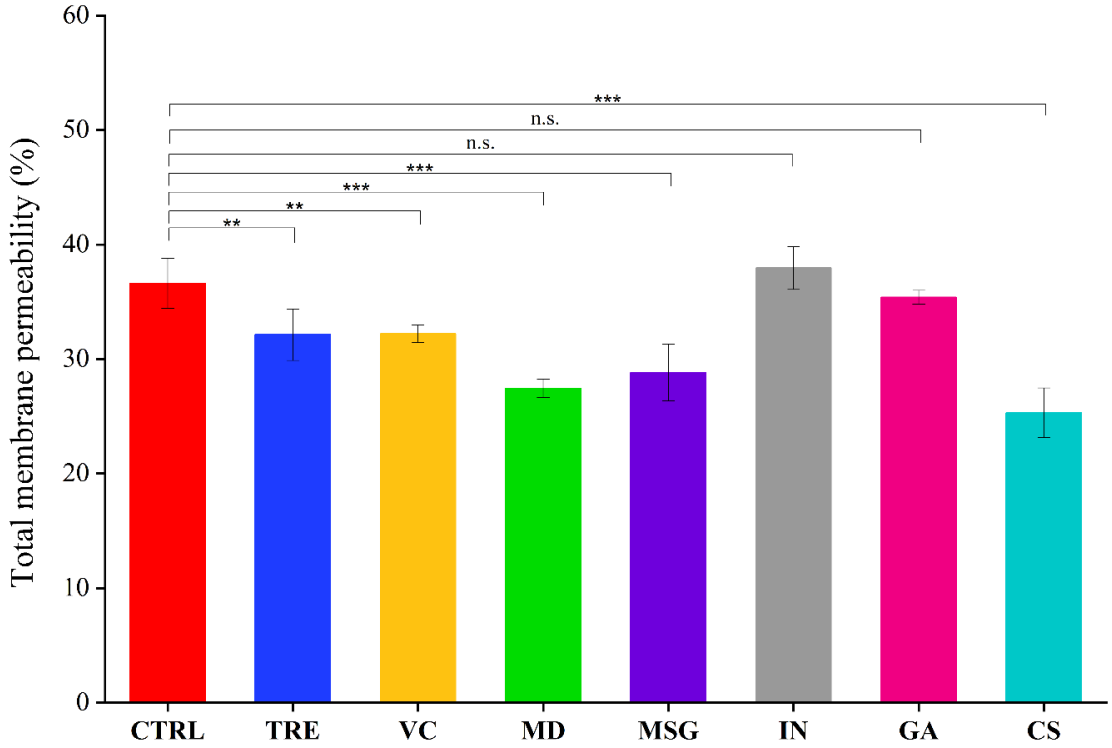

Figure 15. Results of total membrane permeability for *L. plantarum* exposed to trehalose (TRE), vitamin C (VC), maltodextrin (MD), monosodium glutamate (MSG), inulin (IN), gum arabic (GA), and corn starch (CS). The control sample (CTRL) represents free (untreated) cells. Comparisons without asterisks are not statistically significant (n.s.). Statistical significance: (**) $p < 0.01$; (***) $p < 0.001$.

Results of the CR assay (Figure 16) showed that treatment with TRE, VC, MD, IN, GA, and CS resulted in decreased cell surface hydrophobicity, indicating a shift toward a more hydrophilic surface. In contrast, MSG treatment increased surface hydrophobicity to 15.82 ± 0.67% ($p = 0.001$), indicating modified surface properties that may favor hydrophobic interactions. Taken together, these results indicate that PPAs modulate surface characteristics of *L. plantarum* in distinct ways. This is consistent with changes in surface composition or organization after exposure to PPAs, which has been linked to different interactions with the surrounding environment [134].

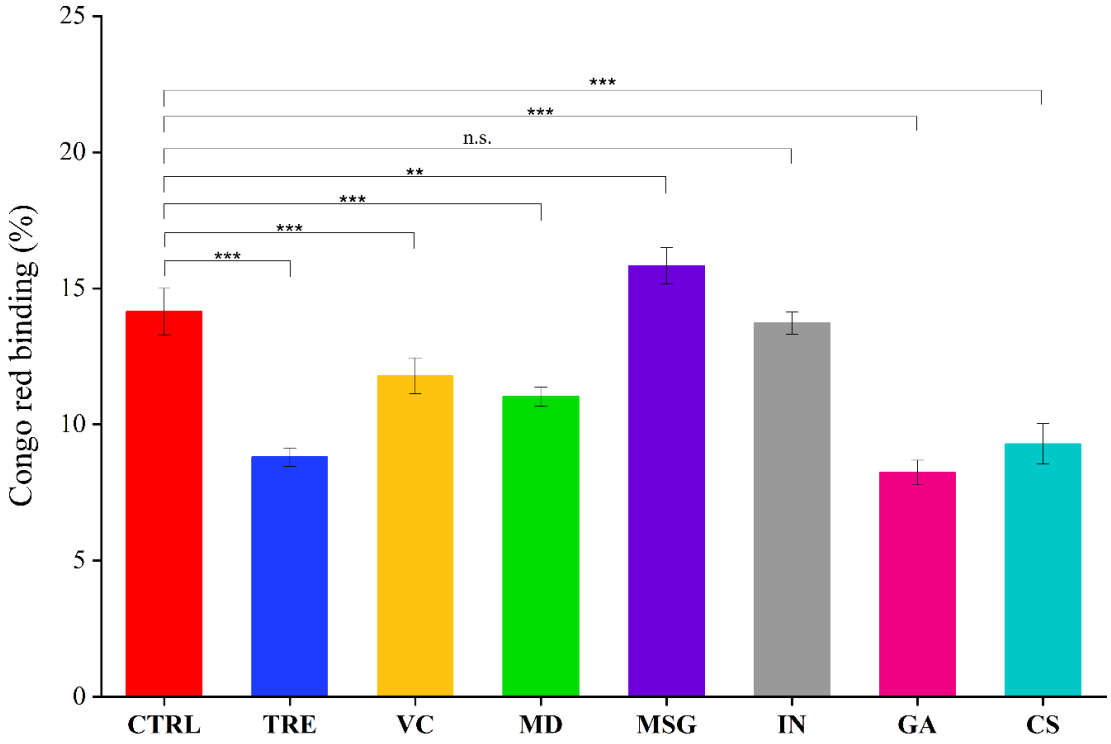

Figure 16. Results of Congo red binding for *L. plantarum* exposed to trehalose (TRE), vitamin C (VC), maltodextrin (MD), monosodium glutamate (MSG), inulin (IN), gum arabic (GA), and corn starch (CS). The control sample (CTRL) represents free (untreated) cells. Comparisons without asterisks are not statistically significant (n.s.). Statistical significance: (**) $p < 0.01$; (***) $p < 0.001$.

Lacticaseibacillus rhamnosus

As shown in Figure 17, treatment with VC and IN resulted in a significant increase in membrane permeability in *L. rhamnosus*, reaching 14.19 ± 1.34 and 17.52 ± 0.27%, respectively ($p < 0.001$ for both), indicating changed membrane barrier properties relative to the CTRL. Changes in permeability were also observed following exposure to MD and MSG, suggesting that both compounds affected membrane integrity under the applied conditions.

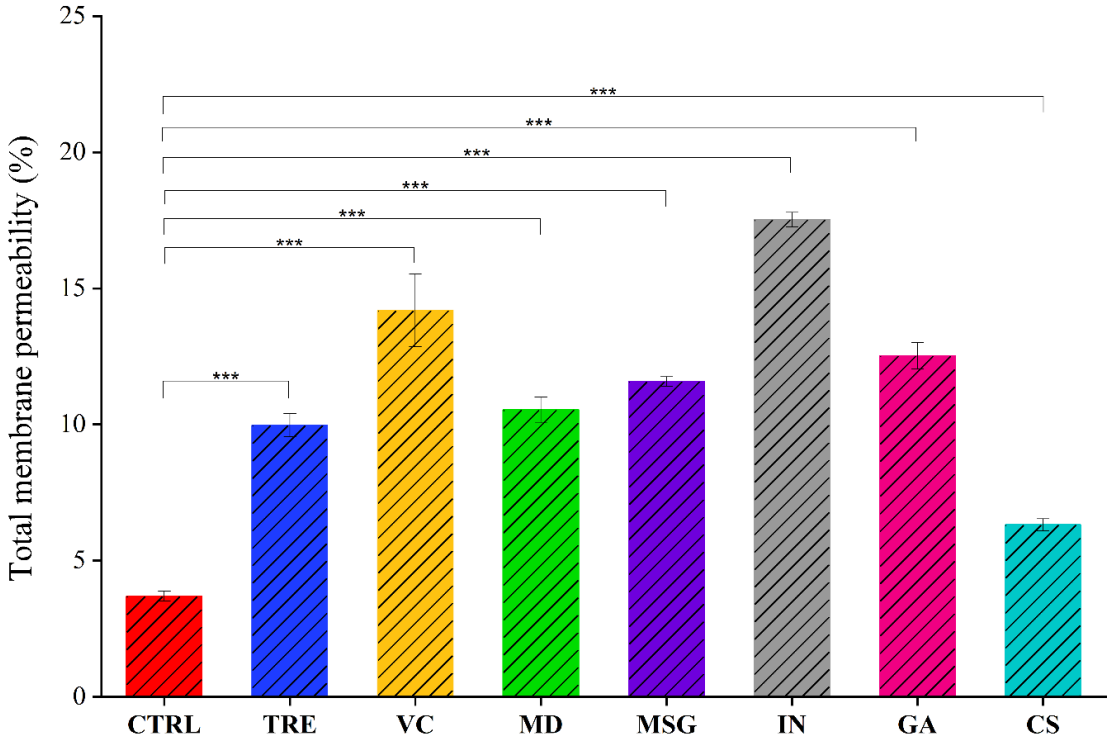

Figure 17. Results of total membrane permeability for *L. rhamnosus* exposed to trehalose (TRE), vitamin C (VC), maltodextrin (MD), monosodium glutamate (MSG), inulin (IN), gum arabic (GA), and corn starch (CS). The control sample (CTRL) represents free (untreated) cells. Statistical significance: (***) $p < 0.001$.

According to Figure 18, treatment with TRE and VC was associated with increased cell surface hydrophobicity in *L. rhamnosus*. In contrast, exposure to MD and CS resulted in a significant reduction in hydrophobicity, with values of 12.78 ± 1.20 and 8.03 ± 1.11%, respectively ($p < 0.001$ for both), indicating a shift toward a more hydrophilic surface. Such changes may represent an adaptive response associated with reduced hydrophobic interactions at the cell surface [135]. Treatments with MSG, IN, and GA resulted in comparatively minor changes in surface hydrophobicity, indicating a limited effect on cell surface properties under the tested conditions.

Lacticaseibacillus paracasei

Analysis of membrane permeability in *L. paracasei* (Figure 19) showed increases after exposure to TRE, MSG, and IN, consistent with adaptive responses under the tested conditions. In contrast, treatment with MD, GA, and CS resulted in statistically significant reductions in membrane permeability to 28.31 ± 2.41, 34.90 ± 1.17, and 27.48 ± 1.42%, respectively ($p < 0.001$ for all). These changes are consistent with enhanced barrier properties, which may

be related to the formation of stabilizing surface interactions that limit environmental exposure [136]. VC and MSG did not result in statistically significant changes in membrane permeability.

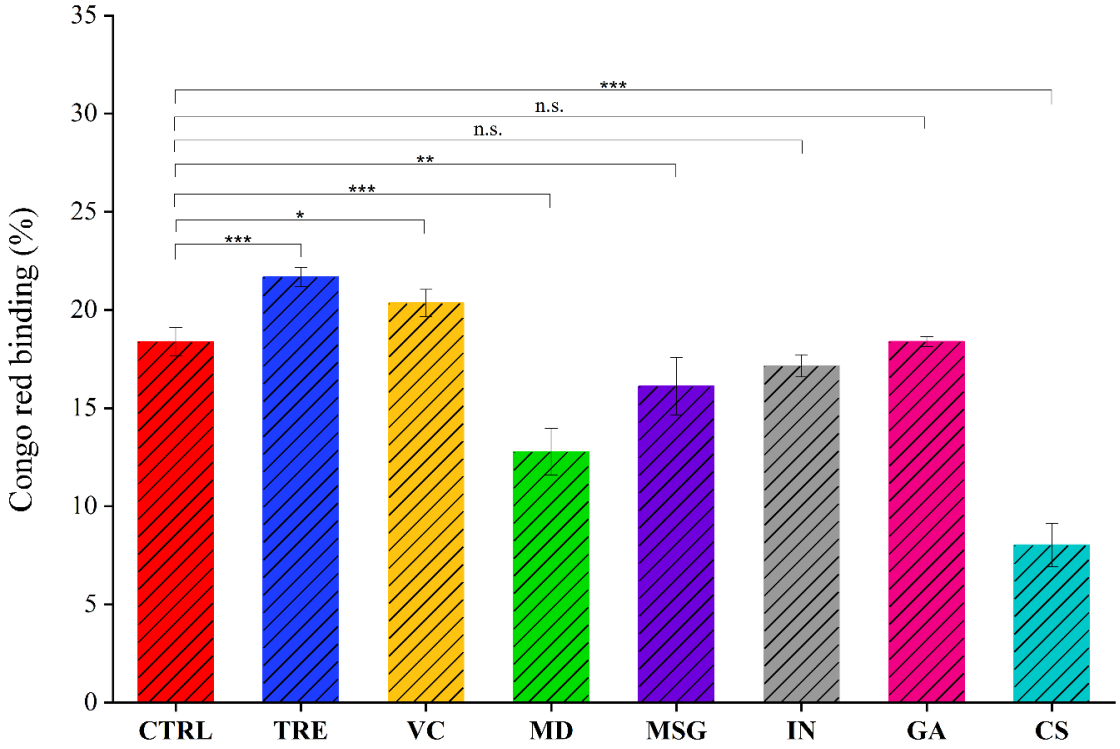

Figure 18. Results of Congo red binding for *L. rhamnosus* exposed to trehalose (TRE), vitamin C (VC), maltodextrin (MD), monosodium glutamate (MSG), inulin (IN), gum arabic (GA), and corn starch (CS). The control sample (CTRL) represents free (untreated) cells. Comparisons without asterisks are not statistically significant (n.s.). Statistical significance: (*) $p < 0.05$; (**) $p < 0.01$; (***) $p < 0.001$.

As shown in Figure 20, treatment with TRE, VC, IN, GA, and CS was associated with statistically significant reductions in cell surface hydrophobicity in *L. paracasei*. MD also resulted in a decrease in hydrophobicity to 21.50 ± 0.85% ($p < 0.001$), consistent with its stabilizing effect on membrane permeability. In contrast, MSG caused only a modest reduction in hydrophobicity, indicating a more limited effect on surface properties. PPAs associated with increased membrane permeability, such as TRE and IN, should be linked to increased oxidative stress markers, whereas compounds that reduced permeability, including MD, GA, and CS, should be associated with lower levels of oxidative stress indicators [137]. Overall, most PPAs reduced cell surface hydrophobicity, shifting *L. paracasei* toward a more hydrophilic surface profile under the applied conditions.

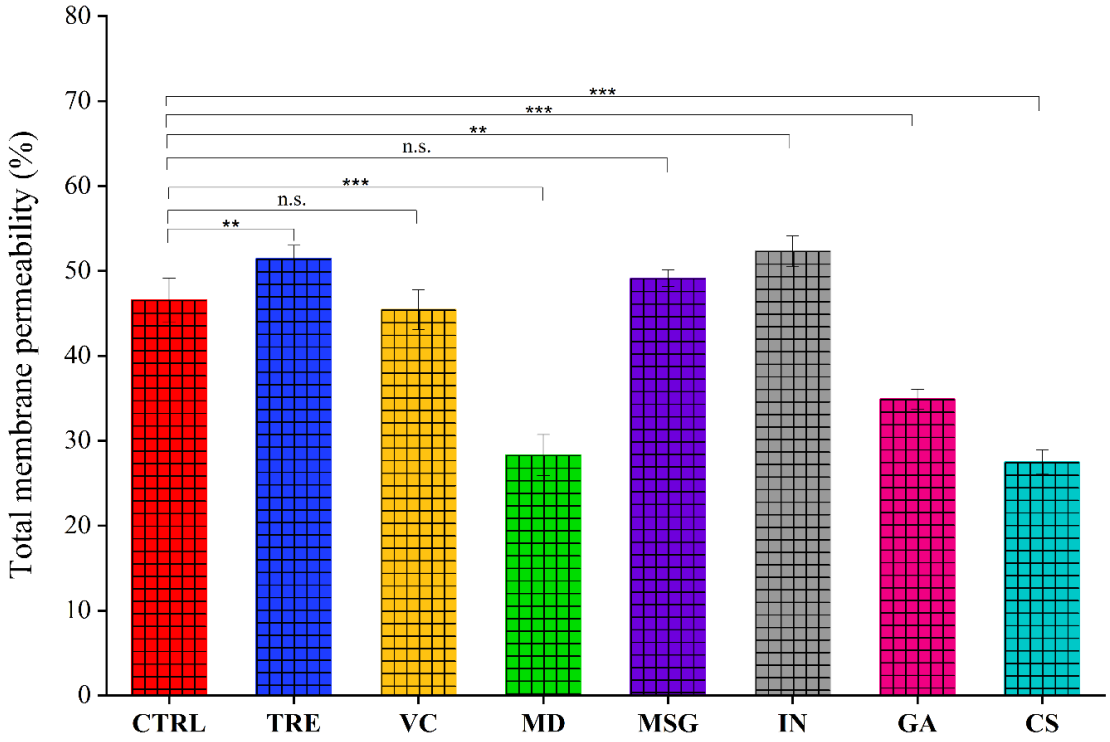

Figure 19. Results of total membrane permeability for *L. paracasei* exposed to trehalose (TRE), vitamin C (VC), maltodextrin (MD), monosodium glutamate (MSG), inulin (IN), gum arabic (GA), and corn starch (CS). The control sample (CTRL) represents free (untreated) cells. Comparisons without asterisks are not statistically significant (n.s.). Statistical significance: (**) $p < 0.01$; (***) $p < 0.001$.

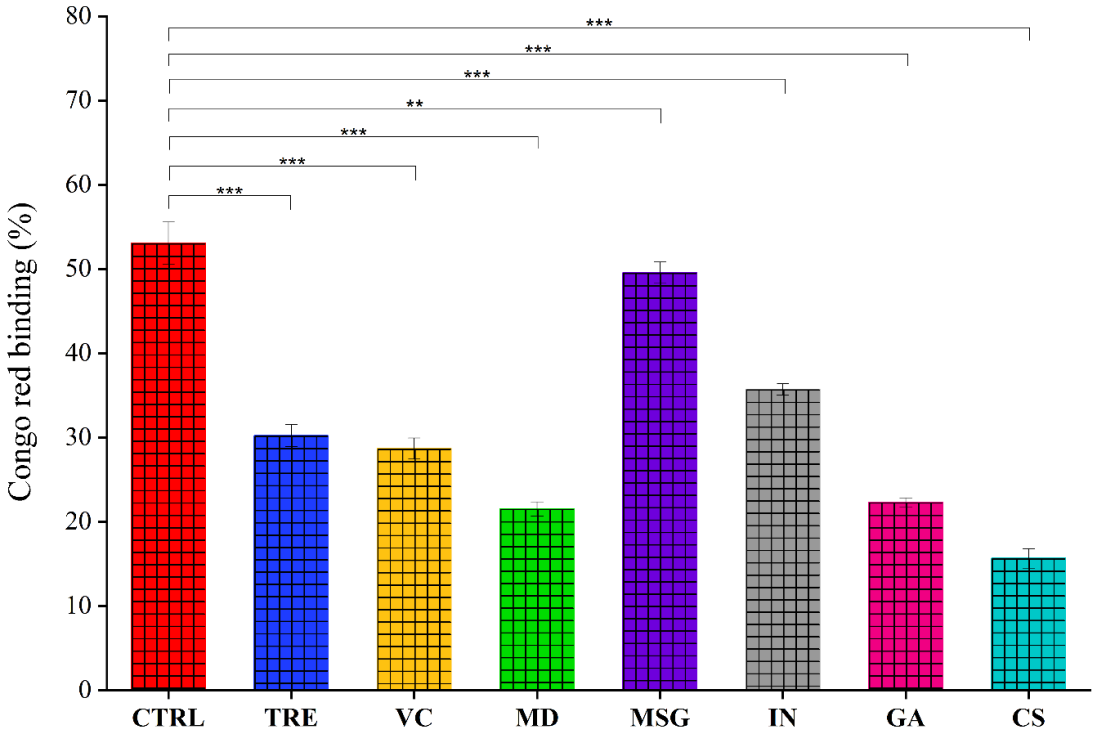

Figure 20. Results of Congo red binding for *L. paracasei* exposed to trehalose (TRE), vitamin C (VC), maltodextrin (MD), monosodium glutamate (MSG), inulin (IN), gum arabic (GA), and corn starch (CS). The control sample (CTRL) represents free (untreated) cells. Statistical significance: (**) $p < 0.01$; (***) $p < 0.001$.

After comparing responses across all *Lactobacillus* strains, treatment with TRE and IN was consistently associated with increased membrane permeability. In contrast, exposure to MD, GA, and CS resulted in reduced membrane permeability. Changes in cell surface hydrophobicity were also observed, with TRE, VC, and MD associated with decreased hydrophobicity. Such modifications indicate a shift toward a more hydrophilic surface profile, which may reduce interactions with potentially harmful compounds and contribute to improved cellular stability.

1.3. Adaptive stress response

The combined analysis of GSTs activity and protein carbonyl content (PCC) provides an integrated view of the adaptive stress responses of probiotic bacteria to the applied PPAs. GSTs activity reflects cellular defense mechanisms against oxidative stress, whereas PCC shows the level of oxidative protein damage.

Lactiplantibacillus planatrum

As shown in Table 7 for *L. plantarum*, treatment with TRE and GA resulted in an increase in GSTs activity, reaching 0.24 ± 0.02 and 0.25 ± 0.01 μmol·min^{-1}·mg^{-1} of protein, respectively ($p < 0.001$ for both). This increase indicates activation of detoxification pathways and suggests the induction of an oxidative stress response, despite the established protective role of TRE against stress and the generally stabilizing character of GA [138]. In contrast, exposure to VC resulted in a significant decrease in GSTs activity to 0.04 ± 0.01 μmol·min^{-1}·mg^{-1} of protein ($p < 0.001$), indicating reduced stress response mechanisms in *L. plantarum*. However, this observation was accompanied by increased PCC, suggesting that reduced GSTs activity does not necessarily exclude the occurrence of oxidative protein damage under the tested conditions. Treatment with MD, MSG, IN, and CS resulted in only minor changes in GSTs activity and PCC relative to the CTRL, suggesting their neutral role as metabolic substrates for *L. plantarum*. This study shows that exposure to TRE and VC resulted in a significant increase in PCC, indicating enhanced oxidative modification of cellular proteins and suggesting pro-oxidant effects under the applied conditions. These observations highlight the dual nature of PPAs in probiotic formulations, in which protective or pro-oxidant effects depend on environmental conditions, additive concentration, and interactions with cellular redox systems, including the involvement of transition metals [130,139,140].

Integration of these results with cell viability analyses for *L. plantarum* indicates that exposure to TRE and VC was associated with a significant increase in metabolic activity, accompanied by elevated oxidative stress markers. This observation suggests that enhanced metabolic activity may occur together with increased oxidative burden. Despite this, results from cytotoxicity assays and flow cytometry showed that TRE and VC maintained or increased overall cellular viability. This response may be related to the ability of *L. plantarum* to activate adaptive antioxidant and detoxification mechanisms that mitigate the impact of oxidative stress and preserve cellular function [141].

Lacticaseibacillus rhamnosus

As shown in Table 7 for *L. rhamnosus*, TRE and VC were associated with increased GSTs activity, indicating activation of oxidative stress response pathways, while showing different effects on PCC. TRE was related with a significant decrease in PCC (0.74 ± 0.07 nmol·μg^{-1} of protein, $p < 0.001$), in contrast to VC, which resulted in higher PCC values (4.93 ± 0.28 nmol· μg^{-1} of protein, n.s.). This difference may be related to the distinct role of TRE in

intracellular osmoregulation and protection against desiccation, which can indirectly reduce oxidative protein damage by stabilizing cellular structures and functions [129]. GA was associated with the highest GSTs activity, reaching 0.42 ± 0.05 $\mu mol \cdot min^{-1} \cdot mg^{-1}$ of protein ($p < 0.001$) In the presence of CS, a reduction in GSTs activity and PCC was observed, indicating a protective effect under the applied conditions. Overall, TRE was associated with increased metabolic activity together with reduced oxidative protein damage, whereas VC increased metabolic activity without a corresponding reduction in oxidative stress markers. Other PPAs, showed relatively limited effects on a cellular redox balance and viability.

Lacticaseibacillus paracasei

As shown in Table 7 for *L. paracasei*, TRE and VC exhibited contrasting effects on stress markers. TRE was related with reduced protein oxidation, as showed by decreased PCC, whereas VC resulted in increased PCC despite increased GSTs activity. In contrast, treatment with MD and IN resulted in reductions in GSTs activity (0.14 ± 0.02 and 0.14 ± 0.01 $\mu mol \cdot min^{-1} \cdot mg^{-1}$ of protein, respectively, $p < 0.001$ for both) and PCC (1.03 ± 0.03 and 0.90 ± 0.06 $nmol \cdot \mu g^{-1}$ of protein, respectively; $p < 0.001$ for both), showing a more balanced stress levels under the tested conditions. GA was associated with a modest increase in GSTs activity without significant changes in PCC. CS exhibited a protective effect characterized by reduced both stress indicators. Overall, TRE was associated with reduced protein damage together with increased metabolic activity, indicating a protective response in *L. paracasei*. In contrast, VC exhibited pro-oxidant tendencies, showed by increased PCC (the highest from tested PPAs). The combined reduction of GSTs activity and PCC observed for MD and IN suggests favorable effects on cellular redox balance and viability in *L. paracasei* under the applied conditions [142].

Strain-specific stress responses contribute to the observed differences, reflecting variability in detoxification capacity and metabolic regulation. Certain PPAs appear to stimulate metabolic processes, resulting in increased GSTs activity as part of an adaptive response to oxidative challenge, without leading to protein oxidation. These observations suggest that activation of antioxidant defense mechanisms may occur as a cellular response to anticipated oxidative stress rather than only as a consequence of protein damage.

Table 7. Results of GSTs activity and protein carbonyl content (PCC) for *L. plantarum*, *L. rhamnosus*, and *L. paracasei* exposed to trehalose (TRE), vitamin C (VC), maltodextrin (MD), monosodium glutamate (MSG), inulin (IN), gum arabic (GA), and corn starch (CS). The control sample (CTRL) represents free (untreated) cells. Data are expressed as mean ± standard deviation. Comparisons without asterisks are not statistically significant (n.s.). Statistical significance: (*) $p < 0.05$; (**) $p < 0.01$; (***) $p < 0.001$.

	L. plantarum		***L. rhamnosus***		***L. paracasei***	
	GSTs activity ($\mu mol \cdot min^{-1} \cdot mg^{-1}$ of protein)	**PCC ($nmol \cdot \mu g^{-1}$ of protein)**	**GSTs activity ($\mu mol \cdot min^{-1} \cdot mg^{-1}$ of protein)**	**PCC ($nmol \cdot \mu g^{-1}$ of protein)**	**GSTs activity ($\mu mol \cdot min^{-1} \cdot mg^{-1}$ of protein)**	**PCC ($nmol \cdot \mu g^{-1}$ of protein)**
CTRL	0.15 ± 0.01	0.78 ± 0.05	0.30 ± 0.02	4.75 ± 0.11	0.20 ± 0.01	2.95 ± 0.17
TRE	0.24 ± 0.02 (***)	5.69 ± 0.14 (***)	0.39 ± 0.02 (***)	0.74 ± 0.07 (***)	0.11 ± 0.01 (***)	1.95 ± 0.28 (***)
VC	0.04 ± 0.01 (***)	5.09 ± 0.43 (***)	0.39 ± 0.01 (***)	4.93 ± 0.28 (n.s.)	0.10 ± 0.01 (***)	4.62 ± 0.25 (***)
MD	0.14 ± 0.01 (n.s.)	0.75 ± 0.06 (n.s.)	0.28 ± 0.02 (n.s.)	2.73 ± 0.26 (***)	0.14 ± 0.02 (***)	1.03 ± 0.03 (***)
MSG	0.16 ± 0.01 (n.s.)	0.75 ± 0.04 (n.s.)	0.37 ± 0.04 (***)	3.37 ± 0.19 (***)	0.20 ± 0.01 (n.s.)	3.72 ± 0.23 (***)
IN	0.16 ± 0.01 (n.s.)	0.65 ± 0.07 (n.s.)	0.25 ± 0.02 (**)	3.20 ± 0.08 (***)	0.14 ± 0.01 (***)	0.90 ± 0.06 (***)
GA	0.25 ± 0.01 (***)	0.68 ± 0.07 (n.s.)	0.42 ± 0.05 (***)	2.61 ± 0.01 (***)	0.23 ± 0.01 (***)	3.06 ± 0.29 (n.s.)
CS	0.18 ± 0.03 (*)	1.26 ± 0.06 (**)	0.13 ± 0.01 (***)	0.45 ± 0.04 (***)	0.18 ± 0.01 (**)	1.90 ± 0.30 (***)

1.4. Morphological and topographical characterization

Atomic force microscopy was used to characterize cell surface roughness (Ra), topography, and cell dimensions. AFM analysis allowed evaluation of whether exposure to PPAs was associated with protective adaptation or stress-related damage.

AFM imaging (Figures 21-23) revealed clear topographical differences among *Lactobacillus* strains exposed to individual PPAs.

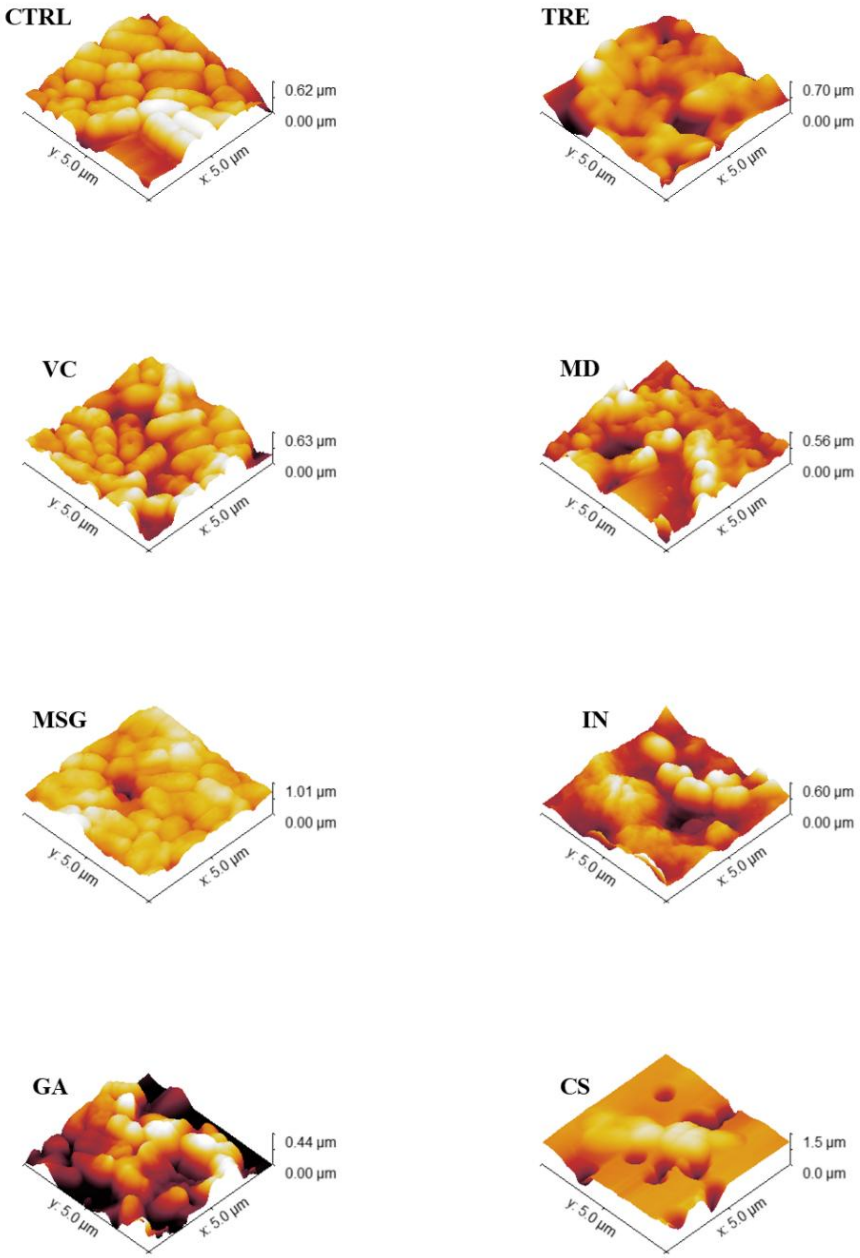

Figure 21. Representative AFM images illustrating the topography of *L. plantarum* after exposure to trehalose (TRE), vitamin C (VC), maltodextrin (MD), monosodium glutamate (MSG), inulin (IN), gum arabic (GA), and corn starch (CS). The control sample (CTRL) represents free (untreated) cells.

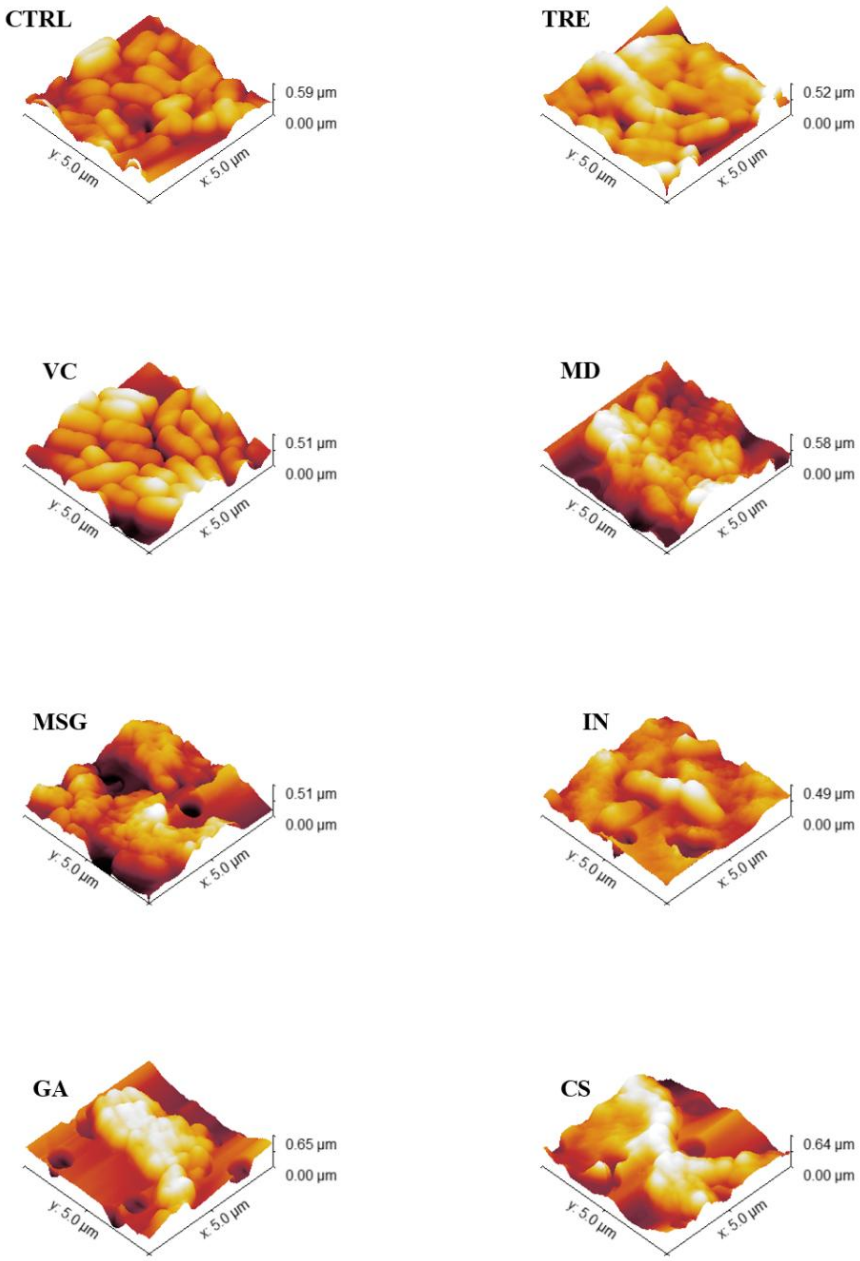

Figure 22. Representative AFM images illustrating the topography of *L. rhamnosus* after exposure to trehalose (TRE), vitamin C (VC), maltodextrin (MD), monosodium glutamate (MSG), inulin (IN), gum arabic (GA), and corn starch (CS). The control sample (CTRL) represents free (untreated) cells.

Control cells exhibited relatively smooth surfaces with minor undulations, consistent with typical bacterial morphology. Exposure to TRE caused surface smoothing in *L. plantarum*, whereas surface disruptions were observed in *L. rhamnosus* and *L. paracasei*. Compared to the CTRL, treatment with VC resulted in a more granular and non-uniform surface appearance. MD induced increased surface irregularity accompanied by cell aggregation, while MSG and IN caused only minor surface alterations. GA was associated with surface coating across all tested strains, whereas CS resulted in pronounced surface disruption.

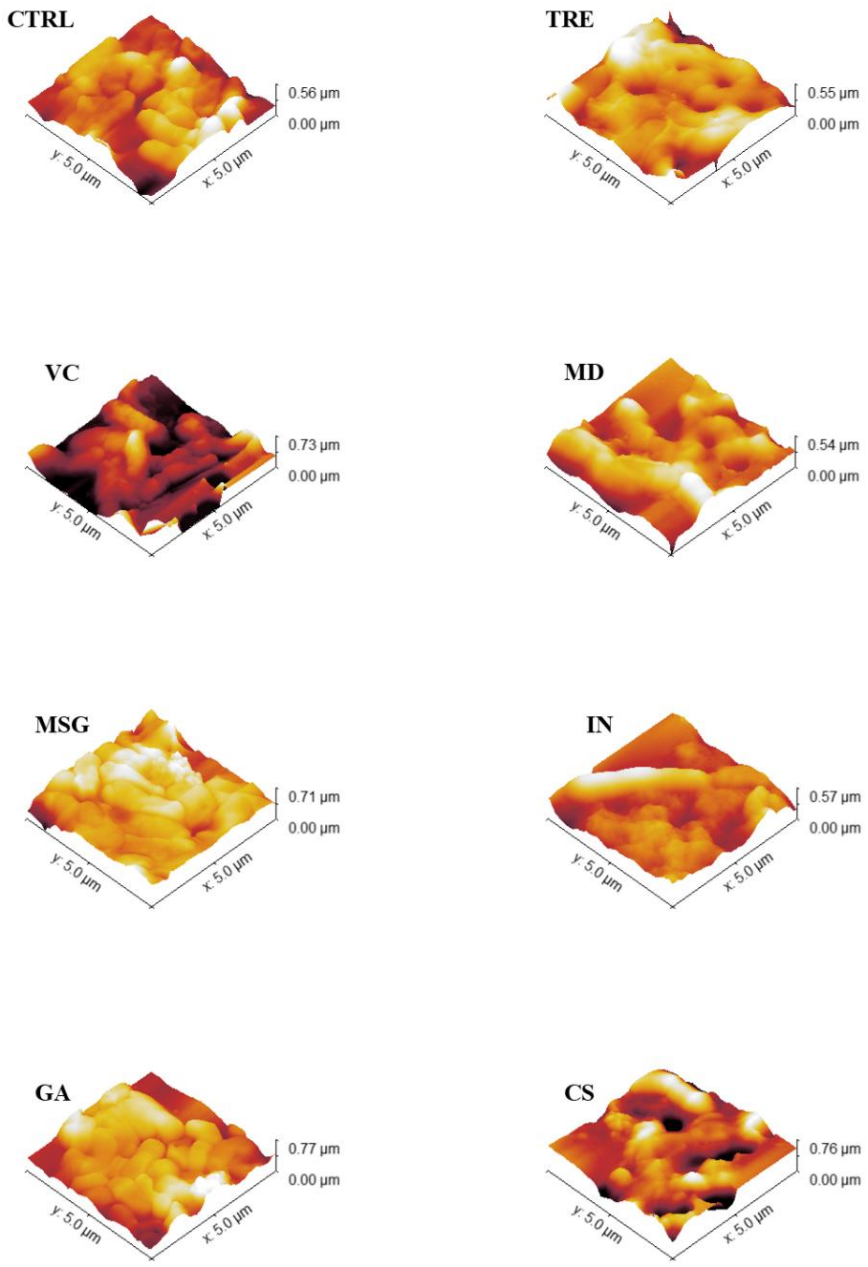

Figure 23. Representative AFM images illustrating the topography of *L. paracasei* after exposure to trehalose (TRE), vitamin C (VC), maltodextrin (MD), monosodium glutamate (MSG), inulin (IN), gum arabic (GA), and corn starch (CS). The control sample (CTRL) represents free (untreated) cells.

AFM analysis revealed changes in Ra of *L. plantarum* after exposure to selected PPAs (Table 8). Control cells reached an Ra value of 4.91 ± 0.22 nm, whereas treatment with TRE resulted in a significant reduction to 3.00 ± 0.51 nm ($p < 0.001$). This decrease indicates surface smoothing and may reflect a protective response associated with surface stabilization or mitigation of stress-related roughness [143]. In contrast, exposure to VC and GA resulted in increased Ra values of 7.90 ± 0.23 and 7.91 ± 0.64 nm, respectively ($p < 0.001$ for both), indicating changed surface properties relative to the CTRL. Exposure to PPAs also affected

bacterial cell dimensions (Table 8). In *L. plantarum*, treatment with TRE resulted in significant increases in cell length (1.45 ± 0.18 μm, $p < 0.001$) and width (0.80 ± 0.10 μm, $p < 0.001$). In contrast, MD and CS were associated with reduced cell length, producing a more compact cell morphology, whereas VC, MSG, and GA did not result in statistically significant changes in cell size. These morphological changes, including surface smoothing, elongation, or compaction, are consistent with adaptive responses to osmotic or environmental stress and could influence the survival and functional properties of *L. plantarum* under the tested conditions [144].

Treatment with TRE resulted in a significant decrease in the Ra value of *L. rhamnosus* to 1.95 ± 0.18 nm ($p < 0.001$), indicating surface smoothing relative to the CTRL. In contrast, exposure to VC, MSG, IN, GA, and CS resulted in increased Ra values, with GA showing the most pronounced effect, reaching 7.94 ± 0.26 nm ($p < 0.001$). As shown in Table 8, treatment with TRE, VC, and IN was related with increased cell length in *L. rhamnosus*, indicating elongation under the tested conditions. Changes in cell width were also observed, including slight reductions after TRE and MSG treatment and a marked increase in the presence of IN. The increased Ra values observed in *L. rhamnosus* after exposure to selected PPAs may indicate a stress response associated with structural surface adaptations. In contrast, surface smoothing observed under other conditions is consistent with a stabilizing effect on the cell envelope. Changes in cell size and surface features may therefore represent adaptive responses to environmental pressure [143,145].

Treatment with MD and IN resulted in a significant reduction of Ra in *L. paracasei* to 1.62 ± 0.17 and 1.60 ± 0.25 nm, respectively ($p < 0.001$ for both). This surface smoothing is consistent with a stabilizing effect on the cell envelope, which may contribute to increased cellular resilience through improved organization of surface proteins and lipid membranes. Such stabilization can influence adhesion properties and other surface functions of probiotic cells. In contrast, exposure to VC resulted in a significant increase in Ra (7.34 ± 0.20 nm, $p < 0.001$), indicating major change in surface characteristics relative to the CTRL. As shown in Table 8, treatment with IN was associated with increased cell length and width, indicating cell elongation and swelling under the tested conditions. Exposure to VC and GA was also associated with increased cell length, whereas CS resulted in reduced cell dimensions, indicating a more compact cell morphology. These morphological responses are consistent with strain-specific adaptive strategies to stress [143,145].

Table 8. Results of cell dimensions and cell surface roughness (Ra) for *Lactobacillus* strains exposed to trehalose (TRE), vitamin C (VC), maltodextrin (MD), monosodium glutamate (MSG), inulin (IN), gum arabic (GA), and corn starch (CS). The control sample (CTRL) represents free (untreated) cells. Data are expressed as mean ± standard deviation. Comparisons without asterisks are not statistically significant (n.s.). Statistical significance: (*) $p < 0.05$; (**) $p < 0.01$; (***) $p < 0.001$.

	Cell dimensions (µm) and cell surface roughness – Ra (nm)								
	L. plantarum			***L. rhamnosus***			***L. paracasei***		
	Cell length	**Cell width**	**Ra**	**Cell length**	**Cell width**	**Ra**	**Cell length**	**Cell width**	**Ra**
CTRL	1.18 ± 0.09	0.65 ± 0.10	4.91 ± 0.22	1.17 ± 0.09	0.59 ± 0.07	3.23 ± 0.22	2.04 ± 0.25	0.63 ± 0.10	4.38 ± 0.23
TRE	1.45 ± 0.18 (***)	0.80 ± 0.10 (***)	3.00 ± 0.51 (***)	1.31 ± 0.10 (***)	0.54 ± 0.05 (*)	1.95 ± 0.18 (***)	1.99 ± 0.25 (n.s.)	0.68 ± 0.07 (n.s.)	2.63 ± 0.08 (***)
VC	1.25 ± 0.15 (n.s.)	0.63 ± 0.09 (n.s.)	7.90 ± 0.23 (***)	1.29 ± 0.09 (***)	0.60 ± 0.08 (n.s.)	5.12 ± 0.15 (***)	1.66 ± 0.13 (***)	0.67 ± 0.08 (n.s.)	7.34 ± 0.20 (***)
MD	1.03 ± 0.19 (**)	0.48 ± 0.09 (***)	6.75 ± 0.34 (***)	1.00 ± 0.10 (***)	0.49 ± 0.10 (***)	4.83 ± 0.20 (***)	1.34 ± 0.14 (***)	0.63 ± 0.09 (n.s.)	1.62 ± 0.17 (***)
MSG	1.20 ± 0.20 (n.s.)	0.66 ± 0.09 (n.s.)	5.37 ± 0.60 (***)	1.18 ± 0.10 (n.s.)	0.53 ± 0.06 (*)	6.19 ± 0.24 (***)	1.44 ± 0.16 (***)	0.62 ± 0.09 (n.s.)	2.89 ± 0.37 (***)
IN	0.94 ± 0.18 (***)	0.58 ± 0.09 (*)	6.14 ± 0.27 (***)	1.88 ± 0.15 (***)	0.68 ± 0.09 (**)	6.15 ± 0.23 (***)	2.34 ± 0.18 (***)	0.72 ± 0.13 (**)	1.60 ± 0.25 (***)
GA	1.14 ± 0.15 (n.s.)	0.62 ± 0.07 (n.s.)	7.91 ± 0.64 (***)	0.99 ± 0.12 (***)	0.45 ± 0.08 (***)	7.94 ± 0.26 (***)	1.67 ± 0.16 (***)	0.58 ± 0.12 (n.s.)	3.19 ± 0.32 (***)
CS	0.97 ± 0.11 (**)	0.50 ± 0.06 (***)	7.15 ± 0.26 (***)	0.97 ± 0.12 (***)	0.44 ± 0.06 (***)	6.96 ± 0.20 (***)	0.86 ± 0.06 (***)	0.41 ± 0.04 (***)	2.39 ± 0.19 (***)

AFM analysis showed that exposure to TRE and IN was associated with reduced Ra values across all tested *Lactobacillus* strains, indicating a consistent surface smoothing effect under the applied conditions. In contrast, treatment with VC resulted in increased Ra values across strains, consistent with changed surface properties. CS was associated with reduced cell length, indicating an effect on cell morphology. To support the AFM observations, selected samples (CTRL, TRE, VC, and GA) were further examined using TEM (Figures 24-26).

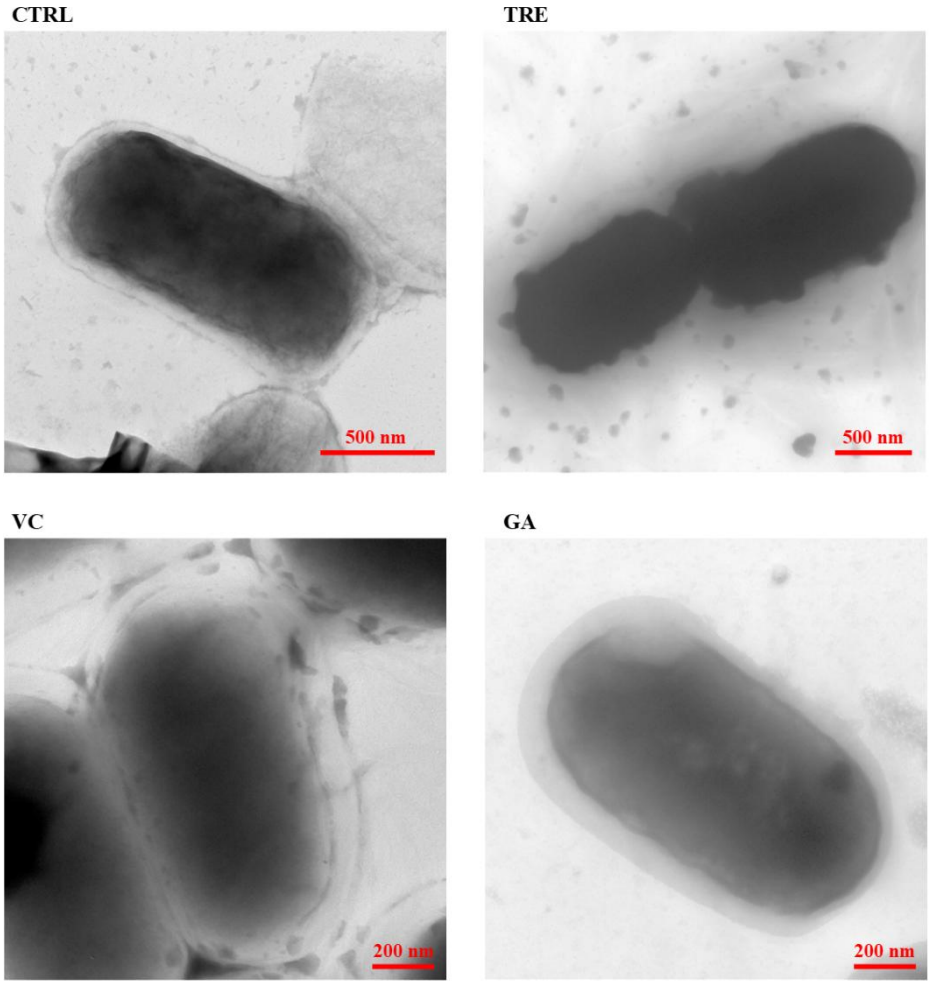

Figure 24. Representative TEM images illustrating the topography of *L. plantarum* after exposure to trehalose (TRE), vitamin C (VC), and gum arabic (GA). The control sample (CTRL) represents free (untreated) cells.

AFM and TEM analyses revealed consistent effects of PPAs on bacterial cell morphology. In the case of *L. plantarum*, TEM images showed cellular integrity after exposure to TRE, which is consistent with the surface profiles observed by AFM. In contrast, AFM and TEM analyses of *L. rhamnosus* and *L. paracasei* suggested that TRE treatment was associated with surface and structural changes under the applied conditions. Samples treated with VC showed

features in TEM images of cellular stress or damage, including cell aggregation and irregular structural appearance. These observations are consistent with the increased surface roughness and irregularity detected by AFM. Conversely, AFM and TEM observations showed that GA treatment was not associated with adverse effects on bacterial cell integrity under the tested conditions.

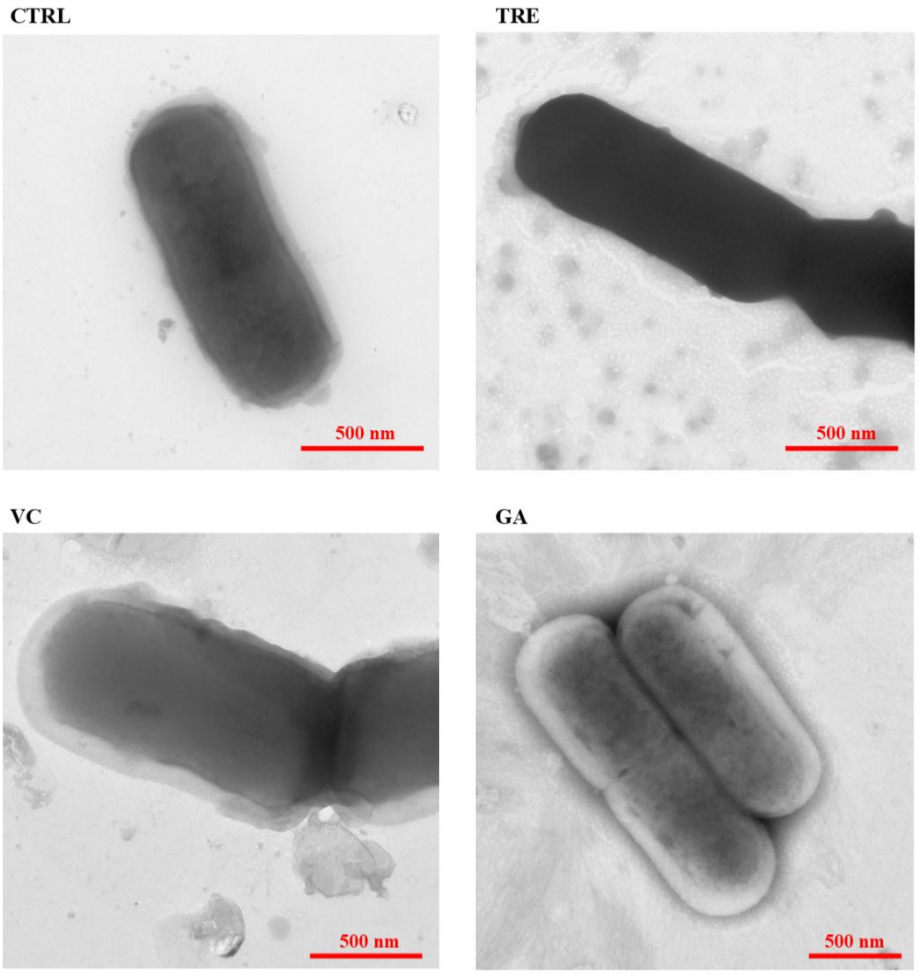

Figure 25. Representative TEM images illustrating the topography of *L. rhamnosus* after exposure to trehalose (TRE), vitamin C (VC), and gum arabic (GA). The control sample (CTRL) represents free (untreated) cells.

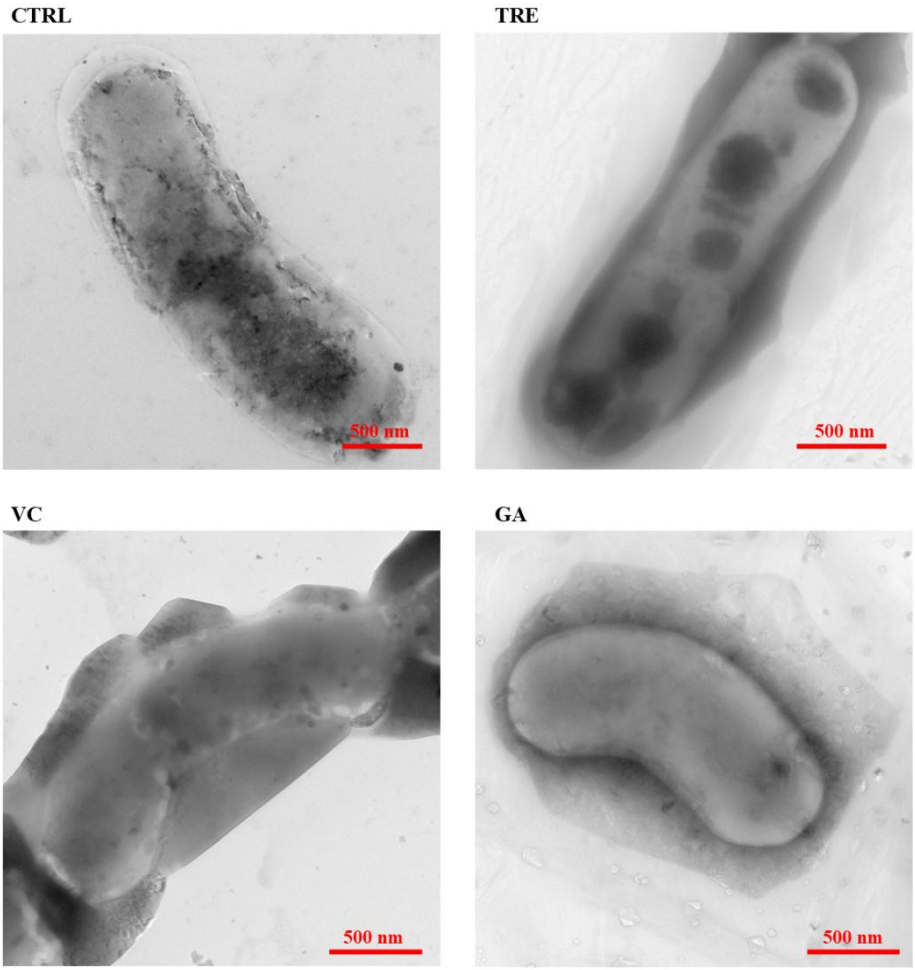

Figure 26. Representative TEM images illustrating the topography of *L. paracasei* after exposure to trehalose (TRE), vitamin C (VC), and gum arabic (GA). The control sample (CTRL) represents free (untreated) cells.

1.5. Stability of bacterial suspensions

Assessment of zeta potential and particle size distribution (PSD) provides insight into how PPAs influence the stability and physicochemical behavior of bacterial suspensions.

Lactiplantibacillus plantarum

As shown in Table 9, compared with CTRL, treatment with VC and CS resulted in a shift of the zeta potential of *L. plantarum* toward less negative values, reaching -9.39 ± 0.25 and -13.06 ± 0.66 mV, respectively ($p < 0.001$ for both). These results indicate changes in surface charge density that may influence suspension stability by modifying cell-cell interactions within the medium. In contrast, exposure to IN resulted in a significant shift toward more negative zeta potential values (-34.80 ± 0.95 mV, $p < 0.001$), consistent with enhanced suspension stability associated with increased electrostatic repulsion between cells. Such stabilization is relevant

for maintaining uniform dispersions, which contributes to consistent functional performance of probiotic suspensions under applied conditions [146]. Minimal changes in zeta potential were observed after treatment with TRE, MSG, and GA, indicating a neutral effect on the suspension stability of *L. plantarum*.

Table 9. Results of zeta potential measurements for *Lactobacillus* strains exposed to trehalose (TRE), vitamin C (VC), maltodextrin (MD), monosodium glutamate (MSG), inulin (IN), gum arabic (GA), and corn starch (CS). The control sample (CTRL) represents free (untreated) cells. Comparisons without asterisks are not statistically significant (n.s.). Statistical significance: (*) $p < 0.05$; (**) $p < 0.01$; (***) $p < 0.001$.

	Zeta potential (mV)		
	L. plantarum	***L. rhamnosus***	***L. paracasei***
CTRL	-30.33 ± 1.33	-29.67 ± 1.67	-26.21 ± 1.88
TRE	-29.79 ± 1.39 (n.s.)	-28.01 ± 1.09 (**)	-16.40 ± 0.99 (***)
VC	-9.39 ± 0.25 (***)	-21.68 ± 0.98 (***)	-4.40 ± 0.37 (***)
MD	-18.06 ± 1.78 (***)	-19.05 ± 1.40 (***)	-11.33 ± 0.56 (***)
MSG	-31.33 ± 3.20 (*)	-33.99 ± 1.12 (***)	-29.58 ± 0.85 (***)
IN	-32.15 ± 3.32 (***)	-33.83 ± 0.84 (***)	-17.10 ± 1.28 (***)
GA	-29.23 ± 1.32 (**)	-30.18 ± 1.24 (n.s.)	-22.32 ± 0.82 (***)
CS	-13.06 ± 0.66 (***)	-19.44 ± 1.69 (***)	-9.20 ± 0.94 (***)

Results of PSD analysis (Figure 27) provided additional insight into suspension homogeneity of *L. plantarum*, and revealed different effects for TRE and VC. TRE treatment was related with a reduction in particle size accompanied by an increase in PDI (1106 nm, 0.30 ± 0.04), indicating increased variability within the suspension. In contrast, VC increased both particle size and PDI (1484 nm, 0.50 ± 0.07), consistent with reduced homogeneity and the presence of larger aggregates. MSG was related with improved suspension uniformity, characterized by a narrower size distribution (1281 nm, 0.16 ± 0.02). In contrast, GA resulted in increased particle size and PDI, indicating reduced suspension homogeneity. The most clear aggregation

was observed after CS treatment, which led to increased particle size and PDI values (2305 nm, 0.90 ± 0.05), indicating a highly heterogeneous suspension.

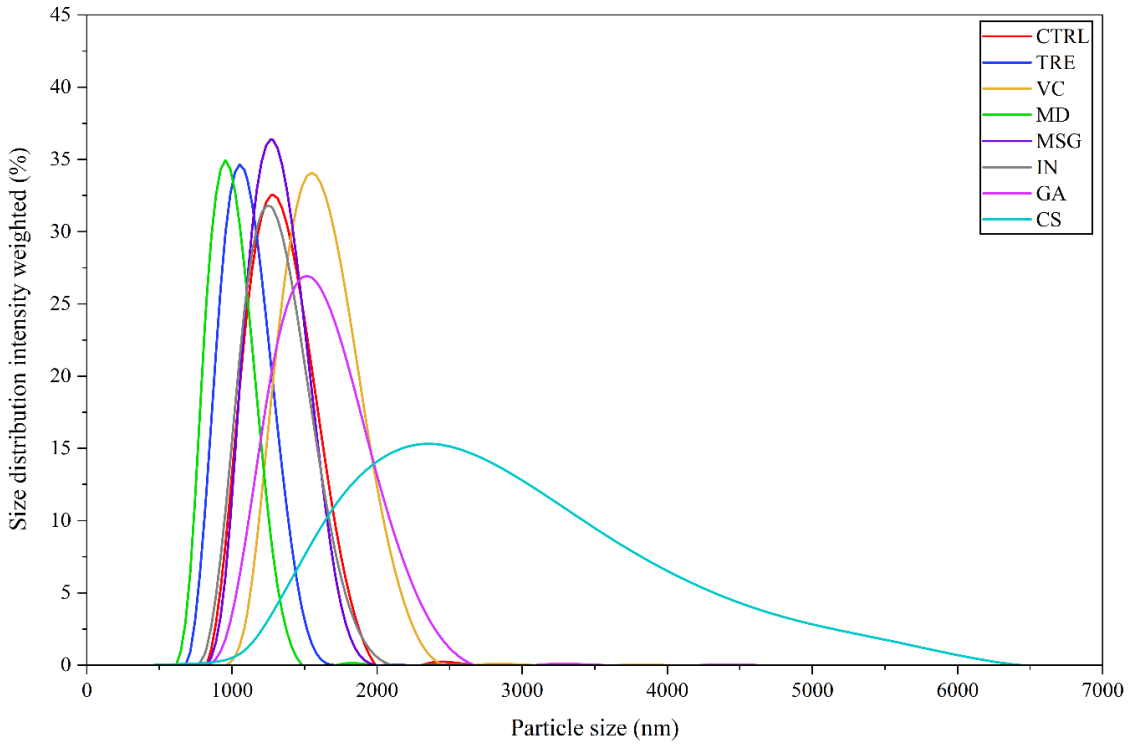

Figure 27. Results of particle size distribution for *L. plantarum* exposed to trehalose (TRE), vitamin C (VC), maltodextrin (MD), monosodium glutamate (MSG), inulin (IN), gum arabic (GA), and corn starch (CS). The control sample (CTRL) represents free (untreated) cells.

Lacticaseibacillus rhamnosus

As shown in Table 9, compared with CTRL, treatment with VC and MD resulted in a shift of the zeta potential of *L. rhamnosus* toward less negative values, reaching -21.68 ± 0.98 and -19.05 ± 1.40 mV, respectively ($p < 0.001$ for both), indicating reduced electrostatic repulsion between cells. In contrast, treatment with MSG and IN resulted in a shift toward more negative zeta potential values (-33.99 ± 1.12 and -33.83 ± 0.84 mV, respectively; $p < 0.001$ for both), indicating increased electrostatic repulsion and a reduced tendency toward aggregation. This observation is consistent with the established relationship between higher absolute zeta potential values and increased suspension stability [146].

According to Figure 28, exposure to TRE and MD was associated with reduced particle size of *L. rhamnosus* suspensions (955.4 nm), accompanied by low PDIs (0.16 ± 0.03 and 0.14 ± 0.03, respectively), indicating a more uniform PSD. GA also reduced particle size to 1106 nm with a PDI of 0.17 ± 0.01, further indicating improved suspension homogeneity [147].

In contrast, treatment with VC and CS resulted in increased particle size to 1718 nm, with corresponding increases in PDI values to 0.64 ± 0.20 and 0.87 ± 0.09, respectively, indicating aggregation and reduced homogeneity of the suspension.

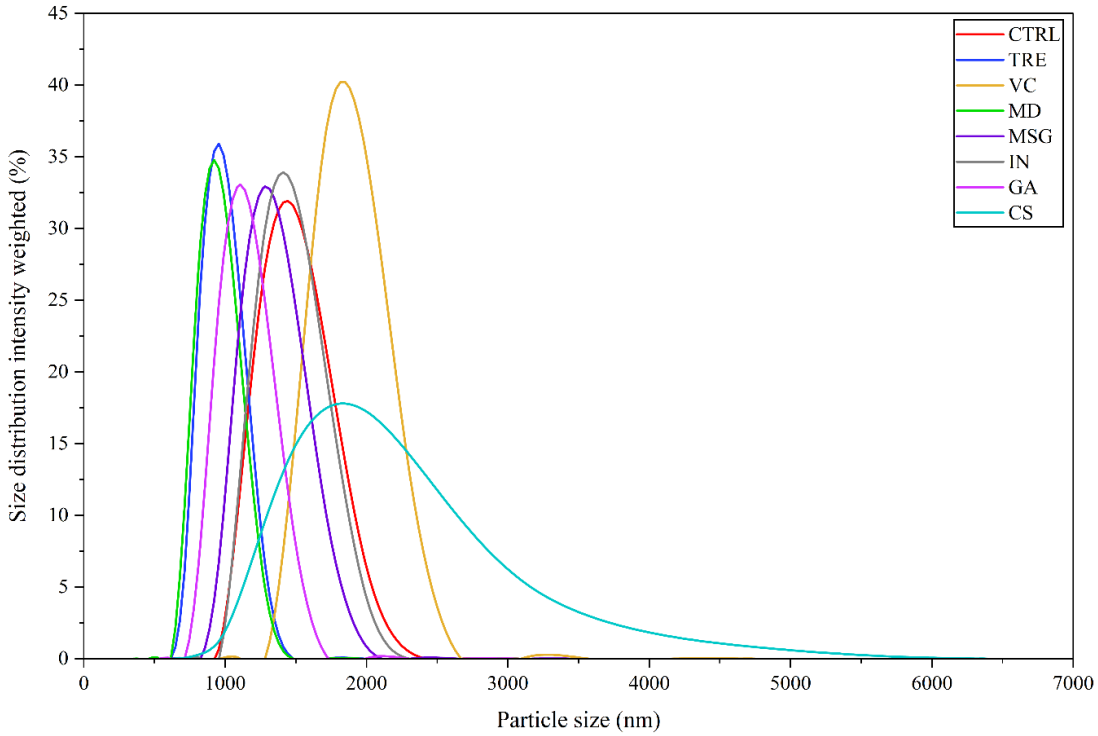

Figure 28. Results of particle size distribution for *L. rhamnosus* exposed to trehalose (TRE), vitamin C (VC), maltodextrin (MD), monosodium glutamate (MSG), inulin (IN), gum arabic (GA), and corn starch (CS). The control sample (CTRL) represents free (untreated) cells.

Lacticaseibacillus paracasei

As shown in Table 9, compared with CTRL, treatment with VC and CS resulted in a shift of the zeta potential of *L. paracasei* toward less negative values, with VC showing the strongest effect (-4.40 ± 0.37 mV, $p < 0.001$). This shift indicates altered electrostatic conditions that may increase the tendency toward aggregation and influence suspension stability under the tested conditions. In contrast, MSG shifted the zeta potential toward more negative values (-29.58 ± 0.85 mV, $p < 0.001$), indicating enhanced electrostatic repulsion and improved suspension stability.

The PSD analysis (Figure 29) for *L. paracasei* showed that TRE was related with a reduction in particle size to 1281 nm, together with an increase in PDI to 0.53 ± 0.08, indicating increased heterogeneity within the suspension. Treatment with VC resulted in increased particle size (2669 nm) and PDI (0.88 ± 0.06), consistent with a higher degree of aggregation. In contrast,

MD and MSG were associated with improved suspension uniformity, with MD showing a clear effect by reducing particle size to 1106 nm and lowering PDI to 0.21 ± 0.04. These observations are consistent with reports describing the stabilizing role of carbohydrate-based additives in suspension systems [147–149]. For CS, a reduction in particle size to 825 nm was observed. However, this was together with a high PDI value (0.72 ± 0.01), indicating substantial heterogeneity. This pattern highlights the complex relationship between particle size and suspension stability, showing that reduced particle size does not necessarily correspond to improved homogeneity or functional stability.

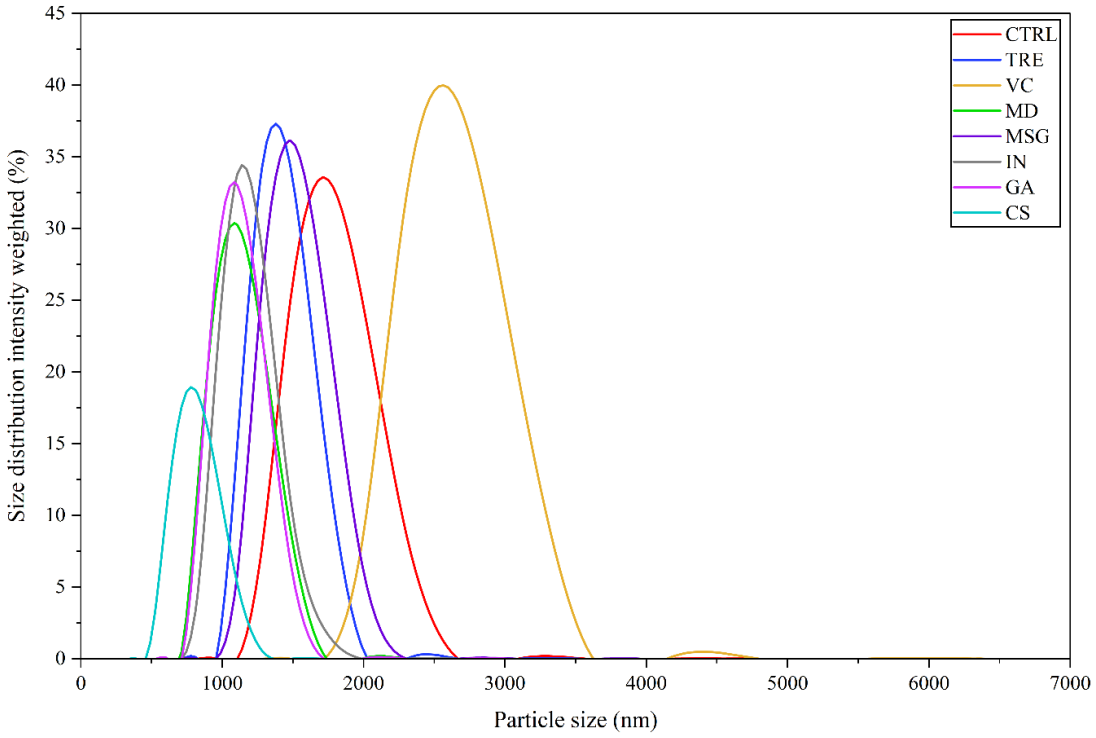

Figure 29. Results of particle size distribution for *L. paracasei* exposed to trehalose (TRE), vitamin C (VC), maltodextrin (MD), monosodium glutamate (MSG), inulin (IN), gum arabic (GA), and corn starch (CS). The control sample (CTRL) represents free (untreated) cells.

Comparison of zeta potential and PSD shows that electrostatic interactions and surface properties vary depending on the composition of the *Lactobacillus* cell envelope. Differences in hydrodynamic behavior and aggregation tendencies were observed, especially in the destabilizing effect of VC on *L. paracasei* suspensions. In contrast, MSG was associated with reduced particle size and improved suspension homogeneity, showing a stabilizing effect under the tested conditions. Divergent responses observed for other PPAs, including IN and GA, indicate that interactions between PPAs and probiotic cells are highly strain-dependent.

1.6. Summary and selection of PPAs for hydrogel formulations

Across the three *Lactobacillus* strains, multi-assay screening showed consistent yet strain-specific patterns in the way PPAs modulated bacterial physiology. TRE was consistently related with increased metabolic activity and maintenance of a high proportion of active cells, together with surface smoothing in *L. plantarum*, reduced membrane permeability, and decreased surface hydrophobicity. Together, these features indicate increased stability of the cell envelope under the tested conditions. VC increased metabolic activity but was often associated with increased oxidative stress indicators or other stress responses, indicating that its effects are strongly dependent on concentration and strain. MD and MSG were generally associated with improved suspension stability and cell viability. CS showed protective effects in individual assays but was also associated with reduced suspension stability. IN elicited mixed responses at the single cell level in *L. plantarum*, while improving suspension stability and showing comparatively favorable oxidative stress profiles. GA consistently reduced surface hydrophobicity without detectable changes in membrane permeability. Overall, these results indicate that evaluation of PPAs requires a multiple parameter approach, as individual metrics alone do not fully capture their complex, strain-dependent effects on probiotic cell physiology.

Based on the combined performance observed across the applied assays and the functional rationale for protective matrix design, TRE, IN, and GA were selected for further development of hydrogel-based formulations. TRE was selected due to its consistent association with preservation of cellular function and cell envelope stability. IN was chosen for its dual role as a synbiotic component and a physicochemical stabilizer. GA was selected because of its film-forming properties and compatibility with alginate, supporting reinforcement of hydrogel bead structure. Moreover, *L. plantarum* was selected as the model strain for next encapsulation studies based on its robust growth characteristics, balanced response across viability and stability parameters, and favorable cell envelope properties observed during the screening studies.

Specific research aim (A) is fully achieved here. This stage provided a link between the initial exploratory phase and following formulation development by identifying additives that support probiotic cell performance. In this context, the outcomes of the screening are consistent with the overall objective of the dissertation and support the formulated research hypothesis.

2. PERFORMANCE OF HYDROGEL-BASED PROBIOTIC FORMULATIONS

This stage focused on evaluating the functional performance of alginate-based hydrogel beads as protective carriers for *L. plantarum*. Alginate beads were prepared with the addition of gum arabic (GA) or psyllium husk (PH). The aim was to assess how hydrogel matrix composition and the incorporation of selected prebiotic components (inulin – IN, trehalose – TRE, and their mixture – IN/TRE) influence probiotic viability, membrane integrity, and physicochemical stability. The analyses compared encapsulated cells with non-encapsulated control sample to evaluate the protective effect of the hydrogel environment and to determine whether the developed synbiotic matrices support improved cell survival and maintenance of structural integrity under the tested conditions.

The following abbreviations were used for the samples:

- CTRL – non-encapsulated probiotic cells,
- PH-IN – alginate probiotic beads with the addition of psyllium husk and with the incorporation of inulin,
- PH-TRE – alginate probiotic beads with the addition of psyllium husk and with the incorporation of trehalose,
- PH-IN/TRE – alginate probiotic beads with the addition of psyllium husk and with the incorporation of the mixture of inulin and trehalose,
- GA-IN – alginate probiotic beads with the addition of gum arabic and with the incorporation of inulin,
- GA-TRE – alginate probiotic beads with the addition of gum arabic and with the incorporation of trehalose,
- GA-IN/TRE – alginate probiotic beads with the addition of gum arabic and with the incorporation of the mixture of inulin and trehalose.

2.1. Viability and metabolic assessment

This stage evaluated whether alginate-based hydrogels provide a more supportive microenvironment for *L. plantarum* compared with non-encapsulated cells. Metabolic activity was assessed by the MTT assay, potential cytotoxicity by the AlamarBlue (AB) assay, and viable cell numbers by plate count method.

As shown in Figure 30, all tested alginate-based hydrogels were associated with a statistically significant increase in metabolic activity of *L. plantarum* compared with the non-encapsulated

control cells. The highest increases were observed for GA-reinforced beads. For GA-TRE, GA-IN, and GA-IN/TRE formulations, MRU values reached 0.89 ± 0.01, 0.85 ± 0.02, and 0.77 ± 0.01, respectively ($p < 0.001$ for all). PH-reinforced beads also showed significantly increased metabolic activity, although to a lesser extent, with MRU values of 0.30 ± 0.01 for PH-TRE, 0.30 ± 0.01 for PH-IN/TRE, and 0.26 ± 0.01 for PH-IN ($p < 0.001$ for all).

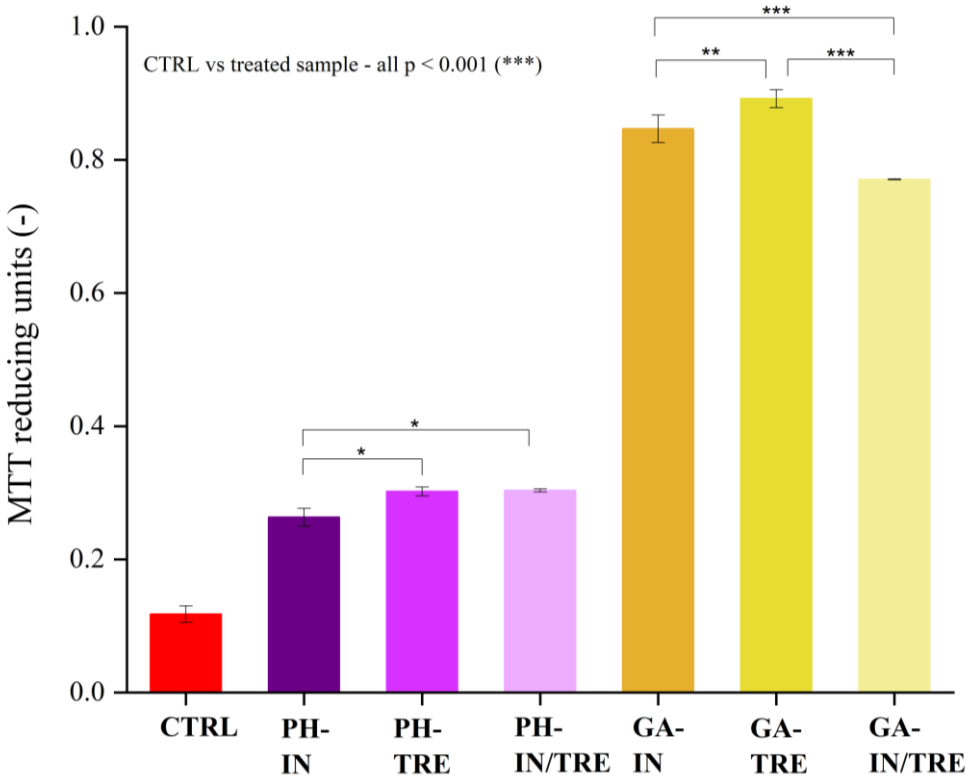

Figure 30. Results of metabolic activity (MTT reducing units – MRU) for *L. plantarum* cells encapsulated in alginate beads with the addition of gum arabic (GA) or psyllium husk (PH), and with the incorporation of selected prebiotic components (inulin – IN, trehalose – TRE, and their mixture – IN/TRE). The control sample (CTRL) represents non-encapsulated cells. Statistical significance: (*) $p < 0.05$; (**) $p < 0.01$; (***) $p < 0.001$.

Because the MTT signal in bacterial cells reflects NAD(P)H-dependent tetrazolium reduction mediated by cellular oxidoreductases, increased MRU values indicate elevated redox-related metabolic activity within the hydrogel environment, particularly in GA-based matrices [150]. Differences between formulations may be related to matrix composition and water-structuring properties of TRE and IN, which can influence the microenvironment surrounding encapsulated cells [151]. The higher MRU values observed for GA-based hydrogels are consistent with the film-forming characteristics of GA, which can promote moisture retention and formation of stable interfacial layers within the beads [90]. In contrast, PH-based hydrogels formed a more

viscous, water-binding network, which may limit diffusion and moderate metabolic activity, resulting in lower but still statistically significant increases in MTT signal [152].

AlamarBlue responses differed between the tested hydrogel matrix types (Figure 31). Relative to the non-encapsulated CTRL, PH-based beads showed significantly higher AlamarBlue reduction, reaching 191.38 ± 3.77% for PH-IN, 186.46 ± 0.03% for PH-TRE, and 206.88 ± 7.84% for PH-IN/TRE ($p < 0.001$ for all). In contrast, GA-based beads exhibited significantly lower AB reduction values, with 15.90 ± 0.32% for GA-IN, 24.52 ± 0.26% for GA-TRE, and 9.12 ± 0.19% for GA-IN/TRE ($p < 0.001$ for all).

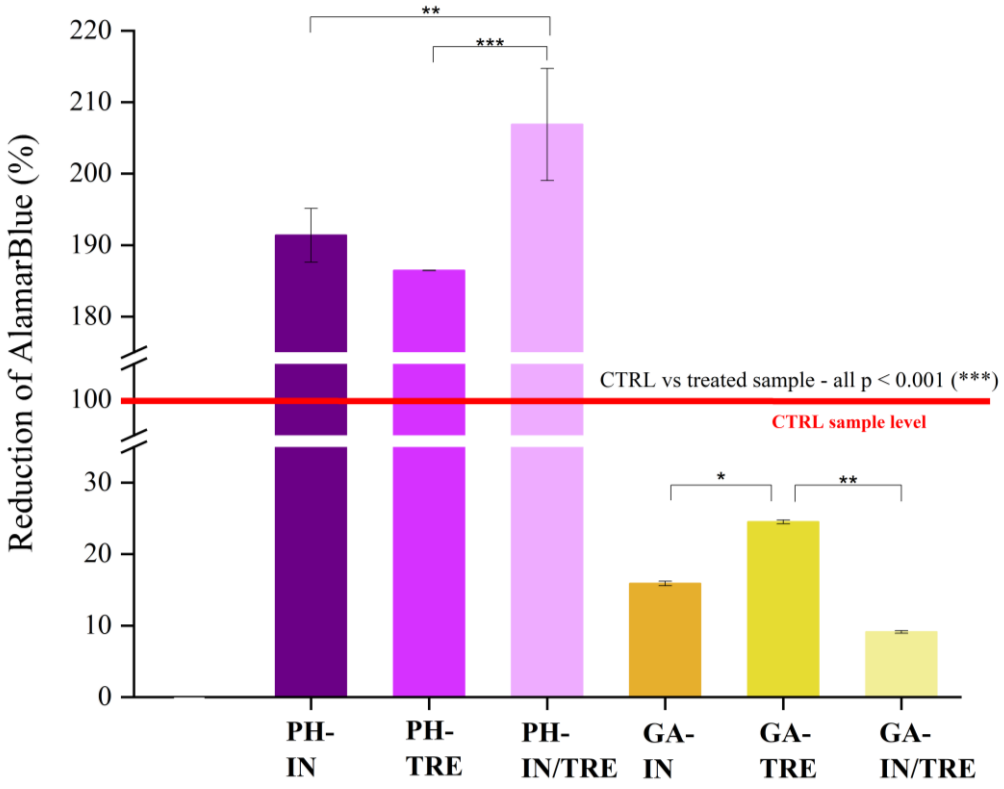

Figure 31. Results of cytotoxicity for *L. plantarum* cells encapsulated in alginate beads with the addition of gum arabic (GA) or psyllium husk (PH), and with the incorporation of selected prebiotic components (inulin – IN, trehalose – TRE, and their mixture – IN/TRE). The control sample (CTRL) represents non-encapsulated cells. Statistical significance: (*) $p < 0.05$; (**) $p < 0.01$; (***) $p < 0.001$.

In bacterial systems, the AB assay reflects cellular reductase activity and dye accessibility, but the measured response can also be influenced by matrix-dependent mass transfer effects [153]. The elevated AB reduction observed in PH-based beads is consistent with a highly hydrated microenvironment formed by the arabinoxylan-rich PH network, which swells extensively and may facilitate reagent diffusion while moderating physicochemical stress [154]. Conversely, the reduced AB signals observed in GA-based beads may be related to restricted

diffusion and altered local redox conditions, as the arabinogalactan protein structure of GA can form dense interfacial layers within the hydrogel matrix [155].

Viable cell counts (Table 10) revealed a clear distinction between metabolic activity and colony forming ability of encapsulated *L. plantarum*. The PH-IN formulation gave the highest number of viable cells, reaching $8.55 \pm 1.41 \cdot 10^9$ CFU·mL^{-1} ($p < 0.001$), which was significantly higher than the CTRL ($6.52 \pm 2.48 \cdot 10^8$ CFU·mL^{-1}). The PH-IN/TRE formulation did not differ significantly from the CTRL, whereas PH-TRE showed an increase to $2.57 \pm 1.51 \cdot 10^9$ CFU·mL^{-1} ($p = 0.046$). In contrast, all GA-based formulations exhibited lower viable cell counts, with values of $2.33 \pm 0.56 \cdot 10^7$ CFU·mL^{-1} for GA-IN, $3.21 \pm 1.11 \cdot 10^7$ CFU·mL^{-1} for GA-TRE, and $9.00 \pm 0.51 \cdot 10^6$ CFU·mL^{-1} for GA-IN/TRE. These differences, however, were not statistically significant.

Table 10. Results of viable cell counts for *L. plantarum* encapsulated in alginate beads with the addition of gum arabic (GA) or psyllium husk (PH), and with the incorporation of selected prebiotic components (inulin – IN, trehalose – TRE, and their mixture – IN/TRE). The control sample (CTRL) represents non-encapsulated cells. Data are expressed as mean ± standard deviation. Comparisons without asterisks are not statistically significant (n.s.). Statistical significance: (*) $p < 0.05$; (***) $p < 0.001$.

	Viable cells (CFU·mL^{-1})	Statistical significance
CTRL	$6.52 \pm 2.48 \cdot 10^8$	-
PH-IN	$8.55 \pm 1.41 \cdot 10^9$	(***)
PH-TRE	$2.57 \pm 1.51 \cdot 10^9$	(*)
PH-IN/TRE	$7.73 \pm 1.93 \cdot 10^8$	(n.s.)
GA-IN	$2.33 \pm 0.56 \cdot 10^7$	(n.s.)
GA-TRE	$3.21 \pm 1.11 \cdot 10^7$	(n.s.)
GA-IN/TRE	$9.00 \pm 0.51 \cdot 10^6$	(n.s.)

The higher CFU recovery observed for the PH-IN formulation may be attributed to two complementary factors. IN acts as a fermentable prebiotic that can support *L. plantarum* following release from the matrix, while also influencing hydrogel hydration and diffusion properties, which have been associated with improved survival in alginate-prebiotic systems [156]. In parallel, the PH network provides strong water-holding capacity and increased viscosity, creating a less abrasive microenvironment that may favor recovery of viable cells [100]. By comparison, the low CFU values observed for GA-based formulations, despite

increased metabolic activity in MTT assays, suggest limited recovery of culturable cells or a shift toward a viable but non-culturable (VBNC) state. In such a state, bacterial cells remain metabolically active but are unable to form colonies under standard cultivation conditions, a response that has been widely reported for bacteria exposed to environmental stress [157].

Considering all results, PH-reinforced hydrogels, particularly the PH-IN formulation, exhibited the most favorable overall profile, combining moderate metabolic activation, increased AlamarBlue reduction, and high recovery of viable cells. This behavior is consistent with the properties of the arabinoxylan-rich mucilage of PH, which forms hydrated and viscous gel networks that buffer bacterial cells against rapid environmental fluctuations while maintaining sufficient diffusion to support metabolic activity. Under these conditions, enzyme function, membrane integrity, and culturability after release are preserved [152]. IN further supports this effect by modulating water structure and osmotic balance within the hydrogel matrix [158]. TRE acts as an osmoprotective disaccharide that stabilizes cellular membranes and proteins. However, under the present conditions, its positive effects on metabolic activity did not translate into increased culturability, indicating a balance between osmotic stabilization and post-release growth recovery [159]. In contrast, GA-reinforced hydrogels were associated with high metabolic activity but lower AB reduction and reduced viable cell counts. The arabinogalactan polysaccharide protein complexes of GA can form dense interfacial layers that restrict diffusion of oxygen and small solutes. Such compact films may also limit rehydration and external diffusion of cells during bead disintegration, reducing colony recovery and favoring the appearance of VBNC state under standard plate count conditions [160].

2.2. Cell envelope properties

A comprehensive assessment was conducted to evaluate how matrix components of alginate-based hydrogels influence the cell envelope of *L. plantarum*. Membrane permeability and disruption were quantified using the CV assay, while surface hydrophobicity was assessed by the CR assay.

As shown in Figure 32, PH-based beads were associated with modest increases in membrane permeability compared with the CTRL. TMP values reached 21.72 ± 0.08 ($p = 0.027$) and 24.17 ± 1.12% ($p = 0.001$) for PH-IN and PH-TRE, respectively, whereas the PH-IN/TRE formulation did not differ significantly from the CTRL. In contrast, GA-based beads exhibited higher TMP values, reaching 31.18 ± 0.69% for GA-IN, 37.34 ± 2.28% for GA-TRE, and 40.06 ± 0.40% for GA-IN/TRE ($p < 0.001$ for all).

The membrane disruption index followed a similar pattern (Table 11). Starting from a value of 1.00 ± 0.000 in the CTRL, the index increased slightly for PH-IN (1.16 ± 0.01, p = 0.027) and PH-TRE (1.29 ± 0.06, p = 0.002), remained not statistically significant for PH-IN/TRE, and increased markedly for GA-IN (1.67 ± 0.04), GA-TRE (1.89 ± 0.12), and GA-IN/TRE (2.14 ± 0.02) ($p < 0.001$ for all). These data indicate that PH-reinforced alginate matrices generally maintain membrane permeability close to CTRL levels, with the IN/TRE combination limiting the modest increases observed when IN or TRE were applied individually.

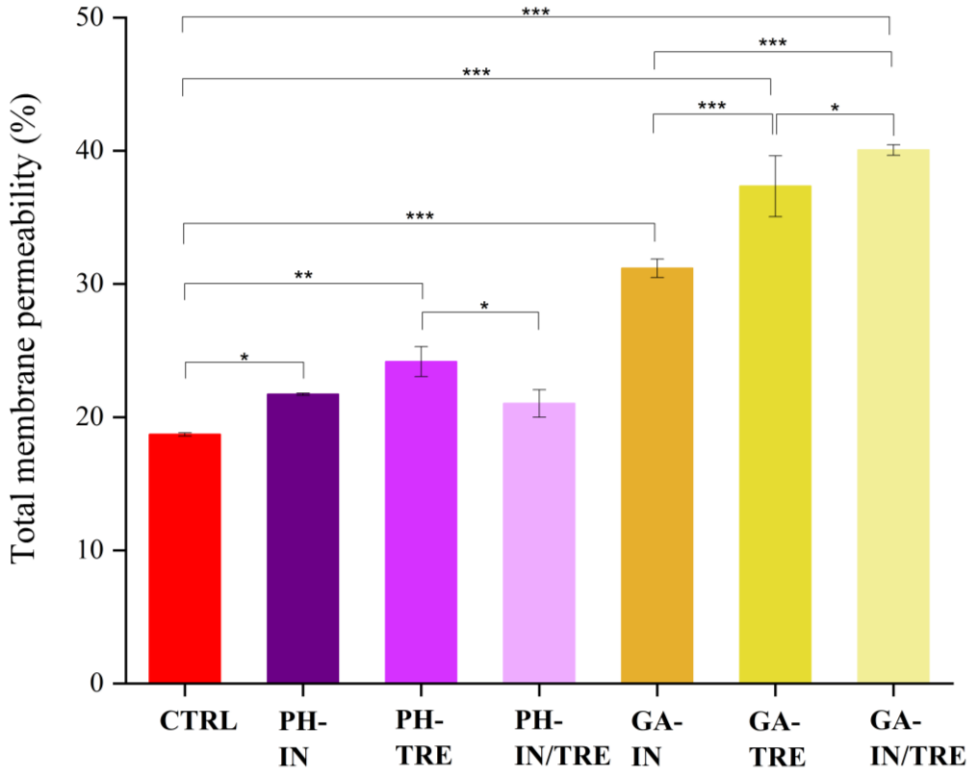

Figure 32. Results of total membrane permeability for *L. plantarum* cells encapsulated in alginate beads with the addition of gum arabic (GA) or psyllium husk (PH), and with the incorporation of selected prebiotic components (inulin – IN, trehalose – TRE, and their mixture – IN/TRE). The control sample (CTRL) represents non-encapsulated cells. Comparisons without asterisks are not statistically significant (n.s.). Statistical significance: (*) $p < 0.05$; (**) $p < 0.01$; (***) $p < 0.001$.

This observation is consistent with the properties of PH gels, which exhibit high water retention and moderated diffusive fluxes, thereby buffering membrane strain and supporting barrier function at the bead-cell interface [161]. The reduced permeability observed for PH-IN/TRE suggests that the water-replacement effect of TRE and the water-structuring role of IN may act synergistically within the PH matrix to stabilize lipid organization and limit transient membrane defects, reducing mechanical stress during encapsulation and release [74]. In contrast, GA-

reinforced hydrogels were associated with greater membrane perturbation under the tested conditions. One possible explanation is that GA alters interfacial organization and pore architecture within the alginate network, affecting effective cross-link density or creating microdomains with higher local porosity [162]. This interpretation is consistent with reports describing tunable porosity in alginate-based systems, where co-polymers can influence pore size distribution and local hydration environments surrounding encapsulated cells [163].

Table 11. Relative hydrophobicity index and membrane disruption index for *L. plantarum* cells encapsulated in alginate beads with the addition of gum arabic (GA) or psyllium husk (PH), and with the incorporation of selected prebiotic components (inulin – IN, trehalose – TRE, and their mixture – IN/TRE). The control sample (CTRL) represents non-encapsulated cells. Data are expressed as mean ± standard deviation. Comparisons without asterisks are not statistically significant (n.s.). Statistical significance: (*) $p < 0.05$; (**) $p < 0.01$; (***) $p < 0.001$.

	Relative hydrophobicity index (-)	**Membrane disruption index (-)**
CTRL	1.00 ± 0.00	1.00 ± 0.00
PH-IN	1.16 ± 0.01 (*)	0.98 ± 0.07 (n.s.)
PH-TRE	1.29 ± 0.06 (**)	1.12 ± 0.09 (n.s.)
PH-IN/TRE	1.12 ± 0.06 (n.s.)	0.83 ± 0.02 (*)
GA-IN	1.67 ± 0.04 (***)	1.16 ± 0.09 (*)
GA-TRE	1.99 ± 0.12 (***)	2.41 ± 0.02 (***)
GA-IN/TRE	2.14 ± 0.02 (***)	2.62 ± 0.05 (***)

Congo red binding (CRB) differentiated the tested formulations with respect to cell surface hydrophobicity (Figure 33). Relative to the CTRL (10.87 ± 1.11%), PH-IN (10.63 ± 0.77%) and PH-TRE (12.17 ± 0.99%) did not show statistically significant changes, whereas PH-IN/TRE exhibited a significant decrease in CRB to 9.01 ± 0.16% ($p = 0.045$). In contrast,

GA-based formulations showed markedly higher CRB values, reaching 26.20 ± 0.24% for GA-TRE and 28.46 ± 0.53% for GA-IN/TRE ($p < 0.001$ for both).

The relative hydrophobicity index supported these observations (Table 11). For PH-based formulations, PH-IN and PH-TRE did not show statistically significant differences relative to the CTRL, whereas PH-IN/TRE exhibited a significant decrease to 0.83 ± 0.02 ($p = 0.022$). In contrast, GA-based formulations showed higher relative hydrophobicity values, with GA-IN reaching 1.16 ± 0.09 ($p = 0.029$), GA-TRE 2.41 ± 0.02, and GA-IN/TRE 2.62 ± 0.05 ($p < 0.001$ for both). As CRB values increase when hydrophobic cell surface components or extracellular polymers are more exposed, the reduced index observed for PH-IN/TRE is consistent with a more hydrophilic and less stress-exposed cell envelope. In contrast, the higher values observed for GA-TRE and GA-IN/TRE indicate increased exposure of hydrophobic surface domains or stronger interactions between the dye and extracellular polymers [122].

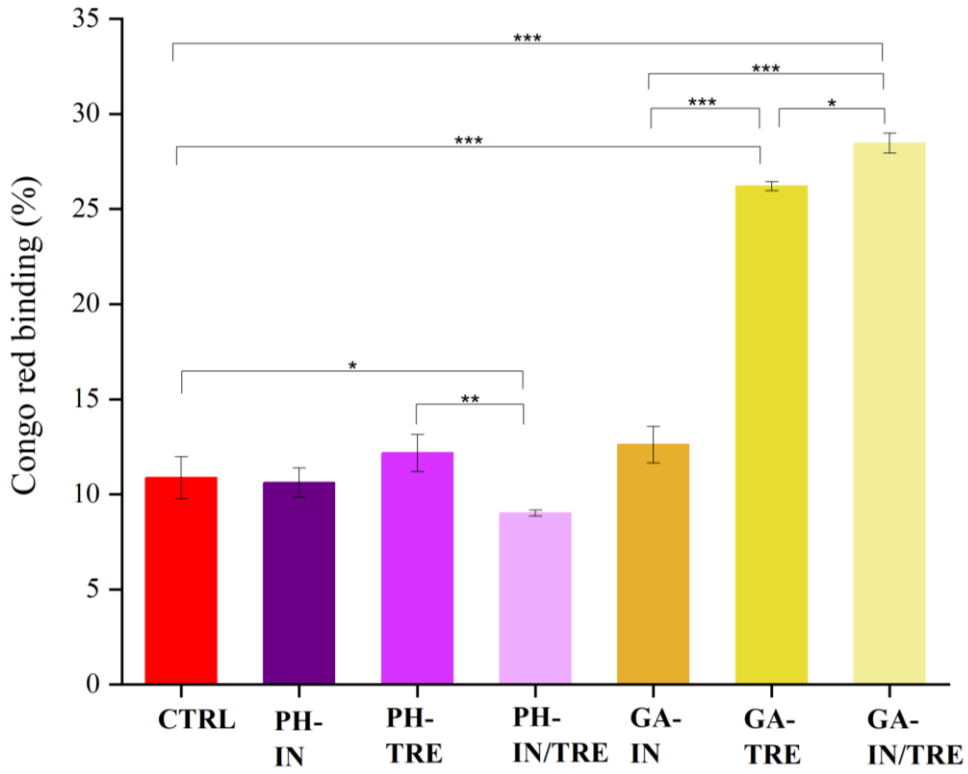

Figure 33. Results of Congo red binding for *L. plantarum* cells encapsulated in alginate beads with the addition of gum arabic (GA) or psyllium husk (PH), and with the incorporation of selected prebiotic components (inulin – IN, trehalose – TRE, and their mixture – IN/TRE). The control sample (CTRL) represents non-encapsulated cells. Statistical significance: (*) $p < 0.05$; (**) $p < 0.01$; (***) $p < 0.001$.

The PH matrix was associated with maintenance of a highly hydrated microenvironment around bacterial cells, which may limit exposure of hydrophobic membrane domains, particularly when

IN and TRE were present simultaneously. IN can modulate *L. plantarum* surface properties by reducing hydrophobicity or smoothing the cell envelope, consistent with the hydrophilic profile observed for PH-IN/TRE [164]. TRE further stabilizes lipid bilayers and membrane proteins, and within the hydrated PH network this stabilization may reduce the exposure of hydrophobic surface regions, resulting in lower Congo red binding indices [74]. In contrast GA forms dense interfacial films that, when combined with alginate, can modify hydration dynamics and increase exposure of hydrophobic protein or lipid domains. This behavior is consistent with the pronounced increases in CRB and surface hydrophobicity observed for GA-TRE and GA-IN/TRE formulations [165]. Although increased hydrophobicity may enhance adhesion under certain GI conditions, it can also reflect stress-related remodeling of the cell envelope. Consequently, the functional impact of GA-induced surface modifications is likely context dependent and should be considered together with membrane permeability data [166].

The combined CV and CR results indicate that PH-reinforced alginate beads, particularly the PH-IN/TRE formulation, provide a more hydrated and less disruptive interface for *L. plantarum*, supporting membrane stabilization and reduced surface hydrophobicity. In contrast, GA-reinforced beads were associated with increased membrane permeability and surface hydrophobicity, reflecting the influence of GA on network structure and water dynamics. These observations identify PH-IN/TRE as a low-permeability, hydrophilic formulation and suggest that GA-based systems may require targeted optimization to balance surface properties and functional performance [167].

2.3. Intracellular trace metal homeostasis

To assess whether hydrogel composition modulates ionic homeostasis, intracellular concentrations of manganese (^{55}Mn), iron (^{56}Fe), and zinc (^{66}Zn) were quantified in *L. plantarum* cells released from alginate beads. These trace metals were selected due to their established roles in LAB physiology and their close association with probiotic robustness. Manganese supports oxidative stress defense and the activity of key redox enzymes, while iron is required for multiple oxidoreductases and electron transfer processes but must be tightly regulated to prevent uncontrolled Fenton reactions. Zinc functions as both a structural and catalytic cofactor, with intracellular levels actively controlled in Gram-positive bacteria [168–170].

As shown in Figure 34, PH-reinforced beads were associated with increased intracellular manganese levels across all formulations compared with the CTRL (4.96 ± 0.02 mg·L^{-1}). Mn concentrations reached 5.38 ± 0.04 mg·L^{-1} for PH-IN ($p < 0.001$), 5.27 ± 0.02 mg·L^{-1} for PH-IN/TRE ($p = 0.001$), and 5.11 ± 0.01 mg·L^{-1} for PH-TRE ($p < 0.001$). In contrast, GA-reinforced beads were associated with slightly lower intracellular Mn levels, reaching 4.86 ± 0.02 mg·L^{-1} for GA-IN ($p = 0.003$), 4.81 ± 0.02 mg·L^{-1} for GA-IN/TRE ($p < 0.001$), and 4.76 ± 0.02 mg·L^{-1} for GA-TRE ($p < 0.001$).

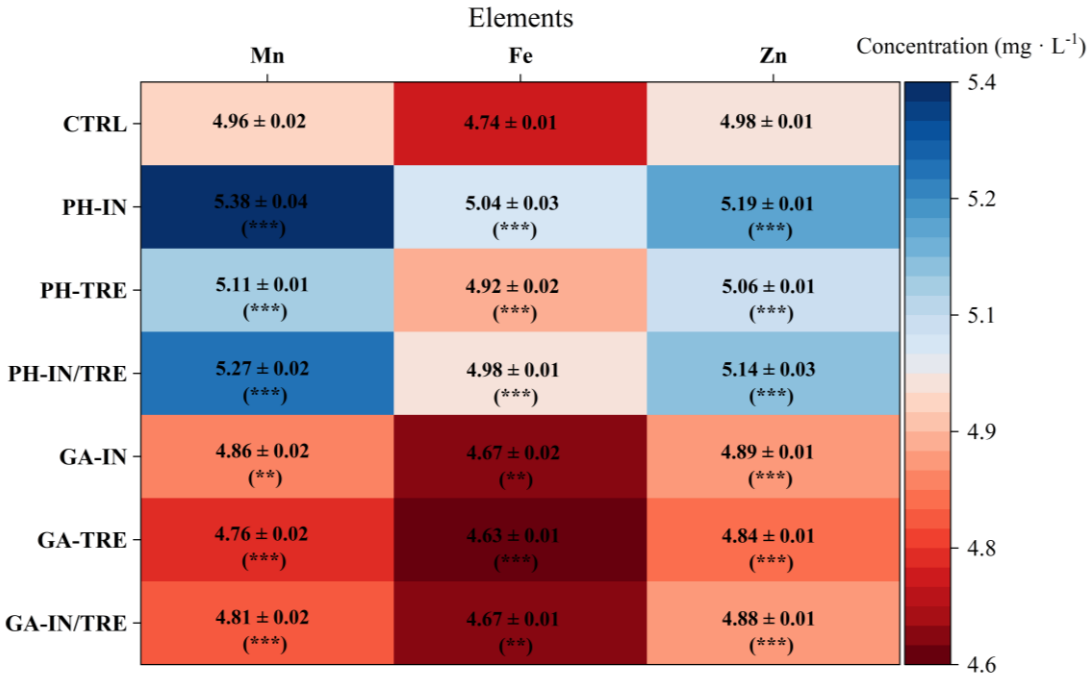

Figure 34. Heatmap illustrating trace metal (manganese – Mn, iron – Fe, and zinc – Zn) concentrations in *L. plantarum* cells encapsulated in alginate beads with the addition of gum arabic (GA) or psyllium husk (PH), and with the incorporation of selected prebiotic components (inulin – IN, trehalose – TRE, and their mixture – IN/TRE). The control sample (CTRL) represents non-encapsulated cells. Data are expressed as mean ± standard deviation. Statistical significance: (**) $p < 0.01$; (***) $p < 0.001$.

In *L. plantarum*, increased intracellular Mn levels are consistent with increased capacity for oxidative stress management and cofactor availability, as this species is known to accumulate high Mn levels to buffer reactive oxygen species and support Mn-dependent enzymes. Accordingly, the PH-associated increase in intracellular Mn suggests a more supportive, redox-competent microenvironment within these beads that facilitates Mn access and retention [171,172]. From a materials perspective, this pattern may be related to two factors. First, the PH network strongly retains water and forms hydrated, open structures that may facilitate

Mn diffusion toward the bacterial surface. Second, GA forms denser interfacial films that can slow ion exchange near cells, thereby limiting Mn availability within GA-based beads [90,154].

As shown in Figure 34, a PH-reinforced beads were associated with increased Fe levels compared with the CTRL (4.74 ± 0.01 $mg \cdot L^{-1}$). Fe concentrations reached 5.04 ± 0.03 $mg \cdot L^{-1}$ for PH-IN, 4.98 ± 0.01 $mg \cdot L^{-1}$ for PH-IN/TRE, and 4.92 ± 0.02 $mg \cdot L^{-1}$ for PH-TRE ($p < 0.001$ for all). In contrast, GA-reinforced beads were associated with modest reductions in intracellular Fe, reaching 4.67 ± 0.02 $mg \cdot L^{-1}$ for GA-IN ($p = 0.002$), 4.67 ± 0.01 $mg \cdot L^{-1}$ for GA-IN/TRE ($p = 0.002$), and 4.63 ± 0.01 $mg \cdot L^{-1}$ for GA-TRE ($p = 0.001$).

As iron is both essential for cellular metabolism and potentially pro-oxidant, the moderate Fe enrichment observed in PH-based systems is consistent with improved bioavailability without excessive intracellular accumulation. In contrast, the lower Fe levels associated with GA-based beads suggest restricted access under the applied conditions. Matrix-controlled mass transfer, governed by factors such as pore size, tortuosity, and water distribution, is likely to influence Fe availability. Previous studies have reported that alginate hydrogels contain distinct water domains with element-dependent mobility. Accordingly, co-polymers that maintain hydration and open diffusion pathways, such as PH, may facilitate Fe uptake, whereas denser interfacial layers, as formed by GA, may limit it [173,174].

As shown in Figure 34, intracellular zinc followed a pattern similar to that observed for manganese and iron. PH-based beads were associated with increased intracellular Zn levels relative to the CTRL (4.98 ± 0.01 $mg \cdot L^{-1}$), with the highest concentration observed for PH-IN at 5.19 ± 0.01 $mg \cdot L^{-1}$ ($p < 0.001$). In contrast, GA-based beads were associated with slightly reduced intracellular Zn levels, with the lowest value observed for GA-TRE (4.84 ± 0.01 $mg \cdot L^{-1}$, $p < 0.001$).

In Gram-positive LAB, high-affinity Zn uptake is mediated by ATP-binding cassette (ABC) transport systems, in which a surface-associated binding protein captures Zn and facilitates its transport across the membrane [175]. Accordingly, a hydrogel matrix that maintains hydrated, low-resistance diffusion pathways may improve Zn availability to these transport systems. The higher intracellular Zn levels observed in PH-based beads compared with GA-based beads are consistent with this transport mechanism and with previously reported Zn-tolerant or Zn-accumulating phenotypes in certain *L. plantarum* strains [176,177].

Across all three analyzed elements, alginate beads reinforced with PH were associated with increased intracellular levels of Mn, Fe, and Zn, particularly when IN was present

as a co-additive. In contrast, beads containing GA generally maintained or slightly reduced intracellular metal levels relative to the CTRL. This pattern indicates a close relationship between hydrogel material properties and bacterial ionic responses. PH forms hydrated and porous gel networks that facilitate ionic diffusion and exchange, whereas GA tends to form denser interfacial layers that restrict ion mobility and reduce local ion availability [178–180]. Among the tested protective additives, IN was generally associated with a more balanced intracellular ion profile than TRE, which may be related to its water-structuring properties and its ability to maintain a moderate osmotic microenvironment [181]. These observations suggest that selection of alginate co-polymers can be used to modulate pore structure, hydration, and ion transport, informing the rational design of encapsulation matrices [182].

2.4. Bead morphology and dimensional analysis

This section integrates whole-bead morphology and near-surface topography data obtained using an inspection microscope and a digital optical microscope, with dimensional measurements obtained from inspection images acquired at 90x magnification.

Across all PH-based formulations, inspection microscopy at 90x magnification revealed beads with high sphericity indicating that the rim was not sharp (Figure 35). Bead interiors appeared optically uniform, with no visible macropores or fractures. Corresponding surface close-up images showed continuous surface layers characterized by shallow undulations and occasional small surface features. Observations obtained using a digital optical microscope at 20x magnification corroborated these findings. Bead outlines appeared smoothly rounded, and interior brightness was uniform. Bead diameters measured by inspection microscopy were 2.78 ± 0.01 mm for PH-TRE, 3.32 ± 0.02 mm for PH-IN, and 3.35 ± 0.03 mm for PH-IN/TRE. Within this group, PH-TRE exhibited the smallest mean diameter. A weak circular feature observed in the PH-IN/TRE formulation at 20x magnification was attributed to illumination or reflection effects rather than to a structural discontinuity.

The smooth, hydrated surface layers observed for PH-based beads are consistent with the swelling behavior of PH, which exhibits high water-holding capacity and gel-forming properties [183,184]. This composition supports the formation of an ion-permeable and compliant interfacial zone rather than a dehydrated outer shell. Such an interfacial phenotype is commonly associated with reduced diffusion resistance and a less restrictive microenvironment for encapsulated cells [185]. The measured bead diameters of PH-based hydrogels are in the millimeter size range, where mass transport is influenced by both shell

architecture and diffusion path length. However, the optically observed hydrated surfaces indicate limited shell densification, which is characteristic of well-controlled external Ca^{2+} gelation processes [186]. The smaller diameter of PH-TRE beads is likely related to feed properties, such as rheology and surface tension, affecting droplet formation during extrusion. These size differences do not indicate reduced interfacial quality, as surface layers remained continuous and hydrated. IN contributes to water structuring, while TRE stabilizes biomolecular and interfacial organization. Together, these effects are consistent with the uniform surface characteristics observed for PH-IN/TRE beads. Such behavior agrees with reports describing enhanced hydration and structural uniformity in composite hydrogels containing these additives [187].

GA-based formulations observed at 90x magnification exhibited a well-defined and sharply outlined rim surrounding optically homogeneous core (Figure 35). Surface close-up images showed generally smooth outer layers without visible cracks or macropores. Corresponding digital optical images at 20x magnification revealed the same clearly defined edge and highlighted the compact outer zone. Bead diameters measured for GA-based formulations were 3.46 ± 0.03 mm for GA-IN, 3.58 ± 0.05 mm for GA-TRE, and 3.81 ± 0.03 mm for GA-IN/TRE. Compared with PH-based beads, GA-based beads were generally larger and exhibited a more compact edge.

The presence of a well-defined rim is consistent with the behavior of arabinogalactan protein fractions present in GA, which are known to adsorb at interfaces and form cohesive films with measurable viscoelastic properties [188]. In alginate hydrocolloid composite systems, such interfacial films can locally densify the bead shell and influence mass transfer, even when the interior remains hydrated. The larger diameters observed for GA-based beads further increase diffusion path length, contributing to enhanced shell control under otherwise comparable conditions. Both droplet size and shell density are recognized factors influencing transport in millimeter-scale alginate beads [189]. Recent studies on alginate systems combined with natural hydrocolloids have shown that co-polymer selection affects bead architecture and release behavior. Complementary interfacial investigations of GA-stabilized systems further demonstrate the formation of stable and films at aqueous interfaces [190]. These observations are consistent with the compact outer regions observed for GA-based beads in the present study and with the observed size trend indicating that the GA matrix promotes tighter skin formation after gelation.

PH-based beads exhibited hydrated, smooth surfaces with continuous outer layers, whereas GA-based beads displayed sharper, more compact rims and slightly larger diameters. These structural features are consistent with earlier functional observations, in which PH-based matrices were associated with higher cellular activity and increased intracellular metal retention, while GA-based systems showed reduced uptake and higher stress-related responses. The microscopic observations align with established models of core-shell formation and diffusion behavior in alginate hydrogels [191].

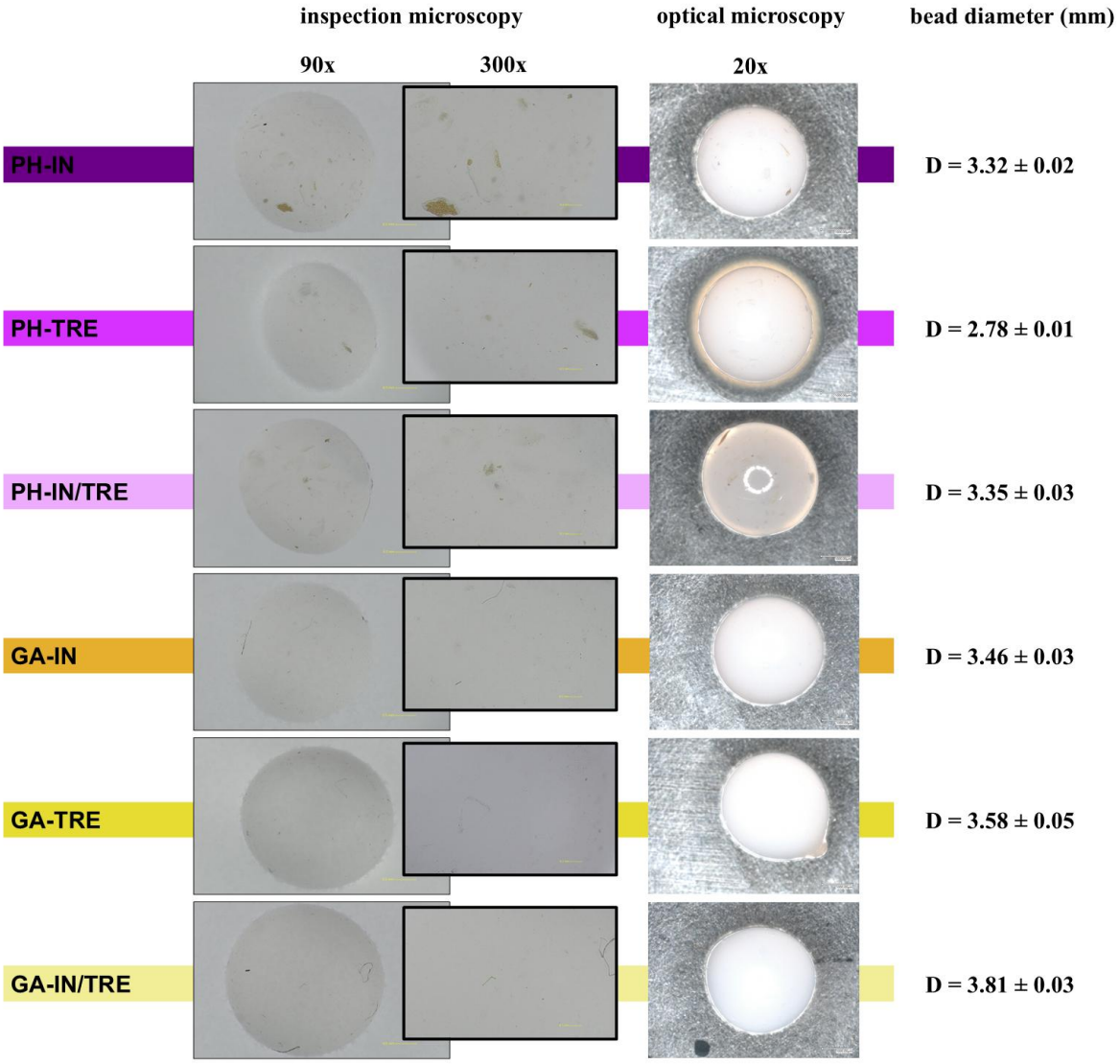

Figure 35. Images obtained with inspection (90x, 300x) and optical microscopy (20x) of *L. plantarum* cells encapsulated in alginate beads with the addition of gum arabic (GA) or psyllium husk (PH), and with the incorporation of selected prebiotic components (inulin – IN, trehalose – TRE, and their mixture – IN/TRE). Bead diameters (D, mm) are expressed as mean ± standard deviation. Representative scale bars correspond to 0.5 mm (90x), 0.1 mm (300x), and 1 mm (20x).

2.5. Summary of hydrogel-based probiotic formulations

Encapsulation of *L. plantarum* in alginate beads reinforced with PH or GA and supplemented with IN, TRE, or their combination provided a more supportive environment than that observed for non-encapsulated cells. Measurements of metabolic activity and colony forming showed that PH-based matrices containing IN, and to a lesser extent IN/TRE, were associated with the most favorable maintenance of cell viability. In contrast, GA-based matrices primarily increased metabolic activity without a corresponding improvement in colony forming ability, indicating that the two matrix types differentially influence how metabolic activation translates into recoverable cells.

At the level of the cell envelope, PH-based beads maintained membrane barrier properties close to those of the CTRL and promoted a more hydrophilic surface profile, particularly in the presence of the IN/TRE combination. This pattern is consistent with the formation of a hydrated and less restrictive microenvironment around the bacterial cells. In contrast, GA-based beads were associated with increased membrane permeability and a shift toward higher surface hydrophobicity, consistent with denser interfacial layers that impose stronger physical and chemical constraints on the cells. These differences help explain why PH-based formulations containing IN produced a more balanced cellular characteristic. Intracellular metal profiles supported this interpretation. PH-based beads were associated with higher intracellular levels of Mn, Fe, and Zn, which serve as key cofactors in oxidative stress defense and central metabolic processes, whereas GA-based beads tended to limit their accumulation. The PH matrix appears to provide a more hydrated environment that supports ionic balance, while the GA matrix is associated with more restricted ion transport at the bead-cell interface.

Whole-bead morphology further supported these findings. PH-based beads were nearly spherical and exhibited smooth, hydrated surfaces with diffuse edges, whereas GA-based beads were larger and displayed a sharper, more compact outer region. The PH bead architecture favors mass transfer and gentler mechanical conditions, while the GA bead structure reflects stronger shell control and tighter interfacial packing. These structural characteristics provide a physical basis for the functional differences observed between the two matrix systems.

Taken together, these results support the selection of PH-IN as the lead hydrogel-based probiotic formulation. At this stage, the work addresses *Specific research aims (B-E)* related to the formulation of functional hydrogel carriers, characterization of their structural and physicochemical properties, demonstration of improved probiotic viability within the complete

system, and evaluation of formulation stability under relevant conditions. These outcomes contribute to the overall objective of the dissertation and support the formulated research hypothesis.

3. FUNCTIONAL EVALUATION OF LIPID-STABILIZED PROBIOTIC SYSTEMS

This stage evaluated the functional performance of *Lactococcus lactis* coated with a DMPC-based lipid layer. In this system, lipid nanoparticles did not encapsulate bacterial cells internally but assembled at the cell-medium interface, forming an external stabilizing corona. The objective was to assess whether this lipid coating influences probiotic bacteria during storage by examining its effects on cellular activity, viability, physiological stability, and colloidal behavior under two temperature conditions (4 °C and room temperature). By monitoring coated and uncoated cells over multiple time points, this stage examined whether surface-associated lipid layers can act as protective structures and contribute to improved survival and functional stability of probiotic cells.

The following abbreviations were used for the samples:

- CTRL – free (uncoated) probiotic cells,
- L/P – lipid-coated (DMPC-coated) probiotic cells,
- L – formulation with liposomes alone (without probiotic cells).

3.1. Viability and metabolic performance

This section examined whether a DMPC-based lipid corona can maintain metabolic activity and viability of *L. lactis* during storage. Two storage conditions were compared over 1, 7, 14, 21, and 28 days, with analyses performed for lipid-coated and uncoated CTRL.

As shown in Figure 36, the metabolic activity profile at 4 °C differed between coated and uncoated cells over the 28-day storage period. On day 1, the DMPC-coated sample exhibited a significantly higher metabolic activity than the CTRL (2.39 ± 0.11 vs 1.06 ± 0.04, $p < 0.001$). By day 7, both groups reached higher MRU values, although coated cells showed a slight but statistically significant reduction compared with CTRL. From day 14, MRU values remained low and no statistically significant from CTRL. By day 28, coated cells showed a modest, non-significant increase relative to CTRL (0.44 ± 0.01 vs 0.38 ± 0.01). Overall, storage at 4 °C was associated with an early increase in metabolic activity in L/P sample, followed by comparable activity levels in both groups at later time points.

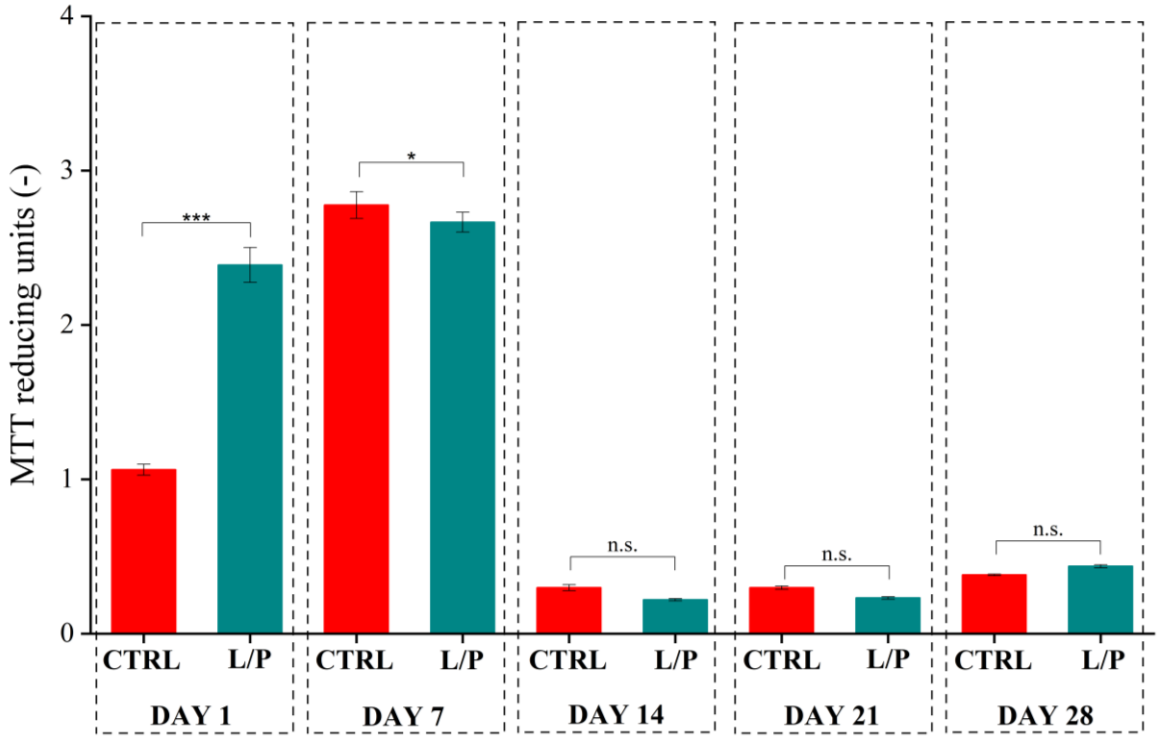

Figure 36. Results of metabolic activity (MTT reducing units – MRU) for *L. lactis* stored at 4 °C. The control sample (CTRL) represents free (uncoated) cells. The L/P sample represents lipid-coated cells. Comparisons without asterisks are not statistically significant (n.s.). Statistical significance: (*) $p < 0.05$; (***) $p < 0.001$.

At room temperature, the metabolic effect of the lipid coating was more clear during early storage (Figure 37). Coated cells showed significantly higher MRU values than controls on day 1 (2.50 ± 0.10 vs 0.93 ± 0.01, $p < 0.001$), and this difference remained clear on day 7 (1.38 ± 0.05 vs 0.41 ± 0.02, $p < 0.001$) and day 14 (0.35 ± 0.01 vs 0.23 ± 0.01, $p = 0.001$). By day 21, MRU values converged and no statistically significant differences were detected. On day 28, a small increase was again observed in L/P sample. Overall, at room temperature, the lipid coating was associated with higher metabolic activity during early and mid-storage periods.

At 4 °C, viable cell counts on day 1 were comparable between L/P samples and CTRL (Table 12). A clear separation in favor of coated cells was observed by day 7 ($5.27 \pm 0.50 \cdot 10^9$ vs $2.34 \pm 0.11 \cdot 10^9$ CFU·mL^{-1}, $p < 0.001$). From day 14 through day 28, coated samples consistently showed higher CFU values than CTRL, often differing by two to three orders of magnitude. Storage at 4 °C was associated with improved viability of lipid-coated cells over time.

At room temperature, L/P samples exhibited slightly lower CFU counts than CTRL on day 1. From day 7, coated samples displayed markedly higher CFU values, with statistically

significant differences relative to CTRL on day 7 ($2.88 \pm 0.06 \cdot 10^{10}$ vs $2.50 \pm 0.13 \cdot 10^{8}$ CFU·mL^{-1}, $p < 0.001$) and day 14 ($6.37 \pm 0.47 \cdot 10^{8}$ vs $3.23 \pm 0.25 \cdot 10^{5}$ CFU·mL^{-1}, $p = 0.002$). By days 21 and 28, coated samples continued to exceed CTRL values by two to four orders of magnitude. At room temperature, the lipid corona was associated with improved viability.

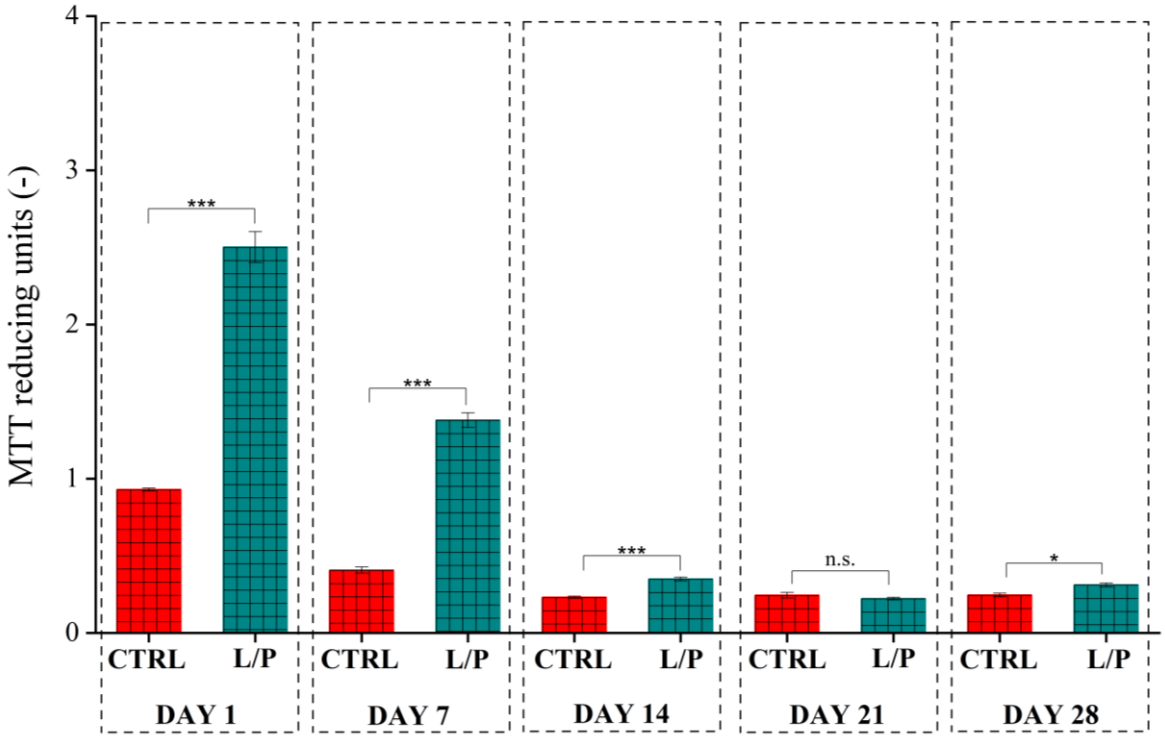

Figure 37. Results of metabolic activity (MTT reducing units – MRU) for *L. lactis* stored at room temperature. The control sample (CTRL) represents free (uncoated) cells. The L/P sample represents lipid-coated cells. Comparisons without asterisks are not statistically significant (n.s.). Statistical significance: (*) $p < 0.05$; (***) $p < 0.001$.

Because bacterial cells are larger than DMPC vesicles, internal encapsulation is not feasible. Instead, multiple vesicles assemble on the bacterial surface, forming a pericellular lipid corona. Such lipid coatings are recognized as a distinct class of cell-surface stabilization strategies and have been reported to modulate interfacial hydration, protect cells from environmental stressors, and influence transport processes at the cell boundary [192]. The observed early increase in metabolic activity and the higher viable cell counts in coated samples, particularly under room temperature storage, are consistent with the expected function of the lipid corona, which provides a protective microenvironment at the cell-medium interface. A defining property of DMPC is its main-chain melting transition at approximately 23-24 °C [193].

Table 12. Results of viable cell counts of *L. lactis* stored at 4 °C and room temperature (RT). The control sample (CTRL) represents free (uncoated) cells. The L/P sample represents lipid-coated cells. Comparisons without asterisks are not statistically significant (n.s.). Statistical significance: (**) $p < 0.01$; (***) $p < 0.001$.

Day	Viable cells (CFU·mL^{-1}) at 4 °C	
	CTRL	**L/P**
1	$3.53 \pm 0.12 \cdot 10^{8}$	$3.73 \pm 0.11 \cdot 10^{8}$ (n.s.)
7	$2.34 \pm 0.11 \cdot 10^{9}$	$5.27 \pm 0.50 \cdot 10^{9}$ (***)
14	$1.49 \pm 0.27 \cdot 10^{6}$	$1.80 \pm 0.55 \cdot 10^{8}$ (n.s.)
21	$4.87 \pm 0.67 \cdot 10^{3}$	$2.55 \pm 1.26 \cdot 10^{6}$ (n.s.)
28	$2.53 \pm 0.32 \cdot 10^{1}$	$2.10 \pm 0.10 \cdot 10^{4}$ (n.s.)
Day	**Viable cells (CFU·mL^{-1}) at RT**	
	CTRL	**L/P**
1	$7.63 \pm 0.76 \cdot 10^{8}$	$5.59 \pm 0.04 \cdot 10^{8}$ (n.s.)
7	$2.50 \pm 0.13 \cdot 10^{8}$	$2.88 \pm 0.06 \cdot 10^{10}$ (***)
14	$3.23 \pm 0.25 \cdot 10^{5}$	$6.37 \pm 0.47 \cdot 10^{8}$ (**)
21	$2.37 \pm 0.31 \cdot 10^{4}$	$2.37 \pm 0.25 \cdot 10^{6}$ (n.s.)
28	$3.83 \pm 0.49 \cdot 10^{1}$	$2.55 \pm 0.32 \cdot 10^{5}$ (n.s.)

At room temperature, the lipid coating predominantly exists in the liquid-crystalline phase, in which lipid molecules are more fluid and flexible and can accommodate minor defects [194]. In contrast, at 4 °C the coating remains in the gel phase, characterized by reduced molecular mobility. Accordingly, the stronger and more sustained increase in metabolic activity observed at room temperature during early storage (days 1-14), together with the pronounced increases in viable cell counts (particularly between days 7 and 14), are consistent with a phase-dependent

protective effect of the lipid corona [195]. A fluid lipid layer at room temperature can better adapt to physical and chemical stress and help maintain favorable conditions that support cellular recovery, whereas the more rigid gel phase coating at 4 °C provides more limited dynamic protection, although measurable benefits were still observed at specific time points. Independent studies generally report improved long-term survival of LAB at lower temperatures, the presence of a surface-associated lipid layer can modify the local microenvironment and alter this trend over short- to mid-term storage periods [196].

Cases in which increased MTT signal was not immediately accompanied by higher CFU counts are consistent with the established dissociation between metabolic activity and culturability. The MTT assay reflects cellular redox activity and reducing capacity, whereas CFU enumeration measures the ability of cells to divide under standard growth conditions [197,198]. Under stress, bacterial populations may enter intermediate physiological states, such as viable but non-culturable (VBNC) state, in which metabolic activity is retained while colony formation is reduced. The pattern observed here, early metabolic activation followed by delayed recovery of culturability between days 7 and 14, is consistent with this model and highlights the importance of interpreting metabolic and viability assays in parallel [199,200].

3.2. Temporal changes in optical density

This section examined changes in optical density (OD_{600}) during storage of *L. lactis*, comparing samples with and without a DMPC lipid corona. Measurements were collected on days 0, 1, 2, 3, 4, 6, 7, 10, 14, 21, and 28 under both temperature conditions.

As shown in Figure 38, at 4 °C both coated and control samples started with low OD_{600} values on day 0, with the CTRL measuring approximately 0.24 ± 0.01 and the L/P sample approximately 0.31 ± 0.01. By day 1, the coated sample showed a clear early increase in OD_{600} (0.49 ± 0.07), exceeding the CTRL (0.33 ± 0.01). From day 2 through day 10, OD_{600} values of L/P samples remained consistently higher than those of the CTRL. Thereafter, both groups gradually approached similar moderate plateau levels by day 28, with the CTRL reaching approximately 0.36 ± 0.01 and the L/P sample approximately 0.40 ± 0.01. The lipid corona was associated with a modest but persistent increase in cell density at low temperature, most clear during early and mid-storage.

At room temperature, the difference between coated and control samples was more visible (Figure 39). Starting from comparable baseline values on day 0 (0.24 ± 0.01 for CTRL and 0.31 ± 0.01 for L/P), OD_{600} values of coated samples increased rapidly to 0.99 ± 0.02 by day 1 and

remained relatively stable over the 28-day storage period, with limited variability. In contrast, CTRL increased only to 0.43 ± 0.02 and then plateaued within this range. These observations indicate that, at room temperature, the lipid coating was associated with a rapid and sustained increase in cell density.

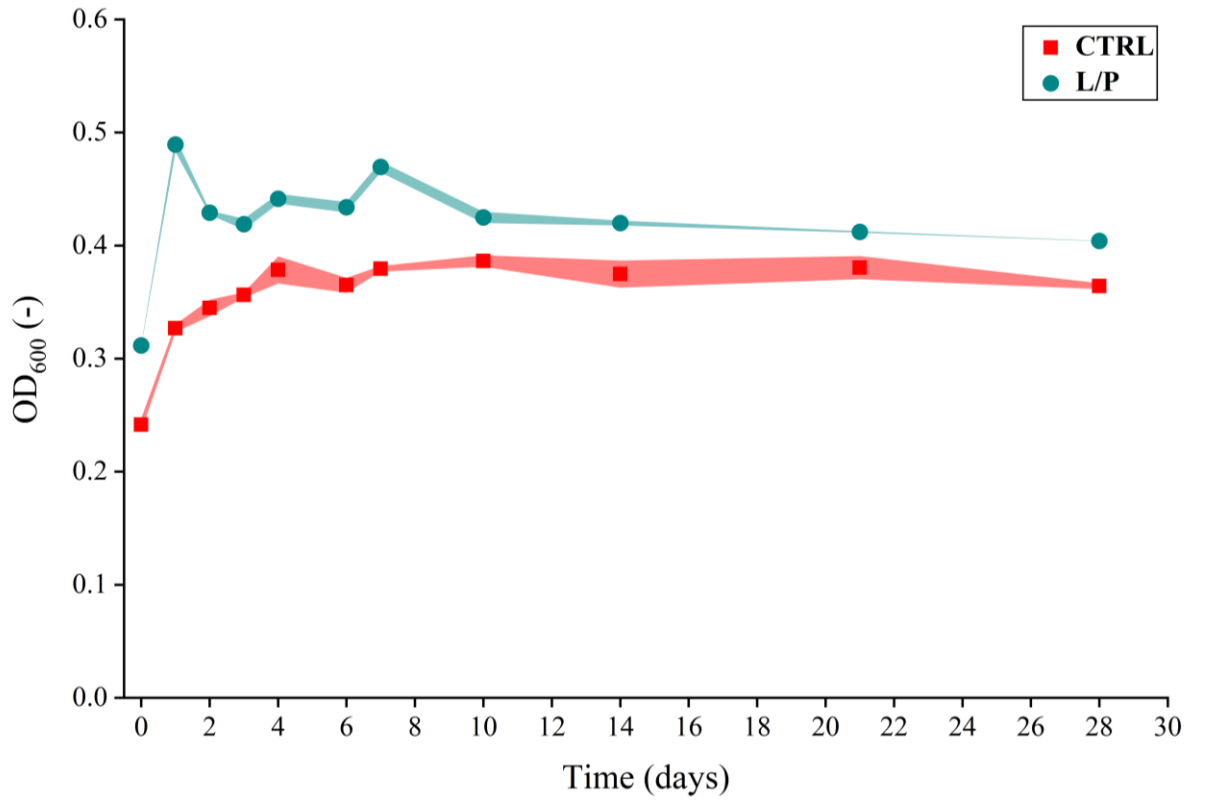

Figure 38. Results of optical density (OD_{600}) for *L. lactis* stored at 4 °C. The control sample (CTRL) represents free (uncoated) cells. The L/P sample represents lipid-coated cells. Shaded areas represent ± standard deviation.

The fluid state of the DMPC coating at room temperature provides a more dynamic pericellular environment than the gel state present at 4 °C. This higher mobility is consistent with the rapid increase of OD_{600} values and their sustained plateau at room temperature, whereas the reduced lipid mobility at 4 °C is associated with smaller OD_{600} increases that gradually stabilize at moderate plateau levels. This phase-state interpretation aligns with the metabolic activity and viable cell trends observed.

For mesophilic LAB such as *L. lactis*, storage at lower temperatures is generally associated with improved long-term viability, although it can delay metabolic reactivation and slow increases in optical density [201]. In contrast, storage at room temperature can promote more rapid outgrowth but may also lead to faster loss of culturability in the absence of protective systems

[202]. In this context, the presence of a DMPC lipid corona appears to modify this balance. At room temperature, the coating was associated with an immediate and stable increase in cell density together with early metabolic enhancement, whereas at 4 °C it provided a smaller but sustained benefit. This behavior is consistent with the ability of protective coatings to modulate the local microenvironment of bacterial cells under temperature stress [203].

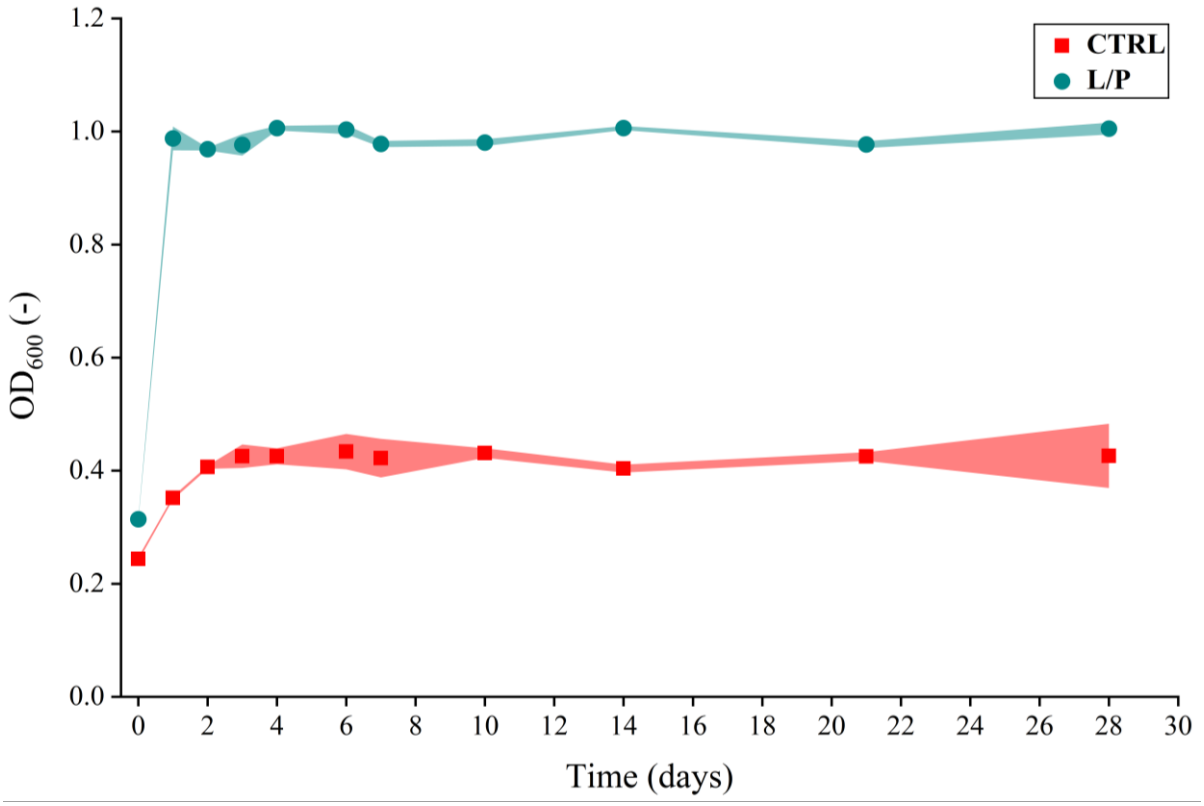

Figure 39. Results of optical density (OD_{600}) for *L. lactis* stored at room temperature. The control sample (CTRL) represents free (uncoated) cells. The L/P sample represents lipid-coated cells. Shaded areas represent ± standard deviation.

When considered together with MTT and viable cell data, the OD_{600} profiles suggest that at room temperature a fluid DMPC corona establishes a favorable pericellular environment that supports rapid functional recovery, followed by increased culturability. At 4 °C, the corona remains in a less dynamic gel phase, resulting in moderate early increases in OD_{600} and more limited functional benefits that persist but do not intensify over time.

3.3. Colloidal stability and surface properties

This section examined how a DMPC lipid corona influences interfacial and dispersion behavior of the probiotic system in comparison with uncoated cells and liposomes alone. Zeta potential and particle size distribution (PSD) were measured on days 0, 1, 7, 14, 21, and 28. The objective

was to assess whether the lipid coating improves colloidal stability, limits aggregation, and maintains a more favorable surface potential relative to uncoated cells.

As shown in Figure 40, at 4 °C uncoated cells exhibited a progressive shift in zeta potential toward less negative values, from -7.92 ± 0.38 mV on day 0 to -1.56 ± 0.06 mV on day 28, indicating an increasing tendency toward flocculation. In contrast, L/P samples maintained substantially more negative zeta potential values throughout the storage period, measuring -17.10 ± 0.41 mV on day 1, -17.44 ± 0.16 mV on day 7, -18.91 ± 0.13 mV on day 14, and -17.31 ± 0.18 mV on day 28, with statistically significant differences relative to CTRL at all time points ($p < 0.001$). Liposomes alone exhibited the most negative zeta potential values across the experiment.

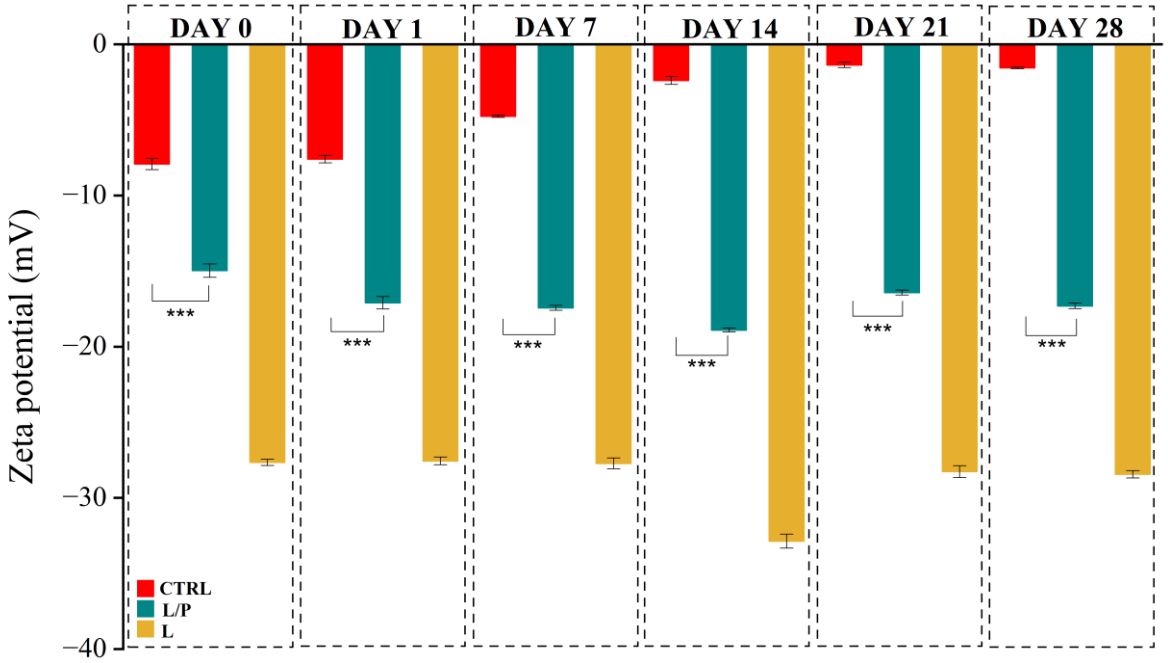

Figure 40. Results of zeta potential measurements for *L. lactis* stored at 4 °C. The control sample (CTRL) represents free (uncoated) cells. The L/P sample represents lipid-coated cells. The L sample represents formulation with liposomes alone. Statistical significance: (***) $p < 0.001$.

At room temperature, a similar but clearer pattern was observed (Figure 41). The uncoated CTRL again shifted toward near-neutral zeta potential values by day 28 (-1.56 ± 0.06 mV), whereas L/P samples remained negative throughout storage, ranging from -15.37 ± 0.22 to -18.88 ± 0.35 mV ($p < 0.001$ for all). Liposomes consistently occupied the most negative region, reflecting strong electrostatic repulsion. According to standard colloidal stability criteria, the movement of CTRL toward 0 mV indicates poor electrostatic stabilization, whereas DMPC-coated probiotic samples remained within a stability-associated range [204].

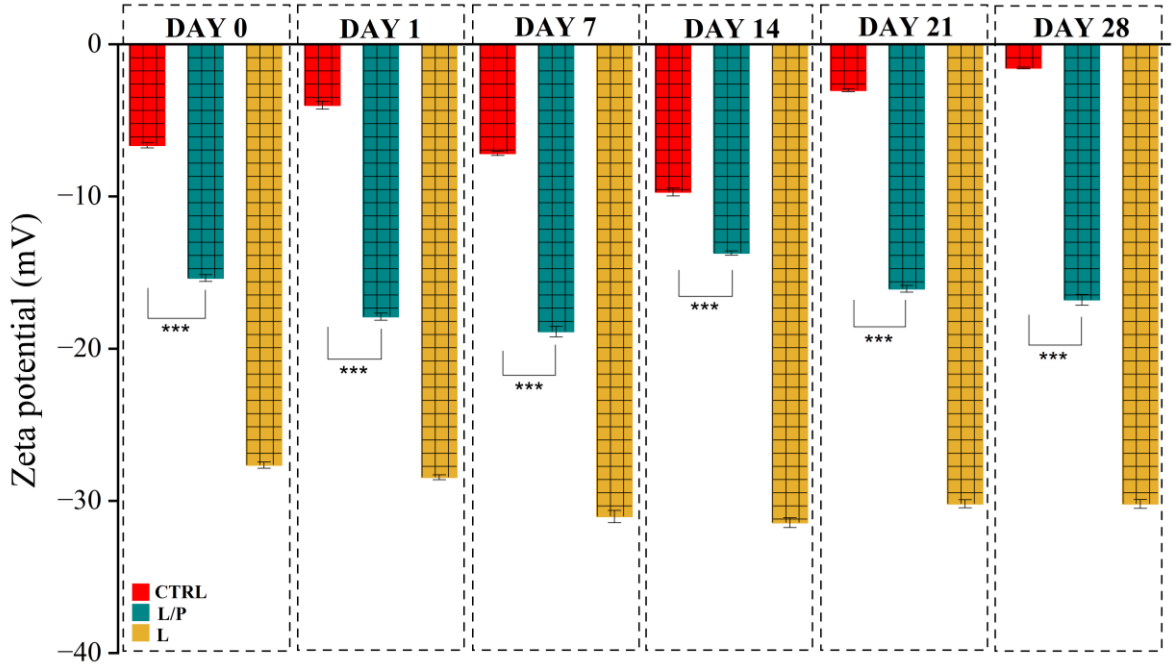

Figure 41. Results of zeta potential measurements for *L. lactis* stored at room temperature. The control sample (CTRL) represents free (uncoated) cells. The L/P sample represents lipid-coated cells. The L sample represents formulation with liposomes alone. Statistical significance: (***) $p < 0.001$.

As summarized in Table 13, DMPC liposomes exhibited narrow and temperature-independent particle size distribution (PSD), remaining within the range of approximately 91.28-164.20 nm across all measured time points. Polydispersity index (PDI) values remained low and stable at both temperatures. The corresponding intensity stayed high, ranging from approximately 68.10 ± 1.26% to 72.51 ± 2.02%. Together, these parameters indicate a uniform and well-controlled population of lipid nanoparticles [205].

For L/P samples, Table 14 shows that the primary PSD remained within the expected micrometric range. Early measurements ranged from approximately 825.00-1281.00 nm and increased moderately during storage, reaching 1106.00-1718.00 nm at 4 °C and 1106.00-2305.00 nm at room temperature by day 28. The intensity associated with this main population remained relatively stable, between 40.39 ± 0.68% and 48.62 ± 1.31%, consistent with the multimodal scattering behavior characteristic of bacterial suspensions. PDI values for DMPC-coated cells were consistently lower than those of uncoated CTRL and increased only slightly over the measurement period, indicating improved size homogeneity and slower aggregation dynamics [206]. In contrast, CTRL showed clear evidence of progressive aggregation, particularly at room temperature.

As shown in Table 15, their PSD broadened substantially over time. PDI values increased into the high-polydispersity range, and the intensity of the main population decreased as larger aggregates increasingly dominated. This behavior is characteristic of biological dispersions in which larger structures dominate light scattering in dynamic light scattering measurements [207].

DMPC liposomes are characterized by a strongly negative zeta potential resulting from exposed phosphate groups and interfacial ion interactions, which accounts for their more negative values relative to bacterial cell samples [208]. As discussed above, the phase behavior of DMPC at the two storage temperatures underlies the stabilization patterns observed in this system [209]. The moderately negative zeta potential values and limited increase in PDI observed for L/P sample at both temperatures are consistent with this phase-dependent behavior. Numerous studies have shown that liposomal membranes can associate with bacterial surfaces through a combination of electrostatic and hydrophobic interactions, forming external coatings that modulate interfacial conditions and aggregation behavior [210]. In the studied system, such adsorption is likely to reduce cell-cell interactions and slow aggregation, consistent with the more negative zeta potential and lower PDI values observed for coated samples compared with uncoated CTRL.

Overall, the DMPC lipid corona was associated with improved colloidal stability and maintenance of a more favorable surface charge over the 28-day storage period at both temperatures, while the liposome component itself retained nanometric size stability.

Table 13. Results of particle size distribution for DMPC liposomes samples stored at 4 °C and room temperature (RT). Data are expressed as mean ± standard deviation. PDI – polydispersity index.

DMPC liposomes						
Day	4 °C			RT		
	Particle size range (nm)	Intensity (%)	PDI (-)	Particle size range (nm)	Intensity (%)	PDI (-)
0	91.28 - 164.2	70.34 ± 1.89	0.22 ± 0.01	91.28 - 164.2	69.32 ± 1.01	0.22 ± 0.02
1	91.28 - 164.2	71.44 ± 1.94	0.23 ± 0.01	91.28 - 164.2	69.73 ± 1.44	0.24 ± 0.01
7	91.28 - 164.2	72.51 ± 2.02	0.24 ± 0.02	91.28 - 164.2	70.82 ± 1.45	0.25 ± 0.01
14	91.28 - 164.2	71.99 ± 1.43	0.25 ± 0.02	91.28 - 164.2	70.16 ± 1.24	0.26 ± 0.01
21	91.28 - 164.2	70.83 ± 1.65	0.24 ± 0.01	91.28 - 164.2	69.13 ± 1.27	0.26 ± 0.03
28	91.28 - 164.2	69.75 ± 1.59	0.26 ± 0.02	91.28 - 164.2	68.10 ± 1.26	0.28 ± 0.02

Table 14. Results of particle size distribution for DMPC-coated cells stored at 4 °C and room temperature (RT). Data are expressed as mean ± standard deviation. PDI – polydispersity index.

DMPC-coated cells						
Day	4 °C			RT		
	Particle size range (nm)	Intensity (%)	PDI (-)	Particle size range (nm)	Intensity (%)	PDI (-)
0	825 - 1281	40.39 ± 0.68	0.36 ± 0.02	825 - 1484	42.41 ± 1.13	0.35 ± 0.01
1	825 - 1281	41.34 ± 0.81	0.36 ± 0.01	825 - 1484	43.54 ± 0.70	0.34 ± 0.03
7	955.4 - 1484	42.59 ± 0.70	0.35 ± 0.00	955.4 - 1718	45.54 ± 1.25	0.36 ± 0.01
14	955.4 - 1484	43.19 ± 0.82	0.37 ± 0.02	955.4 - 1718	46.42 ± 1.04	0.37 ± 0.01
21	1106 - 1718	44.24 ± 0.85	0.38 ± 0.01	1106 - 1990	47.67 ± 0.82	0.40 ± 0.02
28	1106 - 1718	45.26 ± 0.91	0.41 ± 0.01	1106 - 2305	48.62 ± 1.31	0.42 ± 0.00

Table 15. Results of particle size distribution for control uncoated cells stored at 4 °C and room temperature (RT). Data are expressed as mean ± standard deviation. PDI – polydispersity index.

Control uncoated cells						
Day	4 °C			RT		
	Particle size range (nm)	Intensity (%)	PDI (-)	Particle size range (nm)	Intensity (%)	PDI (-)
0	825 - 1281	32.47 ± 0.84	0.46 ± 0.02	825 - 1484	30.53 ± 0.70	0.52 ± 0.01
1	825 - 1484	31.53 ± 1.09	0.52 ± 0.02	955.4 - 1718	29.01 ± 0.75	0.58 ± 0.03
7	955.4 - 1718	30.49 ± 0.67	0.56 ± 0.01	1106 - 1990	27.93 ± 0.65	0.61 ± 0.02
14	955.4 - 1990	29.71 ± 0.83	0.59 ± 0.01	1281 - 2305	26.57 ± 0.34	0.79 ± 0.03
21	1106 - 2305	28.18 ± 0.65	0.66 ± 0.01	1718 - 3091	25.36 ± 0.57	0.72 ± 0.01
28	1281 - 3091	26.86 ± 0.43	0.71 ± 0.03	1990 - 3580	24.24 ± 0.66	0.87 ± 0.04

3.4. Structural verification of the lipid corona

To confirm that DMPC vesicles assemble as an external lipid corona on probiotic cells, three reference states were examined using cryoSEM: uncoated *L. lactis* cells, DMPC liposomes alone, and lipid-coated cells. These images provide direct morphological evidence and complement the zeta potential and PSD data.

The CTRL image (Figure 42(A)) shows densely packed, coccoid *L. lactis* cells with dimensions of approximately 0.8-1.3 µm, as estimated from the 1 µm scale bar, consistent with reported morphological ranges for this species. Cell envelopes appear continuous and relatively smooth, with occasional division furrows characteristic of Gram-positive bacteria with a thick peptidoglycan layer [211,212]. No nanometric spherical features are visible at the cell surface, providing a baseline morphology in the absence of lipid structures.

The DMPC liposome image (Figure 42(B)) shows uniformly spherical nanoscale vesicles distributed across the field of view. Their diameters, estimated from the 100 nm scale bar, range from approximately 100 to 160 nm, in agreement with PSD measurements and with the expected size range of unilamellar vesicles formed by thin-film hydration. The vesicles appear morphologically uniform, consistent with the narrow size distributions observed for phosphatidylcholine dispersions [213,214].

In the lipid-coated cell image (Figure 42(C)), two distinct length scales are evident. Micrometric structures correspond to the bacterial cell envelope. Numerous smooth, nanometric spherical vesicles, comparable in size to those observed in the liposome sample, are clearly associated with the cell surface. These vesicles appear clustered and form bead-like chains that follow the bacterial topography. This morphology is consistent with adsorption of liposomes onto Gram-positive cell walls, resulting in formation of an external lipid corona.

CryoSEM analysis indicates that incubation of *L. lactis* with DMPC vesicles leads to the formation of an external lipid corona. Nanometric, spherical vesicles were observed in close association with the cell-liquid interface. Although previous studies have reported that phosphatidylcholine vesicles can interact with biological surfaces, the specific organization observed in this system (nanometric DMPC vesicles forming a dense, bead-like corona on *L. lactis*) differs from previously described systems [215,216]. To our knowledge, the interfacial pattern documented in Figure 42(C) has not been reported previously for probiotic bacterial systems.

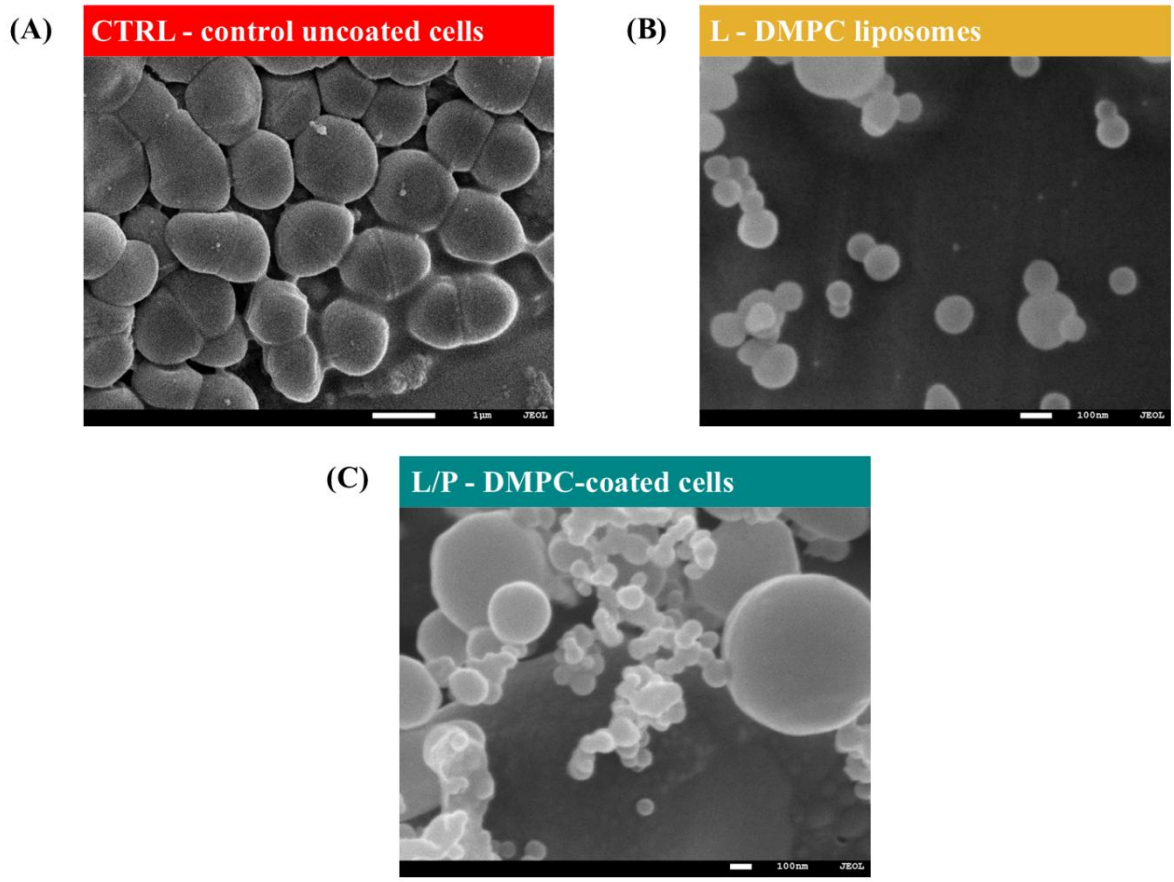

Figure 42. Representative cryoSEM images illustrating (A) control uncoated cells, (B) DMPC liposomes alone, and (C) DMPC-coated cells. Figure A shows cells undergoing cell division.

3.5. Summary of lipid-stabilized probiotic systems

Across all performed assays, DMPC-coated cells showed improved performance relative to uncoated CTRL, particularly under room temperature conditions. Coated samples exhibited earlier metabolic activation, sustained activity over longer periods, and higher cell density. At 4 °C, the beneficial effect was still observed but was reduced in magnitude and duration, consistent with decreased membrane fluidity of DMPC at low temperature and the slower physiological activity of bacteria under cold storage. At later storage time points, differences between coated and uncoated cells decreased. However, the early advantage associated with the lipid corona was consistently observed across all functional readouts.

Electrokinetic and colloidal measurements supported these trends. DMPC-coated cells maintained a more negative and stable zeta potential throughout storage, whereas uncoated cells progressively shifted toward electrostatic neutrality. In addition, coated suspensions retained narrower particle size distributions and lower PDI values, indicating reduced aggregation and

more homogeneous population structure. In contrast, uncoated samples exhibited increasing polydispersity, with aggregation dominating their hydrodynamic profiles. Liposomes alone remained stable over time and served as a reference for a well-defined colloidal system. Together, these parameters indicate that the lipid corona contributes electrostatic repulsion that limits cell-cell interactions and aggregation, supporting improved functional stability.

CryoSEM imaging provided direct structural support for these observations. Coated cells displayed a two-scale organization, with micrometric *L. lactis* envelopes decorated by adherent nanometric vesicles resembling isolated DMPC liposomes. Uncoated control cells lacked these surface-associated nanostructures, while liposomes alone appeared as uniform nanoscale spheres. These observations indicate that DMPC vesicles form an external pericellular lipid corona rather than an encapsulating shell.

Taken together, the findings indicate that prepared colloidal systems can stabilize probiotic cells by modulating their micro- and nanoscale environment, thereby improving both colloidal behavior and biological performance.

At this stage, the work addresses *Specific research aims (B-E)* related to formulation of functional lipid-stabilized probiotic system, characterization of its structural and physicochemical properties, demonstration of improved metabolic activity and viability of cells, and evaluation of stability under relevant storage conditions. These outcomes contribute to the overall objective of the dissertation and support the formulated research hypothesis.

4. FUNCTIONAL EVALUATION OF FLUVASTATIN-LOADED LIPOSOMAL PROBIOTIC SYSTEMS

This stage evaluated the functional performance of colloidal probiotic systems obtained by combining *Lactiplantibacillus plantarum* with DOPG-based liposomes loaded with fluvastatin. In this formulation, probiotic cells were not encapsulated within vesicles but became externally associated with nanoscale liposomes that adsorbed onto the bacterial surface, forming a pericellular lipid corona. The resulting structure represents a dual-component system in which bacterial cells interact with a surrounding layer of DOPG-fluvastatin vesicles. The objective was to assess whether this lipid corona influences biological and physicochemical stability of probiotic cells and to determine how fluvastatin-containing liposomes affect cellular activity, viability, oxidative stress response, and colloidal behavior during storage. This

evaluation allows assessment of the functional role of fluvastatin-loaded liposomal carriers as stabilization platforms within the tested probiotic system.

The following abbreviations were used for the samples:

- CTRL – free (uncoated) probiotic cells,
- B/L – lipid-coated (DOPG-coated) probiotic cells,
- B/L/F – probiotic cells with a surrounding layer of liposomes loaded with fluvastatin.

4.1. Cellular activity

This section examined whether *L. plantarum* maintains metabolic activity during refrigerated storage and how this profile is influenced by formulation. Bacteria were evaluated as free cells (CTRL) and as cells incorporated into two liposomal systems. Measurements were performed on days 1, 7, 14, and 28.

The MTT and AlamarBlue assays were used as a quantitative indicators of metabolic reduction capacity. As shown in Figure 43, on day 1, metabolic activity in the CTRL reached 0.84 ± 0.02 MRU, whereas both formulated systems showed significantly lower values. The strongest reduction was observed in B/L (0.45 ± 0.04, $p < 0.001$), while B/L/F reached 0.63 ± 0.02 ($p < 0.001$). By day 7, MRU values increased across all groups, but both B/L and B/L/F remained significantly lower than the CTRL. A shift was observed on day 14. While B/L continued to exhibit reduced MRU relative to CTRL (1.03 ± 0.05 vs 1.30 ± 0.03, $p < 0.001$), the fluvastatin-loaded system reached 1.31 ± 0.03 and did not differ significantly from the CTRL. At later time point, the divergence between the liposomal systems became more clear. On day 28, the CTRL decreased to 0.93 ± 0.05, while B/L and B/L/F remained higher at 1.19 ± 0.03 and 1.58 ± 0.05, respectively ($p < 0.001$ for both).

As shown in Figure 44, the AlamarBlue assay revealed distinct patterns. On day 1, B/L exhibited increased AB reduction (121.05 ± 1.80%, $p < 0.001$), whereas B/L/F showed reduced values (82.70 ± 2.16%, $p < 0.001$). From day 7, both formulated systems exceeded the CTRL. On day 7, B/L reached 175.12 ± 1.78% and B/L/F reached 109.68 ± 1.29% ($p < 0.001$ for both). Elevated reduction persisted at day 14 (163.40 ± 6.04 and 139.41 ± 0.84%, respectively) and peaked at day 21 (177.66 ± 1.79 and 168.31 ± 2.63%), with all comparisons remaining statistically significant relative to CTRL ($p < 0.001$). By day 28, both systems converged to 132.58 ± 1.57% ($p < 0.001$).

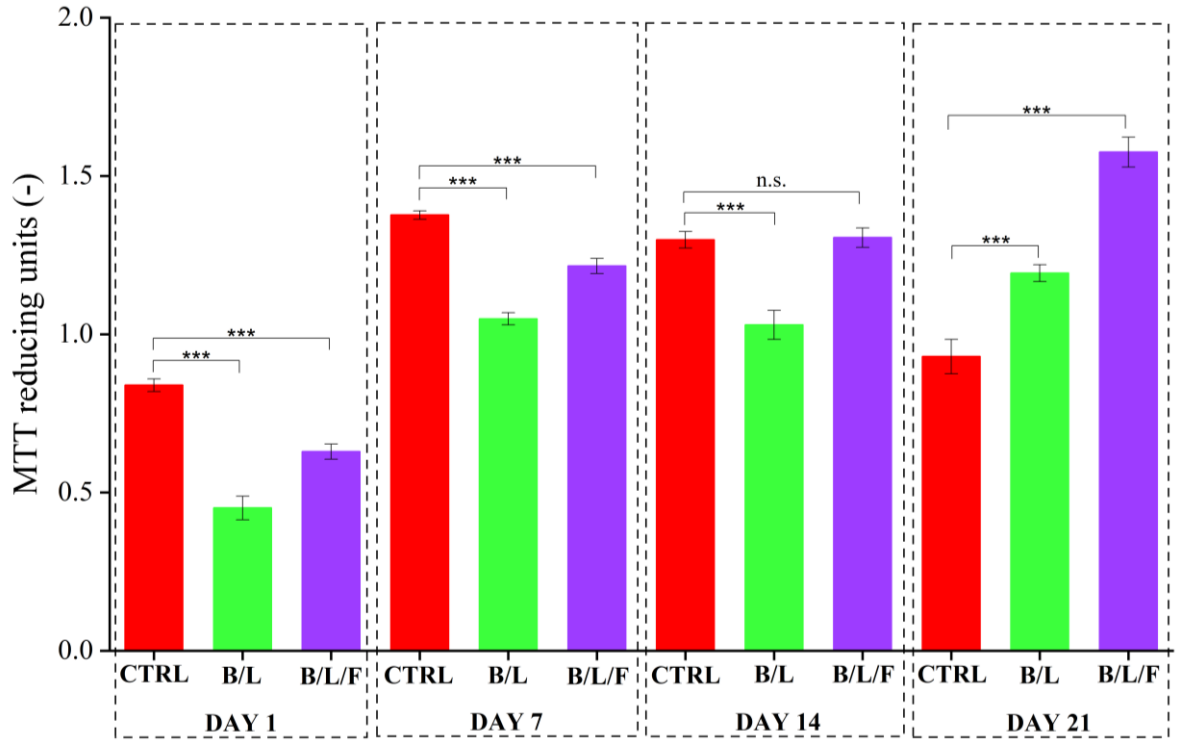

Figure 43. Results of metabolic activity (MTT reducing units – MRU) for *L. plantarum*. The control sample (CTRL) represents free (uncoated) cells. The B/L sample represents lipid-coated cells. The B/L/F sample represents cells with a surrounding layer of liposomes loaded with fluvastatin. Comparisons without asterisks are not statistically significant (n.s.). Statistical significance: (***) $p < 0.001$.

The MTT and AlamarBlue data indicate that formulation primarily modifies the temporal profile of cellular activity rather than leading to a progressive loss of functional competence. This observation is consistent with the broader view that microbial viability and activity represent multidimensional physiological states best characterized using complementary analytical approaches rather than a single endpoint assay [197]. In the present dataset, B/L maintained elevated reducing capacity, while MTT values remained moderately lower than those of the CTRL up to day 21. Such a pattern is consistent with a stabilized physiological state during refrigerated storage. Similar stabilization effects have been reported for liposome-based surface coating strategies that support probiotic performance under stress conditions, even when individual metabolic indices do not uniformly increase across assays [217].

The most distinctive profile was observed for B/L/F. An early reduction in metabolic indicators was followed by normalization by day 14 and then increases in MTT values at last time point This trajectory is consistent with behavior expected for lipophilic compounds incorporated

within lipid bilayers, as liposomal systems are commonly used to accommodate hydrophobic bioactives and modulate their microenvironment during storage and delivery [218].

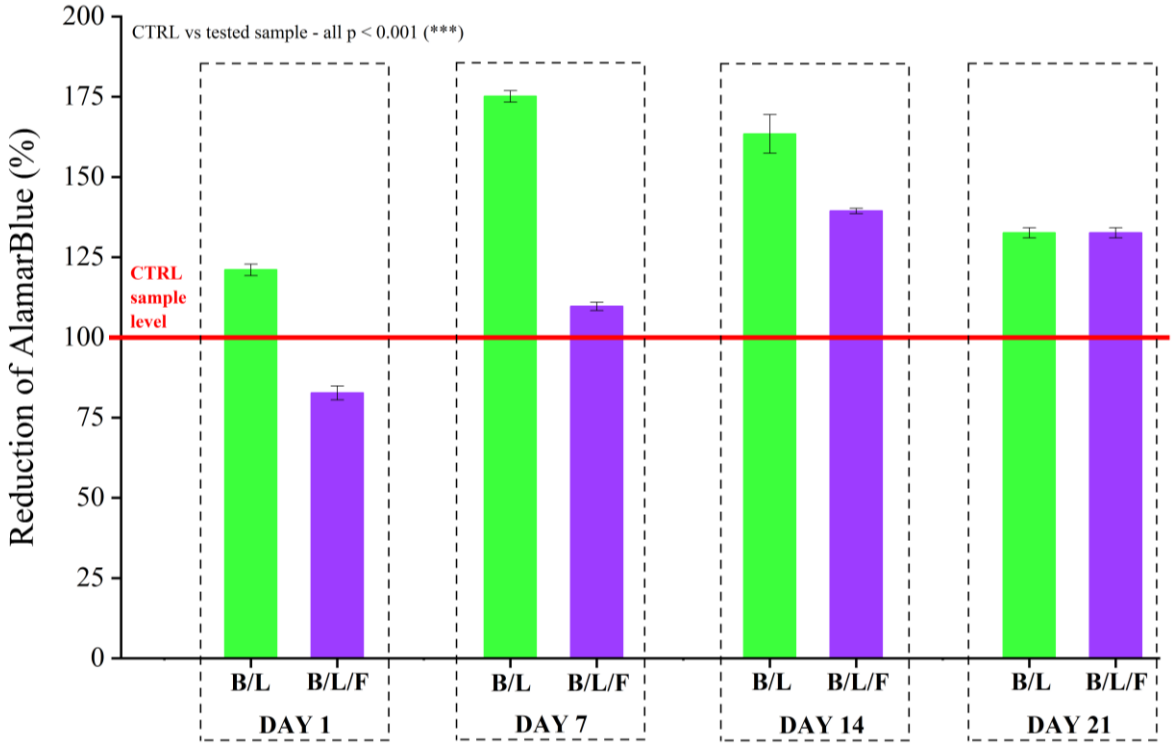

Figure 44. Results of cytotoxicity for *L. plantarum*. The control sample (CTRL) represents free (uncoated) cells. The B/L sample represents lipid-coated cells. The B/L/F sample represents cells with a surrounding layer of liposomes loaded with fluvastatin. Statistical significance: (***) $p < 0.001$.

Fluvastatin, a predominantly lipophilic statin, has been described as interacting with membrane environments and exhibiting distribution influenced by passive diffusion properties [219]. Molecular-level studies further indicate that fluvastatin can associate with and permeate lipid bilayers, and that statin insertion may perturb bilayer structure, providing a plausible basis for transient adaptive responses followed by functional stabilization [220]. From a functional perspective, incorporation of fluvastatin introduces an additional bioactive component within the liposomal probiotic system. Probiotic strains have been associated with cholesterol-related metabolic pathways [221]. In this context, maintaining viable and metabolically competent *L. plantarum* populations while incorporating a clinically used hypolipidemic compound represents a multifunctional formulation approach. The early metabolic modulation observed in B/L/F may therefore reflect adaptation to the lipid-drug environment rather than loss of probiotic function.

4.2. Physiological subpopulation dynamics of cells

Flow cytometry was applied to track shifts in *L. plantarum* physiological heterogeneity within liposomal formulations by resolving four gated subpopulations (active, dormant, injured, and dead). Measurements were performed on days 1, 7, 14, and 28.

Inspection of the dot plots revealed formulation- and time-dependent redistribution of events across the defined gates. In the CTRL the dominant clusters were consistently located within the injured and dead regions, with only limited representation in the active gate across all time points (Figure 45). A gradual shift toward higher propidium iodide (PI) signal intensity became evident by day 28, accompanied by increased event density in the dormant/dead region and minimal occupancy of the active gate.

In bacteria coated with unloaded liposomes (B/L), dot plots showed a more distinct active-gate cluster during mid-storage (days 7-14), while the dead region appeared less populated than in the CTRL at these time points (Figure 46). By day 28, the B/L distribution shifted more toward the dead region, and the active cluster was reduced.

In the fluvastatin-loaded system (B/L/F), a distinct active cluster was detectable on day 1 and remained prominent on days 7 and 14 (Figure 47). At late storage (day 28), reduced active-gate occupancy was observed together with broader event distribution within the injured and dead regions. Overall, the qualitative dot-plot analysis indicates that liposomal surface coating delayed the decline of physiologically active subpopulations, with the fluvastatin-containing system showing the most pronounced enrichment of the active gate during mid-storage.

These qualitative shifts were supported by the fractional composition data (Table 16). In the CTRL, the population was dominated by injured cells on day 1 (67.38 ± 0.76%), with a substantial dead fraction (28.54 ± 0.80%). The active fraction remained minimal reaching only 1.33 ± 0.08% at day 1 and 0.17 ± 0.01% at day 28). The dormant fraction increased to 30.00 ± 0.93% on day 28. In B/L, the active fraction increased during storage, reaching 11.87 ± 0.71% at day 7 and peaking at 20.93 ± 0.68% at day 14, while the dead fraction remained comparatively low at these time points (10.13 ± 0.50 and 9.68 ± 0.25%, respectively). Around day 28, the population changed towards a predominance of dead cells (81.03 ± 0.17%), accompanied by a decrease in the fraction of injured cells (17.89 ± 0.24%) and 2.87 ± 0.12% of active cells. In contrast, B/L/F displayed the highest active fractions during mid-storage, reaching 33.80 ± 0.31% at day 7 and 31.79 ± 0.54% at day 14, together with lower injured fractions relative to the CTRL at those time points (26.68 ± 1.20 and 25.55 ± 1.34%,

respectively). By day 28, the B/L/F distribution shifted toward a higher dead fraction reaching 60.56 ± 0.90%, while a notable injured fraction remained at 31.12 ± 0.96%, and the active fraction decreased. Across the full storage period, the principal trend was a transient enrichment of the active subpopulation during mid-storage in both liposome-coated systems, with the most clear effect observed for B/L/F on days 7 and 14.

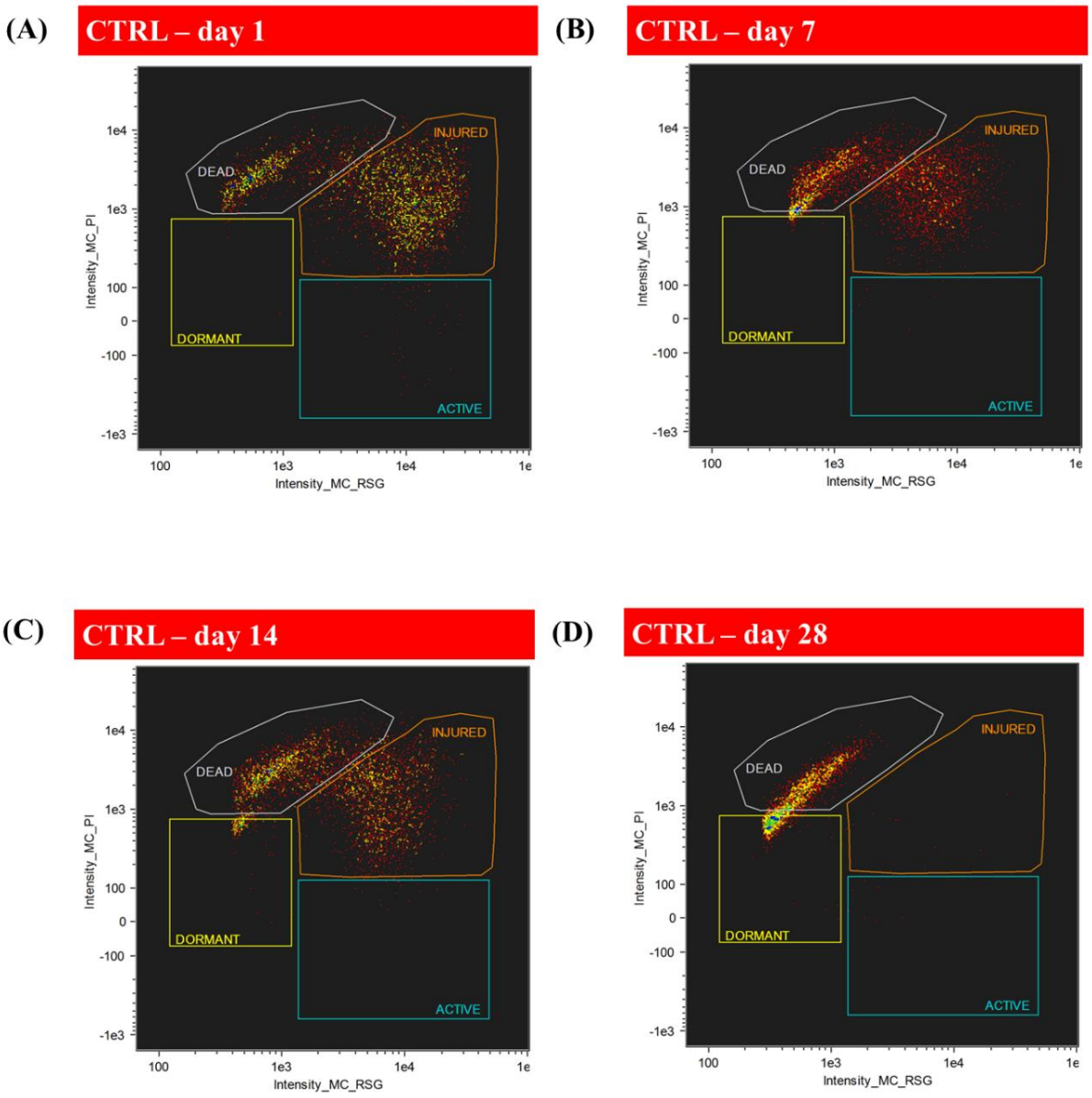

Figure 45. Representative flow cytometry dot plots showing the distribution of bacterial subpopulations in the control sample (CTRL) at days 1, 7, 14, and 28 of storage. Subpopulations (active, dormant, injured, dead) were defined based on the fluorescence intensity of RSG (metabolic activity, X-axis) and propidium iodide (PI; membrane integrity, Y-axis). Logarithmic scale and consistent gating were applied across all time points.

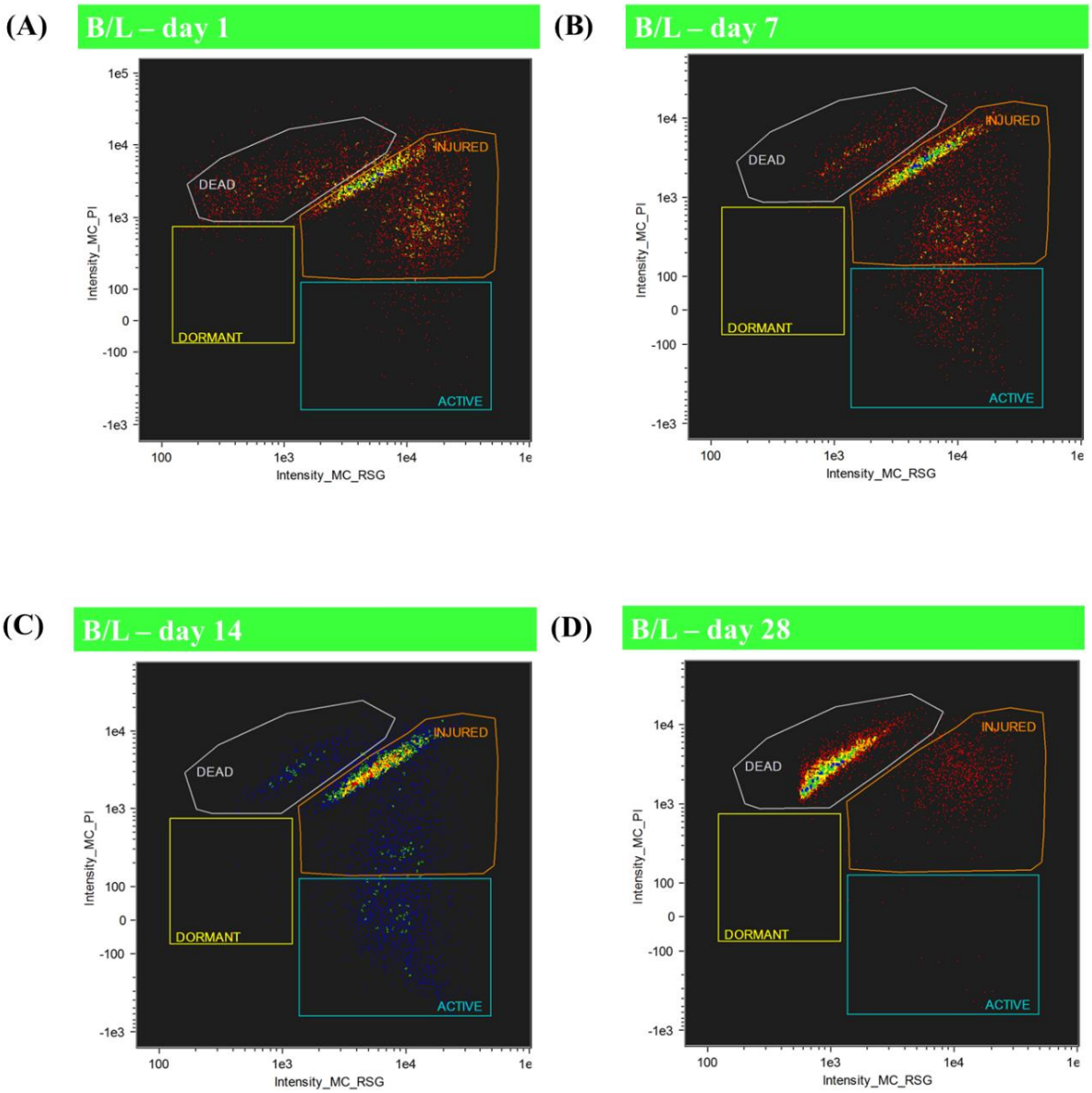

Figure 46. Representative flow cytometry dot plots showing the distribution of bacterial subpopulations in the sample B/L (bacteria coated with unloaded liposomes) at days 1, 7, 14, and 28 of storage. Subpopulations (active, dormant, injured, dead) were defined based on the fluorescence intensity of RSG (metabolic activity, X-axis) and propidium iodide (PI; membrane integrity, Y-axis). Logarithmic scale and consistent gating were applied across all time points.

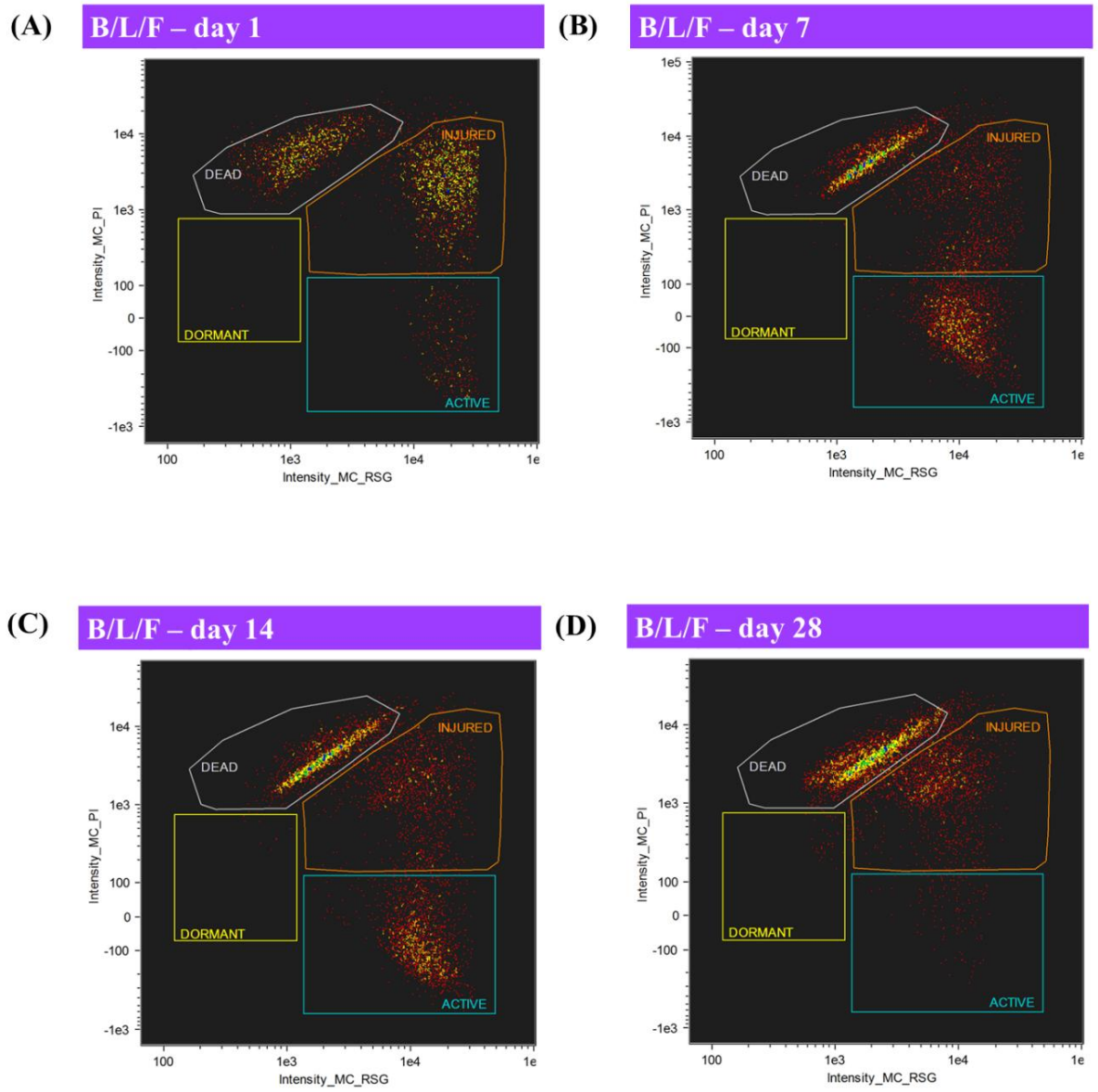

Figure 47. Representative flow cytometry dot plots showing the distribution of bacterial subpopulations in the sample B/L/F (bacteria coated with the fluvastatin-loaded liposomes) at days 1, 7, 14, and 28 of storage. Subpopulations (active, dormant, injured, dead) were defined based on the fluorescence intensity of RSG (metabolic activity, X-axis) and propidium iodide (PI; membrane integrity, Y-axis). Logarithmic scale and consistent gating were applied across all time points.

Table 16. Fractional composition of bacterial cell subpopulations in control sample (CTRL), B/L (bacteria coated with unloaded liposomes) and B/L/F (bacteria coated with the fluvastatin-loaded liposomes) samples. Data are presented as mean ± standard deviation.

Day	Fractional composition of cell populations (%)			
	CTRL			
	active	**dormant**	**injured**	**dead**
1	1.33 ± 0.08	0.28 ± 0.05	67.38 ± 0.76	28.54 ± 0.80
7	0.24 ± 0.03	2.08 ± 0.09	44.52 ± 0.68	47.07 ± 0.94
14	0.71 ± 0.08	5.29 ± 0.25	43.19 ± 0.92	45.48 ± 1.05
28	0.17 ± 0.01	30.00 ± 0.93	0.52 ± 0.05	60.30 ± 0.41
Day	**B/L**			
	active	**dormant**	**injured**	**dead**
1	1.89 ± 0.05	0.39 ± 0.04	68.41 ± 0.37	21.37 ± 0.70
7	11.87 ± 0.71	0.12 ± 0.01	73.75 ± 0.38	10.13 ± 0.50
14	20.93 ± 0.68	0.19 ± 0.01	66.73 ± 0.05	9.68 ± 0.25
28	2.87 ± 0.12	0.05 ± 0.01	17.89 ± 0.24	81.03 ± 0.17
Day	**B/L/F**			
	active	**dormant**	**injured**	**dead**
1	7.62 ± 0.18	0.11 ± 0.02	52.66 ± 0.66	36.28 ± 0.30
7	33.80 ± 0.31	0.05 ± 0.01	26.68 ± 1.20	36.03 ± 0.90
14	31.79 ± 0.54	0.21 ± 0.01	25.55 ± 1.34	39.63 ± 0.30
28	2.57 ± 0.03	0.88 ± 0.07	31.12 ± 0.96	60.56 ± 0.90

The absolute counts of objects were evaluated to capture not only population composition but also the total number of detectable cells within each physiological state (Figure 48). In the CTRL, active cell counts remained low throughout storage (from $2.45 \pm 0.19 \cdot 10^4$ objects·mL^{-1} on day 1 to and $3.40 \pm 0.40 \cdot 10^3$ objects·mL^{-1} on day 28). Liposome coating was associated with a marked increase in absolute active counts during mid-storage. B/L reached $1.03 \pm 0.06 \cdot 10^6$ objects·mL^{-1} on day 7 and $1.54 \pm 0.14 \cdot 10^6$ objects·mL^{-1} on day 14. The fluvastatin-loaded system (B/L/F) showed higher active counts at these time points, reaching $8.69 \pm 1.14 \cdot 10^6$ objects·mL^{-1} on day 7 and $4.27 \pm 0.15 \cdot 10^6$ objects·mL^{-1} on day 14. Although the active fraction of B/L/F decreased by day 28, the absolute number of active events remained elevated ($3.54 \cdot 0.04 \cdot 10^5$ objects·mL^{-1}), exceeding the corresponding values for B/L ($1.14 \pm 0.13 \cdot 10^4$ objects·mL^{-1}) and the CTRL ($3.40 \pm 0.40 \cdot 10^3$ objects·mL^{-1}).

In parallel, late-stage dormancy increased clearly in the CTRL ($5.39 \pm 0.25 \cdot 10^5$ dormant objects·mL^{-1} on day 28), whereas B/L exhibited minimal dormant counts at this time point ($1.67 \pm 0.03 \cdot 10^3$ objects·mL^{-1}) and B/L/F maintained intermediate levels ($1.11 \pm 0.12 \cdot 10^5$ objects·mL^{-1}). The injured subpopulation showed distinct trends. B/L/F retained a large injured pool at day 28 ($4.18 \pm 0.40 \cdot 10^6$ objects·mL^{-1}), while the CTRL injured count decreased to $8.09 \pm 2.32 \cdot 10^3$ objects·mL^{-1}. This analysis indicates that liposome-coated systems, particularly B/L/F, maintained higher numbers of physiologically active cells during mid-storage and preserved a measurable active population at day 28, while also retaining substantial pools of injured cells.

From a functional perspective, these flow cytometric profiles indicate that *L. plantarum* stored under cold conditions does not behave as a uniform population but redistributes into co-existing physiological states whose relative proportions are formulation dependent [222]. This observation has an application for the interpretation of viability in complex probiotic systems. Culture-based enumeration may underestimate physiologically competent cells when dormancy, VBNC, or injury states are present, whereas culture-independent methods provide an important complementary assessment of formulation performance [223].

Within this framework, the CTRL exhibited pattern characterized by increased dormancy and death, consistent with stress-associated transition into low-activity states and later decline in membrane integrity over time. In contrast, both liposome-coated systems showed a transient shift toward higher active fractions and markedly higher numbers of active objects during days 7-14, indicating that an external lipid corona can modulate short- to mid-term physiological

status, potentially through effects on membrane stress buffering, cell-cell interactions, and the local interfacial environment surrounding the bacteria [48].

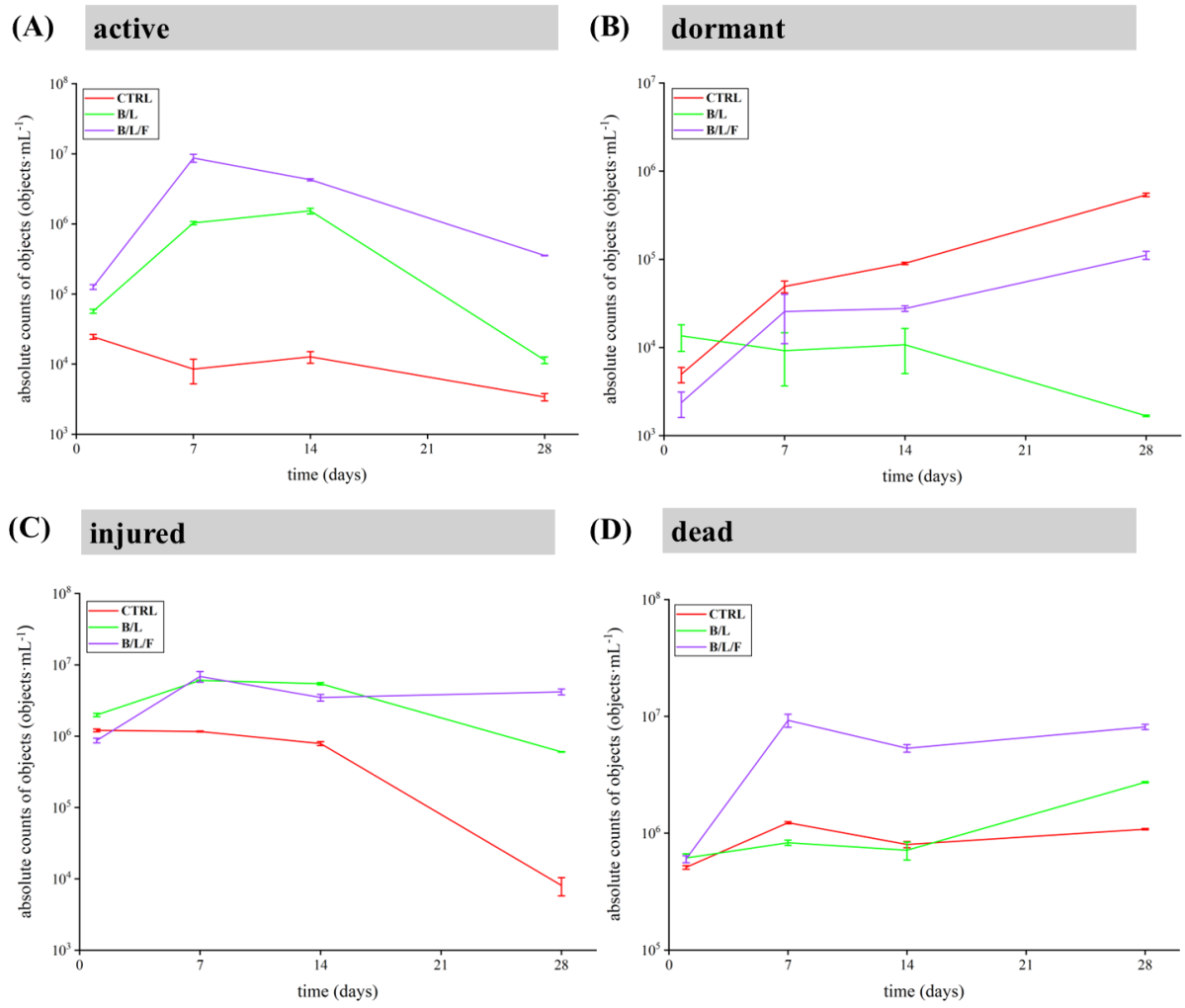

Figure 48. Absolute counts of bacterial cell subpopulations in control sample (CTRL), B/L (bacteria coated with unloaded liposomes) and B/L/F (bacteria coated with the fluvastatin-loaded liposomes) samples.

The value of combining percentage composition with absolute object counts becomes evident at late storage. Despite similarly increased dead fractions by day 28, B/L/F retained a larger absolute active pool than B/L and the CTRL, indicating that the fluvastatin-loaded liposomal architecture preserved a measurable functional subpopulation even as overall deterioration progressed. Such divergence between relative fractions and absolute counts aligns with the ability of flow cytometry to identify physiologically relevant subpopulations (including injured but potentially recoverable cells) which may not be visible by single-endpoint methods and can shift markedly depending on formulation conditions [120].

Finally, the presence of large injured pools, particularly in B/L/F, should not be interpreted entirely as failure, as this injury may represent an intermediate and potentially reversible state. *L. plantarum* has been shown to enter VBNC state in response to technological stresses and then recovering under favorable conditions. This supports the idea that injured and inactive fractions may still be biologically relevant, depending on environmental factors [224].

4.3. Oxidative stress response

The activity of GSTs was measured to evaluate the effect of liposomal coating and fluvastatin loading on the oxidative stress-related detoxification profile of *L. plantarum* during storage. Measurements were performed on days 1, 7, 14, and 28.

As shown in Figure 49, GSTs activity in the CTRL reached 0.65 ± 0.04 $\mu mol \cdot min^{-1} \cdot mg^{-1}$ of protein on day 1, whereas both liposomal systems exhibited significantly lower values. In B/L sample, GSTs activity reached 0.43 ± 0.03 $\mu mol \cdot min^{-1} \cdot mg^{-1}$ of protein ($p < 0.001$), and the lowest activity was observed for B/L/F (0.35 ± 0.02 $\mu mol \cdot min^{-1} \cdot mg^{-1}$ of protein, $p < 0.001$). A similar pattern was observed on day 7. While the CTRL value decreased to 0.46 ± 0.03 $\mu mol \cdot min^{-1} \cdot mg^{-1}$ of protein, coated samples remained significantly lower, with 0.35 ± 0.02 $\mu mol \cdot min^{-1} \cdot mg^{-1}$ of protein for B/L and 0.35 ± 0.02 $\mu mol \cdot min^{-1} \cdot mg^{-1}$ of protein for B/L/F ($p < 0.001$ for both). On day 14, the CTRL values increased to 0.64 ± 0.05 $\mu mol \cdot min^{-1} \cdot mg^{-1}$ of protein, whereas coated systems again displayed significantly reduced GSTs activity. B/L sample reached 0.39 ± 0.02 $\mu mol \cdot min^{-1} \cdot mg^{-1}$ of protein ($p < 0.001$), while B/L/F sample increased to 0.45 ± 0.01 $\mu mol \cdot min^{-1} \cdot mg^{-1}$ of protein ($p < 0.001$), remaining below the CTRL but exceeding B/L at the same time point. By day 28, GSTs activity decreased in all samples, with CTRL reaching 0.42 ± 0.02 $\mu mol \cdot min^{-1} \cdot mg^{-1}$ of protein, B/L reaching 0.28 ± 0.02 $\mu mol \cdot min^{-1} \cdot mg^{-1}$ of protein ($p < 0.001$), and B/L/F reaching 0.32 ± 0.01 $\mu mol \cdot min^{-1} \cdot mg^{-1}$ of protein ($p = 0.001$).

A consistent overall trend was observed during storage. The CTRL exhibited a non-monotonic pattern, with higher GSTs activity on days 1 and 14 and lower values on days 7 and 28. In contrast, both liposomal systems maintained reduced GSTs activity relative to the CTRL throughout the experiment. B/L showed a gradual decrease over time, whereas B/L/F showed a partial increase at day 14 and remained higher than B/L at later time points (days 14 and 28), but still significantly lower than the CTRL.

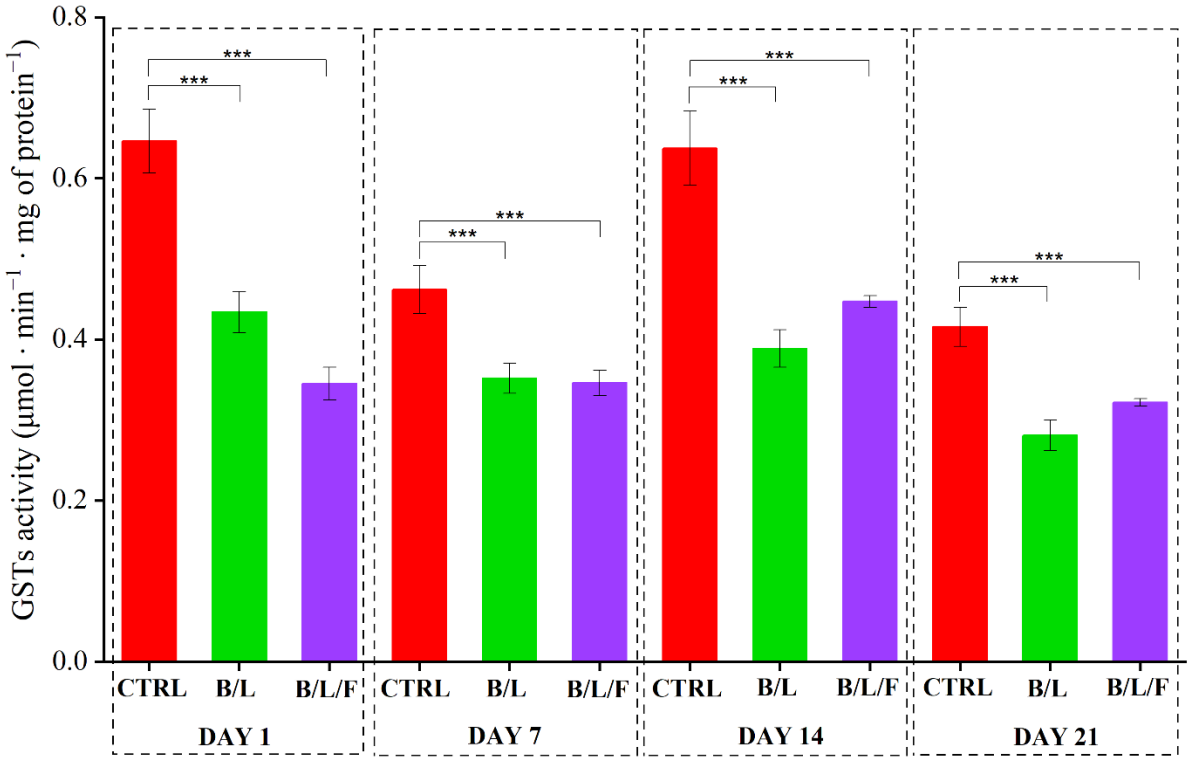

Figure 49. Results of GSTs activity for *L. plantarum* .The control sample (CTRL) represents free (uncoated) cells. The B/L sample represents lipid-coated cells. The B/L/F sample represents cells with a surrounding layer of liposomes loaded with fluvastatin. Statistical significance: (*) $p < 0.05$; (**) $p < 0.01$; (***) $p < 0.001$.

GSTs enzymes contribute to detoxification processes in *Lactobacillus* strains and are commonly induced under stress conditions, supporting their application as functional indicators of oxidative stress-related adaptation in LAB systems [225]. In probiotic bacteria, oxidative stress tolerance is generally governed by coordinated antioxidant and detoxification responses that are strongly influenced by storage conditions and the physicochemical microenvironment [139]. In this context, the consistently lower GST activity observed in both liposomal formulations relative to the control indicates that lipid nanoparticle coating modified the oxidative conditions experienced by the bacteria during storage, reducing the apparent demand for GST-mediated detoxification. This interpretation is consistent with reports describing improved probiotic stability in lipid/liposomal systems, potentially associated with modulation of interfacial environments and reduced stress exposure [217].

The fluvastatin-loaded system showed the lowest GST activity at early time points, followed by a moderate increase at day 14 and higher values than B/L at later storage stages. This pattern suggests that fluvastatin incorporation may introduce a formulation-specific balance between

stress buffering and adaptive response. Statins have been reported to influence oxidative stress pathways and antioxidant enzyme profiles in biological systems, reflecting pleiotropic cellular effects beyond lipid modulation [226]. Fluvastatin in particular has been shown to attenuate oxidative damage in cellular models subjected to oxidative challenge, which is consistent with the reduced early GST activity observed in B/L/F compared with the CTRL [227].

The slightly higher GSTs activity of B/L/F relative to B/L at later time points may reflect a sustained but controlled adaptive component associated with the drug-loaded lipid phase. This pattern remains compatible with the maintenance of functional subpopulations observed by flow cytometry and with the metabolic competence indicated by MTT and AlamarBlue profiles during the same storage intervals.

4.4. Physicochemical stability of probiotic systems

To assess colloidal stability and temperature responsiveness of the probiotic formulations, the systems were characterized by zeta potential and PSD measured at room temperature and at 36.6 °C (physiological temperature). Measurements were performed on days 1, 7, 14, and 28.

Zeta potential measurements showed that all samples maintained a negative surface charge at both temperatures throughout storage. However, the magnitude of the zeta potential and the differences between samples varied depending on the time point. At room temperature (Figure 50), the CTRL sample exhibited a zeta potential of -33.33 ± 1.00 mV on day 1, followed by a shift toward less negative values on day 7 (-21.41 ± 1.89 mV), and then a return to more negative values on days 14 and 28 (-32.94 ± 1.67 mV and -32.11 ± 0.71 mV, respectively). In contrast, both liposomal systems displayed significantly more negative zeta potential values at early storage. On day 1, B/L reached -42.43 ± 3.85 mV ($p < 0.001$) and B/L/F reached -38.49 ± 1.28 mV ($p = 0.009$). A similar pattern was observed on day 7, with B/L at -44.12 ± 3.12 mV and B/L/F at -40.93 ± 1.84 mV ($p < 0.001$ for both), while the CTRL exhibited weaker electrostatic repulsion. By days 14 and 28, zeta potential values converged across all samples, clustering around approximately -32 to -34 mV, indicating progressive equilibration of the effective surface charge over time.

A comparable pattern was observed at 36.6 °C (Figure 51). The CTRL again showed a shift toward less negative zeta potential values on day 7 (-21.64 ± 1.95 mV) compared with day 1 (-33.02 ± 2.09 mV). On both day 1 and day 7, liposomal systems exhibited significantly more negative values than the CTRL. On day 1, the B/L sample reached -37.79 ± 1.19 mV and B/L/F

-38.73 ± 0.89 mV ($p < 0.001$ for both). On day 7, B/L reached -38.25 ± 1.10 mV and B/L/F -41.37 ± 1.86 mV ($p < 0.001$ for both). As observed at room temperature, differences were not statistically significant at later time points, with all samples remaining negative (approximately -29 to -31 mV).

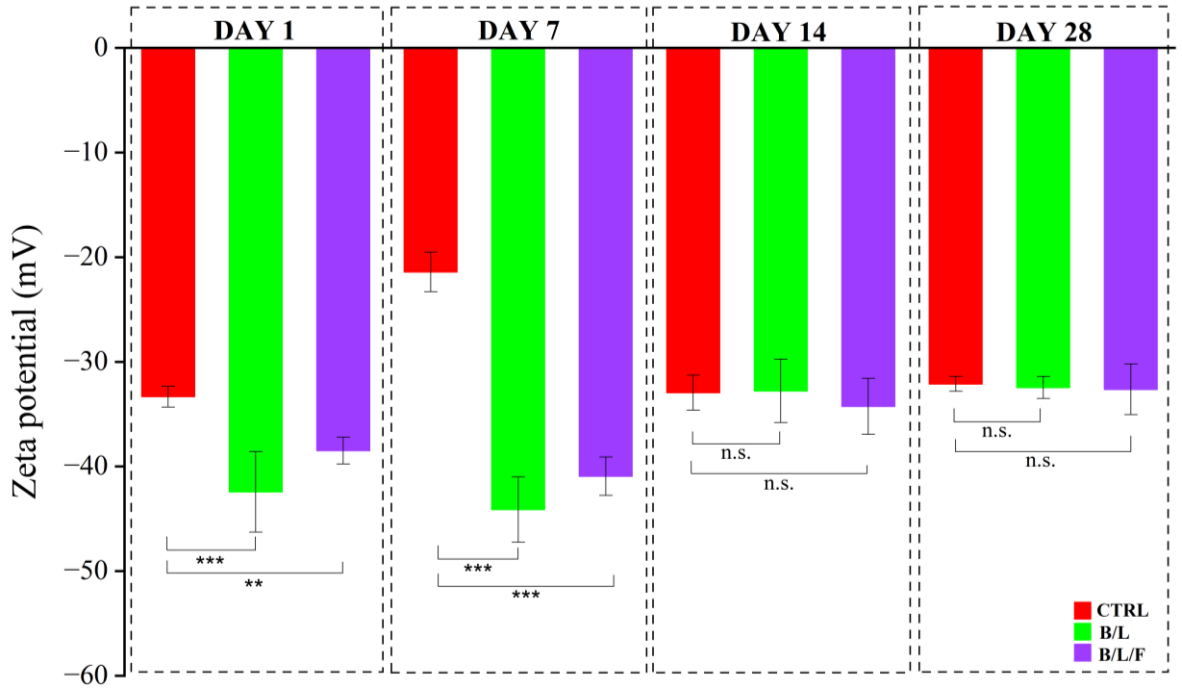

Figure 50. Results of zeta potential measurements for *L. plantarum* performed at room temperature. The control sample (CTRL) represents free (uncoated) cells. The B/L sample represents lipid-coated cells. The B/L/F sample represents cells with a surrounding layer of liposomes loaded with fluvastatin. Comparisons without asterisks are not statistically significant (n.s.). Statistical significance: (**) $p < 0.01$; (***) $p < 0.001$.

Consistent with the zeta potential results, PSD demonstrated a divergence between the CTRL and the liposome-based systems, which was more visible at physiological temperature. At room temperature (Figure 52), the detected size fraction in the CTRL shifted toward larger dimensions over time, reaching 811-1823 nm (32.59 ± 1.27%) on day 14 and remaining elevated on day 28 (460-1319 nm, 17.42 ± 0.84%). In contrast, both B/L and B/L/F consistently exhibited nanometric size fractions throughout storage. For B/L, recorded ranges remained within 91-205 nm (16.48 ± 1.02%) at day 1, 66-307 nm (10.70 ± 0.59%) at day 7, and 61-361 nm (7.25 ± 0.62%) at day 28. The fluvastatin-loaded system showed a similarly stable nanoscale profile, with 91-161 nm (20.50 ± 0.94%) at day 1 and 32-307 nm by day 28 (6.85 ± 0.30%) by day 28.

At 36.6 °C (Figure 53), the CTRL showed a persistent shift toward the micron range beginning at day 1 (636-1430 nm, 22.23 ± 2.47%) and reaching its broadest detected fraction on day 7 (748-2325 nm, 13.02 ± 1.26%). In contrast, both liposomal systems remained within nanometric ranges across all time points at 36.6 °C. B/L ranged from 71-205 nm (18.31 ± 1.93%) at day 1 to 77-174 nm (16.42 ± 0.95%) at day 28, while B/L/F showed a late-storage range of 44-137 nm (11.72% ± 0.72) by day 28. The persistence of nanometric size distributions at physiological temperature indicates that liposomal formulations did not undergo substantial temperature-induced fusion or aggregation within the tested storage period.

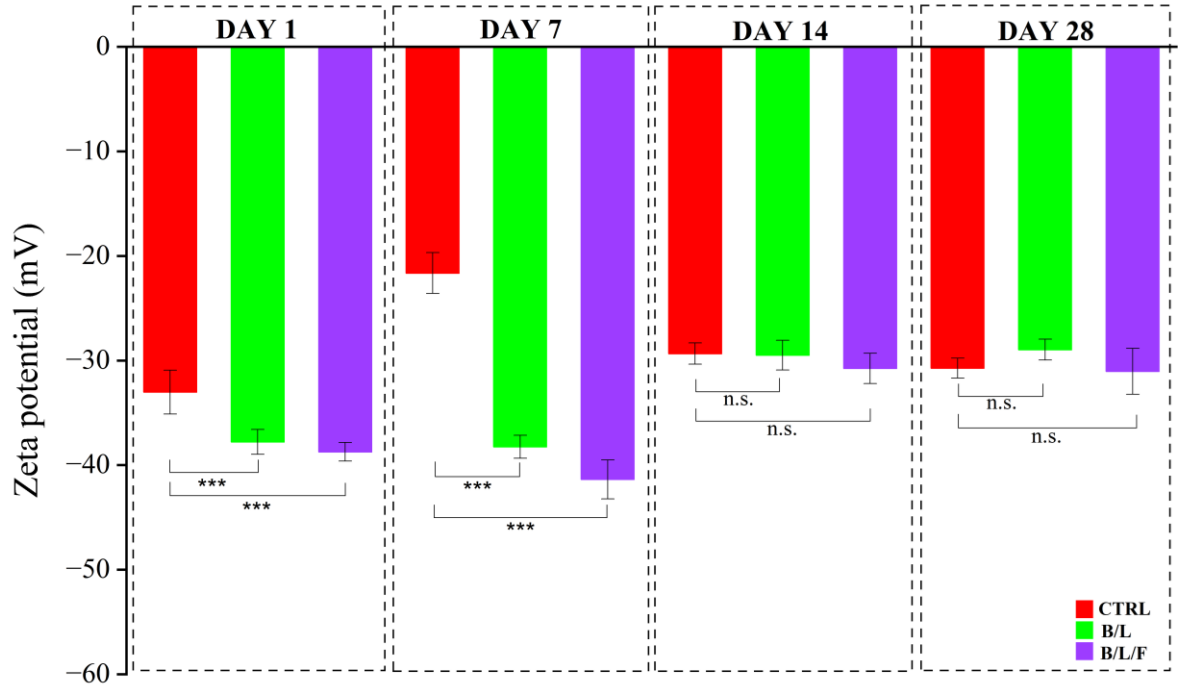

Figure 51. Results of zeta potential measurements for *L. plantarum* performed at 36.6 °C. The control sample (CTRL) represents free (uncoated) cells. The B/L sample represents lipid-coated cells. The B/L/F sample represents cells with a surrounding layer of liposomes loaded with fluvastatin. Comparisons without asterisks are not statistically significant (n.s.). Statistical significance: (***) $p < 0.001$.

From a stability standpoint, zeta potential values of around -30 mV or lower are generally considered to be the practical threshold for electrostatically stabilized dispersions [228]. The early-storage behavior indicates a physicochemical advantage of the liposomal formulations. While the CTRL shifted into a region of weaker electrostatic repulsion at day 7, both B/L and B/L/F maintained strongly negative values, consistent with the presence of an anionic lipid interface and reduced flocculation at that stage.

The lipid composition provides a mechanistic explanation for this charge profile. DOPG liposomes are naturally negatively charged and their interfacial characteristics remain relatively stable across moderate temperature variations within the range of room and physiological conditions [229]. In the present system, the stability of strongly negative zeta values at days 1-7 for B/L and B/L/F supports the interpretation that the bacterial surface was transiently dominated by the DOPG-rich liposomal corona. The later convergence of zeta values among samples is consistent with progressive charge screening or surface conditioning during storage (for example adsorption of bacterial components), without necessarily indicating a loss of the colloidal fraction.

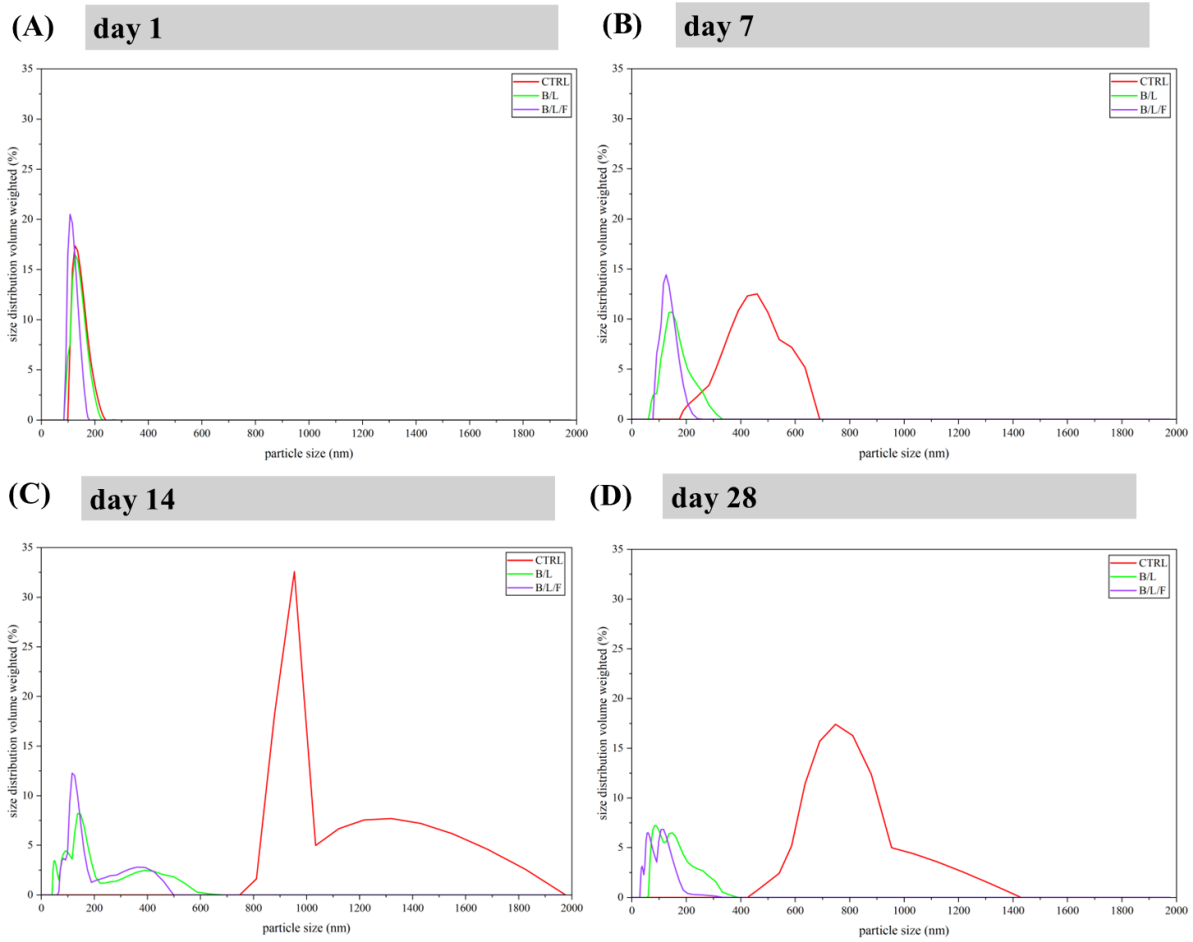

Figure 52. Results of particle size distribution for *L. plantarum* performed at room temperature. The control sample (CTRL) represents free (uncoated) cells. The B/L sample represents lipid-coated cells. The B/L/F sample represents cells with a surrounding layer of liposomes loaded with fluvastatin.

The apparently small size fractions observed for samples containing bacteria can be interpreted in the context of light-scattering behavior in multimodal suspensions. Distributions derived by dynamic light scattering are strongly influenced by sample heterogeneity and by the

coexistence of objects in different size regimes [230]. Therefore, these reported fractions likely correspond primarily to population dominated by nanoparticles, rather than representing the dimensions of individual bacterial cells. This consideration is particularly relevant in systems containing both micron-scale bacteria and a high concentration of nanometric vesicles. In the sample containing bacteria alone, the profile obtained after flow cytometry showed that the population was dominated by membrane-injured cells from day 1 and further shifted toward dormant and dead phenotypes by day 28. This pattern is consistent with an increased contribution of cell-derived nanoscale objects, such as extracellular vesicles and membrane fragments, to the scattering signal. Extracellular vesicles produced by *L. plantarum* have been reported within a size range of the nanometric fraction observed in the present study [231,232].

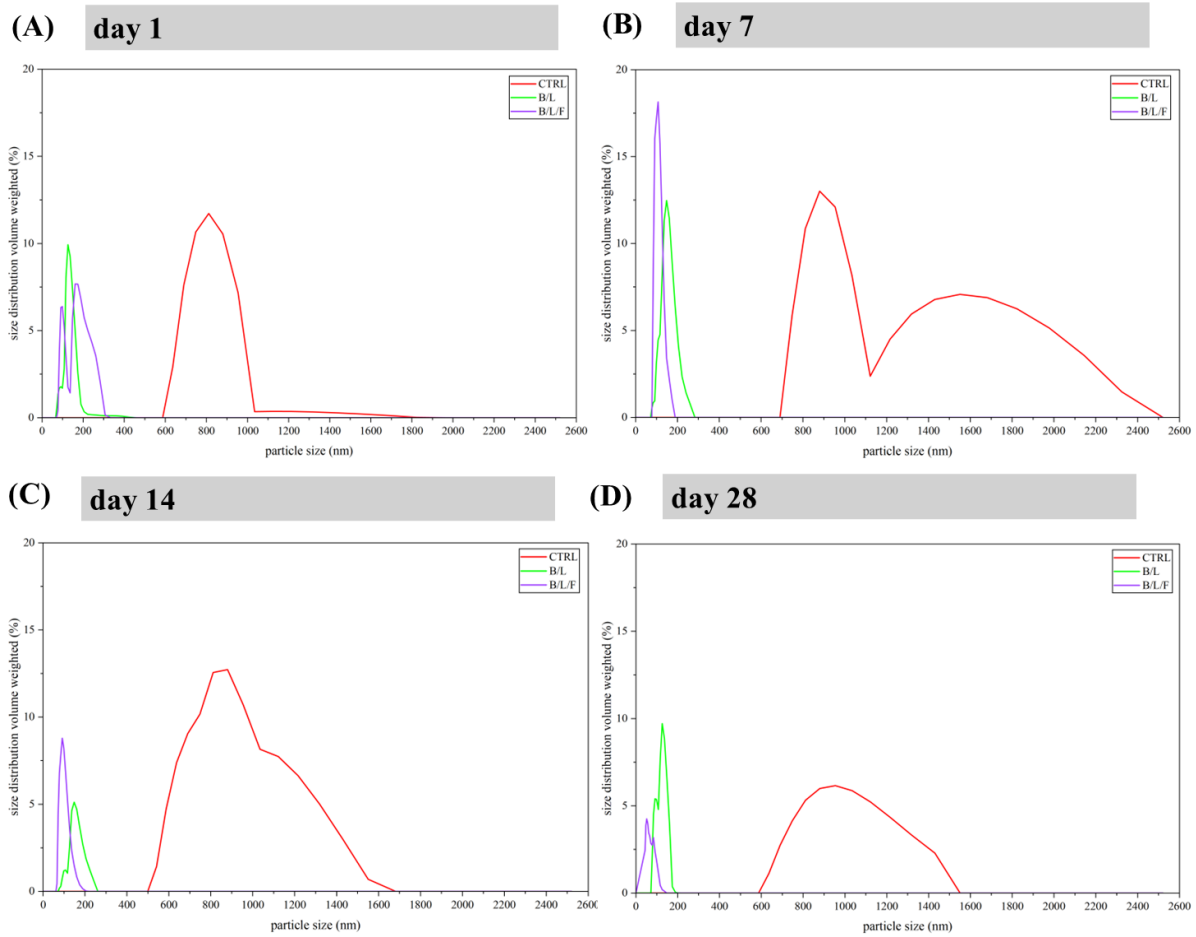

Figure 53. Results of particle size distribution for *L. plantarum* performed at 36.6 °C. The control sample (CTRL) represents free (uncoated) cells. The B/L sample represents lipid-coated cells. The B/L/F sample represents cells with a surrounding layer of liposomes loaded with fluvastatin.

Temperature represents an important stress factor for colloidal lipid systems, as increased bilayer mobility at higher temperatures can promote vesicle restructuring or fusion depending

on composition and environment [233]. Within this framework, the observation that B/L and especially B/L/F maintained narrow nanoscale fractions at 36.6 °C, while the CTRL shifted toward broader microscale distributions, indicates that the liposomes retained colloidal organization under physiologically relevant temperature conditions. This behavior is consistent with reports describing bacteria-colloid formulations as protective structures in which nanoscale particles form a stabilizing coating around probiotic cells [234].

Finally, since the aim of liposome-based probiotic delivery systems is to enhance stability under GI or physiological conditions, physicochemical stability at body temperature is important evidence that the dispersion characteristics are preserved in conditions similar to those of practical use [48].

4.5. Microscopic verification of liposomal systems

CryoSEM was used to visualize the architecture of the probiotic-liposome systems. Three reference states were examined using this method: uncoated *L. plantarum* cells, lipid-coated cells, and cells with a surrounding liposomes loaded with fluvastatin.

As shown in Figure 54(A), in the CTRL, probiotic cells exhibited a typical rod-shaped morphology with no nanoscale particulate layer on the cell envelope. The cells were clearly defined as distinct bacterial objects, with no vesicle-like structures present on their surfaces.

In the B/L sample (Figure 54(B)), vesicle-like spherical nanostructures were observed in the area around the bacterial cells and on or near the cell surface. These features were consistent with liposomal material present as a dispersed nanoscale fraction, with part of the vesicle population appearing adsorbed onto the bacterial envelope rather than forming a continuous coating. The micrograph is consistent with a configuration in which multiple liposomes associate externally with the bacterial surface, creating a non-uniform pericellular lipid layer.

The B/L/F sample showed a distinct organization (Figure 54(C)). Numerous bacterial cells were visible within the field of view, and vesicle-like nanoscale structures were present on and between cells, indicating more extensive lipid-cell association. The presence of liposomal features at intercellular contact regions suggests that liposomes may decorate cell surfaces and also contribute to localized clustering of the lipid fraction, consistent with the formation of a pericellular liposomal corona around individual bacteria within a multicellular arrangement. In the B/L/F formulation contained fluvastatin. However, cryoSEM provides primarily morphological information and does not allow direct discrimination between drug-loaded and unloaded vesicles. The similar surface features observed in B/L and B/L/F samples

indicate that drug loading did not grossly alter the ability of DOPG liposomes to associate with the bacterial surface and form a pericellular corona.

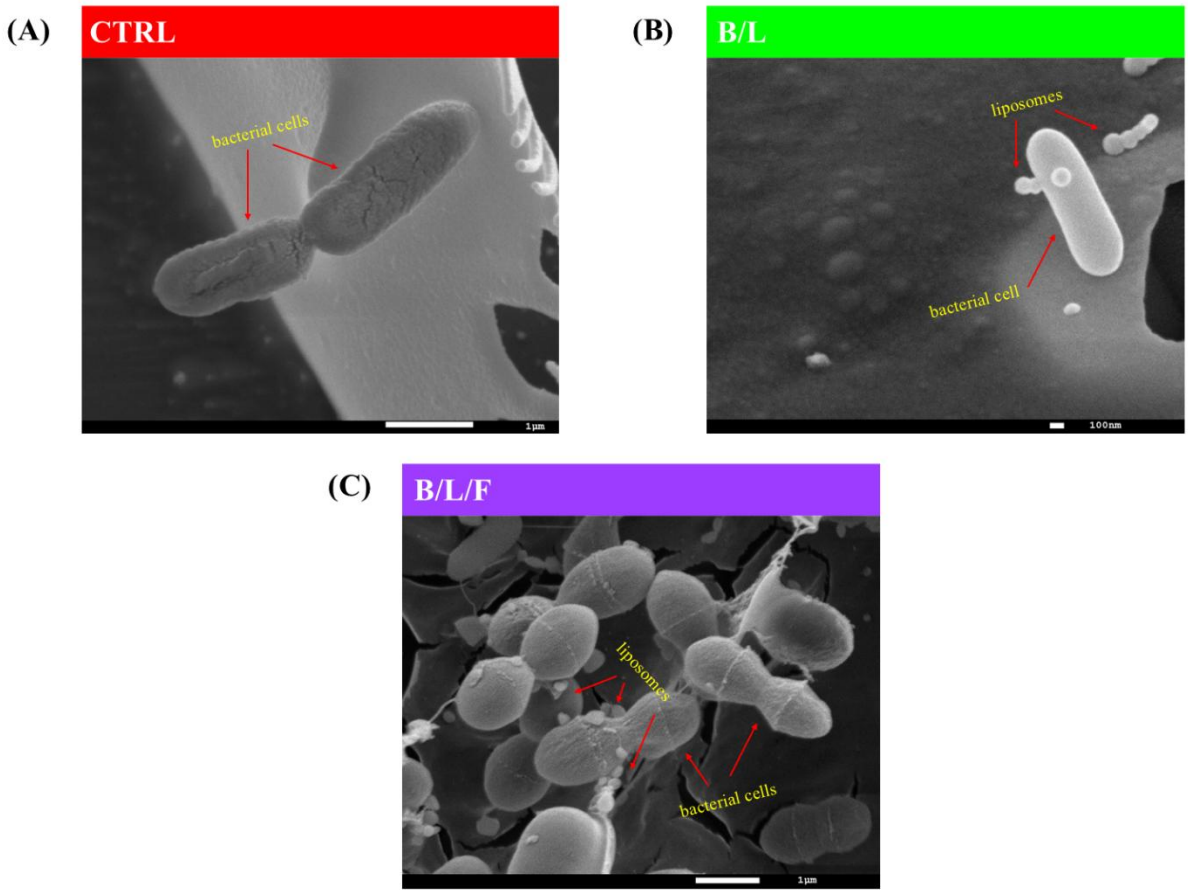

Figure 54. Representative cryoSEM images illustrating (A) control uncoated cells (CTRL), (B) lipid-coated cells (B/L), and (C) cells with a surrounding layer of liposomes loaded with fluvastatin (B/L/F). Figure C shows cells undergoing cell division.

Overall, these representative cryoSEM images provide structural support for the conclusion that liposomes remain as discrete nanoscale objects within the formulations and associate externally with the bacterial envelope, consistent with the intended liposomal corona configuration. CryoSEM is particularly suitable for such verification because it enables high-resolution imaging of hydrated systems (including liposomes and biological samples) in a frozen state that minimizes preparation-related collapse often observed in conventional SEM methods [235].

The external adsorption pattern observed here is consistent with previous reports indicating that liposome-microbe interactions depend on interfacial properties and surface charge, resulting in heterogeneous attachment rather than uniform fusion [236]. From a formulation perspective, the morphology aligns with broader observations that modifying LAB with colloidal materials

can generate structured surface that appear in electron microscopy as non-uniform coatings or shell-like microstructures [237].

Although many liposomal probiotic delivery systems described in the literature emphasize internal probiotic-loaded carriers, microscopy-based verification remains important for distinguishing between true internal entrapment and external coating. The present images are consistent with the second structural arrangement [238].

4.6. Summary of fluvastatin-loaded liposomal probiotic systems

This final stage showed that combining *L. plantarum* with anionic DOPG liposomes resulted in a distinct colloidal probiotic configuration that remained structurally stable during storage and preserved functional cellular competence. Complementary biological and physicochemical results showed that the formation of liposomes modified the behavior of probiotics relative to free cells, while maintaining a measurable fraction of physiologically relevant subpopulations over time.

Metabolic assays indicated an initial formulation-dependent modulation of cellular activity followed by stabilization at later time points. Unloaded liposomes were associated with a sustained increase in overall reducing capacity. In contrast, the fluvastatin-loaded system exhibited an initial transient adjustment phase, followed by stable metabolic performance. Flow cytometry analysis confirmed that these effects reflected dynamic redistribution of physiological states rather than a uniform viability response. Both liposomal systems promoted mid-storage enrichment of physiologically active subpopulations relative to the CTRL, with the fluvastatin-loaded formulation showing the most visible shift. In parallel, GST activity profiles indicated that liposomal incorporation was associated with reduced oxidative stress-linked detoxification demand compared with free bacteria. This is consistent with a formulation-mediated buffering of stress exposure rather than progressive stress escalation.

Physicochemical characterization supported these biological observations by showing that the liposomal systems behaved as organized, negatively charged dispersions at both room and physiological temperatures. Early storage time points were characterized by more negative zeta potential values in liposomal formulations relative to the CTRL, consistent with a dominant contribution of the DOPG interface during corona formation. Particle size distributions further differentiated the formulations. While the CTRL exhibited clear shifts toward larger microscale fractions, particularly at physiological temperature, both liposome-containing systems maintained stable nanometric size fractions throughout storage. CryoSEM provided structural

confirmation that liposomes associate externally with the bacterial surface, supporting formation of a pericellular corona. As expected for a morphology-based technique, cryoSEM did not distinguish between drug-loaded and unloaded vesicles but confirmed that fluvastatin incorporation did not interfere with corona formation.

All findings combined indicate that DOPG liposomal coating can structure probiotic suspensions into stable colloidal systems that retain functional subpopulations during storage and under physiologically relevant temperature conditions. The unloaded liposomal system was primarily associated with stabilization and sustained cellular reducing capacity, whereas the fluvastatin-loaded system introduced an additional functional component while maintaining probiotic physiological competence. In this context, the combined formulation represents a dual-function platform integrating probiotic stabilization with incorporation of a clinically used hypolipidemic agent within the lipid phase.

At this stage, the work focuses on *Specific research aims (B-E)* related to formulation of functional fluvastatin-loaded liposomal probiotic systems, characterization of its structural and physicochemical properties, demonstration of improved metabolic activity and cell viability, and evaluation of stability at both room and physiological temperatures. These outcomes contribute to the overall objective of the dissertation and support the formulated research hypothesis.

V. SUMMARY

148:9781791138

The experimental part of this doctoral dissertation focused on the design, preparation, and multi-parameter evaluation of colloidal systems intended to improve the viability, stability, and functional performance of probiotic bacteria. The study was based on the hypothesis that hydrogel-based encapsulation matrices and liposome-based carriers would provide more favorable storage conditions than non-encapsulated cells, and that incorporation of supportive components, such as prebiotic compounds or bioactive agent, could further modulate the functionality of the developed formulations.

To address this hypothesis, a stepwise research strategy was applied, beginning with preformulation screening of candidate additives, followed by development of hydrogel- and lipid-based probiotic systems, their physicochemical and structural characterization, and comprehensive evaluation of biological performance during storage.

The results indicate that properties of the surrounding colloidal matrix influence probiotic physiology, membrane integrity, oxidative balance, and colloidal stability, and that appropriately designed carrier systems were associated with improved probiotic performance relative to free-cell controls.

The most important conclusions of the experimental part are summarized below:

1. The preformulation stage indicated that the effect of formulation additives on probiotics is strain dependent and requires evaluation using a multi-parameter approach. Screening performed on *L. plantarum*, *L. rhamnosus*, and *L. paracasei* showed that no single parameter adequately described the overall biological response of free probiotic cells. Among the tested additives, trehalose, inulin, and gum arabic were associated with the most favorable combined performance and were selected for further formulation studies. Moreover, *L. plantarum* was identified as a suitable model strain for further experimental stages.
2. Hydrogel-based formulations were associated with a more protective environment for probiotic cells compared with non-encapsulated controls. However, their performance depended on matrix composition. Alginate beads reinforced with psyllium husk or gum arabic and supplemented with inulin, trehalose, or their combination differed in their ability to support metabolic activity, cell viability, membrane integrity, and structural stability. Among the tested hydrogel systems, the psyllium husk/inulin formulation exhibited the most balanced performance profile, suggesting that a more hydrated and

less restrictive bead microenvironment supports probiotic survival and functionality during storage.

3. The hydrogel results indicate that probiotic protection depends not only on physical entrapment but also on the microenvironment established around the cells. Differences in cell envelope properties, intracellular trace metal homeostasis, and bead morphology suggest that matrix composition influences mass transfer, hydration, and cell-matrix interactions. These findings support the view that rational design of hydrogel carriers requires simultaneous consideration of biological and physicochemical parameters, rather than only colony counts or general viability endpoints.
4. Lipid-based stabilization using DMPC indicated that probiotic cells can be supported by an externally associated lipid layer forming a pericellular corona. In this model, bacterial cells were not entrapped within vesicles. Instead, nanoscale lipid structures assembled at the cell surface and modified the immediate microenvironment. This approach was associated with improved metabolic performance, higher apparent cell density, and enhanced colloidal stability relative to uncoated controls, particularly during room temperature storage. CryoSEM observations verified the external character of the lipid coating and showed that the developed systems represented organized colloidal structures rather than conventional encapsulates.
5. The fluvastatin-loaded liposomal systems extended this approach by combining probiotic cells with a bioactive liposomal phase, forming a dual-function formulation. In these systems, *L. plantarum* cells became externally coated with multiple DOPG liposomes, including fluvastatin-loaded vesicles, rather than being encapsulated within them. The results indicated that both liposomal systems retained structural organization during storage, while the fluvastatin-containing variant introduced an additional functional component without compromising probiotic physiological competence. Biological analyses showed that liposome-associated systems modified metabolic profiles, preserved physiologically relevant subpopulations, and were associated with reduced oxidative stress markers relative to free-cell controls. Moreover, physicochemical analyses demonstrated stable electrokinetic behavior and maintenance of nanometric fractions at both room temperature and physiologically relevant temperature.
6. The dissertation demonstrates the value of integrating biological, physicochemical, and structural methods in the evaluation of probiotic formulations. The combined use of culture-based enumeration, metabolic assays, flow cytometry, membrane and surface

analyses, oxidative stress markers, colloidal measurements, and microscopic imaging enabled assessment of complementary aspects of probiotic performance that would not be captured by a single analytical approach. This integrated methodology was essential for distinguishing between apparent culturability, physiological heterogeneity, stress adaptation, and formulation-dependent stability.

7. Taken together, the results support the main objective of the dissertation and are consistent with the formulated research hypothesis within the scope of the performed study. The developed colloidal systems, both hydrogel-based and lipid-based, were associated with more favorable conditions for probiotic stability compared with non-encapsulated cells, although the extent of protection depended on matrix composition and system architecture. The study further indicates that formation of an external lipid corona represents a feasible strategy for probiotic stabilization and that such systems can be functionally extended through incorporation of bioactive compounds, including fluvastatin.
8. The conducted research contributes to current knowledge on the design and evaluation of colloidal probiotic carriers that combine structural stabilization with added functional components. In particular, the work expands understanding of how hydrogel matrices, external lipid coatings, and drug-loaded liposomal phases influence probiotic physiology and storage behavior. From an application-oriented perspective, the fluvastatin-loaded liposomal probiotic system may be considered as a conceptual framework for multifunctional formulations integrating probiotic activity with a lipid-phase hypolipidemic component.
9. All specific objectives of the dissertation were addressed. The work covered preformulation screening, formulation development, structural and physicochemical characterization, biological evaluation, and storage stability assessment of the developed systems. The experimental part of the dissertation therefore provides a coherent evaluation of the proposed research concept within the defined scope.
10. Further studies are needed to extend the application potential of the developed systems. In particular, future investigations should examine their behavior under simulated gastrointestinal conditions, including exposure to acidic pH, digestive enzymes, and bile salts, as well as the release profile of incorporated components. Such studies would represent a logical next step toward practical implementation of the developed probiotic colloidal systems in food, nutraceutical, or biomedical applications.

REFERENCES

1. Reid, G.; Gadir, A.A.; Dhir, R. Probiotics: Reiterating What They Are and What They Are Not. *Front. Microbiol.* 2019, *10*, 424, doi:10.3389/fmicb.2019.00424.
2. Sarita, B.; Samadhan, D.; Hassan, M.Z.; Kovaleva, E.G. A Comprehensive Review of Probiotics and Human Health-Current Prospective and Applications. *Front. Microbiol.* 2025, *15*, 1487641, doi:10.3389/fmicb.2024.1487641.
3. Zheng, J.; Wittouck, S.; Salvetti, E.; Franz, C.M.A.P.; Harris, H.M.B.; Mattarelli, P.; O'Toole, P.W.; Pot, B.; Vandamme, P.; Walter, J.; et al. A Taxonomic Note on the Genus *Lactobacillus*: Description of 23 Novel Genera, Emended Description of the Genus *Lactobacillus* Beijerinck 1901, and Union of *Lactobacillaceae* and *Leuconostocaceae*. *Int. J. Syst. Evol. Microbiol.* 2020, *70*, 2782–2858, doi:10.1099/ijsem.0.004107.
4. Sibanda, T.; Marole, T.A.; Thomashoff, U.L.; Thantsha, M.S.; Buys, E.M. *Bifidobacterium* Species Viability in Dairy-Based Probiotic Foods: Challenges and Innovative Approaches for Accurate Viability Determination and Monitoring of Probiotic Functionality. *Front. Microbiol.* 2024, *15*, 1327010, doi:10.3389/fmicb.2024.1327010.
5. Jung, M.Y.; Lee, C.; Seo, M.-J.; Roh, S.W.; Lee, S.H. Characterization of a Potential Probiotic Bacterium *Lactococcus raffinolactis* WiKim0068 Isolated from Fermented Vegetable Using Genomic and in Vitro Analyses. *BMC Microbiol.* 2020, *20*, 136, doi:10.1186/s12866-020-01820-9.
6. Binda, S.; Hill, C.; Johansen, E.; Obis, D.; Pot, B.; Sanders, M.E.; Tremblay, A.; Ouwehand, A.C. Criteria to Qualify Microorganisms as "Probiotic" in Foods and Dietary Supplements. *Front. Microbiol.* 2020, *11*, 1662, doi:10.3389/fmicb.2020.01662.
7. Shivani, T.M.; Sathiavelu, M. Probiotic Evaluation, Adherence Capability and Safety Assessment of *Lactococcus lactis* Strain Isolated from an Important Herb "Murraya Koenigii." *Sci. Rep.* 2024, *14*, 15565, doi:10.1038/s41598-024-66597-7.
8. Tuomola, E.; Crittenden, R.; Playne, M.; Isolauri, E.; Salminen, S. Quality Assurance Criteria for Probiotic Bacteria. *Am. J. Clin. Nutr.* 2001, *73*, 393s–398s, doi:10.1093/ajcn/73.2.393s.
9. Chandrasekaran, P.; Weiskirchen, S.; Weiskirchen, R. Effects of Probiotics on Gut Microbiota: An Overview. *Int. J. Mol. Sci.* 2024, *25*, 6022, doi:10.3390/ijms25116022.
10. Mazziotta, C.; Tognon, M.; Martini, F.; Torreggiani, E.; Rotondo, J.C. Probiotics Mechanism of Action on Immune Cells and Beneficial Effects on Human Health. *Cells* 2023, *12*, 184, doi:10.3390/cells12010184.

11. Momin, E.S.; Khan, A.A.; Kashyap, T.; Pervaiz, M.A.; Akram, A.; Mannan, V.; Sanusi, M.; Elshaikh, A.O. The Effects of Probiotics on Cholesterol Levels in Patients With Metabolic Syndrome: A Systematic Review. *Cureus* 2023, doi:10.7759/cureus.37567.
12. Barkhidarian, B.; Roldos, L.; Iskandar, M.M.; Saedisomeolia, A.; Kubow, S. Probiotic Supplementation and Micronutrient Status in Healthy Subjects: A Systematic Review of Clinical Trials. *Nutrients* 2021, *13*, 3001, doi:10.3390/nu13093001.
13. Wendel, U. Assessing Viability and Stress Tolerance of Probiotics-A Review. *Front. Microbiol.* 2022, *12*, 818468, doi:10.3389/fmicb.2021.818468.
14. Gardiner, G.E.; O'Sullivan, E.; Kelly, J.; Auty, M.A.E.; Fitzgerald, G.F.; Collins, J.K.; Ross, R.P.; Stanton, C. Comparative Survival Rates of Human-Derived Probiotic *Lactobacillus paracasei* and *L. salivarius* Strains during Heat Treatment and Spray Drying. *Appl. Environ. Microbiol.* 2000, *66*, 2605–2612, doi:10.1128/AEM.66.6.2605-2612.2000.
15. Gaucher, F.; Bonnassie, S.; Rabah, H.; Marchand, P.; Blanc, P.; Jeantet, R.; Jan, G. Review: Adaptation of Beneficial *Propionibacteria*, *Lactobacilli*, and *Bifidobacteria* Improves Tolerance Toward Technological and Digestive Stresses. *Front. Microbiol.* 2019, *10*, 841, doi:10.3389/fmicb.2019.00841.
16. Wong, S.; Kabeir, B.M.; Mustafa, S.; Mohamad, R.; Hussin, A.S.M.; Manap, M.Y. Viability of *Bifidobacterium Pseudocatenulatum* G4 after Spray-Drying and Freeze-Drying. *Microbiol. Insights* 2010, *3*, MBI.S2728, doi:10.4137/MBI.S2728.
17. Sin, P.Y.; Tan, S.H.; Farida Asras, M.F.; Karmawan, L.U. From Preparation to Product: Factors Influencing Probiotic Viability in Spray Drying. *Curr. Sci. Technol.* 2024, *4*, 22–35, doi:10.15282/cst.v4i1.11125.
18. Wang, J.; Wu, P.; Dhital, S.; Yu, A.; Chen, X.D. Impact of Freezing and Freeze Drying on *Lactobacillus rhamnosus* GG Survival: Mechanisms of Cell Damage and the Role of Pre-Freezing Conditions and Cryoprotectants. *Foods* 2025, *14*, 1817, doi:10.3390/foods14101817.
19. Broeckx, G.; Vandenheuvel, D.; Claes, I.J.J.; Lebeer, S.; Kiekens, F. Drying Techniques of Probiotic Bacteria as an Important Step towards the Development of Novel Pharmabiotics. *Int. J. Pharm.* 2016, *505*, 303–318, doi:10.1016/j.ijpharm.2016.04.002.
20. Santivarangkna, C.; Kulozik, U.; Foerst, P. Inactivation Mechanisms of Lactic Acid Starter Cultures Preserved by Drying Processes. *J. Appl. Microbiol.* 2008, *105*, 1–13, doi:10.1111/j.1365-2672.2008.03744.x.

21. Huang, S.; Vignolles, M.-L.; Chen, X.D.; Le Loir, Y.; Jan, G.; Schuck, P.; Jeantet, R. Spray Drying of Probiotics and Other Food-Grade Bacteria: A Review. *Trends Food Sci. Technol.* 2017, *63*, 1–17, doi:10.1016/j.tifs.2017.02.007.
22. Marcial-Coba, M.S.; Cieplak, T.; Cahú, T.B.; Blennow, A.; Knøchel, S.; Nielsen, D.S. Viability of Microencapsulated *Akkermansia Muciniphila* and *Lactobacillus Plantarum* during Freeze-Drying, Storage and *in Vitro* Simulated Upper Gastrointestinal Tract Passage. *Food Funct.* 2018, *9*, 5868–5879, doi:10.1039/C8FO01331D.
23. Fonseca, F.; Cenard, S.; Passot, S. Freeze-Drying of Lactic Acid Bacteria. In *Cryopreservation and Freeze-Drying Protocols*; Wolkers, W.F., Oldenhof, H., Eds.; Methods in Molecular Biology; Springer New York: New York, NY, 2015; Vol. 1257, pp. 477–488 ISBN 978-1-4939-2192-8.
24. Fu, N.; Chen, X.D. Towards a Maximal Cell Survival in Convective Thermal Drying Processes. *Food Res. Int.* 2011, *44*, 1127–1149, doi:10.1016/j.foodres.2011.03.053.
25. Cutting, S.M. Bacillus Probiotics. *Food Microbiol.* 2011, *28*, 214–220, doi:10.1016/j.fm.2010.03.007.
26. Adibpour, N.; Hosseininezhad, M.; Pahlevanlo, A.; Hussain, M.A. A Review on *Bacillus coagulans* as a Spore-Forming Probiotic. *Appl. Food Biotechnol.* 2019, *6*, doi:10.22037/afb.v6i2.23958.
27. You, S.; Ma, Y.; Yan, B.; Pei, W.; Wu, Q.; Ding, C.; Huang, C. The Promotion Mechanism of Prebiotics for Probiotics: A Review. *Front. Nutr.* 2022, *9*, 1000517, doi:10.3389/fnut.2022.1000517.
28. Gomez Quintero, D.F.; Kok, C.R.; Hutkins, R. The Future of Synbiotics: Rational Formulation and Design. *Front. Microbiol.* 2022, *13*, 919725, doi:10.3389/fmicb.2022.919725.
29. Hill, C.; Guarner, F.; Reid, G.; Gibson, G.R.; Merenstein, D.J.; Pot, B.; Morelli, L.; Canani, R.B.; Flint, H.J.; Salminen, S.; et al. The International Scientific Association for Probiotics and Prebiotics Consensus Statement on the Scope and Appropriate Use of the Term Probiotic. *Nat. Rev. Gastroenterol. Hepatol.* 2014, *11*, 506–514, doi:10.1038/nrgastro.2014.66.
30. Ma, L.; Tu, H.; Chen, T. Postbiotics in Human Health: A Narrative Review. *Nutrients* 2023, *15*, 291, doi:10.3390/nu15020291.
31. Vesaratchanon, S.; Nikolov, A.; Wasan, D.T. Sedimentation in Nano-Colloidal Dispersions: Effects of Collective Interactions and Particle Charge. *Adv. Colloid Interface Sci.* 2007, *134–135*, 268–278, doi:10.1016/j.cis.2007.04.026.

32. Mo, S.; Shao, X.; Chen, Y.; Cheng, Z. Increasing Entropy for Colloidal Stabilization. *Sci. Rep.* 2016, *6*, 36836, doi:10.1038/srep36836.
33. Wang, B.; LvYe, J.; Yang, S.; Shi, Y.; Chen, Q. Critical Review of Food Colloidal Delivery System for Bioactive Compounds: Physical Characterization and Application. *Foods* 2024, *13*, 2596, doi:10.3390/foods13162596.
34. Kwiecień, I.; Kwiecień, M. Application of Polysaccharide-Based Hydrogels as Probiotic Delivery Systems. *Gels* 2018, *4*, 47, doi:10.3390/gels4020047.
35. Garcia-Brand, A.J.; Quezada, V.; Gonzalez-Melo, C.; Bolaños-Barbosa, A.D.; Cruz, J.C.; Reyes, L.H. Novel Developments on Stimuli-Responsive Probiotic Encapsulates: From Smart Hydrogels to Nanostructured Platforms. *Fermentation* 2022, *8*, 117, doi:10.3390/fermentation8030117.
36. Milovanović, J.; Banjanac, K.; Nikolić, J.; Nikodinović-Runić, J.; Prlainović, N.Ž. The Organic-Functionalized Silica Nanoparticles as Lipase Carriers for Biocatalytic Application: Future Perspective in Biodegradation. *Catalysts* 2025, *15*, 54, doi:10.3390/catal15010054.
37. Leiper, K.A.; Miedl, M. Colloidal Stability of Beer. In *Beer*; Elsevier, 2009; pp. 111–161 ISBN 978-0-12-669201-3.
38. Parhi, R. Cross-Linked Hydrogel for Pharmaceutical Applications: A Review. *Adv. Pharm. Bull.* 2017, *7*, 515–530, doi:10.15171/apb.2017.064.
39. Cao, H.; Duan, L.; Zhang, Y.; Cao, J.; Zhang, K. Current Hydrogel Advances in Physicochemical and Biological Response-Driven Biomedical Application Diversity. *Signal Transduct. Target. Ther.* 2021, *6*, 426, doi:10.1038/s41392-021-00830-x.
40. Kvakova, M.; Bertkova, I.; Stofilova, J.; Savidge, T.C. Co-Encapsulated Synbiotics and Immobilized Probiotics in Human Health and Gut Microbiota Modulation. *Foods* 2021, *10*, 1297, doi:10.3390/foods10061297.
41. Singh, S.; Gupta, R.; Chawla, S.; Gauba, P.; Singh, M.; Tiwari, R.K.; Upadhyay, S.; Sharma, S.; Chanda, S.; Gaur, S. Natural Sources and Encapsulating Materials for Probiotics Delivery Systems: Recent Applications and Challenges in Functional Food Development. *Front. Nutr.* 2022, *9*, 971784, doi:10.3389/fnut.2022.971784.
42. Campos-Espinoza, F.; Castaño-Agudelo, J.; Rodriguez-Llamazares, S. Polysaccharides Systems for Probiotic Bacteria Microencapsulation: Mini Review. *Food Sci. Technol.* 2022, *42*, e95121, doi:10.1590/fst.95121.
43. Wang, X.; Sun, H.; Wu, J.; Wang, Y.; Ai, Z.; Wang, X.; Nan, B.; Cao, Y.; Li, X.; Liu, J.; et al. Improved Viability of Trehalose on *Lactobacillus plantarum* Embedded with Whey

Protein Concentrate/Pullulan in Simulated Gastrointestinal Conditions and Its Application in Acid Juice. *Food Sci. Hum. Wellness* 2024, *13*, 3614–3623, doi:10.26599/FSHW.2023.9250043.

44. Tomnikova, A.; Orgonikova, A.; Krizek, T. Liposomes: Preparation and Characterization with a Special Focus on the Application of Capillary Electrophoresis. *Monatshefte Für Chem. - Chem. Mon.* 2022, *153*, 687–695, doi:10.1007/s00706-022-02966-0.
45. Liu, P.; Chen, G.; Zhang, J. A Review of Liposomes as a Drug Delivery System: Current Status of Approved Products, Regulatory Environments, and Future Perspectives. *Molecules* 2022, *27*, 1372, doi:10.3390/molecules27041372.
46. Burdaev, N.I.; Nikolaeva, L.L.; Kosenko, V.V.; Shprakh, Z.S.; Bunyatyan, N.D. Liposomes as Drug Carriers: Classification, Preparation Methods, and Medicinal Use. *Bull. Sci. Cent. Expert Eval. Med. Prod. Regul. Res. Med. Eval.* 2023, *13*, 316–332, doi:10.30895/1991-2919-2023-508.
47. Ajeeshkumar, K.K.; Aneesh, P.A.; Raju, N.; Suseela, M.; Ravishankar, C.N.; Benjakul, S. Advancements in Liposome Technology: Preparation Techniques and Applications in Food, Functional Foods, and Bioactive Delivery: A Review. *Compr. Rev. Food Sci. Food Saf.* 2021, *20*, 1280–1306, doi:10.1111/1541-4337.12725.
48. Liu, J.; Sun, Z.; Liu, S.; Lu, Y.; Guo, C.; Cao, J.; Wang, X.; Wang, X. Liposome-Mediated Encapsulation of Probiotics: Current Status, Challenges and Future Directions. *Crit. Rev. Food Sci. Nutr.* 2025, 1–18, doi:10.1080/10408398.2025.2480169.
49. Rudzińska, M.; Grygier, A.; Knight, G.; Kmiecik, D. Liposomes as Carriers of Bioactive Compounds in Human Nutrition. *Foods* 2024, *13*, 1814, doi:10.3390/foods13121814.
50. Ashaolu, T.J. Nanoemulsions for Health, Food, and Cosmetics: A Review. *Environ. Chem. Lett.* 2021, *19*, 3381–3395, doi:10.1007/s10311-021-01216-9.
51. Rathnasinghe, N.L.; Kaushani, K.G.; Rajapakshe, P.S.; De Silva, A.; Jayasinghe, R.A.; Liyanage, R.N.; Tissera, N.D.; Wijesena, R.N.; Priyadarshana, G. Current Trends on Unique Features and Role of Nanomaterials in Personal Care Products. *Cosmetics* 2024, *11*, 152, doi:10.3390/cosmetics11050152.
52. Dickinson, E. Colloids in Food: Ingredients, Structure, and Stability. *Annu. Rev. Food Sci. Technol.* 2015, *6*, 211–233, doi:10.1146/annurev-food-022814-015651.
53. Mohammadi, K.; Sani, M.A.; Azizi-Lalabadi, M.; McClements, D.J. Recent Progress in the Application of Plant-Based Colloidal Drug Delivery Systems in the Pharmaceutical Sciences. *Adv. Colloid Interface Sci.* 2022, *307*, 102734, doi:10.1016/j.cis.2022.102734.

54. Li, M.; He, X.; Zhao, R.; Shi, Q.; Nian, Y.; Hu, B. Hydrogels as Promising Carriers for the Delivery of Food Bioactive Ingredients. *Front. Nutr.* 2022, *9*, doi:10.3389/fnut.2022.1006520.
55. Klojdová, I.; Milota, T.; Smetanová, J.; Stathopoulos, C. Encapsulation: A Strategy to Deliver Therapeutics and Bioactive Compounds? *Pharmaceuticals* 2023, *16*, 362, doi:10.3390/ph16030362.
56. Luo, M.; Oomah, B.D.; Akoetey, W.; Zhang, Y.; Daneshfozoun, H.; Hosseinian, F. Liposomes as Sustainable Delivery Systems in Food, Cosmetic, and Pharmaceutical Applications. *J. Am. Oil Chem. Soc.* 2025, *102*, 547–568, doi:10.1002/aocs.12907.
57. Atrooz, O.; Kerdari, E.; Mozafari, M.R.; Reihani, N.; Asadi, A.; Torkaman, S.; Alavi, M.; Taghavi, E. A Comparative Review of Tocosomes, Liposomes, and Nanoliposomes as Potent and Novel Nanonutraceutical Delivery Systems for Health and Biomedical Applications. *Biomedicines* 2024, *12*, 2002, doi:10.3390/biomedicines12092002.
58. Sun, Q.; Yin, S.; He, Y.; Cao, Y.; Jiang, C. Biomaterials and Encapsulation Techniques for Probiotics: Current Status and Future Prospects in Biomedical Applications. *Nanomaterials* 2023, *13*, 2185, doi:10.3390/nano13152185.
59. D'Amico, V.; Cavaliere, M.; Ivone, M.; Lacassia, C.; Celano, G.; Vacca, M.; La Forgia, F.M.; Fontana, S.; De Angelis, M.; Denora, N.; et al. Microencapsulation of Probiotics for Enhanced Stability and Health Benefits in Dairy Functional Foods: A Focus on Pasta Filata Cheese. *Pharmaceutics* 2025, *17*, 185, doi:10.3390/pharmaceutics17020185.
60. Agriopoulou, S.; Tarapoulouzi, M.; Varzakas, T.; Jafari, S.M. Application of Encapsulation Strategies for Probiotics: From Individual Loading to Co-Encapsulation. *Microorganisms* 2023, *11*, 2896, doi:10.3390/microorganisms11122896.
61. Vijayaram, S.; Sinha, R.; Faggio, C.; Ringø, E.; Chou, C.-C. Biopolymer Encapsulation for Improved Probiotic Delivery: Advancements and Challenges. *AIMS Microbiol.* 2024, *10*, 986–1023, doi:10.3934/microbiol.2024043.
62. Rajam, R.; Subramanian, P. Encapsulation of Probiotics: Past, Present and Future. *Beni-Suef Univ. J. Basic Appl. Sci.* 2022, *11*, 46, doi:10.1186/s43088-022-00228-w.
63. Khodashenas, M.; Jouki, M. Optimization of Stabilized Probiotic Doogh Formulation by Edible Gums and Response Surface Methodology: Assessment of Stability, Viability and Organoleptic Attributes. *J. Food Sci. Technol.* 2020, *57*, 3201–3210, doi:10.1007/s13197-020-04351-3.

64. Rojas-Muñoz, Y.V.; Santagapita, P.R.; Quintanilla-Carvajal, M.X. Probiotic Encapsulation: Bead Design Improves Bacterial Performance during In Vitro Digestion. *Polymers* 2023, *15*, 4296, doi:10.3390/polym15214296.
65. Iravani, S.; Korbekandi, H.; Mirmohammadi, S.V. Technology and Potential Applications of Probiotic Encapsulation in Fermented Milk Products. *J. Food Sci. Technol.* 2015, *52*, 4679–4696, doi:10.1007/s13197-014-1516-2.
66. Yoha, K.S.; Nida, S.; Dutta, S.; Moses, J.A.; Anandharamakrishnan, C. Targeted Delivery of Probiotics: Perspectives on Research and Commercialization. *Probiotics Antimicrob. Proteins* 2022, *14*, 15–48, doi:10.1007/s12602-021-09791-7.
67. Malos, I.G.; Pasarin, D.; Ghizdareanu, A.-I.; Frunzareanu, B. A Promising Approach for the Food Industry: Enhancing Probiotic Viability Through Microencapsulated Synbiotics. *Microorganisms* 2025, *13*, 336, doi:10.3390/microorganisms13020336.
68. Bhutto, R.A.; Bhutto, N.U.A.H.; Mahar, H.; Khanal, S.; Wang, M.; Iqbal, S.; Fan, Y.; Yi, J. Recent Trends in Co-Encapsulation of Probiotics with Prebiotics and Their Applications in the Food Industry. *Trends Food Sci. Technol.* 2025, *156*, 104829, doi:10.1016/j.tifs.2024.104829.
69. George Kerry, R.; Patra, J.K.; Gouda, S.; Park, Y.; Shin, H.-S.; Das, G. Benefaction of Probiotics for Human Health: A Review. *J. Food Drug Anal.* 2018, *26*, 927–939, doi:10.1016/j.jfda.2018.01.002.
70. Colautti, A.; Ginaldi, F.; Camprini, L.; Comi, G.; Reale, A.; Iacumin, L. Investigating Safety and Technological Traits of a Leading Probiotic Species: *Lacticaseibacillus paracasei*. *Nutrients* 2024, *16*, 2212, doi:10.3390/nu16142212.
71. Rocchetti, M.T.; Russo, P.; Spano, G.; De Santis, L.; Iarusso, I.; De Simone, N.; Brahimi, S.; Fiocco, D.; Capozzi, V. Exploring the Probiotic Potential of Dairy Industrial-Relevant *Lactobacilli*. *Appl. Sci.* 2022, *12*, 4989, doi:10.3390/app12104989.
72. Bosch, S.; De Beaurepaire, L.; Allard, M.; Mosser, M.; Heichette, C.; Chrétien, D.; Jegou, D.; Bach, J.-M. Trehalose Prevents Aggregation of Exosomes and Cryodamage. *Sci. Rep.* 2016, *6*, 36162, doi:10.1038/srep36162.
73. Jeznienė, S.; Bružaitė, I.; Šipailienė, A. Application of Biomacromolecules Encapsulation Systems for the Long-Term Storage of *Lactobacillus plantarum* F1 and *Lactobacillus reuteri* 182. *Heliyon* 2024, *10*, e26566, doi:10.1016/j.heliyon.2024.e26566.
74. Kuczyńska-Wiśnik, D.; Stojowska-Swędrzyńska, K.; Laskowska, E. Intracellular Protective Functions and Therapeutical Potential of Trehalose. *Molecules* 2024, *29*, 2088, doi:10.3390/molecules29092088.

75. Nadali, N.; Pahlevanlo, A.; Sarabi-Jamab, M.; Balandari, A. Effect of Maltodextrin with Different Dextrose Equivalents on the Physicochemical Properties of Spray-Dried Barberry Juice (Berberis Vulgaris L.). *J. Food Sci. Technol.* 2022, *59*, 2855–2866, doi:10.1007/s13197-021-05308-w.
76. Hofman, D.L.; Van Buul, V.J.; Brouns, F.J.P.H. Nutrition, Health, and Regulatory Aspects of Digestible Maltodextrins. *Crit. Rev. Food Sci. Nutr.* 2016, *56*, 2091–2100, doi:10.1080/10408398.2014.940415.
77. Corrêa-Filho, L.C.; Moldão-Martins, M.; Alves, V.D. Advances in the Application of Microcapsules as Carriers of Functional Compounds for Food Products. *Appl. Sci.* 2019, *9*, 571, doi:10.3390/app9030571.
78. Xiao, Z.; Xia, J.; Zhao, Q.; Niu, Y.; Zhao, D. Maltodextrin as Wall Material for Microcapsules: A Review. *Carbohydr. Polym.* 2022, *298*, 120113, doi:10.1016/j.carbpol.2022.120113.
79. Gregório, M.; Araújo, M.; Albuquerque, A.; Rodrigues, T.; Santos, N.C.; Fonseca, M.T.; Costa, M.E.D.; Tomé, A.; Gomes, J.; Gouveia, D.; et al. Probiotication of Plum Pulp and Conditions Effects Freeze-Drying in Cell Viability, Functional Properties and Antioxidant Activity. *Foods* 2024, *13*, 3551, doi:10.3390/foods13223551.
80. Alberts, A.; Moldoveanu, E.-T.; Niculescu, A.-G.; Grumezescu, A.M. Vitamin C: A Comprehensive Review of Its Role in Health, Disease Prevention, and Therapeutic Potential. *Molecules* 2025, *30*, 748, doi:10.3390/molecules30030748.
81. Harran University Agricultural Faculty, Department of Food Engineering, 63040 Şanlıurfa, Turkey; Akın, M.B. Effects of Ascorbic Acid and Glucose Oxidase Levels on the Viability of Probiotic Bacteria and the Physical and Sensory Characteristics in Symbiotic Ice-Cream. *Mljekarstvo* 2015, 121–129, doi:10.15567/mljekarstvo.2015.0206.
82. Srianta, I.; Kusdiyantini, E.; Zubaidah, E.; Ristiarini, S.; Nugerahani, I.; Alvin, A.; Iswanto, N.; Zhang, B.-B. Utilization of Agro-Industrial by-Products in Monascus Fermentation: A Review. *Bioresour. Bioprocess.* 2021, *8*, 129, doi:10.1186/s40643-021-00473-4.
83. Thuy, L.N.; Salanță, L.C.; Tofană, M.; Socaci, S.A.; Fărcaș, A.C.; Pop, C.R. Mini Review About Monosodium Glutamate. *Bull. Univ. Agric. Sci. Vet. Med. Cluj-Napoca Food Sci. Technol.* 2020, *77*, 1–12, doi:10.15835/buasvmcn-fst:2019.0029.
84. Tanimomo, J.; Delcenserie, V.; Taminiau, B.; Daube, G.; Saint-Hubert, C.; Durieux, A. Growth and Freeze-Drying Optimization of <I>Bifidobacterium Crudilactis</I> *Food Nutr. Sci.* 2016, *07*, 616–626, doi:10.4236/fns.2016.77063.

85. Pyar, H.; Peh, K.-K. Cost Effectiveness of Cryoprotective Agents and Modified De-Man Rogosa Sharpe Medium on Growth of *Lactobacillus acidophilus*. *Pak. J. Biol. Sci.* 2014, *17*, 462–471, doi:10.3923/pjbs.2014.462.471.
86. Shoaib, M.; Shehzad, A.; Omar, M.; Rakha, A.; Raza, H.; Sharif, H.R.; Shakeel, A.; Ansari, A.; Niazi, S. Inulin: Properties, Health Benefits and Food Applications. *Carbohydr. Polym.* 2016, *147*, 444–454, doi:10.1016/j.carbpol.2016.04.020.
87. Teferra, T.F. Possible Actions of Inulin as Prebiotic Polysaccharide: A Review. *Food Front.* 2021, *2*, 407–416, doi:10.1002/fft2.92.
88. Ramírez-Damián, M.; Garfias-Noguez, C.; Bermúdez-Humarán, L.G.; Sánchez-Pardo, M.E. Synbiotic Microencapsulation of *Lactobacillus* Strains from Mexican Fermented Beverages for Enhanced Probiotic Functionality. *Molecules* 2025, *30*, 1185, doi:10.3390/molecules30051185.
89. Krasaekoopt, W.; Watcharapoka, S. Effect of Addition of Inulin and Galactooligosaccharide on the Survival of Microencapsulated Probiotics in Alginate Beads Coated with Chitosan in Simulated Digestive System, Yogurt and Fruit Juice. *LWT - Food Sci. Technol.* 2014, *57*, 761–766, doi:10.1016/j.lwt.2014.01.037.
90. Mohamed, S.A.; Elsherbini, A.M.; Alrefaey, H.R.; Adelrahman, K.; Moustafa, A.; Egodawaththa, N.M.; Crawford, K.E.; Nesnas, N.; Sabra, S.A. Gum Arabic: A Commodity with Versatile Formulations and Applications. *Nanomaterials* 2025, *15*, 290, doi:10.3390/nano15040290.
91. Ozogul, Y.; Karsli, G.T.; Durmuş, M.; Yazgan, H.; Oztop, H.M.; McClements, D.J.; Ozogul, F. Recent Developments in Industrial Applications of Nanoemulsions. *Adv. Colloid Interface Sci.* 2022, *304*, 102685, doi:10.1016/j.cis.2022.102685.
92. Kamwa, R.; Khurajog, B.; Muangsin, N.; Pupa, P.; Hampson, D.J.; Prapasarakul, N. Water-Soluble Microencapsulation Using Gum Arabic and Skim Milk Enhances Viability and Efficacy of *Pediococcus acidilactici* Probiotic Strains for Application in Broiler Chickens. *Anim. Biosci.* 2024, *37*, 1440–1451, doi:10.5713/ab.23.0446.
93. Yu, J.-K.; Moon, Y.-S. Corn Starch: Quality and Quantity Improvement for Industrial Uses. *Plants* 2021, *11*, 92, doi:10.3390/plants11010092.
94. Bashir, K.; Aggarwal, M. Physicochemical, Structural and Functional Properties of Native and Irradiated Starch: A Review. *J. Food Sci. Technol.* 2019, *56*, 513–523, doi:10.1007/s13197-018-3530-2.
95. Azarnejad, N.; Celletti, S.; Ghorbani, M.; Fedeli, R.; Loppi, S. Dose-Dependent Effects of a Corn Starch-Based Bioplastic on Basil (*Ocimum basilicum* L.): Implications for Growth,

Biochemical Parameters, and Nutrient Content. *Toxics* 2024, *12*, 80, doi:10.3390/toxics12010080.

96. Velloso, C.C.V.; Lopes, M.M.; Badino, A.C.; Farinas, C.S. Exploring the Roles of Starch for Microbial Encapsulation through a Systematic Mapping Review. *Carbohydr. Polym.* 2023, *306*, 120574, doi:10.1016/j.carbpol.2023.120574.
97. Lee, K.Y.; Mooney, D.J. Alginate: Properties and Biomedical Applications. *Prog. Polym. Sci.* 2012, *37*, 106–126, doi:10.1016/j.progpolymsci.2011.06.003.
98. Abka-khajouei, R.; Tounsi, L.; Shahabi, N.; Patel, A.K.; Abdelkafi, S.; Michaud, P. Structures, Properties and Applications of Alginates. *Mar. Drugs* 2022, *20*, 364, doi:10.3390/md20060364.
99. Tan, L.L.; Ang, K.L.; Loo, S.C.J. Alginate Encapsulation Improves Probiotics Survival in Carbonated Sodas and Beers. *PLOS ONE* 2023, *18*, e0283745, doi:10.1371/journal.pone.0283745.
100. Przybyszewska, J.; Kuźmiński, A.; Przybyszewski, M.; Popławski, C. The Role and Therapeutic Effectiveness of Plantago Ovata Seed Husk (Psyllium Husk) in the Prevention and Non-Pharmacological Treatment of Gastrointestinal Diseases. Part 1. Clinical Use of Psyllium Husk in the Treatment of Irritable Bowel Syndrome, Ulcerative Colitis, and Colorectal Cancer. *Gastroenterol. Rev.* 2024, *19*, 121–126, doi:10.5114/pg.2024.139209.
101. Franco, E.A.N.; Sanches-Silva, A.; Ribeiro-Santos, R.; De Melo, N.R. Psyllium (Plantago Ovata Forsk): From Evidence of Health Benefits to Its Food Application. *Trends Food Sci. Technol.* 2020, *96*, 166–175, doi:10.1016/j.tifs.2019.12.006.
102. McRorie, J.W.; Gibb, R.D.; Sloan, K.J.; McKeown, N.M. Psyllium: The Gel-Forming Nonfermented Isolated Fiber That Delivers Multiple Fiber-Related Health Benefits. *Nutr. Today* 2021, *56*, 169–182, doi:10.1097/NT.0000000000000489.
103. Lotfipour, F.; Mirzaeei, S.; Maghsoodi, M. Preparation and Characterization of Alginate and Psyllium Beads Containing *Lactobacillus acidophilus*. *Sci. World J.* 2012, *2012*, 1–8, doi:10.1100/2012/680108.
104. Hite, R.K.; Li, Z.; Walz, T. Principles of Membrane Protein Interactions with Annular Lipids Deduced from Aquaporin-0 2D Crystals. *EMBO J.* 2010, *29*, 1652–1658, doi:10.1038/emboj.2010.68.
105. Najm, A.; Bîrcă, A.C.; Niculescu, A.-G.; Alberts, A.; Grumezescu, A.M.; Gălățeanu, B.; Vasile, B. Ștefan; Beuran, M.; Gaspar, B.S.; Turculeț, C. Ștefan; et al. DMPC-Based Liposomal Vesicles for Encapsulation and Controlled Release of NMN and Matrigel in Sarcopenia Therapy. *Int. J. Mol. Sci.* 2025, *26*, 5594, doi:10.3390/ijms26125594.

106. Chen, C.; Zhu, Z. Recent Advances in the Nanoshells Approach for Encapsulation of Single Probiotics. *Drug Des. Devel. Ther.* 2023, *Volume 17*, 2763–2774, doi:10.2147/DDDT.S419897.

107. Ta, Hp.; Clarisse, C.; Maes, E.; Yamakawa, N.; Guérardel, Y.; Krzewinski, F.; Zarzycka, W.; Touboul, D.; Girardeau, A.; Fonseca, F.; et al. Membrane Lipid Composition of *Carnobacterium maltaromaticum* CNCM I-3298, a Highly Cryoresistant Lactic Bacterium. *Chem. Phys. Lipids* 2023, *255*, 105326, doi:10.1016/j.chemphyslip.2023.105326.

108. Pan, J.; Heberle, F.A.; Tristram-Nagle, S.; Szymanski, M.; Koepfinger, M.; Katsaras, J.; Kučerka, N. Molecular Structures of Fluid Phase Phosphatidylglycerol Bilayers as Determined by Small Angle Neutron and X-Ray Scattering. *Biochim. Biophys. Acta BBA - Biomembr.* 2012, *1818*, 2135–2148, doi:10.1016/j.bbamem.2012.05.007.

109. Viera Herrera, C.; O'Connor, P.M.; Ratrey, P.; Paul Ross, R.; Hill, C.; Hudson, S.P. Anionic Liposome Formulation for Oral Delivery of Thuricin CD, a Potential Antimicrobial Peptide Therapeutic. *Int. J. Pharm.* 2024, *654*, 123918, doi:10.1016/j.ijpharm.2024.123918.

110. Frallicciardi, J.; Melcr, J.; Siginou, P.; Marrink, S.J.; Poolman, B. Membrane Thickness, Lipid Phase and Sterol Type Are Determining Factors in the Permeability of Membranes to Small Solutes. *Nat. Commun.* 2022, *13*, 1605, doi:10.1038/s41467-022-29272-x.

111. Luévano-Martínez, L.A.; Kowaltowski, A.J. Phosphatidylglycerol-Derived Phospholipids Have a Universal, Domain-Crossing Role in Stress Responses. *Arch. Biochem. Biophys.* 2015, *585*, 90–97, doi:10.1016/j.abb.2015.09.015.

112. El-Helw, A.-R.; Fahmy, U. Improvement of Fluvastatin Bioavailability by Loading on Nanostructured Lipid Carriers. *Int. J. Nanomedicine* 2015, 5797, doi:10.2147/IJN.S91556.

113. Asif, A.; Desu, P.; Alavala, R.; Rao, G.; Sreeharsha, N.; Meravanige, G. Development, Statistical Optimization and Characterization of Fluvastatin Loaded Solid Lipid Nanoparticles: A 32 Factorial Design Approach. *Pharmaceutics* 2022, *14*, 584, doi:10.3390/pharmaceutics14030584.

114. Tiwari, R.; Pathak, K. Statins Therapy: A Review on Conventional and Novel Formulation Approaches. *J. Pharm. Pharmacol.* 2011, *63*, 983–998, doi:10.1111/j.2042-7158.2011.01273.x.

115. Wang, J.; Chen, J.; Gao, M.; Ouyang, Z.; Li, Y.; Liu, D.; Zhu, M.; Sun, H. Research Progress on the Mechanism of Action and Screening Methods of Probiotics for Lowering Blood Lipid Levels. *Foods* 2025, *14*, 1583, doi:10.3390/foods14091583.

116. Benov, L. Improved Formazan Dissolution for Bacterial MTT Assay. *Microbiol. Spectr.* 2021, *9*, e01637-21, doi:10.1128/spectrum.01637-21.

117. Pacholak, A.; Burlaga, N.; Frankowski, R.; Zgoła-Grześkowiak, A.; Kaczorek, E. Azole Fungicides: (Bio)Degradation, Transformation Products and Toxicity Elucidation. *Sci. Total Environ.* 2022, *802*, 149917, doi:10.1016/j.scitotenv.2021.149917.

118. *ISO 7218:2024. Microbiology of the Food Chain — General Requirements and Guidance for Microbiological Examinations*; International Organization for Standardization; Geneva, Switzerland, 2024.

119. *ISO 15214:1998. Microbiology of Food and Animal Feeding Stuffs — Horizontal Method for the Enumeration of Mesophilic Lactic Acid Bacteria — Colony-Count Technique at 30 °C*; International Organization for Standardization; Geneva, Switzerland, 1998.

120. Sielatycka, K.; Juzwa, W.; Śliwa-Dominiak, J.; Kaczmarczyk, M.; Łoniewski, I.; Marlicz, W. Multiparameter Flow Cytometric Enumeration of Probiotic-Containing Commercial Powders. *Innov. Food Sci. Emerg. Technol.* 2021, *68*, 102598, doi:10.1016/j.ifset.2020.102598.

121. Halder, S.; Yadav, K.K.; Sarkar, R.; Mukherjee, S.; Saha, P.; Haldar, S.; Karmakar, S.; Sen, T. Alteration of Zeta Potential and Membrane Permeability in Bacteria: A Study with Cationic Agents. *SpringerPlus* 2015, *4*, 672, doi:10.1186/s40064-015-1476-7.

122. Ambalam, P.; Kondepudi, K.K.; Nilsson, I.; Wadström, T.; Ljungh, Å. Bile Stimulates Cell Surface Hydrophobicity, Congo Red Binding and Biofilm Formation of Lactobacillus Strains. *FEMS Microbiol. Lett.* 2012, *333*, 10–19, doi:10.1111/j.1574-6968.2012.02590.x.

123. Pacholak, A.; Burlaga, N.; Kaczorek, E. Evaluating the Effect of Azole Antifungal Agents on the Stress Response and Nanomechanical Surface Properties of *Ochrobactrum anthropi* Aspcl2.2. *Molecules* 2020, *25*, 3348, doi:10.3390/molecules25153348.

124. Vašková, J.; Kočan, L.; Vaško, L.; Perjési, P. Glutathione-Related Enzymes and Proteins: A Review. *Molecules* 2023, *28*, 1447, doi:10.3390/molecules28031447.

125. *Glutathione S-Transferase (GST) Assay Kit - Technical Bulletin*; Sigma-Aldrich Catalog No. CS0410; St. Louis, USA, 2007.

126. Rodríguez-García, A.; García-Vicente, R.; Morales, M.L.; Ortiz-Ruiz, A.; Martínez-López, J.; Linares, M. Protein Carbonylation and Lipid Peroxidation in Hematological Malignancies. *Antioxidants* 2020, *9*, 1212, doi:10.3390/antiox9121212.

127. *Protein Carbonyl Content Assay Kit - Technical Bulletin*; Sigma-Aldrich Catalog No. MAK094; St. Louis, USA, 2021.

128. Li, X.-Y.; Meng, L.; Shen, L.; Ji, H.-F. Regulation of Gut Microbiota by Vitamin C, Vitamin E and β-Carotene. *Food Res. Int.* 2023, *169*, 112749, doi:10.1016/j.foodres.2023.112749.

129. Nawaz, M.; Hassan, M.U.; Chattha, M.U.; Mahmood, A.; Shah, A.N.; Hashem, M.; Alamri, S.; Batool, M.; Rasheed, A.; Thabit, M.A.; et al. Trehalose: A Promising Osmo-Protectant against Salinity Stress—Physiological and Molecular Mechanisms and Future Prospective. *Mol. Biol. Rep.* 2022, *49*, 11255–11271, doi:10.1007/s11033-022-07681-x.

130. Rastall, R.A.; Diez-Municio, M.; Forssten, S.D.; Hamaker, B.; Meynier, A.; Moreno, F.J.; Respondek, F.; Stahl, B.; Venema, K.; Wiese, M. Structure and Function of Non-Digestible Carbohydrates in the Gut Microbiome. *Benef. Microbes* 2022, *13*, 95–168, doi:10.3920/BM2021.0090.

131. Nami, Y.; Haghshenas, B.; Yari Khosroushahi, A. Effect of Psyllium and Gum Arabic Biopolymers on the Survival Rate and Storage Stability in Yogurt of *Enterococcus Durans* IW 3 Encapsulated in Alginate. *Food Sci. Nutr.* 2017, *5*, 554–563, doi:10.1002/fsn3.430.

132. Romyasamit, C.; Saengsuwan, P.; Boonserm, P.; Thamjarongwong, B.; Singkhamanan, K. Optimization of Cryoprotectants for Freeze-Dried Potential Probiotic *Enterococcus faecalis* and Evaluation of Its Storage Stability. *Dry. Technol.* 2022, *40*, 2283–2292, doi:10.1080/07373937.2021.1931294.

133. Zandi, P.; Schnug, E. Reactive Oxygen Species, Antioxidant Responses and Implications from a Microbial Modulation Perspective. *Biology* 2022, *11*, 155, doi:10.3390/biology11020155.

134. Cai, Z.; Guo, Y.; Zheng, Q.; Liu, Z.; Zhong, G.; Zeng, L.; Huang, M.; Pan, D.; Wu, Z. Screening of a Potential Probiotic *Lactiplantibacillus plantarum* NUC08 and Its Synergistic Effects with Yogurt Starter. *J. Dairy Sci.* 2023, S0022030223020131, doi:10.3168/jds.2023-24113.

135. Chua, J.C.L.; Hale, J.D.F.; Silcock, P.; Bremer, P.J. Bacterial Survival and Adhesion for Formulating New Oral Probiotic Foods. *Crit. Rev. Food Sci. Nutr.* 2020, *60*, 2926–2937, doi:10.1080/10408398.2019.1669528.

136. Rowlett, V.W.; Mallampalli, V.K.P.S.; Karlstaedt, A.; Dowhan, W.; Taegtmeyer, H.; Margolin, W.; Vitrac, H. Impact of Membrane Phospholipid Alterations in *Escherichia coli* on Cellular Function and Bacterial Stress Adaptation. *J. Bacteriol.* 2017, *199*, doi:10.1128/JB.00849-16.

137. Bridges, D.F.; Lacombe, A.; Wu, V.C.H. Integrity of the *Escherichia coli* O157:H7 Cell Wall and Membranes After Chlorine Dioxide Treatment. *Front. Microbiol.* 2020, *11*, 888, doi:10.3389/fmicb.2020.00888.

138. Das, A.; Ringu, T.; Ghosh, S.; Pramanik, N. A Comprehensive Review on Recent Advances in Preparation, Physicochemical Characterization, and Bioengineering Applications of Biopolymers. *Polym. Bull.* 2023, *80*, 7247–7312, doi:10.1007/s00289-022-04443-4.

139. Feng, T.; Wang, J. Oxidative Stress Tolerance and Antioxidant Capacity of Lactic Acid Bacteria as Probiotic: A Systematic Review. *Gut Microbes* 2020, *12*, 1801944, doi:10.1080/19490976.2020.1801944.

140. Papadimitriou, K.; Alegría, Á.; Bron, P.A.; De Angelis, M.; Gobbetti, M.; Kleerebezem, M.; Lemos, J.A.; Linares, D.M.; Ross, P.; Stanton, C.; et al. Stress Physiology of Lactic Acid Bacteria. *Microbiol. Mol. Biol. Rev.* 2016, *80*, 837–890, doi:10.1128/MMBR.00076-15.

141. Wu, S.; Chen, Y.; Chen, Z.; Zhou, Q.; Wei, F.; Li, P.; Gu, Q. Antioxidant Properties and Molecular Mechanisms of *Lactiplantibacillus plantarum* ZJ316: A Potential Probiotic Resource. *LWT* 2023, *187*, 115269, doi:10.1016/j.lwt.2023.115269.

142. García-Núñez, I.M.; Santacruz, A.; Serna-Saldívar, S.O.; Hernandez, S.L.C.; Amaya Guerra, C.A. Assessment of Potential Probiotic and Synbiotic Properties of Lactic Acid Bacteria Grown In Vitro with Starch-Based Soluble Corn Fiber or Inulin. *Foods* 2022, *11*, 4020, doi:10.3390/foods11244020.

143. Zhang, X.; Yang, C.; Xi, T.; Zhao, J.; Yang, K. Surface Roughness of Cu-Bearing Stainless Steel Affects Its Contact-Killing Efficiency by Mediating the Interfacial Interaction with Bacteria. *ACS Appl. Mater. Interfaces* 2021, *13*, 2303–2315, doi:10.1021/acsami.0c19655.

144. Wennerström, H.; Oliveberg, M. On the Osmotic Pressure of Cells. *QRB Discov.* 2022, *3*, e12, doi:10.1017/qrd.2022.3.

145. Kumar Bajaj, B.; J.J. Claes, I.; Lebeer, S. FUNCTIONAL MECHANISMS OF PROBIOTICS. *J. Microbiol. Biotechnol. Food Sci.* 2015, *4*, 321–327, doi:10.15414/jmbfs.2015.4.4.321-327.

146. Krithika, B.; Preetha, R. Formulation of Protein Based Inulin Incorporated Synbiotic Nanoemulsion for Enhanced Stability of Probiotic. *Mater. Res. Express* 2019, *6*, 114003, doi:10.1088/2053-1591/ab4d1a.

147. Nale, Z.; Tontul, I.; Aşçi Arslan, A.; Sahin Nadeem, H.; Kucukcetin, A. Microbial Viability, Physicochemical and Sensory Properties of Kefir Microcapsules Prepared Using Maltodextrin/Arabic Gum Mixes. *Int. J. Dairy Technol.* 2018, *71*, 61–72, doi:10.1111/1471-0307.12402.

148. De Andrade, D.P.; Ramos, C.L.; Botrel, D.A.; Borges, S.V.; Schwan, R.F.; Ribeiro Dias, D. Stability of Microencapsulated Lactic Acid Bacteria under Acidic and Bile Juice Conditions. *Int. J. Food Sci. Technol.* 2019, *54*, 2355–2362, doi:10.1111/ijfs.14114.

149. Oluwatosin, S.O.; Tai, S.L.; Fagan-Endres, M.A. Sucrose, Maltodextrin and Inulin Efficacy as Cryoprotectant, Preservative and Prebiotic – towards a Freeze Dried Lactobacillus Plantarum Topical Probiotic. *Biotechnol. Rep.* 2022, *33*, e00696, doi:10.1016/j.btre.2021.e00696.

150. Stindlova, M.; Peroutka, V.; Jencova, V.; Havlickova, K.; Lencova, S. Application of MTT Assay for Probing Metabolic Activity in Bacterial Biofilm-Forming Cells on Nanofibrous Materials. *J. Microbiol. Methods* 2024, *224*, 107010, doi:10.1016/j.mimet.2024.107010.

151. Murray, A.; Kilbride, P.; Gibson, M.I. Trehalose in Cryopreservation. Applications, Mechanisms and Intracellular Delivery Opportunities. *RSC Med. Chem.* 2024, *15*, 2980–2995, doi:10.1039/D4MD00174E.

152. Chen, X.; Gao, X.; Chen, J.; Liu, Y.; Song, C.; Liu, W.; Wan, Y.; Kong, X.; Guan, Y.; Qiu, Z.; et al. Application of Psyllium Husk as a Friendly Filtrate Reducer for High-Temperature Water-Based Drilling Fluids. *ACS Omega* 2022, *7*, 27787–27797, doi:10.1021/acsomega.1c04999.

153. Lavogina, D.; Lust, H.; Tahk, M.-J.; Laasfeld, T.; Vellama, H.; Nasirova, N.; Vardja, M.; Eskla, K.-L.; Salumets, A.; Rinken, A.; et al. Revisiting the Resazurin-Based Sensing of Cellular Viability: Widening the Application Horizon. *Biosensors* 2022, *12*, 196, doi:10.3390/bios12040196.

154. Strkalj, L.; Yakubov, G.E.; Burton, R.A.; Cowley, J.M. Structural and Functional Properties of Fiber From Psyllium (*Plantago ovata*) Husk: Current Knowledge and Strategies to Expand Its Application in Food and Beyond. *Compr. Rev. Food Sci. Food Saf.* 2025, *24*, e70297, doi:10.1111/1541-4337.70297.

155. Gao, B.; Lei, X.; Huang, X.; Rao, C.; Qin, Y.; Song, Y.; Ye, D.; Liu, Y. The Enhancement Mechanism of Gum Acacia and Mannoproteins through Hydrogen Bonding and the Development Strategy for Taste-Masking Films. *Food Hydrocoll.* 2025, *164*, 111216, doi:10.1016/j.foodhyd.2025.111216.

156. Kirmizigul Peker, A.; Guney, D.; Sengun, I. Survival of Free and Alginate-Based Microencapsulated *Lactiplantibacillus plantarum* and *Pediococcus parvulus* in Sauerkraut. *Food Biosci.* 2024, *59*, 104201, doi:10.1016/j.fbio.2024.104201.

157. Snaidr, L.; Mühlhahn, P.; Beimfohr, C.; Kreuzer, C.; Richly, C.; Snaidr, J. Specific Cultivation-Independent Enumeration of Viable Cells in Probiotic Products Using a Combination of Fluorescence in Situ Hybridization and Flow Cytometry. *Front. Microbiol.* 2024, *15*, 1410709, doi:10.3389/fmicb.2024.1410709.

158. Gao, R.; Zhao, D.; Zhou, X.; Wan, Z.; Wang, X.; Rao, H.; Liu, X.; Gao, X.; Hao, J. Advances in Polysaccharide-Based Biopolymers for Probiotic Encapsulation: From Single Polysaccharides to Composite Systems. *Curr. Res. Food Sci.* 2025, *11*, 101186, doi:10.1016/j.crfs.2025.101186.

159. Venturoli, G.; Mamedov, M.D.; Vitukhnovskaya, L.A.; Semenov, A.Y.; Francia, F. Trehalose Interferes with the Photosynthetic Electron Transfer Chain of *Cereibacter* (Rhodobacter) Sphaeroides Permeating the Bacterial Chromatophore Membrane. *Int. J. Mol. Sci.* 2024, *25*, 13420, doi:10.3390/ijms252413420.

160. Pazos-Rojas, L.A.; Cuellar-Sánchez, A.; Romero-Cerón, A.L.; Rivera-Urbalejo, A.; Van Dillewijn, P.; Luna-Vital, D.A.; Muñoz-Rojas, J.; Morales-García, Y.E.; Bustillos-Cristales, M.D.R. The Viable but Non-Culturable (VBNC) State, a Poorly Explored Aspect of Beneficial Bacteria. *Microorganisms* 2023, *12*, 39, doi:10.3390/microorganisms12010039.

161. Bartkiene, E.; Kungiene, G.; Starkute, V.; Klupsaite, D.; Zokaityte, E.; Cernauskas, D.; Kamarauskiene, E.; Özogul, F.; Rocha, J.M. Psyllium Husk Gel Used as an Alternative and More Sustainable Scalding Technology for Wheat Bread Quality Improvement and Acrylamide Reduction. *Front. Nutr.* 2023, *10*, 1277980, doi:10.3389/fnut.2023.1277980.

162. Gao, Y.; Liu, R.; Liang, H. Food Hydrocolloids: Structure, Properties, and Applications. *Foods* 2024, *13*, 1077, doi:10.3390/foods13071077.

163. Colin, C.; Akpo, E.; Perrin, A.; Cornu, D.; Cambedouzou, J. Encapsulation in Alginates Hydrogels and Controlled Release: An Overview. *Molecules* 2024, *29*, 2515, doi:10.3390/molecules29112515.

164. Bevilacqua, A.; Petruzzi, L.; Speranza, B.; Campaniello, D.; Sinigaglia, M.; Corbo, M.R. Changes of the Cell Surface Hydrophobicity of *Lactobacillus acidophilus* La-5 in Response to pH, Temperature and Inulin. *Int. J. Food Sci. Technol.* 2018, *53*, 1262–1268, doi:10.1111/ijfs.13706.

165. Atgié, M.; Masbernat, O.; Roger, K. Emulsions Stabilized by Gum Arabic: Composition and Packing within Interfacial Films. *Langmuir* 2019, *35*, 962–972, doi:10.1021/acs.langmuir.8b02715.

166. M'hamed, A.C.; Ncib, K.; Merghni, A.; Migaou, M.; Lazreg, H.; Snoussi, M.; Noumi, E.; Mansour, M.B.; Maaroufi, R.M. Characterization of Probiotic Properties of *Lacticaseibacillus paracasei* L2 Isolated from a Traditional Fermented Food "Lben." *Life* 2022, *13*, 21, doi:10.3390/life13010021.

167. Kapoor, D.U.; Pareek, A.; Sharma, S.; Prajapati, B.G.; Thanawuth, K.; Sriamornsak, P. Alginate Gels: Chemistry, Gelation Mechanisms, and Therapeutic Applications with a Focus on GERD Treatment. *Int. J. Pharm.* 2025, *675*, 125570, doi:10.1016/j.ijpharm.2025.125570.

168. Martin, J.E.; Waters, L.S. Regulation of Bacterial Manganese Homeostasis and Usage During Stress Responses and Pathogenesis. *Front. Mol. Biosci.* 2022, *9*, 945724, doi:10.3389/fmolb.2022.945724.

169. Seyoum, Y.; Baye, K.; Humblot, C. Iron Homeostasis in Host and Gut Bacteria – a Complex Interrelationship. *Gut Microbes* 2021, *13*, 1874855, doi:10.1080/19490976.2021.1874855.

170. Huynh, U.; Nguyen, H.N.; Trinh, B.K.; Elhaj, J.; Zastrow, M.L. A Bioinformatic Analysis of Zinc Transporters in Intestinal *Lactobacillaceae*. *Metallomics* 2023, *15*, mfad044, doi:10.1093/mtomcs/mfad044.

171. Bosma, E.F.; Rau, M.H.; van Gijtenbeek, L.A.; Siedler, S. Regulation and Distinct Physiological Roles of Manganese in Bacteria. *FEMS Microbiol. Rev.* 2021, *45*, fuab028, doi:10.1093/femsre/fuab028.

172. Huynh, U.; Qiao, M.; King, J.; Trinh, B.; Valdez, J.; Haq, M.; Zastrow, M.L. Differential Effects of Transition Metals on Growth and Metal Uptake for Two Distinct *Lactobacillus* Species. *Microbiol. Spectr.* 2022, *10*, e01006-21, doi:10.1128/spectrum.01006-21.

173. El Hariri El Nokab, M.; Es Sayed, J.; De Witte, F.; Dewettinck, K.; Elshewy, A.; Zhang, Z.; Van Steenberge, P.H.M.; Wang, T.; Sebakhy, K.O. A Comparative Analytical Study for the Different Water Pools Present in Alginate Hydrogels: Qualitative vs. Quantitative Approaches. *Food Hydrocoll.* 2024, *154*, 110159, doi:10.1016/j.foodhyd.2024.110159.

174. Wang, Y.; Shen, Z.; Wang, H.; Song, Z.; Yu, D.; Li, G.; Liu, X.; Liu, W. Progress in Research on Metal Ion Crosslinking Alginate-Based Gels. *Gels* 2024, *11*, 16, doi:10.3390/gels11010016.

175. Lam, L.N.; Brunson, D.N.; Molina, J.J.; Flores-Mireles, A.L.; Lemos, J.A. The AdcACB/AdcAII System Is Essential for Zinc Homeostasis and an Important Contributor of *Enterococcus faecalis* Virulence. *Virulence* 2022, *13*, 592–608, doi:10.1080/21505594.2022.2056965.

176. Kang, S.; Li, R.; Jin, H.; You, H.J.; Ji, G.E. Effects of Selenium- and Zinc-Enriched *Lactobacillus plantarum* SeZi on Antioxidant Capacities and Gut Microbiome in an ICR Mouse Model. *Antioxidants* 2020, *9*, 1028, doi:10.3390/antiox9101028.

177. Irfan, J.; Hussain, M.A.; Haseeb, M.T.; Ali, A.; Farid-ul-Haq, M.; Tabassum, T.; Hussain, S.Z.; Hussain, I.; Naeem-ul-Hassan, M. A pH-Sensitive, Stimuli-Responsive, Superabsorbent, Smart Hydrogel from Psyllium (*Plantago Ovata*) for Intelligent Drug Delivery. *RSC Adv.* 2021, *11*, 19755–19767, doi:10.1039/D1RA02219A.

178. Savić Gajić, I.M.; Savić, I.M.; Svirčev, Z. Preparation and Characterization of Alginate Hydrogels with High Water-Retaining Capacity. *Polymers* 2023, *15*, 2592, doi:10.3390/polym15122592.

179. Menegatti, T.; Kopač, T.; Žnidaršič-Plazl, P. Tuning Mechanical Characteristics and Permeability of Alginate Hydrogel by Polyvinyl Alcohol and Deep Eutectic Solvent Addition. *Bioengineering* 2024, *11*, 371, doi:10.3390/bioengineering11040371.

180. Chen, Q.; Wang, X.; Wang, Y.; Guo, T.; Guan, P.; Hou, J.; Chen, Z. Effects of Inulin with Different Polymerization Degrees on the Structural and Gelation Properties of Potato Protein. *Food Chem. X* 2024, *22*, 101405, doi:10.1016/j.fochx.2024.101405.

181. Pérez-Flores, J.G.; García-Curiel, L.; Pérez-Escalante, E.; Contreras-López, E.; Olloqui, E.J. Arabinoxylans Matrixes as a Potential Material for Drug Delivery Systems Development - A Bibliometric Analysis and Literature Review. *Heliyon* 2024, *10*, e25445, doi:10.1016/j.heliyon.2024.e25445.

182. Farahmand, A.; Ghorani, B.; Emadzadeh, B.; Sarabi-Jamab, M.; Emadzadeh, M.; Modiri, A.; Mendes, A.C. Double Protection of Probiotics in Alginate Hydrogel through Emulsification Incorporated with Freeze Drying and Coaxial Wet-Electrospraying: Survivability and Targeted Delivery. *LWT* 2024, *204*, 116459, doi:10.1016/j.lwt.2024.116459.

183. Zhao, J.; Guo, Q.; Huang, W.; Zhang, T.; Wang, J.; Zhang, Y.; Huang, L.; Tang, Y. Shape Tuning and Size Prediction of Millimeter-Scale Calcium-Alginate Capsules with Aqueous Core. *Polymers* 2020, *12*, 688, doi:10.3390/polym12030688.

184. Liang, X.; Lin, D.; Zhang, W.; Chen, S.; Ding, H.; Zhong, H.-J. Progress in the Preparation and Application of Inulin-Based Hydrogels. *Polymers* 2024, *16*, 1492, doi:10.3390/polym16111492.

185. Vinciguerra, D.; Gelb, M.B.; Maynard, H.D. Synthesis and Application of Trehalose Materials. *JACS Au* 2022, *2*, 1561–1587, doi:10.1021/jacsau.2c00309.

186. Zhang, C.; Grossier, R.; Candoni, N.; Veesler, S. Preparation of Alginate Hydrogel Microparticles by Gelation Introducing Cross-Linkers Using Droplet-Based Microfluidics: A Review of Methods. *Biomater. Res.* 2021, *25*, 41, doi:10.1186/s40824-021-00243-5.

187. Cortés-Camargo, S.; Román-Guerrero, A.; Alvarez-Ramirez, J.; Alpizar-Reyes, E.; Velázquez-Gutiérrez, S.K.; Pérez-Alonso, C. Microstructural Influence on Physical Properties and Release Profiles of Sesame Oil Encapsulated into Sodium Alginate-Tamarind Mucilage Hydrogel Beads. *Carbohydr. Polym. Technol. Appl.* 2023, *5*, 100302, doi:10.1016/j.carpta.2023.100302.

188. Niu, H.; Chen, X.; Luo, T.; Chen, H.; Fu, X. The Interfacial Behavior and Long-Term Stability of Emulsions Stabilized by Gum Arabic and Sugar Beet Pectin. *Carbohydr. Polym.* 2022, *291*, 119623, doi:10.1016/j.carbpol.2022.119623.

189. Renard, D.; Davantès, A.; D'orlando, A.; Cahier, K.; Molinari, M.; Nigen, M.; Chalier, P.; Sanchez, C. Adsorption of Arabinogalactan-Proteins from Acacia Gums (Senegal and Seyal) and Its Molecular Fractions onto Latex Particles. *Food Hydrocoll.* 2022, *125*, 107360, doi:10.1016/j.foodhyd.2021.107360.

190. Sıçramaz, H.; Dönmez, A.B.; Güven, B.; Ünal, D.; Aşbay, E. Microstructure and Release Behavior of Alginate–Natural Hydrocolloid Composites: A Comparative Study. *Polymers* 2025, *17*, 531, doi:10.3390/polym17040531.

191. Chen, N.; Feng, Z.-J.; Gao, H.-X.; He, Q.; Zeng, W.-C. Core-Shell Structured Alginate-Based Hydrogel Beads Modified by Starch and Protocatechuic Acid: Preparation, Characterization, Phenolic Slow Release and Stable Antioxidant Potential. *Food Chem.* 2024, *459*, 140389, doi:10.1016/j.foodchem.2024.140389.

192. Cao, Z.; Liu, J. Coated Bacteria: Advanced Living Materials for Microbial Therapy. *Acc. Mater. Res.* 2024, *5*, 872–883, doi:10.1021/accountsmr.4c00116.

193. Kim, S.-Y.; Park, Y.-L.; Ji, H.-E.; Lee, H.-S.; Chang, H.-J.; Bang, G.-H.; Lee, J.-H. High-Purity 1,2-Dimyristoyl-Sn-Glycero-3-Phosphocholine: Synthesis and Emulsifying Performance Evaluation. *Front. Nutr.* 2024, *11*, 1408937, doi:10.3389/fnut.2024.1408937.

194. Subczynski, W.K.; Widomska, J. 5-PC as a Lipid Probe Molecule and as a Second Phospholipid in Binary Phospholipid Mixtures: Saturation Recovery EPR Studies. *Int. J. Mol. Sci.* 2024, *25*, 12913, doi:10.3390/ijms252312913.

195. Drabik, D.; Chodaczek, G.; Kraszewski, S.; Langner, M. Mechanical Properties Determination of DMPC, DPPC, DSPC, and HSPC Solid-Ordered Bilayers. *Langmuir* 2020, *36*, 3826–3835, doi:10.1021/acs.langmuir.0c00475.

196. Ghandi, A.; Powell, I.B.; Broome, M.; Adhikari, B. Survival, Fermentation Activity and Storage Stability of Spray Dried *Lactococcus lactis* Produced via Different Atomization Regimes. *J. Food Eng.* 2013, *115*, 83–90, doi:10.1016/j.jfoodeng.2012.09.022.

197. Braissant, O.; Astasov-Frauenhoffer, M.; Waltimo, T.; Bonkat, G. A Review of Methods to Determine Viability, Vitality, and Metabolic Rates in Microbiology. *Front. Microbiol.* 2020, *11*, 547458, doi:10.3389/fmicb.2020.547458.

198. Ghasemi, M.; Turnbull, T.; Sebastian, S.; Kempson, I. The MTT Assay: Utility, Limitations, Pitfalls, and Interpretation in Bulk and Single-Cell Analysis. *Int. J. Mol. Sci.* 2021, *22*, 12827, doi:10.3390/ijms222312827.

199. Cai, Y.; Liu, J.; Li, G.; Wong, P.K.; An, T. Formation Mechanisms of Viable but Nonculturable Bacteria through Induction by Light-Based Disinfection and Their Antibiotic Resistance Gene Transfer Risk: A Review. *Crit. Rev. Environ. Sci. Technol.* 2022, *52*, 3651–3688, doi:10.1080/10643389.2021.1932397.

200. Oh, Y.J.; Hong, J. Application of the MTT-Based Colorimetric Method for Evaluating Bacterial Growth Using Different Solvent Systems. *LWT* 2022, *153*, 112565, doi:10.1016/j.lwt.2021.112565.

201. Velly, H.; Fonseca, F.; Passot, S.; Delacroix-Buchet, A.; Bouix, M. Cell Growth and Resistance of *Lactococcus lactis* Subsp. *lactis* TOMSC161 Following Freezing, Drying and Freeze-Dried Storage Are Differentially Affected by Fermentation Conditions. *J. Appl. Microbiol.* 2014, *117*, 729–740, doi:10.1111/jam.12577.

202. Johanson, A.; Goel, A.; Olsson, L.; Franzén, C.J. Respiratory Physiology of *Lactococcus lactis* in Chemostat Cultures and Its Effect on Cellular Robustness in Frozen and Freeze-Dried Starter Cultures. *Appl. Environ. Microbiol.* 2020, *86*, e02785-19, doi:10.1128/AEM.02785-19.

203. Ghosh, R.; De, M. Liposome-Based Antibacterial Delivery: An Emergent Approach to Combat Bacterial Infections. *ACS Omega* 2023, *8*, 35442–35451, doi:10.1021/acsomega.3c04893.

204. Bhattacharjee, S. DLS and Zeta Potential – What They Are and What They Are Not? *J. Controlled Release* 2016, *235*, 337–351, doi:10.1016/j.jconrel.2016.06.017.

205. John, R.; Monpara, J.; Swaminathan, S.; Kalhapure, R. Chemistry and Art of Developing Lipid Nanoparticles for Biologics Delivery: Focus on Development and Scale-Up. *Pharmaceutics* 2024, *16*, 131, doi:10.3390/pharmaceutics16010131.

206. Rodriguez-Loya, J.; Lerma, M.; Gardea-Torresdey, J.L. Dynamic Light Scattering and Its Application to Control Nanoparticle Aggregation in Colloidal Systems: A Review. *Micromachines* 2023, *15*, 24, doi:10.3390/mi15010024.

207. Falke, S.; Betzel, C. Dynamic Light Scattering (DLS): Principles, Perspectives, Applications to Biological Samples. In *Radiation in Bioanalysis*; Pereira, A.S., Tavares, P., Limão-Vieira, P., Eds.; Bioanalysis; Springer International Publishing: Cham, 2019; Vol. 8, pp. 173–193 ISBN 978-3-030-28246-2.

208. Chibowski, E.; Szcześ, A. Zeta Potential and Surface Charge of DPPC and DOPC Liposomes in the Presence of PLC Enzyme. *Adsorption* 2016, *22*, 755–765, doi:10.1007/s10450-016-9767-z.

209. Sreij, R.; Dargel, C.; Schweins, R.; Prévost, S.; Dattani, R.; Hellweg, T. Aescin-Cholesterol Complexes in DMPC Model Membranes: A DSC and Temperature-Dependent Scattering Study. *Sci. Rep.* 2019, *9*, 5542, doi:10.1038/s41598-019-41865-z.

210. Moreira, L.; Guimarães, N.M.; Pereira, S.; Santos, R.S.; Loureiro, J.A.; Pereira, M.C.; Azevedo, N.F. Liposome Delivery of Nucleic Acids in Bacteria: Toward *In Vivo* Labeling of Human Microbiota. *ACS Infect. Dis.* 2022, *8*, 1218–1230, doi:10.1021/acsinfecdis.1c00601.

211. Rohde, M. The Gram-Positive Bacterial Cell Wall. *Microbiol. Spectr.* 2019, *7*, 7.3.10, doi:10.1128/microbiolspec.GPP3-0044-2018.

212. Yerlikaya, O. Probiotic Potential and Biochemical and Technological Properties of *Lactococcus lactis* ssp. *lactis* Strains Isolated from Raw Milk and Kefir Grains. *J. Dairy Sci.* 2019, *102*, 124–134, doi:10.3168/jds.2018-14983.

213. Quinn, S.D.; Dresser, L.; Graham, S.; Conteduca, D.; Shepherd, J.; Leake, M.C. Crowding-Induced Morphological Changes in Synthetic Lipid Vesicles Determined Using smFRET. *Front. Bioeng. Biotechnol.* 2022, *10*, 958026, doi:10.3389/fbioe.2022.958026.

214. Lombardo, D.; Kiselev, M.A. Methods of Liposomes Preparation: Formation and Control Factors of Versatile Nanocarriers for Biomedical and Nanomedicine Application. *Pharmaceutics* 2022, *14*, 543, doi:10.3390/pharmaceutics14030543.

215. Garcia-Manyes, S.; Oncins, G.; Sanz, F. Effect of Ion-Binding and Chemical Phospholipid Structure on the Nanomechanics of Lipid Bilayers Studied by Force Spectroscopy. *Biophys. J.* 2005, *89*, 1812–1826, doi:10.1529/biophysj.105.064030.

216. Rukavina, Z.; Vanić, Ž. Current Trends in Development of Liposomes for Targeting Bacterial Biofilms. *Pharmaceutics* 2016, *8*, 18, doi:10.3390/pharmaceutics8020018.

217. Han, M.; Yang, S.; Song, J.; Gao, Z. Layer-by-Layer Coated Probiotics with Chitosan and Liposomes Demonstrate Improved Stability and Antioxidant Properties in Vitro. *Int. J. Biol. Macromol.* 2024, *258*, 128826, doi:10.1016/j.ijbiomac.2023.128826.

218. Mankan, E.; Karakas, C.Y.; Saroglu, O.; Mzoughi, M.; Sagdic, O.; Karadag, A. Food-Grade Liposome-Loaded Delivery Systems: Current Trends and Future Perspectives. *Foods* 2025, *14*, 2978, doi:10.3390/foods14172978.

219. Climent, E.; Benaiges, D.; Pedro-Botet, J. Hydrophilic or Lipophilic Statins? *Front. Cardiovasc. Med.* 2021, *8*, 687585, doi:10.3389/fcvm.2021.687585.

220. Belletto, D.; Cova, T.F.G.G.; Mazzone, G.; Pais, A.A.C.C.; Sicilia, E. Investigation of Simvastatin and Fluvastatin Permeation across Cell Membrane Models Using Molecular Dynamics Simulations. *J. Chem. Phys.* 2025, *163*, 065101, doi:10.1063/5.0280981.

221. Agolino, G.; Pino, A.; Vaccalluzzo, A.; Cristofolini, M.; Solieri, L.; Caggia, C.; Randazzo, C.L. Bile Salt Hydrolase: The Complexity behind Its Mechanism in Relation to Lowering-Cholesterol *Lactobacilli* Probiotics. *J. Funct. Foods* 2024, *120*, 106357, doi:10.1016/j.jff.2024.106357.

222. Kiepś, J.; Juzwa, W.; Dembczyński, R. Imaging Flow Cytometry Demonstrates Physiological and Morphological Diversity within Treated Probiotic Bacteria Groups. *Int. J. Mol. Sci.* 2023, *24*, 6841, doi:10.3390/ijms24076841.

223. Arroyo-Moreno, S.; Saiz-Gonzalo, G.; McSweeney, S.; Bleiel, S.B. Probiotic Viability Reconsidered: Integrating VBNC Resuscitation and Culture-Independent Methods for Accurate Probiotic Enumeration. *Microorganisms* 2025, *13*, 2479, doi:10.3390/microorganisms13112479.

224. Shangguan, Y.; Yang, D.; Zhao, L.; Rao, L.; Liao, X. High-Pressure-Induced Viable but Non-Culturable Lactic Acid Bacteria Inhibit Its Post-Acidification. *Bioresour. Technol.* 2025, *422*, 132221, doi:10.1016/j.biortech.2025.132221.

225. Al-Madboly, L.A.; Ali, S.M.; Fakharany, E.M.E.; Ragab, A.E.; Khedr, E.G.; Elokely, K.M. Stress-Based Production, and Characterization of Glutathione Peroxidase and Glutathione S-Transferase Enzymes From Lactobacillus Plantarum. *Front. Bioeng. Biotechnol.* 2020, *8*, 78, doi:10.3389/fbioe.2020.00078.

226. Zinellu, A.; Mangoni, A.A. A Systematic Review and Meta-Analysis of the Effect of Statins on Glutathione Peroxidase, Superoxide Dismutase, and Catalase. *Antioxidants* 2021, *10*, 1841, doi:10.3390/antiox10111841.

227. Wang, M.; Wang, J.; Liu, M.; Chen, G. Fluvastatin Protects Neuronal Cells from Hydrogen Peroxide-Induced Toxicity with Decreasing Oxidative Damage and Increasing PI3K/Akt/mTOR Signalling. *J. Pharm. Pharmacol.* 2021, *73*, 515–521, doi:10.1093/jpp/rgaa058.

228. Németh, Z.; Csóka, I.; Semnani Jazani, R.; Sipos, B.; Haspel, H.; Kozma, G.; Kónya, Z.; Dobó, D.G. Quality by Design-Driven Zeta Potential Optimisation Study of Liposomes with Charge Imparting Membrane Additives. *Pharmaceutics* 2022, *14*, 1798, doi:10.3390/pharmaceutics14091798.

229. Hamal, P.; Subasinghege Don, V.; Nguyenhuu, H.; Ranasinghe, J.C.; Nauman, J.A.; McCarley, R.L.; Kumar, R.; Haber, L.H. Influence of Temperature on Molecular Adsorption and Transport at Liposome Surfaces Studied by Molecular Dynamics Simulations and Second Harmonic Generation Spectroscopy. *J. Phys. Chem. B* 2021, *125*, 10506–10513, doi:10.1021/acs.jpcb.1c04263.

230. Farkas, N.; Kramar, J.A. Dynamic Light Scattering Distributions by Any Means. *J. Nanoparticle Res.* 2021, *23*, 120, doi:10.1007/s11051-021-05220-6.

231. Kowalik, K.; Kulig, K.; Karnas, E.; Barczyk-Woznicka, O.; Zuba-Surma, E.; Pyza, E.; Rapala-Kozik, M.; Karkowska-Kuleta, J. Extracellular Vesicles of *Lactiplantibacillus plantarum* PCM 2675 and *Lacticaseibacillus rhamnosus* PCM 489: An Introductory Characteristic. *Extracell. Vesicles Circ. Nucleic Acids* 2024, doi:10.20517/evcna.2024.49.

232. Kurata, A.; Kiyohara, S.; Imai, T.; Yamasaki-Yashiki, S.; Zaima, N.; Moriyama, T.; Kishimoto, N.; Uegaki, K. Characterization of Extracellular Vesicles from *Lactiplantibacillus plantarum*. *Sci. Rep.* 2022, *12*, 13330, doi:10.1038/s41598-022-17629-7.

233. Hoseini, B.; Jaafari, M.R.; Golabpour, A.; Momtazi-Borojeni, A.A.; Karimi, M.; Eslami, S. Application of Ensemble Machine Learning Approach to Assess the Factors Affecting Size and Polydispersity Index of Liposomal Nanoparticles. *Sci. Rep.* 2023, *13*, 18012, doi:10.1038/s41598-023-43689-4.

234. Zhang, C.; Gao, X.; Ren, X.; Xu, T.; Peng, Q.; Zhang, Y.; Chao, Z.; Jiang, W.; Jia, L.; Han, L. Bacteria-Induced Colloidal Encapsulation for Probiotic Oral Delivery. *ACS Nano* 2023, *17*, 6886–6898, doi:10.1021/acsnano.3c00600.

235. Liang, J.; Koo, B.; Wu, Y.; Manna, S.; Noble, J.M.; Patel, M.; Park, J.H.; Kozak, D.; Wang, Y.; Zheng, J. Characterization of Complex Drug Formulations Using Cryogenic Scanning Electron Microscopy (Cryo-SEM). *Curr. Protoc.* 2022, *2*, e406, doi:10.1002/cpz1.406.

236. Amer, A.M.; Charnock, C.; Nguyen, S. The Impact of Surface Charge on the Interaction of Cholesterol-Free Fusogenic Liposomes with Planktonic Microbial Cells and Biofilms. *Int. J. Pharm.* 2025, *669*, 125088, doi:10.1016/j.ijpharm.2024.125088.

237. Jiang, X.; Martens, H.J.; Shekarforoush, E.; Muhammed, M.K.; Whitehead, K.A.; Arneborg, N.; Risbo, J. Multi-Species Colloidosomes by Surface-Modified Lactic Acid Bacteria with Enhanced Aggregation Properties. *J. Colloid Interface Sci.* 2022, *622*, 503–514, doi:10.1016/j.jcis.2022.04.136.

238. Hosseini, S.F.; Ansari, B.; Gharsallaoui, A. Polyelectrolytes-Stabilized Liposomes for Efficient Encapsulation of *Lactobacillus rhamnosus* and Improvement of Its Survivability under Adverse Conditions. *Food Chem.* 2022, *372*, 131358, doi:10.1016/j.foodchem.2021.131358.

SCIENTIFIC ACHIEVEMENTS

Publications

1. Marta Wojcieszak, **Natalia Burlaga**, Jacek Różański, Ewa Kaczorek, Katarzyna Materna*; Emulgels powered by coco-glucoside: A stable and effective synbiotics delivery system for skin care*; International Journal of Pharmaceutics - 2025, vol. 683, s. 126070-1-126070-11; **IF 5.2, MNiSW points 100**
2. Monika Zielińska, Amanda Pacholak, **Natalia Burlaga**, Ewa Chmielewska, Adam Voelkel, Ewa Kaczorek; *Determination of bisphosphonate properties in terms of bioavailability, bone affinity, and cytotoxicity*; Pharmacological Reports - 2024, vol. 76, iss. 4; **IF 3.8, MNiSW points 100**
3. **Natalia Burlaga**, Amanda Pacholak, Wojciech Juzwa, Ewa Kaczorek; *Functional insights into the interaction of Lactobacillus spp. and potentially protective agents*; Food Bioscience - 2024, vol. 61, s. 105002-1-105002-10; **IF 5.9, MNiSW points 70**
4. Damian Krystian Kaczmarek, Amanda Pacholak, **Natalia Burlaga**, Marta Wojcieszak, Katarzyna Materna, Dariusz Kruszka, Piotr Dąbrowski, Karolina Sobańska, Ewa Kaczorek; *Dicationic Ionic Liquids with an Indole-3-butyrate Anion – Plant Growth Stimulation and Ecotoxicological Evaluations*; ACS Sustainable Chemistry & Engineering - 2023, vol. 11, iss. 36, s. 13282-13297; **IF 7.1, MNiSW points 140**
5. Amanda Pacholak, **Natalia Burlaga**, Robert Frankowski, Agnieszka Zgoła-Grześkowiak, Ewa Kaczorek; *Azole fungicides: (Bio)degradation, transformation products and toxicity elucidation*; Science of the Total Environment - 2022, vol. 802, s. 149917-1-149917-13; **IF 9.8, MNiSW points 200**
6. Wojciech Smułek, **Natalia Burlaga**, Michal Hricovíni, Alzbeta Medvedova, Ewa Kaczorek, Zuzana Hricovíniová; *Evaluation of surface active and antimicrobial properties of alkyl D-lyxosides and alkyl L-rhamnosides as green surfactants*; Chemosphere - 2021, vol. 271, s. 129818-1-129818-8; **IF 8.943, MNiSW points 140**
7. Amanda Pacholak, **Natalia Burlaga**, Urszula Guzik, Ewa Kaczorek; *Investigation of the bacterial cell envelope nanomechanical properties after long-term exposure to nitrofurans*; Journal of Hazardous Materials - 2021, vol. 407, s. 124352-1-124352-15; **IF 14.224, MNiSW points 200**
8. Amanda Pacholak, **Natalia Burlaga**, Ewa Kaczorek; *Evaluating the effect of azole antifungal agents on the stress response and nanomechanical surface properties of*

Ochrobactrum anthropi Aspcl2.2; Molecules - 2020, vol. 25, iss. 15, s. 3348-1-3348-18; **IF 4.411, MNiSW points 100**

Total IF: 59.378; total MNiSW points: 1050; h-index 6; citation count: 147 (ResearchGate), 154 (Google Scholar), 136 (Scopus) – as of the date of 10.03.2026.

Conference paper

Natalia Burlaga, Magdalena Bartolewska, Matej Buzgo, Aiva Simaite; *Optimization of the Emulsion Electrospinning for Increased Activity of Biopharmaceuticals*; Proceedings - 2021, vol. 78, iss. 1, s. 39-1-39-9; MNiSW points 5

Chapters in scientific monographs

1. Marta Wojcieszak-Michalak, Julia Kowalska, Amelia Wojciechowska, Natalia Szymczak, **Natalia Burlaga**, Ewa Kaczorek, Katarzyna Materna; *Charakterystyka i analiza emulżeli na bazie synbiotyków jako zaawansowanych środków do pielęgnacji skóry*; V Sympozjum Chemii Bioorganicznej, Organicznej i Biomateriałów: materiały konferencyjne; Poznan, Poland, 2025 - s. 284-285; MNiSW points 20
2. Michał Kapczyński, Adam Grzywaczyk, **Natalia Burlaga**, Ewa Kaczorek; *Waloryzacja odpadów przemysłu spożywczego jako źródła węgla w syntezie polihydroksyalkanianów*; III Ogólnopolska Konferencja Naukowa PUTChemikon: materiały konferencyjne; Poznan, Poland, 2025 - s. 84-86; MNiSW points 20
3. **Natalia Burlaga**, Adam Grzywaczyk, Paulina Laufer, Ewa Kaczorek; *Zmiany w komórkach bakterii probiotycznych w obecności farmaceutyków*; V Sympozjum Chemii Bioorganicznej, Organicznej i Biomateriałów: materiały konferencyjne; Poznan, Poland, 2025 - s. 66-68; MNiSW points 20
4. Michał Kapczyński, Adam Grzywaczyk, **Natalia Burlaga**, Ewa Kaczorek; *Zrównoważone zagospodarowanie odpadowej biomasy jako surowiec do syntezy polihydroksyalkanianów*; II Ogólnopolska Konferencja Naukowa PUTChemikon: materiały konferencyjne; Poznan, Poland, 2024 - s. 153-155; MNiSW points 20
5. **Natalia Burlaga**, Irina Nagorichna; *Efektywność procesu dezintegracji komórek w uzyskaniu protein pochodzenia bakteryjnego*; BioOrg 2022 - IV Ogólnopolskie Sympozjum Chemii Bioorganicznej, Organicznej i Biomateriałów: materiały konferencyjne; Poznan, Poland, 2022 - s. 67-69; MNiSW points 20

6. Amanda Pacholak, **Natalia Burlaga**, Ewa Kaczorek; *Wpływ azolowych związków przeciwgrzybiczych na bakterie środowiskowe*; BioOrg 2022 - IV Ogólnopolskie Sympozjum Chemii Bioorganicznej, Organicznej i Biomateriałów: materiały konferencyjne; Poznan, Poland, 2022 - s. 166-168; MNiSW points 20
7. **Natalia Burlaga**, Amanda Pacholak, Ewa Kaczorek; *Wytwarzanie preparatów probiotycznych a właściwości komórek bakteryjnych*; BioOrg 2022 - IV Ogólnopolskie Sympozjum Chemii Bioorganicznej, Organicznej i Biomateriałów: materiały konferencyjne; Poznan, Poland, 2022 - s. 65-66; MNiSW points 20
8. **Natalia Burlaga**, Amanda Pacholak, Ewa Kaczorek; *Wpływ wybranych leków przeciwgrzybiczych na właściwości komórek bakterii środowiskowych*; BioOrg 2019 - III Ogólnopolskie Sympozjum Chemii Bioorganicznej, Organicznej i Biomateriałów: materiały konferencyjne; Poznan, Poland, 2019 - s. 297-298; MNiSW points 20

Intellectual property

1. Patent application Pat.249169; Amanda Pacholak, Filip Jaworski, **Natalia Burlaga**, Ewa Kaczorek; *Sposób przygotowania próbki żywych komórek bakteryjnych do ich obrazowania za pomocą mikroskopii sił atomowych*; patent granted in 2025
2. Patent application P.446869; **Natalia Burlaga**, Adam Grzywaczyk, Amanda Pacholak, Ewa Kaczorek; *Układ do dostarczania mikroorganizmów probiotycznych stabilizowany za pomocą nanocząstek lipidowych*; patent pending
3. Newly isolated bacterial strain reported to the GenBank database (*Lacticaseibacillus rhamnosus* Z2; ON429035.1); **Natalia Burlaga**, Amanda Pacholak, Ariel Marchlewicz, Urszula Guzik, Ewa Kaczorek; 2022
4. Newly isolated bacterial strain reported to the GenBank database (*Companilactobacillus heilongjiangensis* Z1; ON429027.1); **Natalia Burlaga**, Amanda Pacholak, Ariel Marchlewicz, Urszula Guzik, Ewa Kaczorek; 2022
5. Newly isolated bacterial strain reported to the GenBank database (*Lactiplantibacillus plantarum* P1; ON429026.1); **Natalia Burlaga**, Amanda Pacholak, Ariel Marchlewicz, Urszula Guzik, Ewa Kaczorek; 2022

Projects and grants

1. *MiCo: new microbe-colloids for oral delivery of probiotics* - PRELUDIUM 22

2024-01 – 2027-01
Registration number: 2023/49/N/NZ9/02128
Source of funding: National Science Centre
Role in the project: **Project manager**, Principal Investigator

2. *Natural insecticides used in organic farming - multi-aspect assessment of their microbiological safety* - SONATA 17

2022-10 – 2026-10
Registration number: 2021/41/D/NZ9/01201
Source of funding: National Science Centre
Role in the project: Investigator

3. *A comprehensive approach to 3D printing - from application to environmental impact*

2025-04 – 2025-11
Registration number: 0912/SBAD/2513
Source of funding: Poznan University of Technology
Role in the project: Investigator

4. *Innovative biocomposite product using industrial hemp fibers for high-value sustainable applications*

2025-03 – 2025-05
Registration number: 12450235
Source of funding: INDUSAC program funded from the European Union's Horizon Europe Program under grant agreement No 101070297
Role in the project: Investigator

5. *Effect of pharmacologically active substances on the development of resistance mechanisms of environmental microorganisms*

2024-04 – 2024-11
Registration number: 0912/SBAD/2404
Source of funding: Poznan University of Technology
Role in the project: Investigator

6. *Microbial removal of environmental pollutants by single strain and microbial consortia*

2023-04 – 2023-11
Registration number: 0912/SBAD/2311
Source of funding: Poznan University of Technology
Role in the project: Investigator

7. *STER - Internationalisation of doctoral schools* - STER Mobility scholarship

2022-03 – 2023-06
Source of funding: NAWA Polish National Agency for Academic Exchange
Role in the project: Scholar

8. *Impact of natural and anthropogenic bioactive compounds on human and environmental microbiota*

2022-04 – 2022-11
Registration number: 0912/SBAD/2211
Source of funding: Poznan University of Technology
Role in the project: Investigator

9. *Biotechnological methods in the assessment of the properties of pharmaceuticals and new biomedical materials*

2021-04 – 2021-11
Registration number: 0912/SBAD/2115
Source of funding: Poznan University of Technology
Role in the project: Investigator

10. *The use of compounds of plant origin as protective compounds in the storage of probiotic bacteria*

2020-04 – 2020-11
Registration number: 0912/SBAD/2015
Source of funding: Poznan University of Technology
Role in the project: Investigator

11. *ORBIS Open Research Biopharmaceutical Internship Support* - Research and Innovation Staff Exchange

2018-03 – 2023-08
Registration number: H2020-MSCA-RISE-2017 No 778051
Source of funding: MSCA – Horizon 2020
Role in the project: Trainee

12. *Biodegradation of nitrofuran derivatives by environmental bacteria - from metabolic pathway to changes in genome and proteome* - OPUS 14

2018-07 – 2022-07
Registration number: 2017/27/B/NZ9/01603
Source of funding: National Science Centre
Role in the project: Investigator

Prizes and awards

- Selection as one of the Top 1000 Innovators of Poland in Silicon Valley (2025)
- 1st Place – atTRACTION DemoDay for the excellent presentation of an innovative deep tech startup and the highest marks from the jury (2025)
- 1st Place – EU Sparks for Climate Hackathon World Championships founded by European Commission (2024)

- 1st Place – Pitch Final Contest within the Deep Tech Innovators program for AGRIfood (2024)
- 1st Place – BASF Drive Innovation Competition for the Solutions for Sustainable Development (2024)
- 2nd Place – PUT START UP competition for the best business idea (2023)
- Santander Scholarship for Outstanding Doctoral Students (2023)
- Beneficiary of the PUT Rector's scientific scholarship for the best doctoral students (2022/23)
- Elevation of Doctoral Scholarship for Outstanding Performance (2022/23)
- Beneficiary of INPUTDoc STER Mobility Grant (2022/23)
- Beneficiary of the PUT Rector's scientific scholarship for the best doctoral students (2020/21)

Scientific internships

1. 2023-03 – 2023-07 – Scientific internship as part of the INPUTDoc project at University of Technology Sydney (Sydney, Australia)
2. 2022-09 – 2022-12 – Scientific internship under the ORBIS program at Zentiva k.s. (Prague, Czech Republic)
3. 2022-01 – 2022-02 – Scientific internship under the ORBIS program at Farmak JSC (Kiev, Ukraine)
4. 2020-09 – 2020-12 – Scientific internship under the Erasmus+ program at InoCure s.r.o. (Prague, Czech Republic)
5. 2019-12 – Scientific training at State Higher Vocational School (Gniezno, Poland)

Summer schools

1. 2024-07 – REUNICE Summer School on Multifunctional Materials and Sustainability (Catania, Italy)
2. 2023-09 – Summer school on Applied and interdisciplinary artificial intelligence (Poznan, Poland)
3. 2022-09 – 4th ORBIS School on Biopharmaceutical Evaluation of Dosage Forms and Drug Delivery (Prague, Czech Republic)

Conference presentations in person

1. **Natalia Burlaga**, Ewa Kaczorek; *Układy hydrożelowe jako nośniki probiotyków w przeciwdziałaniu negatywnym skutkom terapii onkologicznych*; XII Sympozjum Onkologia i Żywienie, Bydgoszcz, Poland, 2026; **Poster**
2. **Natalia Burlaga**, Adam Grzywaczyk, Paulina Laufer, Ewa Kaczorek; *Zmiany w komórkach bakterii probiotycznych w obecności farmaceutyków*; V Sympozjum Chemii Bioorganicznej, Organicznej i Biomateriałów, Poznan, Poland, 2025; **Oral presentation**
3. **Natalia Burlaga**, Ewa Kaczorek; *Układy koloidalne do dostarczania probiotyków*; XI Kongres Technologii Chemicznej, Poznan, Poland, 2024; **Oral presentation**
4. **Natalia Burlaga**, Amanda Pacholak, Ewa Kaczorek; *Impact of potentially protective agents on lactic acid bacteria in probiotic formulations*; 2nd REUNICE Workshop on Multifuntional Materials and Sustainability, Catania, Italy, 2024; **Poster**
5. **Natalia Burlaga**, Amanda Pacholak, Ewa Kaczorek; *Cellular changes occurring in LABs under the influence of additives commonly used in the production of probiotics*; 14th Symposium on Lactic Acid Bacteria, Egmond aan Zee, Netherlands, 2023; **Poster**
6. **Natalia Burlaga**, Jakub Hert, Ewa Bartosińska, Ondrej Dammer, Josef Beranek, Ewa Kaczorek; *Compatibility studies of the API and excipients (in the drug formulation) with the use of novel technological approaches*; ORBIS Final Conference, Poznan, Poland, 2023; **Poster**
7. **Natalia Burlaga**, Amanda Pacholak, Ewa Kaczorek; *Wytwarzanie preparatów probiotycznych a właściwości komórek bakteryjnych*; BioOrg 2022 - IV Ogólnopolskie Sympozjum Chemii Bioorganicznej, Organicznej i Biomateriałów, Poznan, Poland, 2022; **Poster**
8. **Natalia Burlaga**, Irina Nagorichna; *Efektywność procesu dezintegracji komórek w uzyskaniu protein pochodzenia bakteryjnego*; BioOrg 2022 - IV Ogólnopolskie Sympozjum Chemii Bioorganicznej, Organicznej i Biomateriałów, Poznan, Poland, 2022; **Poster**
9. **Natalia Burlaga**, Amanda Pacholak, Ewa Kaczorek; *The effect of bacterial cells exposure to nitrofuran antibiotics on the properties of environmental strains*; FEMS Conference on Microbiology, Belgrade, Serbia, 2022; **Poster**

10. **Natalia Burlaga**, Amanda Pacholak, Ewa Kaczorek; *Analysis of the influence of additives used for probiotic production on LAB properties*; 10th European Young Engineers Conference, Warsaw, Poland, 2022; **Oral presentation**
11. **Natalia Burlaga**, Ewa Kaczorek; *Wpływ dodatków wykorzystywanych w produkcji probiotyków na żywotność bakterii rodzaju Lactobacillus*; XIV Kopernikańskie Seminarium Doktoranckie, Torun, Poland, 2021; **Oral presentation**
12. **Natalia Burlaga**, Ewa Kaczorek; *The presence of azole fungicides in the environment - a perspective of environmental microbes*; Science: Polish Perspectives, Zurich, Switzerland, 2021; **Poster**
13. **Natalia Burlaga**, Ewa Kaczorek; *Korzyści zdrowotne mikroorganizmów probiotycznych oraz ich zastosowanie w żywności funkcjonalnej*; II Pomorskie Studenckie Sympozjum Chemiczne, Gdansk, Poland, 2021; **Oral presentation**
14. **Natalia Burlaga**, Amanda Pacholak, Ewa Kaczorek; *Zmiany właściwości komórek bakteryjnych w obecności klotrimazolu*; Ogólnopolska Studencka Konferencja Naukowa "Bliżej Chemii", Cracow, Poland, 2021; **Poster**
15. **Natalia Burlaga**, Amanda Pacholak, Ewa Kaczorek; *Porównanie biologicznych i fizykochemicznych metod degradacji wybranych azolowych związków przeciwgrzybiczych*; E-Zjazd Zimowy Sekcji Studenckiej Polskiego Towarzystwa Chemicznego, 2020; **Oral presentation**
16. **Natalia Burlaga**, Magdalena Bartolewska, Matej Buzgo, Aiva Simaite; *Optimization of the Emulsion Electrospinning for Increased Activity of Biopharmaceuticals*; The 1st International Electronic Conference on Pharmaceutics, 2020; **Oral presentation**
17. **Natalia Burlaga**, Amanda Pacholak, Ewa Kaczorek; *Wpływ wybranych leków przeciwgrzybiczych na właściwości komórek bakterii środowiskowych*; BioOrg 2019 - III Ogólnopolskie Sympozjum Chemii Bioorganicznej, Organicznej i Biomateriałów, Poznan, Poland, 2019; **Poster**

Other conferences

1. Marta Wojcieszak-Michalak, Julia Kowalska, Amelia Wojciechowska, Natalia Szymczak, **Natalia Burlaga**, Ewa Kaczorek, Katarzyna Materna; *Charakterystyka i analiza emulżeli na bazie synbiotyków jako zaawansowanych środków do pielęgnacji skóry*; V Sympozjum Chemii Bioorganicznej, Organicznej i Biomateriałów, Poznan, Poland, 2025; Poster

2. Michał Kapczyński, Adam Grzywaczyk, **Natalia Burlaga**, Ewa Kaczorek; *Waloryzacja odpadów przemysłu spożywczego jako źródła węgla w syntezie polihydroksyalkanianów*; III Ogólnopolska Konferencja Naukowa PUTChemikon, Poznan, Poland, 2025; Poster
3. Monika Zielińska, Amanda Pacholak, **Natalia Burlaga**, Ewa Chmielewska, Adam Voelkel, Ewa Kaczorek; *Określenie właściwości bisfosfonianów pod względem cytotoksyczności, biodostępności i powinowactwa do kości*; XI Kongres Technologii Chemicznej, Poznan, Poland, 2024; Poster
4. Amanda Pacholak, Adam Grzywaczyk, **Natalia Burlaga**, Aleksandra Makiej, Agata Zdarta, Wojciech Smułek, Ewa Kaczorek; *Surfaktanty pochodzenia naturalnego a aktywność metaboliczna antybiotyków*; XI Kongres Technologii Chemicznej, Poznan, Poland, 2024; Poster
5. Amanda Pacholak, **Natalia Burlaga**, Adam Grzywaczyk, Aleksandra Makiej, Agata Zdarta, Wojciech Smułek, Ewa Kaczorek; *Właściwości mikroorganizmów środowiskowych uczestniczących w biodegradacji ksenobiotyków*; XI Kongres Technologii Chemicznej, Poznan, Poland, 2024; Poster
6. Michał Kapczyński, **Natalia Burlaga**, Adam Grzywaczyk, Oliwia Rożnowska, Ewa Kaczorek; *Sustainable management of waste biomass through biotransformation into polyhydroxyalkanoates*; 6th Symposium on Biotransformations for Pharmaceutical and Cosmetic Industry, Cracow, Poland, 2024; Poster
7. Michał Kapczyński, Adam Grzywaczyk, Natalia Burlaga, Ewa Kaczorek; *Zrównoważone zagospodarowanie odpadowej biomasy jako surowiec do syntezy polihydroksyalkanianów*; II Ogólnopolska Konferencja Naukowa PUTChemikon, Poznan, Poland, 2024; Poster
8. Wojciech Smułek, **Natalia Burlaga**, Adam Grzywaczyk, Aleksandra Makiej, Amanda Pacholak, Agata Zdarta, Ewa Kaczorek; *Bioavailability of antibiotics modified with plant surfactants*; 2nd French-Polish Chemistry Congress, Montpellier, France, 2023; Oral presentation
9. Amanda Pacholak, **Natalia Burlaga**, Ewa Kaczorek; *Wpływ azolowych związków przeciwgrzybiczych na bakterie środowiskowe*; BioOrg 2022 - IV Ogólnopolskie Sympozjum Chemii Bioorganicznej, Organicznej i Biomateriałów, Poznan, Poland, 2022; Poster

10. Amanda Pacholak, **Natalia Burlaga**, Ewa Kaczorek; *Azole fungicides - do they affect the properties of environmental bacterial strains?*; FEMS Online Conference on Microbiology, 2020; Oral presentation

Other achievements

- A CEO and co-founder of MiCo Scientific sp. z o. o. – Poznan University of Technology spin-off company
- A member of Polish Microbiological Society
- A member of Polish Chemical Society
- A member of PUT Chemistry Student Research Group